Numerical modelling studies on the impact of horizontal resolution, explicit convection and SST boundary forcing on the prediction of Tropical Cyclones over North Indian Ocean

By

RESHMI MOHAN P

Enrolment No: PHYS02201504027

Indira Gandhi Centre for Atomic Research, Kalpakkam,

Tamil Nadu, India, 603102

A thesis submitted to the

Board of Studies in Physical Sciences

In partial fulfillment of requirements

for the Degree of

DOCTOR OF PHILOSOPHY

of

HOMI BHABHA NATIONAL INSTITUTE

December 2020

Homi Bhabha National Institute

Recommendations of the Viva Voce Committee

As members of the Viva Voce Committee, we certify that we have read the dissertation prepared by Reshmi Mohan P entitled," **Numerical modelling studies on the impact of horizontal resolution, explicit convection and SST boundary forcing on the prediction of Tropical Cyclones over North Indian Ocean**" and recommend that it may be accepted as fulfilling the thesis requirement for the award of Degree of Doctor of Philosophy.

Chairman –Dr. R. Bhaskaran	by VC for	**Date**
Guide / Convener –Dr. C.V. Srinivas		**Date** 15-5-2021
Examiner - Prof. S. Balachandran	by VC for	**Date**
Member 1- Dr. K. Devan		**Date** 15/5/2021
Member 2- Dr. V. Jayaraman		**Date** 15.05.2021.
Technology Advisor- Dr. D.K. Mohapatra	by VC for	**Date**

Final approval and acceptance of this thesis is contingent upon the candidate's submission of the final copies of the thesis to HBNI.

I/We hereby certify that I/we have read this thesis prepared under my/our direction and recommend that it may be accepted as fulfilling the thesis requirement.

Date: 15/05/2021

Place: Kalpakkam.

Dr. C.V. Srinivas

Guide

Homi Bhabha National Institute

Recommendations of the Viva Voce Committee

As members of the Viva Voce Committee, we certify that we have read the dissertation prepared by Reshmi Mohan P entitled," **Numerical modelling studies on the impact of horizontal resolution, explicit convection and SST boundary forcing on the prediction of Tropical Cyclones over North Indian Ocean**" and recommend that it may be accepted as fulfilling the thesis requirement for the award of Degree of Doctor of Philosophy.

Chairman –Dr. R. Bhaskaran	by VC for [signature]	**Date**	
Guide / Convener –Dr. C.V. Srinivas	[signature]	**Date**	15-5-2021
Examiner - Prof. S. Balachandran	by VC for [signature]	**Date**	
Member 1- Dr. K. Devan	[signature]	**Date**	15/5/2021
Member 2- Dr. V. Jayaraman	[signature]	**Date**	15.05.2021.
Technology Advisor- Dr. D.K. Mohapatra	by VC for [signature]	**Date**	

Final approval and acceptance of this thesis is contingent upon the candidate's submission of the final copies of the thesis to HBNI.

I/We hereby certify that I/we have read this thesis prepared under my/our direction and recommend that it may be accepted as fulfilling the thesis requirement.

Date: 15/05/2021

Place: Kalpakkam.

[signature]

Dr. C.V. Srinivas

Guide

STATEMENT BY AUTHOR

This dissertation has been submitted in partial fulfillment of requirements for an advanced degree at Homi Bhabha National Institute (HBNI) and is deposited in the Library to be made available to borrowers under rules of the HBNI.

Brief quotations from this dissertation are allowable without special permission, provided that accurate acknowledgement of source is made. Requests for permission for extended quotation from or reproduction of this manuscript in whole or in part may be granted by the Competent Authority of HBNI when in his or her judgment the proposed use of the material is in the interests of scholarship. In all other instances, however, permission must be obtained from the author.

Reshmi Mohan P

DECLARATION

I, hereby declare that the investigation presented in the thesis has been carried out by me. The work is original and has not been submitted earlier as a whole or in part for a degree / diploma at this or any other Institution / University.

Reshmi Mohan P

List of Publications arising from the thesis

Journal

1. "Tropical Cyclone Simulations over Bay of Bengal with ARW model: Sensitivity to cloud microphysics schemes", **P. Reshmi Mohan,** C.V. Srinivas, V. Yesubabu, R. Bhaskaran, B. Venkatraman, *Atmos. Res.*, **2019**, *230,* 104651 (16 pp).

2. "Simulation of a heavy rainfall event over Chennai in Southeast India using WRF: Sensitivity to microphysics parameterization", **P. Reshmi Mohan,** C. V. Srinivas, V. Yesubabu, R. Bhaskaran, B. Venkatraman, *Atmos. Res.*, **2018**, *210*, 83-89.

3. "Impact of convection permitting high resolution simulations with WRF on Tropical cyclone predictions over the North Indian Ocean", **P. Reshmi Mohan,** C.V. Srinivas, B. Venkatraman, *Journal of Atmospheric Research* (**Under Review**).

4. "A numerical investigation of the rapid-intensification of pre-monsoon cyclones Fani and Amphan in the Bay of Bengal using WRF", **P. Reshmi Mohan,** C. V. Srinivas, B. Venkatraman, *Journal of Atmospheric Research* (**Under Review**).

5. "Representation of convection in explicit simulations of Cyclones Fani and Gaja", **P. Reshmi Mohan,** C. V. Srinivas, V. Yesubabu, B. Venkatraman, (**Manuscript under preparation**).

Conference Presentations

1. "Effect of parameterized and explicit convection physics schemes on the simulation of Tropical cyclones over the Bay of Bengal", **P. Reshmi Mohan,** C.V. Srinivas, V. Yesubabu, R. Venkatesan, R. Bhaskaran, *International Workshop on Modeling Atmospheric-Oceanic Processes for Weather and Climate Extremes (MAPEX-2019)*, 28-29 March 2019, IIT Delhi, India (**Poster Presentation – Third position for Best Poster**).

2. “Numerical simulation of Tropical Cyclone Vardha, 2016: Analysis of Intensity Parameters”, **P. Reshmi Mohan,** C. V. Srinivas and R. Bhaskaran, *Research Scholars Meet on Material Science and Engineering of Nuclear Materials (RSM-MSENM-2018)*, 7-9 May 2018, Indira Gandhi Centre for Atomic Research, Kalpakkam, India **(Poster Presentation)**.

3. “Sensitivity of Tropical Cyclone simulations to microphysics parameterizations in WRF”, **P. Reshmi Mohan,** C.V. Srinivas, V. Yesubabu, R. Bhaskaran and B. Venkatraman, *Indian Association for Radiation Protection International Conference (IARPIC-2018)*, 16-20 January 2018, Bhabha Atomic Research Centre, Mumbai, India **(Poster Presentation)**.

4. “Sensitivity of Heavy Rainfall simulations of December 2015 over Chennai, southeast India, to Microphysics Parameterizations in WRF Model”, **P. Reshmi Mohan,** C.V. Srinivas, R. Bhaskaran and B. Venkatraman, *India Conference on Radar Meteorology (iRAD-2017)*, 8-11 January 2017, IIT Kharagpur, India **(Oral Presentation – Second position for Best Oral Presentation)**.

Publications not included in the thesis

1. “Impact of boundary layer physics on Tropical Cyclone simulations in the Bay of Bengal using the WRF model”, J. R. Rajeswari, C. V. Srinivas, **P. Reshmi Mohan** and B. Venkatraman, *Pure Appl. Geophys.*, **2020**, *177*, 5523-5550.

Reshmi Mohan P

DEDICATED

to

My Brother and Sister

ACKNOWLEDGEMENTS

I would like to thank all the people who have directly or indirectly played a role in shaping this thesis to completion and developing my personal and academic career. In the first place, I would like to express my sincere gratitude to my thesis supervisor Dr. C.V. Srinivas, for his constant and extensive support, both academically and personally, throughout the tenure of my thesis works. I admire his utmost dedication towards planning the thesis works and correcting the manuscripts. Without his persistent support, the thesis would not have been in its present shape.

Besides my advisor, I am also thankful to my Doctoral Committee (DC) members, Dr. R. Bhaskaran (Chairman), Dr. V. Jayaraman, Dr. D.K. Mohapatra and Dr. K. Devan for the rich discussions, productive criticisms and intuitive comments which helped me step forward and broaden my knowledge in various perspectives.

I would like to thank my research collaborator Dr. V. Yesubabu from National Atmospheric Research Laboratory, Tirupati for providing observational data and his valuable comments and suggestions for improving my research works. I am also thankful to the providers of all scientific datasets and software used in this thesis. I am greatly indebted to my seniors Dr. Greeshma and Dr. Hariprasad for their kind and valuable help throughout my thesis tenure. Sincere thanks and love to my dear juniors Rajeswari and Revanth for creating a vibrant atmosphere in lab and for their immense support and help. I also thank Mr. P.T. Rakesh for his valuable suggestions during my tenure.

I am privileged to thank Dr. A. K. Bhaduri, Director, IGCAR and Dr. S. A. V. Satya Murthy (former Director, IGCAR) for providing an opportunity to carry out my research at IGCAR. I would also like to thank Dr. B. Venkatraman, Director, *SQ&RMG for his constant support and encouragement. I thank Dr. R. Rajaraman, Dean, Physical Sciences, Dr. N. V. Chandra Shekar and Dr. B. V. R. Tata (former Deans, Physical Sciences) for their constant support in all my academic endeavors at IGCAR. I also thank the IGCAR management for providing the accommodation and for all the other help and support during the tenure of my thesis. I sincerely thank the Department of Atomic Energy (DAE), Government of India for providing fellowship.*

I thank Dr. Radhikesh, Dr. Irshad and all my seniors for their friendly nature and support. I thank all my batch mates Bala, Dhilipan, Rajitha K, Rajitha R, Velraj, Akshaya and Jakathamani for making the stay at IGCAR and JRF enclave cheerful and memorable. My heartfelt thanks and love to Bala, my best friend, for his care, affection and advices, and being the constant source of encouragement during the ups and downs of my life. I would also like to thank all my juniors and other friends at JRF enclave for creating a joyful environment during my stay at JRF enclave.

I thank all the members of JRF Enclave Residence committee (JRC) for the collective role they played in representing our issues to higher authorities. I also thank all the players of Enclave Badminton League and fellow participants of Freshers day cultural programme for providing the most memorable and entertaining moments during my stay at IGCAR.

I take this opportunity to acknowledge all my Professors at Department of Atmospheric Sciences, CUSAT for building my knowledge and research interest in Meteorology. I also thank my dear friends, seniors and juniors at CUSAT for all the cherished moments we spent together. I would also like to express my thanks to all my teachers for playing a significant role in my life.

I am deeply indebted to the most important part of my life, my family for their immense support and encouragement throughout my life. Words would not be sufficient to express my deep and heartfelt gratitude to my dear brother Mr. Rangit R.K, without whose continuous support and love, my Ph.D dream would not have come true. Enormous thanks and love to my dear sister Mrs. Meera Rangit who has always been my mentor and pillar of strength. My deepest appreciation to my beloved parents Mr. P. Mohanakrishnan and Mrs. Thara Mohan for their unconditional love, care and affection. It will be incomplete without asserting the role of my husband Mr. Vaisagh Menon and my parents-in-law whose love, understanding and patience made the completion of this thesis possible.

CONTENTS

LIST OF FIGURES

LIST OF TABLES

LIST OF ABBREVIATIONS

AMSU	:	Advanced Microwave Sounding Unit
ARW	:	Advanced Research Weather Research and Forecasting
AS	:	Arabian Sea
AWS	:	Automatic Weather Station
BOB	:	Bay of Bengal
CAPE	:	Convective Available Potential Energy
CIRA	:	Cooperative Institute for Research in Atmosphere
CISK	:	Conditional Instability of Second Kind
CMP	:	Cloud Microphysics
CP	:	Cumulus/Convective Parameterization
CS	:	Cyclonic Storm
CSLP	:	Central Sea Level Pressure
CSU	:	Colorado State University
D	:	Depression
DD	:	Deep Depression
DWR	:	Doppler Weather Radar
ESCS	:	Extremely Severe Cyclonic Storm
FAQ	:	Frequently Asked Questions
GFDL	:	Geophysical Fluid Dynamics Laboratory
GFS	:	Global Forecasting System
HWRF	:	Hurricane Weather Research and Forecasting
IMD	:	India Meteorological Department
ITCZ	:	Inter Tropical Convergence Zone

L	:	Low pressure
LHF	:	Latent Heat Flux
LSM	:	Land Surface Model
MJO	:	Madden Julian Oscillation
MM5	:	Fifth-Generation Penn State/NCAR Mesoscale Model
MMAB	:	Marine Modelling and Analysis Branch
MST	:	Mesosphere-Stratosphere-Troposphere
MSW	:	Maximum Sustained Winds
MYNN	:	Mellor-Yamada Nakanishi and Niino
NARL	:	National Atmospheric Research Laboratory
NCAR	:	National Center for Atmospheric Research
NCEP	:	National Center for Environmental Prediction
NHC	:	National Hurricane Centre
NIO	:	North Indian Ocean
NOAA	:	National Oceanic Atmospheric Administration
OISST	:	Optimum Interpolation Sea Surface Temperature
PBL	:	Planetary Boundary Layer
RAMMB	:	Regional and Mesoscale Meteorology Branch
RH	:	Relative Humidity
RI	:	Rapid Intensification
RMW	:	Radius of Maximum Winds
RRTM	:	Rapid Radiative Transfer Model
RSMC(s)	:	Regional Specialized Meteorological Center(s)
RTG_SST	:	Real Time Global_SST

SCS	:	Severe Cyclonic Storm
SHF	:	Sensible Heat Flux
SSHS	:	Saffir-Simpson Hurricane Scale
SSHWS	:	Saffir-Simpson Hurricane Wind Scale
SST	:	Sea Surface Temperature
SuCS	:	Super Cyclonic Storm
TC(s)	:	Tropical Cyclone(s)
TCM3	:	Triply Nested Movable Mesh Primitive Equation Model
TRMM	:	Tropical Rainfall Measuring Mission
UCAR	:	University Corporation for Atmospheric Research
VSCS	:	Very Severe Cyclonic Storm
WISHE	:	Wind-Induced Surface Heat Exchange
WRF	:	Weather Research and Forecasting
WRF-DA	:	WRF-Var Data Assimilation
WSM3	:	WRF Single Moment 3-class
WSM6	:	WRF Single Moment 6-class
YSU	:	Yonsei University

Chapter 7

Summary, conclusions and scope of future work

The information on the genesis, intensification and movement of the TCs over tropical oceanic regions is considered highly important for advanced preparations needed in disaster mitigation along the highly vulnerable tropical coastal areas. The prediction of the movement, intensity and structure of TCs over global tropical oceans has been a challenging task for the research community. The Bay of Bengal of North Indian Ocean is one of the potential basins with high annual frequency for intensive TCs. The east-coast of India is highly vulnerable to the TC related natural disasters due to the shallow and plain topography, curved coast line and the intensive TCs that form in the BOB region. Reliable numerical atmospheric models incorporating all the physical processes especially of convection are highly essential to produce robust predictions of the TCs. The previous modelling studies of TCs over the NIO mainly used coarse grids (≥9 km) with parameterized convection for TC intensity and track forecasting. With advances in high resolution models convection can be explicitly represented to resolve the cloud and convection processes which would offer advantages over the traditional approach of using implicit convection.

In this study an attempt is made to study the impact of horizontal resolution and explicit convection, sensitivity of high resolution predictions to cloud microphysical processes on the track and intensity predictions of TCs over BOB region of NIO, and the role of SST in rapidly intensifying TCs using the WRF-ARW mesoscale numerical

weather prediction modelling system. To achieve these objectives towards improving the TC predictions over the NIO, the study is organized into four major chapters i) impact of convection permitting high resolution simulations ii) sensitivity of high resolution simulations to cloud microphysics schemes and iii) role of SST boundary forcing on the rapid intensification of TCs using GFS model analysis SST, satellite-derived SST and climatological SST data sets. Results of simulations are compared with various available observational datasets. A summary of the results of various simulations focused on the above aspects are presented in this chapter along with the conclusions, their applications and constraints. Discussions on comparisons with the earlier studies conducted and extension of the study as a future scope are also provided in the current chapter.

In essence, the increased grid resolution of 3 km better resolved the inflow, convergence and vertical motions and also produced higher diabatic heating due to explicit treatment of cloud microphysical processes and therefore produced improvements for both track and intensity predictions over low-resolution simulations (9 km) using cumulus parameterization. Among various microphysics schemes, the Thompson scheme produced stronger convergence and vertical motion up to 6 km and stronger upper air divergence associated with strong cyclonic vorticity in the atmosphere and also captured the time evolution of different hydrometeors that led to produce the observed pattern of the rainfall associated with a low-pressure system both spatially and temporally. Also, the Thompson scheme produced least errors for track and intensity and good prediction of thermodynamic parameters which suggest that it is more suitable for high-resolution operational TC forecasting in the NIO. The SST played a significant role in the rapid intensification of TC Amphan due to large positive SST anomaly from climatological mean associated with a high wind shear, whereas it has shown only a minor influence in RI phase of Fani due to smaller SST anomaly associated with low wind-shear. This suggests the RI phase is caused

mainly by SST anomaly for Amphan and low wind-shear for Fani cyclones. The chapter wise summary and conclusions of the study are given below.

In **Chapter 1** an introduction on the general characteristics of the TCs like formation, structure etc. of global TCs along with the climatology, intensity and a review of earlier numerical modelling studies of TCs over NIO was given. The importance of high-resolution TC simulations with explicit convection in the context of previous studies over NIO and current advancements over other basins and the objectives of the present study were also discussed.

In **Chapter 2**, a detailed description of WRF-ARW modelling system and its components which includes the governing equations, grid nesting, initial and boundary conditions and model physics used for the study were presented. Subsequently, a brief description of the history of the TCs along with their characteristics selected for the simulations were also presented. Finally, the details of the global data sets used for model initialization and integration and various observational data sets that include surface, upper air, DWR and satellite data products used for validation of simulations were provided.

In **Chapter 3** the results of convection permitting high-resolution simulations on the prediction of ten TCs during 2010-2019 in the BOB of NIO were presented. The study was conducted using two horizontal grid resolutions i.e., 9km grid using parameterized convection (9km-CP) and 3km grid using explicit microphysics (3km-MP). The study involved a comparison of the effects of cumulus physics at 9-km resolution with those of microphysics in the finer grids (3km). The results showed that the 3km-MP using explicit convection provided superior track and intensity predictions over the 9-km grids using implicit convection. The track errors in 3km-MP were reduced by 31%, 5%, 28% and 8% at 24h, 48h, 72h and 96h forecast intervals respectively over 9km-CP. The 9km-CP

produced relatively weaker vorticity, thereby the TC experienced stronger environmental steering force which thus led to northward deviating tracks and higher error compared to the 3km-MP which produced stronger vorticity. The 3km-MP produced significant improvements in intensity forecasts. Overall, the errors were reduced by 47%, 78%, 128%, 36% for CSLP and 29%, 31%, 44%, 101% for MSW at 24, 48, 72 and 96 h respectively in 3km-MP over 9km-CP. The study showed that the 9km-CP produced relatively higher (lower) intensity during the growing phases (peak and decay phases) for all cyclones due to producing higher (lower) thermal anomaly than the 3km-MP indicating different impacts of cumulus and microphysics in the respective phases. While both the simulations over-estimated the intensity for a majority of the cyclones, the 3km-MP reduced the overestimation of intensity during growing phases and underestimation during peak and decay phases and also improved the timing of maximum intensification in most cases. Various structural characteristics of the TCs (RMW, surface winds, thermal anomaly, radial winds, cloud reflectivity etc.) were found to be better represented in the 3km-MP as seen from comparison with CIRA multi-satellite observational cyclone products. Overall, the increased resolution of 3km-MP better resolved the inflow, convergence and updrafts and also produced higher diabatic heating due to explicit treatment of cloud microphysical processes and therefore suggests improvements over low-resolution simulations using cumulus parameterization. The results clearly demonstrate better model performance for track and intensity predictions compared to the earlier results reported by Srinivas et al. (2013) using 9 km with parameterized convection which showed considerable overestimation of the intensity. The results of this study using high-resolution modelling framework with explicit convection and statistical error evaluation for a large number of TCs over the BOB of NIO region show promising forecast strategy.

In **Chapter 4**, the results of sensitivity experiments with various cloud microphysical parameterization schemes (Morrison, Lin, WSM3, WSM6, Thompson, Goddard) in the simulation of tropical low-pressure system that produced heavy rainfall over north-coastal Tamilnadu, Chennai and surrounding areas were presented. Simulations revealed that the microphysics schemes affect the location of the low-pressure trough, atmospheric circulation and low-level convergence through changes in the diabatic heating and its coupling to dynamics ultimately influencing the distribution and location of rainfall. It was noticed that among all the schemes the Thompson scheme had realistically produced the low-pressure trough, circulation and rainfall pattern compared to other schemes. While the Morrison and Lin schemes simulated the maximum precipitation over the ocean area adjacent to Chennai, the WSM3, WSM6 and Goddard schemes simulated along the coast but with significantly lower intensity. The Thompson microphysics scheme produced the maximum rainfall (450 mm) over Chennai and its surroundings and the heavy rainfall extension along the coast with its time of occurrence in better agreement with observations compared to all the other schemes. Thompson predicted most of the hydrometeors mixing ratios (except ice), their vertical distribution as well as the time of occurrence coinciding with the maximum observed rainfall event and the corresponding hydrometeor reflectivity better than the other schemes. Based on these sensitivity results the microphysics schemes were further used in the next chapter (Chapter 5) for the prediction of TCs to obtain a better conclusion on the performance of various microphysics schemes for tropical cyclonic storms.

In **Chapter 5**, the sensitivity results of cloud-resolving scale predictions of TCs with a high resolution of 3 km to cloud microphysics schemes were presented. Six TCs which formed over the Bay of Bengal (BOB) were chosen for the study using 5 microphysics schemes. The microphysics schemes (Thompson, Goddard, Lin, Morrison,

WSM6) were chosen based on the results from Chapter 4. Results of simulated CSLP, MSW and track positions indicated that the microphysics schemes mainly affect the intensity and produce moderate impact on track. Overall, based on aggregate error statistics for all the six cyclones it was found that Thompson produced the best predictions for both tracks and intensity. Next to Thompson, Morrison and Goddard gave the best intensity prediction; WSM6 and Lin produced the best track prediction. Moreover, a comparison of simulated vertical winds with the corresponding data from MST radar profiles at Gadanki station during the passage of Gaja and Fani cyclones showed that the simulations with Morrison, Thompson and Goddard schemes produced more realistic representation of vertical motions indicating better prediction of convection in TCs. Overall, the results from the two chapters (Chapters 4 and 5) suggest that the Thompson scheme gave a good prediction of rainfall, thermodynamic variables and least errors for both the track and intensity parameters thus promising the scheme's application for high resolution operational TC forecasting in the NIO.

In **Chapter 6** the results of SST sensitivity experiments on the RI phase of two rapidly intensified cyclones Amphan and Fani that formed over the BOB during pre-monsoon season in 2020 and 2019 respectively were presented. The simulations with real-time SSTs (GFS-SST, NOAA-SST) were compared with a control run in which a 11-year climatological mean SST (CLIM-SST) was taken for SST initial and boundary conditions. The results showed that the anomalous increase in SST from the climatological mean greatly influenced the intensification of TC Amphan which is seen from the GFS-SST and NOAA-SST simulations with higher intensification than the CLIM-SST, though in general all the simulations overestimated the intensity. All the experiments also captured the RI phase for TC Amphan with variation in the intensity according to the observed SST values. The NOAA-SST produced the maximum intensification and CLIM-SST the least. The

simulations for Amphan revealed that the RI phase was associated with a positive SST anomaly and also an increase in vertical shear of horizontal wind in upper atmosphere indicating a greater role of SST in the RI process. However, for TC Fani, an increase in SST from the climatological mean did not influence much the intensification, as the CLIM-SST simulation also produced the highest intensity. Simulations for Fani revealed that though the SST anomaly is relatively small compared to Amphan, there was a low vertical shear of horizontal winds during the RI phase which facilitated the cyclone to undergo rapid intensification. The wind-shear was relatively low in both NOAA-SST and GFS-SST during the RI phase thus producing slightly higher intensification during the RI phase in these experiments. The analysis of surface fluxes and storm thermodynamics conducted for TC Amphan showed that an increase in SST has a great impact on the intensification through a WISHE type of feed-back by increasing the latent and sensible heat fluxes, low-level convergence and the diabatic heating thereby resulting in larger vertical velocities. Overall, the results from this chapter suggest that positive SST anomaly has a major role in rapid intensification as the simulations also showed a higher wind shear during the RI phase. On the other hand, simulations for Fani revealed a less important role of SST during the RI phase which is associated with a low-wind shear.

The present work has conducted numerical modelling studies for 11 TCs during 2010-2020 period and showed very promising results with 3-km resolution using explicit convection for the improvement of TC forecasting over NIO. Though there are a lot of uncertainties associated with the cloud microphysics and convective parameterization schemes in numerical models, the present study finds that the convection permitting simulations in general produce better simulations for TC tracks, intensities and structural parameters than the simulations using convective parameterization. However, these results may be specific to the Kain Fritsch convection scheme in the 9km grid. This may require

further sensitivity analysis with simulations with parameterized convection in the coarse domain to reduce uncertainties in model performance. Although there may be competing effects of decreasing flux moisture convergence and increasing convection at increasing horizontal resolution, numerical modelling studies at 1 km grid resolution are needed to test this limit for further possible improvements in TC intensity especially during the entire life cycle and structure prediction.

It is known that the TC simulations are sensitive to the initial conditions; however, most studies were focused on the impact of data assimilation at 9 km resolutions. The present results with high resolution convective permitting simulations can be further improved by data assimilation for thermodynamical parameters with data from sources such as GPS- Osculati humidity and temperature profiles using data assimilation techniques such as 3DVAR. Also, most of the previous air-sea interaction studies in numerical models were conducted at 9 km resolution. The air-sea coupled simulations need to be conducted at 3 km grid resolution to address the role of accurate air-sea fluxes on cloud-resolving simulations. The present study also finds the best microphysics scheme (Thompson scheme) applicable for both TC tracks, intensity and rainfall, from simulations conducted for six TCs and a tropical low-pressure convective system. However, there is further scope for detailed studies on microphysics sensitivity in the context of development of a large number of new cloud microphysics in WRF-ARW by analyzing the heating profiles associated with hydrometeor phase changes, fall speed and particle size distributions of frozen hydrometeors etc. The SST sensitivity experiments showed that even though SST has an impact in RI phase of cyclones it is not always a dominant factor for TC intensification as evident from the analysis of Amphan and Fani. The results of high SST anomaly and high wind-shear for Amphan and low SST anomaly and low wind-shear for Fani indicate SST influenced the RI phase only for Amphan whereas the wind-

shear played major role for Fani. These results suggest that in order to obtain more robust conclusions on the role of SST for RI further sensitivity studies have to be conducted with longer term climatological mean SST and for more cyclone samples including the post-monsoon cyclones that have undergone rapid intensification.

Chapter 7

Summary, conclusions and scope of future work

The information on the genesis, intensification and movement of the TCs over tropical oceanic regions is considered highly important for advanced preparations needed in disaster mitigation along the highly vulnerable tropical coastal areas. The prediction of the movement, intensity and structure of TCs over global tropical oceans has been a challenging task for the research community. The Bay of Bengal of North Indian Ocean is one of the potential basins with high annual frequency for intensive TCs. The east-coast of India is highly vulnerable to the TC related natural disasters due to the shallow and plain topography, curved coast line and the intensive TCs that form in the BOB region. Reliable numerical atmospheric models incorporating all the physical processes especially of convection are highly essential to produce robust predictions of the TCs. The previous modelling studies of TCs over the NIO mainly used coarse grids (≥9 km) with parameterized convection for TC intensity and track forecasting. With advances in high resolution models convection can be explicitly represented to resolve the cloud and convection processes which would offer advantages over the traditional approach of using implicit convection.

In this study an attempt is made to study the impact of horizontal resolution and explicit convection, sensitivity of high resolution predictions to cloud microphysical processes on the track and intensity predictions of TCs over BOB region of NIO, and the role of SST in rapidly intensifying TCs using the WRF-ARW mesoscale numerical

weather prediction modelling system. To achieve these objectives towards improving the TC predictions over the NIO, the study is organized into four major chapters i) impact of convection permitting high resolution simulations ii) sensitivity of high resolution simulations to cloud microphysics schemes and iii) role of SST boundary forcing on the rapid intensification of TCs using GFS model analysis SST, satellite-derived SST and climatological SST data sets. Results of simulations are compared with various available observational datasets. A summary of the results of various simulations focused on the above aspects are presented in this chapter along with the conclusions, their applications and constraints. Discussions on comparisons with the earlier studies conducted and extension of the study as a future scope are also provided in the current chapter.

In essence, the increased grid resolution of 3 km better resolved the inflow, convergence and vertical motions and also produced higher diabatic heating due to explicit treatment of cloud microphysical processes and therefore produced improvements for both track and intensity predictions over low-resolution simulations (9 km) using cumulus parameterization. Among various microphysics schemes, the Thompson scheme produced stronger convergence and vertical motion up to 6 km and stronger upper air divergence associated with strong cyclonic vorticity in the atmosphere and also captured the time evolution of different hydrometeors that led to produce the observed pattern of the rainfall associated with a low-pressure system both spatially and temporally. Also, the Thompson scheme produced least errors for track and intensity and good prediction of thermodynamic parameters which suggest that it is more suitable for high-resolution operational TC forecasting in the NIO. The SST played a significant role in the rapid intensification of TC Amphan due to large positive SST anomaly from climatological mean associated with a high wind shear, whereas it has shown only a minor influence in RI phase of Fani due to smaller SST anomaly associated with low wind-shear. This suggests the RI phase is caused

mainly by SST anomaly for Amphan and low wind-shear for Fani cyclones. The chapter wise summary and conclusions of the study are given below.

In **Chapter 1** an introduction on the general characteristics of the TCs like formation, structure etc. of global TCs along with the climatology, intensity and a review of earlier numerical modelling studies of TCs over NIO was given. The importance of high-resolution TC simulations with explicit convection in the context of previous studies over NIO and current advancements over other basins and the objectives of the present study were also discussed.

In **Chapter 2**, a detailed description of WRF-ARW modelling system and its components which includes the governing equations, grid nesting, initial and boundary conditions and model physics used for the study were presented. Subsequently, a brief description of the history of the TCs along with their characteristics selected for the simulations were also presented. Finally, the details of the global data sets used for model initialization and integration and various observational data sets that include surface, upper air, DWR and satellite data products used for validation of simulations were provided.

In **Chapter 3** the results of convection permitting high-resolution simulations on the prediction of ten TCs during 2010-2019 in the BOB of NIO were presented. The study was conducted using two horizontal grid resolutions i.e., 9km grid using parameterized convection (9km-CP) and 3km grid using explicit microphysics (3km-MP). The study involved a comparison of the effects of cumulus physics at 9-km resolution with those of microphysics in the finer grids (3km). The results showed that the 3km-MP using explicit convection provided superior track and intensity predictions over the 9-km grids using implicit convection. The track errors in 3km-MP were reduced by 31%, 5%, 28% and 8% at 24h, 48h, 72h and 96h forecast intervals respectively over 9km-CP. The 9km-CP

produced relatively weaker vorticity, thereby the TC experienced stronger environmental steering force which thus led to northward deviating tracks and higher error compared to the 3km-MP which produced stronger vorticity. The 3km-MP produced significant improvements in intensity forecasts. Overall, the errors were reduced by 47%, 78%, 128%, 36% for CSLP and 29%, 31%, 44%, 101% for MSW at 24, 48, 72 and 96 h respectively in 3km-MP over 9km-CP. The study showed that the 9km-CP produced relatively higher (lower) intensity during the growing phases (peak and decay phases) for all cyclones due to producing higher (lower) thermal anomaly than the 3km-MP indicating different impacts of cumulus and microphysics in the respective phases. While both the simulations over-estimated the intensity for a majority of the cyclones, the 3km-MP reduced the overestimation of intensity during growing phases and underestimation during peak and decay phases and also improved the timing of maximum intensification in most cases. Various structural characteristics of the TCs (RMW, surface winds, thermal anomaly, radial winds, cloud reflectivity etc.) were found to be better represented in the 3km-MP as seen from comparison with CIRA multi-satellite observational cyclone products. Overall, the increased resolution of 3km-MP better resolved the inflow, convergence and updrafts and also produced higher diabatic heating due to explicit treatment of cloud microphysical processes and therefore suggests improvements over low-resolution simulations using cumulus parameterization. The results clearly demonstrate better model performance for track and intensity predictions compared to the earlier results reported by Srinivas et al. (2013) using 9 km with parameterized convection which showed considerable overestimation of the intensity. The results of this study using high-resolution modelling framework with explicit convection and statistical error evaluation for a large number of TCs over the BOB of NIO region show promising forecast strategy.

In **Chapter 4**, the results of sensitivity experiments with various cloud microphysical parameterization schemes (Morrison, Lin, WSM3, WSM6, Thompson, Goddard) in the simulation of tropical low-pressure system that produced heavy rainfall over north-coastal Tamilnadu, Chennai and surrounding areas were presented. Simulations revealed that the microphysics schemes affect the location of the low-pressure trough, atmospheric circulation and low-level convergence through changes in the diabatic heating and its coupling to dynamics ultimately influencing the distribution and location of rainfall. It was noticed that among all the schemes the Thompson scheme had realistically produced the low-pressure trough, circulation and rainfall pattern compared to other schemes. While the Morrison and Lin schemes simulated the maximum precipitation over the ocean area adjacent to Chennai, the WSM3, WSM6 and Goddard schemes simulated along the coast but with significantly lower intensity. The Thompson microphysics scheme produced the maximum rainfall (450 mm) over Chennai and its surroundings and the heavy rainfall extension along the coast with its time of occurrence in better agreement with observations compared to all the other schemes. Thompson predicted most of the hydrometeors mixing ratios (except ice), their vertical distribution as well as the time of occurrence coinciding with the maximum observed rainfall event and the corresponding hydrometeor reflectivity better than the other schemes. Based on these sensitivity results the microphysics schemes were further used in the next chapter (Chapter 5) for the prediction of TCs to obtain a better conclusion on the performance of various microphysics schemes for tropical cyclonic storms.

In **Chapter 5**, the sensitivity results of cloud-resolving scale predictions of TCs with a high resolution of 3 km to cloud microphysics schemes were presented. Six TCs which formed over the Bay of Bengal (BOB) were chosen for the study using 5 microphysics schemes. The microphysics schemes (Thompson, Goddard, Lin, Morrison,

WSM6) were chosen based on the results from Chapter 4. Results of simulated CSLP, MSW and track positions indicated that the microphysics schemes mainly affect the intensity and produce moderate impact on track. Overall, based on aggregate error statistics for all the six cyclones it was found that Thompson produced the best predictions for both tracks and intensity. Next to Thompson, Morrison and Goddard gave the best intensity prediction; WSM6 and Lin produced the best track prediction. Moreover, a comparison of simulated vertical winds with the corresponding data from MST radar profiles at Gadanki station during the passage of Gaja and Fani cyclones showed that the simulations with Morrison, Thompson and Goddard schemes produced more realistic representation of vertical motions indicating better prediction of convection in TCs. Overall, the results from the two chapters (Chapters 4 and 5) suggest that the Thompson scheme gave a good prediction of rainfall, thermodynamic variables and least errors for both the track and intensity parameters thus promising the scheme's application for high resolution operational TC forecasting in the NIO.

In **Chapter 6** the results of SST sensitivity experiments on the RI phase of two rapidly intensified cyclones Amphan and Fani that formed over the BOB during pre-monsoon season in 2020 and 2019 respectively were presented. The simulations with real-time SSTs (GFS-SST, NOAA-SST) were compared with a control run in which a 11-year climatological mean SST (CLIM-SST) was taken for SST initial and boundary conditions. The results showed that the anomalous increase in SST from the climatological mean greatly influenced the intensification of TC Amphan which is seen from the GFS-SST and NOAA-SST simulations with higher intensification than the CLIM-SST, though in general all the simulations overestimated the intensity. All the experiments also captured the RI phase for TC Amphan with variation in the intensity according to the observed SST values. The NOAA-SST produced the maximum intensification and CLIM-SST the least. The

simulations for Amphan revealed that the RI phase was associated with a positive SST anomaly and also an increase in vertical shear of horizontal wind in upper atmosphere indicating a greater role of SST in the RI process. However, for TC Fani, an increase in SST from the climatological mean did not influence much the intensification, as the CLIM-SST simulation also produced the highest intensity. Simulations for Fani revealed that though the SST anomaly is relatively small compared to Amphan, there was a low vertical shear of horizontal winds during the RI phase which facilitated the cyclone to undergo rapid intensification. The wind-shear was relatively low in both NOAA-SST and GFS-SST during the RI phase thus producing slightly higher intensification during the RI phase in these experiments. The analysis of surface fluxes and storm thermodynamics conducted for TC Amphan showed that an increase in SST has a great impact on the intensification through a WISHE type of feed-back by increasing the latent and sensible heat fluxes, low-level convergence and the diabatic heating thereby resulting in larger vertical velocities. Overall, the results from this chapter suggest that positive SST anomaly has a major role in rapid intensification as the simulations also showed a higher wind shear during the RI phase. On the other hand, simulations for Fani revealed a less important role of SST during the RI phase which is associated with a low-wind shear.

The present work has conducted numerical modelling studies for 11 TCs during 2010-2020 period and showed very promising results with 3-km resolution using explicit convection for the improvement of TC forecasting over NIO. Though there are a lot of uncertainties associated with the cloud microphysics and convective parameterization schemes in numerical models, the present study finds that the convection permitting simulations in general produce better simulations for TC tracks, intensities and structural parameters than the simulations using convective parameterization. However, these results may be specific to the Kain Fritsch convection scheme in the 9km grid. This may require

further sensitivity analysis with simulations with parameterized convection in the coarse domain to reduce uncertainties in model performance. Although there may be competing effects of decreasing flux moisture convergence and increasing convection at increasing horizontal resolution, numerical modelling studies at 1 km grid resolution are needed to test this limit for further possible improvements in TC intensity especially during the entire life cycle and structure prediction.

It is known that the TC simulations are sensitive to the initial conditions; however, most studies were focused on the impact of data assimilation at 9 km resolutions. The present results with high resolution convective permitting simulations can be further improved by data assimilation for thermodynamical parameters with data from sources such as GPS- Osculati humidity and temperature profiles using data assimilation techniques such as 3DVAR. Also, most of the previous air-sea interaction studies in numerical models were conducted at 9 km resolution. The air-sea coupled simulations need to be conducted at 3 km grid resolution to address the role of accurate air-sea fluxes on cloud-resolving simulations. The present study also finds the best microphysics scheme (Thompson scheme) applicable for both TC tracks, intensity and rainfall, from simulations conducted for six TCs and a tropical low-pressure convective system. However, there is further scope for detailed studies on microphysics sensitivity in the context of development of a large number of new cloud microphysics in WRF-ARW by analyzing the heating profiles associated with hydrometeor phase changes, fall speed and particle size distributions of frozen hydrometeors etc. The SST sensitivity experiments showed that even though SST has an impact in RI phase of cyclones it is not always a dominant factor for TC intensification as evident from the analysis of Amphan and Fani. The results of high SST anomaly and high wind-shear for Amphan and low SST anomaly and low wind-shear for Fani indicate SST influenced the RI phase only for Amphan whereas the wind-

shear played major role for Fani. These results suggest that in order to obtain more robust conclusions on the role of SST for RI further sensitivity studies have to be conducted with longer term climatological mean SST and for more cyclone samples including the post-monsoon cyclones that have undergone rapid intensification.

Chapter 1

Introduction

1.1. Tropical Cyclones

Tropical cyclones (TCs) are intense, rotational low-pressure warm-core extreme weather systems that form over the tropical oceans under favorable environmental conditions such as high sea surface temperature (SST), low atmospheric wind shear, existing incipient low pressure etc. (Gray, 1968). They are associated with strong wind, heavy rain and often with costal storm surges. Severe cyclones cause enormous damage to the life and infrastructure along coastal areas during their landfall and they are the most destructive of all the natural disasters. However, on the positive side, they provide essential rainfall over much of the lands they cross (Anthes, 1982). The typical near surface sustained wind speeds in TCs exceed 17 ms^{-1} (60 kmph, 32 knots). The severe TCs with maximum surface sustained wind speeds equal to or exceeding 33 ms^{-1} (120 kmph, 64 knots) are termed Hurricanes over the Atlantic Ocean, East Pacific Ocean and the Caribbean Sea; Typhoons over the West North Pacific Ocean; Willy-Willies in Australia; and TCs over the Indian Ocean.

Environmental conditions for TC development:

Using composites of observations of a large number of cyclones in the Pacific and Atlantic oceans Gray (1968; 1979) defined the following six favorable environmental conditions for cyclogenesis:

- Warm ocean waters with SST $\geq$ 26.5 C.
- Low-level cyclonic vorticity.

- Minimum Coriolis parameter (>10^{-5}/sec).
- Weak vertical shear of horizontal wind:
- High humidity in the lower and middle atmosphere.
- Large convective instability of the atmosphere ($\frac{\partial \theta}{\partial p}$).

1.1.1. TC formation and structure

An average life cycle of a TC is nine days and includes three stages; genesis, mature and decaying stages. During the genesis, warm ocean waters and high relative humidity facilitates condensation of water vapor into clouds, releases heat energy thereby inducing a drop in pressure which falls gradually. Atmospheric instability encourages formation of huge cumulus cloud convection with condensation of rising air over ocean. The mature stage consists of clouds which are well organized about a center of low pressure and a strong rotational circulation with a large axisymmetric component with the maximum intensification. In the decaying stage TC begins to weaken in terms of its central pressure and extreme winds as soon as its warm moist air supply is abruptly cut off either due to crossing the land or moving over cold water. The circulation weakens, expands in size and becomes asymmetric about the center (Anthes, 1982).

An understanding of the internal structure of TCs is developed from the analysis of the vast observations collected over Atlantic and Pacific regions with respect to temperature, height, moisture, wind and vertical motion (Frank, 1977; 1982). The main features of a TC include the eye, eyewall and the rainbands (Fig. 1.1). Low-level winds spiral cyclonically inward toward the low pressure, with the speed increasing nearer to the center and spiral out at the top in the reverse direction. In the very center of the storm, air sinks forming an “*eye*” that is more or less circular about a diameter of 5-50 km. It is a region of comparatively clear skies and a sudden drop in wind speed. The eye is developed only when the cyclone reaches its maturity. It is an area where the lowest pressure, highest temperatures and highest relative humidity of the storm are found. The air present at the outward edge of eye is dragged upward and outward by the surrounding air. As a result, the low pressure is accentuated and air is induced from above to sink into the eye that will results in the clear skies and high temperatures inside the eye.

The eye is surrounded by the "*eyewall*" which is a wall of cumulonimbus clouds. The eyewall consists of intense thunderstorms in continuous rings with violent vertical motion explosive cumulonimbus growth. Hence, most intense rainfall occurs in this region. There are two spiral bands away from the eyewall that are sometimes hundreds of kilometers long and a few kilometers wide, known as the "*rainbands*" or feederbands. They consist of many individual thunderstorms that produce heavy rainfall, cyclonically spiraling towards the center. The distance between the bands is about 50-80 km near the edge that decreases nearing the center / eye (Siddhartha, 2015).

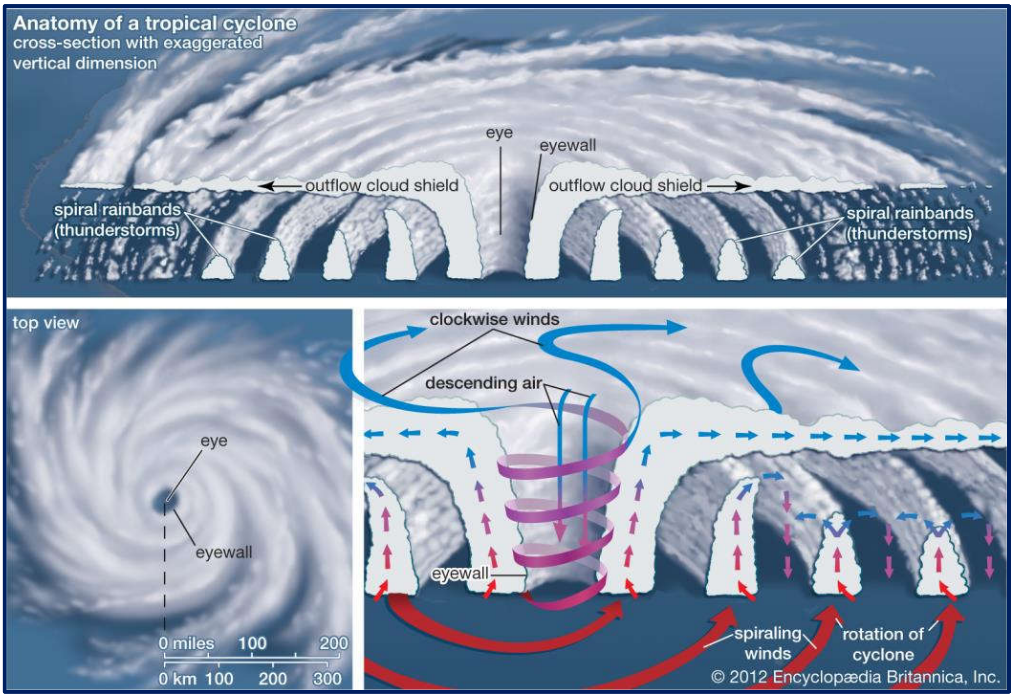

Figure 1.1. *Vertical cross section of a matured TC (adapted from Encyclopaedia Britannica).*

Wind structure:

The TC near-surface wind field is characterized by the rapidly rotating air around a center of circulation while also flowing inwards radially. The air begins to rotate cyclonically as radially flowing inward to conserve angular momentum. At the radius of the eyewall, air begins to ascend to the top of the troposphere. This radius is called the radius of maximum winds (RMW) where near-surface winds of the storm are the strongest. Once aloft, air flows away from the storm's center, producing a shield of cirrus clouds (outflow cloud shield in Fig. 1.1). Thus, wind speeds are low at the center, increase rapidly moving outwards to the RMW, and then decay more gradually with radius to large radii (Fig. 1.2). In the vertical, winds are strongest near the surface and decay with height within the troposphere.

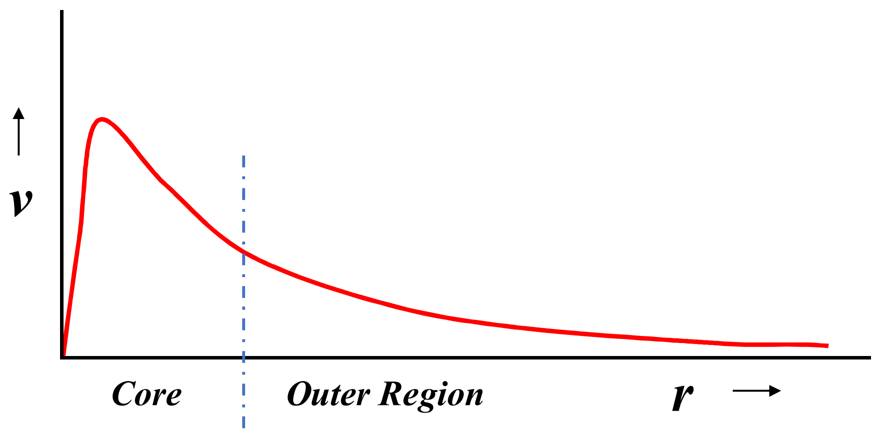

Figure 1.2. *Radial variation of winds in a TC.*

Inflow and outflow layers:

The TC consists of three vertical layers (Fig. 1.3). The lowest layer is the inflow layer that extends up to 3 km that drives the storm due to large momentum and energy transport. Water evaporated from the warm ocean surface subsequently condenses liberating latent heat. This potential energy is converted into kinetic energy in the form of motions that are essentially towards the low-pressure center resulting in convergence of winds at the surface. The middle layer extends from 3 km to 7 km where the main cyclonic circulation of the storm takes place. The airflow in this region is circular in form and not radial. The outflow layer is from 7 km upwards to the tropopause at about 12 km and above. It is a high-pressure region with anti-cyclonic air circulation with outward radial component and divergence of air. Generally, low-level air moves towards the low-pressure (convergence), moves through the chimney (vertical) and then moves out in the outflow (divergence). The air is recycled many times by updrafts and downdrafts before reaching the storm core. The outflow in the TC provides a channel that carries high equivalent-potential temperature air from the convective core region outward to the far environment, where the air is cooled by radiation (Wu and Emanuel, 1994). The study of the impacts of vertical diffusion on the structure and intensity of TCs by Goapalakrishnan et al. (2012) showed that stronger inflow not only increased the spin of the storm, but also resulted in enhanced equivalent potential temperature in the boundary layer, a stronger and warmer core, and, subsequently a stronger storm.

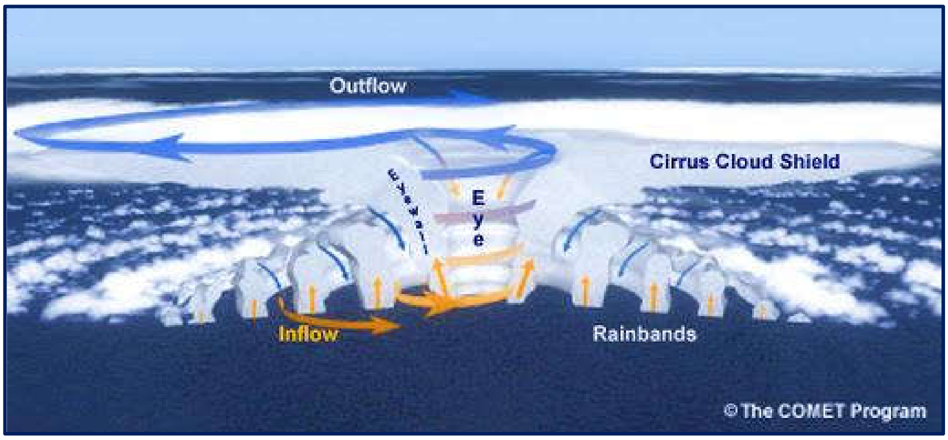

Figure 1.3. *Vertical layers (inflow, middle and outflow) of a TC (adapted from The COMET Program, UCAR).*

Warm core:

Warm oceans supply the energy to the atmosphere in the form of huge amounts of latent heat and sensible heat to a lesser degree. Under favorable atmospheric thermodynamic conditions, the convergence at low-level contribute to the intensification of a surface low-pressure into a cyclonic storm. The increasing surface wind speeds produce an increase of surface enthalpy flux by aerodynamic effect thereby acting as a feedback mechanism that promotes intensification. It is the warm core that maintains the low pressure at the center and thereby high-level outflow. The air within the eye comes from two different sources; (1) mixing and subsidence from surrounding cloud wall, and (2) subsidence through the troposphere through the break in tropopause. Thus, the air in the eye gets warmed adiabatically producing the anomalous warm core of the TC. The study on potential temperature budget analysis of an idealized TC by Stern and Zhang (2013), finds that, the maintenance of the warm core is highly dependent on the sub-grid scale horizontal diffusion of potential temperature. The region of TC from the center to 1° radius (~100 km) is the inner core and the region from 1° to 2.5° (~100 – 250 km) is the outer core.

1.1.2. TC dynamics

The mature TC consists of a horizontal quasi-symmetric circulation on which is superimposed a thermally-direct (warm air rising) vertical (transverse) circulation. These are referred to as primary and secondary circulations respectively, terms which were coined by Ooyama (1982). The combinations of these two component circulations results in a spiraling motion (Smith, 2006). The primary circulation arises due to the drop of pressure towards the storm center due to which, the Centrifugal and Coriolis forces act to move the parcel outwards and balance the pressure-gradient force assuming the friction to be absent. Such a balance of forces is known as the gradient wind balance as illustrated in Figure 1.4. Precisely, in the primary circulation the pressure-gradient force is balanced by the sum of centrifugal force and Coriolis force assuming the absence of friction.

$$\frac{1}{\rho}\frac{dp}{dr} = \frac{V^2}{r} + fV \tag{1.1}$$

where, r is the radius to the axis of rotation, V is the wind speed, f is the Coriolis parameter, p is the pressure and ρ is the density.

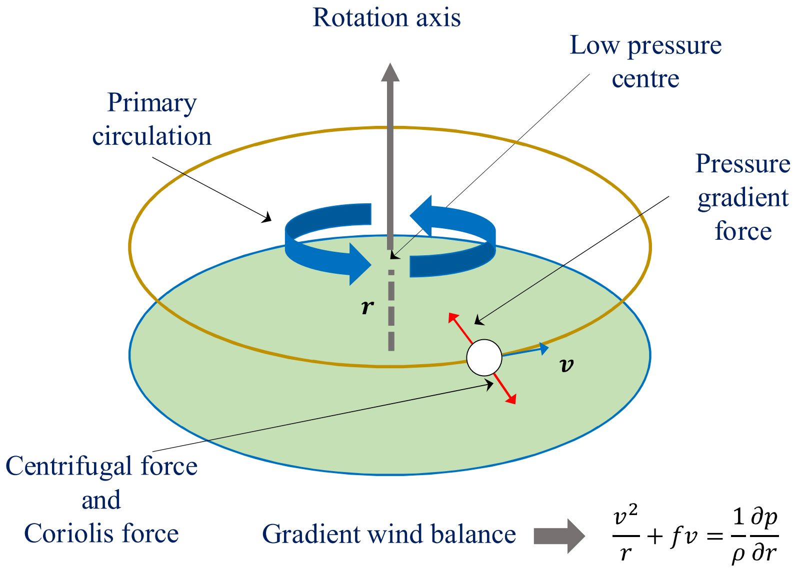

Figure 1.4. *The gradient wind balance and primary circulation in a TC (referred from Smith, 2006).*

However, surface friction exerts a strong influence on the TC dynamics. The secondary circulation is induced by friction by introducing a radial wind component, finally leading to the spiraling motion of the air parcels. Other than within the boundary layer, the flow modification by friction is also found in the higher regions. The friction now reduces the tangential wind which intern reduces the centrifugal and Coriolis forces (Fig. 1.5). As a result, the pressure-gradient force that was unchanged, is now larger than the sum of the two outward forces, and the parcel is drawn inwards towards the center. This will lead to a strong inflow close to the surface in the boundary layer. The primary rotating flow in a TC results from the conservation of angular momentum by the secondary circulation. The velocity of inflow and mass flux towards the center increase at large distances from the cyclone core with decreasing radius. At large radii, this mass flux is balanced through forced subsidence above the boundary layer. At smaller radii, air parcels are moved upward from the boundary layer into the vortex above due to effects of local buoyancy. This indicates that the rigid bottom boundary leads to convergence in lower levels and vertical motion in the vortex above the boundary layer, thereby inducing secondary circulation in the vortex above. The sea surface supply most of the energy to

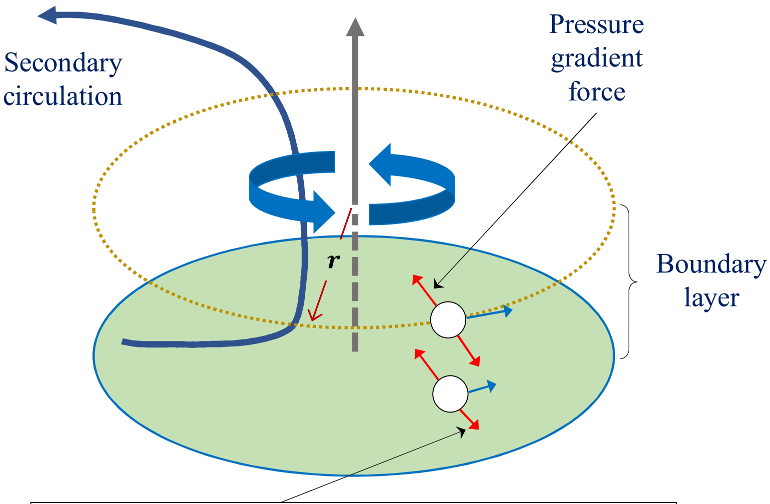

Figure 1.5. *Frictionally-induced convergence and secondary circulation in a TC (referred from Smith, 2006).*

the storm. The warm and highly moist air from the marine atmospheric boundary layer is transported up into the vortex above, through the strong up flow in the eyewall. Thus, the boundary layer is of utmost importance for both the dynamic and thermodynamic processes of a TC (Gopalakrishnan et al., 2016).

The energetics of a TC system is accounted on the secondary circulation and may be idealized as an atmospheric Carnot heat engine (Emanuel, 1986) (Fig. 1.6). The evaporation of water from the warm ocean surface cause the inflowing air near the surface to acquire heat (latent heat). Secondly, the warm air rises and cools within the eyewall while conserving the total heat content (adiabatic cooling). Further, air flows out and loses heat via infrared radiation to the space at the temperature of the cold tropopause. Finally, air subsides and warms at the outer edge of the storm while conserving total heat content. The first and third processes are nearly isothermal, while the second and fourth legs are nearly isentropic. So, the secondary circulation in Carnot perspective provides an upper bound on the maximum wind speed that a storm can attain.

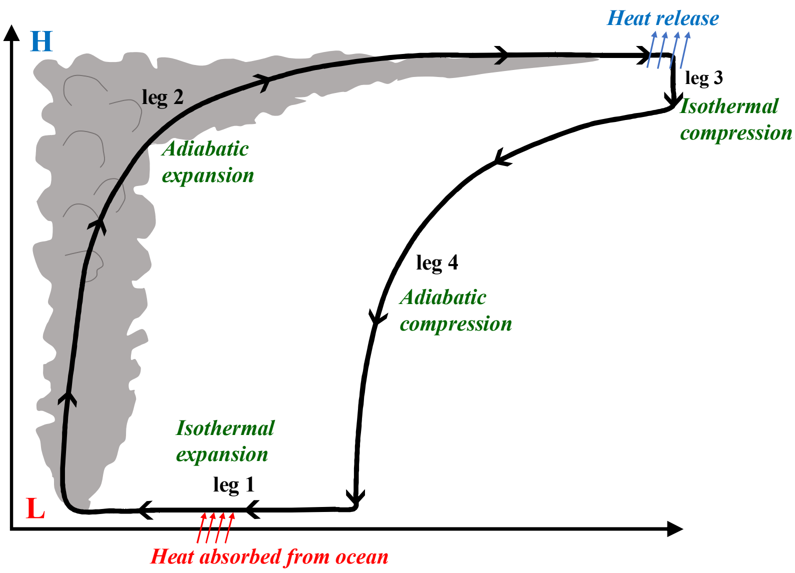

Figure 1.6. Schematic of *Carnot cycle in a matured TC (referred from The COMET Program, UCAR).*

1.1.3. Theories of TC formation

Two theories are evolved on the TC intensification process. The Conditional Instability of Second Kind (CISK) by Charney and Eliassen (1964) and the Cooperative intensification theory by Ooyama (1969) have independently suggested an axisymmetric balance for the cooperative interaction between moisture convergence in the lower atmosphere, heating produced by the convective clouds and the subsequent deepening of the cyclones.

In the CISK theory, the secondary circulation of an incipient large-scale vortex would organize the small-scale randomly distributed cumulus clouds into finite-size area near the center of the vortex. The convection thus organized would then act as a finite-size heat source at the vortex center and consequently intensify it. However, subsequent works contradicted the CISK instability as a genesis mechanism due to questions concerning its linear nature and reliance on inherent convective instability. In this, the role of surface friction and low-level convergence was highlighted in supporting the cyclone intensification. They essentially highlighted two aspects; (a) the main spin up of the vortex occurs via the convergence of angular momentum above the boundary layer, and (b) the boundary layer plays an important role in converging moisture to sustain deep convection, but its dynamical role opposes the spin up by the transfer of momentum between the atmosphere and the ocean. They emphasized on convection, i.e., heating due to cumulus is proportional to integrated moisture convergence mainly in the lower troposphere ignoring the importance of air-sea interactions (Gopalakrishnan et al., 2011).

The currently accepted theory for the source of this heating – and, by extension, the development of the TC warm core – is given by the non-linear Wind-Induced Surface Heat Exchange (WISHE) paradigm of Emanuel (1986) and subsequent works. In the presence of a pre-existing tropical disturbance over a sufficiently warm ocean surface, WISHE states that, the latent heat release in the free troposphere is governed by the evaporation of moisture from the underlying ocean surface as determined primarily by the magnitude of the surface winds. In other words, latent heat energy used to fuel the TC and build the TC warm core is obtained from the underlying surface and not through convective heating processes. The TC warm core is constructed aloft as updrafts, moist convection carries this latent heat energy from the boundary layer to the middle and upper troposphere (Smith, 2006).

1.1.4. TC movement

TCs generally tend to move westward and slowly drift poleward in both the Northern and Southern Hemispheres. The main steering forces are i) large scale winds and

ii) Coriolis force (Riehl, 1954). The tropical easterlies or the trade winds are responsible for the general westward movement of the TCs. The poleward movement is due to i) the presence of subtropical highs over the oceans and associated anticyclonic circulations whose western edges move toward the poles; (ii) the Coriolis force which becomes progressively stronger at higher latitudes. Since the diameter of the TC is large, the Coriolis force has a strong influence toward the poleward side, and hence, the TC is deflected toward the pole.

The movement of TCs is also modified by the horizontal vorticity gradient of the surrounding flow. Vorticity which represents a coupling of the dynamic and thermodynamic processes is an indicator of the movement of the TC (Chan, 2005). The accuracy of the prediction of TC movement is attributed to the accurate prediction of the TC and environment structures, as well as the convection (Chan, 2005). Earlier studies (Chan, 1984; Chan, 2005; Wu and Wang, 2000) have shown that the gradient towards the centre of positive potential vorticity tendency strongly coincides with the direction of the cyclone and so can be used as a tool for the prediction of the movement. A TC tends to move towards areas of maximum potential vorticity time tendency, which is contributed by both the convection and heating processes. Studies like Zheng et al. (2007) and Stern and Zhang, 2013 have also showed that the movement of TCs is highly sensitive to the vertical wind shear.

1.1.5. Classification of TC intensity

The intensity of TCs is specified by the speed of maximum sustained winds (wind speed at the radius of eyewall). The TC intensity scales over different regions are defined by the Regional Specialized Meteorological Centers (RSMCs) as per the characteristics of the cyclones in the respective regions. For TCs in the Atlantic, Eastern Pacific and Central Pacific basins, the intensity is classified based on the Saffir-Simpson Hurricane Scale

(SSHS) from the early 1970s. This scale ranks storms that have already reached hurricane strength. The SSHS was originally created using both wind speed and storm surge, but due to the lack of a well-defined relationship between wind speed and storm surge, the scale was changed to the Saffir-Simpson Hurricane Wind Scale (SSHWS) based on a one-minute maximum sustained wind speed at 10-meter height (Stull, 2015) by the US National Hurricane Center. The SSHWS is given below in Table 1.1.

Table 1.1. *The Saffir-Simpson Hurricane Wind Scale.*

Category	**Wind Speed**		
	ms^{-1}	***kmh^{-1}***	***knots***
1	33-42	119-153	64-82
2	43-49	154-177	83-95
3	50-58	178-209	96-113
4	59-69	210-249	114 - 135
5	>69	>249	>135

The TCs belonging to category 1 cause very dangerous winds with some damage and category 2 will cause extensive damage with extremely dangerous winds. Devastating damage will occur due to category 3 TCs, whereas category 4 and 5 TCs produce catastrophic damage. TCs over North Indian Ocean are monitored by Regional Specialized Meteorological Centre (RSMC), New Delhi, India Meteorological Department (IMD).

1.1.6. TC climatology

The regions of TC development are typically grouped into 7 basins. The intensity and frequency of occurrence of TCs vary over different basins. The annual frequency and season of development of TCs in different basis are provided in Table 1.2. Based on the start of reliable global best track data, about 84 TCs form around the globe each year (Ramsay, 2017). During the 25-year period from 1990-2014 an average annual number of

79 TCs occurred with a standard deviation of about seven, with the most active years being 1992, 2005, and 2013-when 90 TCs formed-while the most inactive years were 1999 (65 TCs) and 2010 (69 TCs) (Maue, 2011). Out of 70% of global total in the Northern Hemisphere, almost one third (31%) develop and track over the warm waters of the Western North Pacific, 19.5% over Eastern North Pacific, 11.5% over Northern Atlantic basins and 6.5% develop over North Indian basin. Out of 30% of cyclones forming over the Southern Hemisphere, 11% develop in the South Indian basin, 12% in the Australian region and 7% in the South Pacific basin (Ramsay, 2017).

Table 1.2. *Global basins, annual frequency and season of development of TCs.*

Basin	Annual Frequency	Season of Occurrence
North Atlantic	12	June - November
Eastern North Pacific	16	May - November
Western North Pacific	24	Throughout the year, August – September (peak)
North Indian Ocean	6	April – June, October - December
South Indian Ocean	9	November - April
South Pacific	6	November - April
Australian region	9	November – April

1.1.7. Damage due to TC

The damage or destruction caused by the TCs are mainly by strong winds and associated rainfall and occasional storm surges which cause inundation. Over recent years, the loss of lives from TCs has significantly decreased especially in the developed countries due to improvement in TC forecasting and warning system. Nevertheless, there is a substantial increase in infrastructure and property loss which is attributed to a high concentration of population and development activity in coastal plains and low-lying areas that are subject to flooding and storm surges. The area of TCs destruction varies from about 25 km in small systems to 500 km or more in large systems (Burton and Burton, 1999).

Strong winds from cyclones can disrupt communication networks, power lines and satellite communication dishes. Besides they damage the roads by wrecking trees and other installations. Strong rotational winds can uproot trees, lift off the roof of thatched and wooden houses and buildings. The winds largely determine the other agents directly or indirectly. They also carry debris of all sizes and turning them to deadly flying projectiles, resulting in economic damage and population of a region. The distribution of winds is hardly symmetrical; low-level winds are typically more intense on the right (left) side of the cyclone with respect to its displacement in the northern (southern) hemisphere, but are extremely variable in both time and space. However, it is not the maximum sustained winds that is accountable for wind damage, but rather variations in intensity and direction which that weaken the structures. These features include maximum wind speed in gusts, duration of high sustained wind speeds, which can subject different elements of a structure with cumulative effects. The variability of intensity and direction increases inland as topography generates small-scale (a few kilometres) but more intense circulations.

Rainfall associated with TCs results in heavy flooding, landslides, disrupts power and electric systems and also caused damage to infrastructures due to inundation. Rainfall due to TCs is also beneficial as it contributes to the water needs of specific regions. If the TC sustains for longer after landfall, torrential rains will develop and successive outbreaks of heavy rain over the same area cause flooding. Floods from TC are dependent on, the rate of precipitation, physical characteristics of the drainage basin such as the soil type and vegetation and eventually the size and speed of the system. A storm surge is an abnormal rise in water due to a cyclone which is an oceanic event responding to meteorological and other driving forces. The important factors in determining the storm surge heights is the maximum wind speed which in turn is closely related to the minimum sea-level pressure, the size and speed of motion of the TC, the topography of the landfall point and the astronomical tides. The low-lying terrain coasts are drastically damaged by surges due to high degree of inland inundation. The surge may penetrate as much as 15 to 30 km inland for a typical landfalling storm. The impacts of storm surges include coastal flooding, beach erosion and the removal of beach materials. Also, the waves that accompany the storm surges may reshape the coastal areas and lead to damage of structures (Burton and Burton, 1999).

1.2. TCs over North Indian Ocean

North Indian Ocean (NIO) is one of the major TC basins where highly intense cyclones develop. The TCs in NIO are highly variable in movement and intensification (Raghavan and Sen Sharma, 2000). The sub-basins include the Bay of Bengal (BOB) and Arabian Sea (AS). The RSMC, New Delhi provides the TC Advisories and TC Weather Outlooks for the benefit of countries bordering the BOB and AS, namely Bangladesh, Myanmar, Oman, Pakistan, Sri Lanka and Thailand. The average annual frequency of TCs in the NIO is about 5 (5-6% of the Global annual average) and in the globe is about 80. The cyclonic disturbances are 5 to 6 times more frequent over the BOB than the AS, the ratio of frequency being 4:1, probably due to the relatively colder SSTs in the AS which inhibits the formation and intensification of the system (FAQ on TCs, IMD). The average annual frequency of TCs is about 5 in the BOB and 1 in the AS (Rao et al., 2001). Moreover, the passage of westward moving remnants of typhoons over northwest Pacific moving across South China Sea to Indian Seas, also helps in more cyclogenesis over the

NIO region. The presence of Inter Tropical Convergence Zone (ITCZ) near the Equatorial region of the BOB due to the advancement or retreat of Monsoon (Southwest or Northeast) during these periods favours the intensification of low-level cyclogenesis to a cyclone. The cyclones over AS either originate insitu over southeast AS or develop from remnants of cyclones from the BOB that move across south peninsula. Since most of the cyclones over the BOB weaken after landfall, migration to AS and further development is less frequent.

The frequencies of Indian Ocean TCs show a bi-modal maximum peaking once from mid-April to mid-June and again from October to mid-December (FAQ on TCs, IMD). The cyclonic storms in the NIO occur in two seasons i.e., pre-monsoon (March-April-May) and post-monsoon (October-November-December) with a higher frequency in October-November period. During the Southwest Monson season (June-September), intense systems usually do not develop due to the northward shift of ITCZ over the land and due to the presence of high vertical wind shear during monsoon resulting from strong westerly winds in the lower troposphere (below 5 km) and strong easterly winds in the upper troposphere (above 9 km). The months of May-June and October-November are known to produce cyclones of severe intensity. It has also been recognized that the lower tropospheric westward travelling disturbances known as the Easterly waves prevailing during October to April period, often serve as the seedling circulations of large proportion of TCs over NIO.

Out of 5-6 TCs forming every year in NIO, 2-3 becomes severe cyclones (FAQ on TCs, IMD). The average life period of a TC over the NIO is 5-6 days. It will have a hurricane intensity (33 m/s) for 2-4 days as against 6 days of global average. The size of a TC over Indian Ocean varies from 50-100 km radius to 2000 km with an average of 300-600 km. IMD, India uses satellite imagery-based pattern recognition techniques (Dvorak, 1975) to determine intensity of cyclones. Intensity can be derived as the near-surface maximum wind speed around the eyewall, or as the minimum surface pressure at the TC pressure centre. IMD uses a 3-minutes averaging for the sustained wind observed at the standard meteorological height of 10 m, whereas, the National Hurricane Centre (NHC) uses a 1-minute averaging time. However, there is no significant difference between the maximum sustained winds reported in different basis with different averaging method. The largest rainfalls associated with TCs over NIO were 50-60 cm per day, with an average of 35-40 cm for a typical cyclonic storm.

The low-pressure systems over Indian region are classified based on the maximum sustained winds speed associated with the system and the pressure deficit / number of closed isobars associated with the system. The detailed intensity classification defined by RSMC, New Delhi based on pressure deficit and maximum sustained winds is shown in Table 1.3.

Table 1.3. *Intensity classification of TCs over NIO by IMD.*

System	**Pressure deficit (hPa)**	**Associated wind speed (kmph/knots)**
Low pressure (L)	1.0	< 31 / < 17
Depression (D)	1.0 - 3.0	31 - 49 / 17 - 27
Deep Depression (DD)	3.0 - 4.5	50 - 61 / 28 - 33
Cyclonic Storm (CS)	6.1 - 10.0	62 - 88 / 34 - 47
Severe Cyclonic Storm (SCS)	15.0	89 - 117 / 48 - 63
Very Severe Cyclonic Storm (VSCS)	20.9 - 29.4	118 - 166 / 64 - 89
Extremely Severe Cyclonic Storm (ESCS)	40.2 - 65.6	167 - 221 / 90 - 119
Super Cyclonic Storm (SuCS)	≥ 80.0	≥ 222 / ≥ 120
1 knot = 1.85 kmph (kilometre per hour)		

1.3. Methods of TC forecasting

One of the challenges faced by weather forecasting agencies is to predict the movement and intensity of TCs during their life cycle. The movement is governed by the non-linear dynamics involving various scales of motion like large scale flow and the storm scale circulations. The intensity predictions are even more challenging given the limitation of observations and limited understanding of the complex interactions between the large scale and storm inner core processes. Various techniques such as i) climatological, ii) synoptic, iii) satellite techniques and iv) dynamical models are used to predict the TC movement (track) and intensity parameters required in disaster management. In the persistence method the future motion is extrapolated from the past motion assuming that the cyclone, the surrounding large-scale flow and the interaction processes remain unaltered. This technique gives reasonable forecasts up to 24 hours. The climatological method is based on the analogy of the movement of present storm to that of past storms of similar average speed and direction near that location. This method is effective only at longer forecast durations. In the Climatology and Persistence method (Sikka and Suryanarayana, 1972) persistence is given weight in the early stages and climatology for periods extending over 36 hours or more. The empirical methods based on steering current concept assume that the TCs tend to move with the speed and direction of the deep layer environmental flow (Srinivasan and Ramamurthy, 1973; Holland, 1984; Mandal, 1991). In the absence of conventional observations satellite remote sensing provides real-time estimates of the size and intensity of TCs over the Oceans. Dvorak (1975) has devised a method to assess the intensity of TCs based on satellite imagery. This technique involves satellite image analysis for various cloud features such as moisture, cloud pattern, their time changes to estimate the cyclone intensity and its evolution. A modified version of this technique called digital Dvorak technique (Velden et al., 2006) has been presently used by various weather forecasting agencies including IMD.

The dynamical atmospheric models solve the non-linear partial differential equations representing the atmospheric motion using appropriate numerical methods for the prediction of the future state. The initial state at various grid points in the model are specified from meteorological analysis generated by the Weather Forecasting Centers (Kalnay, 2003). Numerical models based on fundamental dynamics and physical processes provide an objective basis for advance forecasting of TCs. Simulation of cyclones using numerical models is highly dependent on accurate initial conditions, representation of initial vortex and the physical processes. Since physical processes such as ocean-atmospheric energy exchange, turbulent diffusion in the planetary boundary layer, clouds and convection play an important role in the intensification of TCs, they need to be realistically accounted in models.

1.4. Numerical modelling of TCs

Numerical models provide an objective and deterministic method for forecasting the TCs. However, their predictions are limited by the certain constraints of poor initial conditions and representation of the dynamical and physical processes. The region of high winds defining the cyclone vortex is relatively small compared to the synoptic scale motions. These small-scale features of the cyclone are not adequately represented in the meteorological analysis due to insufficient observations over the ocean areas where cyclones form. With this observational limitation the initial state is not well defined even in high resolution models. Secondly the understanding about the convective motions and cloud scale physical processes in the core of the TC and their interaction with the largescale environment is still evolving. Some of these issues are partly addressed with development of nested grid high resolution models, data assimilation techniques, advanced physics parameterization schemes and advent of high performance computing systems (Singh et al., 2016). There has been a steady improvement in the ability to numerical models to forecast the TC tracks due to increased model resolution, improved physics parameterizations, increased coverage of high-quality satellite observations and data assimilation techniques (Leslie et al., 1998; Houze et al., 2007; Miyoshi et al., 2010; Rogers et al., 2006; Rappaport et al., 2009; Goerss, 2000, Franklin et al., 2003). However, the problem of TC intensity forecasting continues to challenge both weather forecasters and researchers (Montgomery and Smith, 2012; Wada, 2007). Large variability of TC intensity and structure in numerical prediction systems arises from imperfect initial conditions, model physics parameterizations (radiation, convection, microphysics, planetary boundary layer), model resolutions, numerical discretization and approximation to the continuous equations and limits of predictability (Hendricks and Peng, 2012).

1.4.1. Early modelling studies

Initially in the history of TC modelling studies axi-symmetric models were rigorously used to understand various physical and dynamical processes in the TC development. A 19-level axi-symmetric model was used by Kasahara (1961) to study the role of latent heat of condensation in the intense circulation. Charney and Eliassan (1964) using an axi-symmetric model studied the interaction between the cumulus scale and cyclone scale motion. Rosenthal (1964) used a hydrostatic axi-symmetric model to study the role of friction in TCs. It was shown the TC development was very rapid and the meridional circulations were intense when friction was not included and deepening of the system was noticed when friction was included. Kuo (1965) studied the vertical distribution of convective heating through a cumulus parameterization scheme in which the heating is related to the temperature difference between the clouds and their environments. Yamasaki (1968) using a primitive equation axi-symmetric model found that the development of tropical cyclone is directly dependent on the increase of specific humidity and surface drag coefficient. Modelling studies by Ooyama (1969) revealed that the increase of drag coefficient leads to more frictional convergence in the boundary layer and increases the intensification of the cyclone. Rosenthal (1970) found an improvement in the storm structure by increasing the radial resolution from 20 km to 10 km in a primitive-equation axi-symmetric model. During 1971 Anthes et al. (1971 a, b) developed an axi-symmetric model in isentropic coordinates, wherein the mass and momentum equations are integrated by using a constant specific heating function until the inner region of the cyclone reached a steady state. Rotunno and Emanuel (1987) using a time-dependent nonhydrostatic 2-d numerical model studied the role of interaction between ocean and cyclone and showed that a hurricane-like vortex may amplify in an atmosphere which is neutral to cumulus convection. It was shown that the vortex attains intensification as a result of thermodynamic interaction between vortex and ocean and emphasized the crucial role of boundary-layer processes in controlling the structure and evolution of the vortex.

During the 1980s three-dimensional models were developed and extensively used for TC studies. Using a regional model, Tuleya (1988, 1991) found significant changes in the structure, vorticity and equivalent potential temperature tendencies of the storms for initial moisture, surface temperature and surface evaporation. Tuleya (1991) studied the sensitivity of surface boundary conditions on TC development using a nested grid Geophysical Fluid Dynamics Laboratory (GFDL) tropical cyclone model. It was shown that reducing the ocean surface temperature has resulted in weaker storm.

It is possible to simulate TCs with high resolution like 1 km (Montgomery and Smith, 2012) which can better resolve various physical processes like convection, microphysics, turbulent diffusion etc. Several studies have investigated the impact of horizontal grid resolution, cumulus convection, microphysics and planetary boundary layer (PBL) forcing on TC predictions.

1.4.2. Studies using 3-D mesoscale models

Advanced high-resolution mesoscale models such as MM5 (Anthes et al., 1987) and WRF (Skamarock et al., 2008) are developed in the last two decades for improving weather prediction. Studies employing high resolution mesoscale models (Marks and Shay, 1998; Wang, 2001; Braun et al., 2006; Davis et al 2008 among others) show better prediction of the intensity of the system due to better resolving the inner-core dynamics, asymmetric effects and interaction with the environment. The high-resolution numerical models with horizontal grid spacing as small as about 1 km (Montgomery and Smith, 2012) can better resolve various physical processes like convection, microphysics, turbulent diffusion etc. and lead to improvements in predictions. Several studies have investigated the impact of horizontal grid resolution, cumulus convection, microphysics and planetary boundary layer forcing on TC predictions.

1.4.2.1. Studies on impact of horizontal resolution and convection physics

TCs owe their existence to release of latent heat resulting from intense convection. This convection depends on eddy transfers of heat, moisture and momentum at the sea surface and radiative effects, as well as on the TC circulation itself (Anthes, 1982). The intensity is largely determined by the inner core dynamics and its modulation by the large-scale environment (Marks and Shay, 1998; Holland, 1997; Emanuel, 1999). Deep moist convection with hot buoyant plumes (towers) plays a vital role in the internal dynamics (Krishnamurti et al., 2005; Fang and Zhang, 2010, 2011). Apart from that, the horizontal grid resolution of the model and boundary layer forcing such as SST, also impacts the forecasting of TCs. Cloud physical processes play an important role in tropical weather systems through production and distribution of heat, mass and momentum in the atmosphere via precipitation, winds and turbulence (Wang et al., 2009). Thus, application of high-resolution models with proper convection physics may be required for resolving the moist convection for better prediction of TCs. Convection in numerical models is formulated through implicit convective (cumulus) parameterization (CP) schemes and explicit cloud microphysics (CMP) schemes. While CP represents the effects of sub-grid scale convective processes on the grid scale variables and removes the convective instability (Molinari and Dudek, 1992), microphysics schemes explicitly treat the small-scale physical processes governing the cloud formation, growth, and dissipation that play important role in the evolution and development of moist convection (Stensrud, 2007). These schemes produce different vertical profiles of heating and moistening in the atmosphere due to simulating different spatial and temporal precipitation distribution.

Davis et al. (2008) on the prediction of Atlantic hurricanes using Advanced Hurricane ARW model have shown that application of 4-km resolution with explicit convection slightly improved the track forecasts over 12-km grid using parameterized convection. They suggested that the application of high resolution enabled to obtain a better structure representation of could bands and thereby improved simulation of the inner core structure of the storms. Gentry and Lackman (2010) reported the sensitivity of WRF simulations of Hurricane Ivan (2004) to changes in horizontal resolution. It was found that as the grid spacing is reduced from 8 km to 1 km, the intensity of the system increased and most apparent changes in structure and other characteristics occurred near a grid length of 4 km due to better simulation of vertical motions in the eyewall region. The Weather Research and Forecasting (WRF) model has been widely used for operational TC predictions (Roy Bhowmik, 2013) as well as research on TCs over the NIO (Mukhopadhyay et al., 2011; Raju et al., 2011; Singh et al., 2011; Singh et al., 2012; Osuri et al., 2012; Osuri et al., 2013; Srinivas et al., 2013; Mohandas and Ashrit, 2014; Singh and Bhaskaran, 2019 among others). Srinivas et al. (2013) evaluated the performance of double-nested WRF model for a large number of TCs over the NIO with 65 physics sensitivity tests. It has been shown that Kain Fritsch cumulus convection, Yonsei University PBL, Lin or WSM6 microphysics and Noah land surface parameterizations provide best results for TC predictions. Their simulations for 21 TCs during 2001-2011 using parameterized convection in 9-km grid inferred that the model overestimated the intensity with mean errors ranging from -2 to 15 hPa for central pressure, 1 to 22 m/s for winds and 170-250 km in track errors corresponding to 24 to 72 h predictions. Osuri et al. (2013) evaluated WRF for 17 cyclone cases over NIO during 2007–2011 with different horizontal resolutions and it was shown that the prediction at 9 km resolution was more accurate than 27 and 18 km resolutions. Singh and Bhaskaran (2019) evaluated the performance of data assimilative double nested WRF for TCs over the Bay of Bengal during 2013. They suggested that the warm core structure of the TCs was better resolved at 9 km resolution. Mukhopadhyay et al. (2011) studied the sensitivity of simulation of intensity and track for Sidr and Gonu cyclones with triple nested WRF. It was suggested that the 10-km grid (2nd inner domain) with parameterized convection produced a better simulation of TC track and intensity. Further, it was shown that simulations with only explicit CMP at fine resolution of 3.3 km (3rd inner domain) did not yield improved results as it could not properly represent the middle level heating rate in the cyclone core.

The results of high horizontal resolution (≤ 3 km) studies are also related to the convection physics as convection is explicitly resolved with microphysics in these simulations. A few studies (Wang, 2001; Wang, 2002; Deshpande et al., 2010) have found that the track predictions are more sensitive to cumulus physics whereas the intensity predictions are more sensitive to the microphysics. Li and Pu (2006) studied the intensity prediction of hurricane Emily using high resolution (3 to 1 km) WRF with explicit convection schemes. It was suggested that the 1-km grid resolution shows a slight improvement in Emily's intensity forecast over the 3-km grid due to better representing the eyewall convective heating distribution, latent heat flux and high equivalent potential temperature feeding from the ocean surface. Fierro et al. (2009) studied the impact of horizontal grid spacing (1 to 5 km) on the simulation of microphysical, kinematic structure and intensity characteristics of Hurricane Rita (2005). It was shown that despite structural differences (volume, areal coverage, eyewall asymmetry etc.) all the simulations produced nearly similar intensity as the features in high resolution simulations that tend to weaken the TC (smaller area of high surface fluxes and weaker total updraft mass flux), compensate for features that favor TC intensity (smaller amplitude eyewall asymmetries and larger radial gradients). Gopalakrishnan et al. (2012) studied the impact of horizontal resolution (9 km, 3 km) in HWRF on the Atlantic TCs during 2005-2009. It was shown that the 3-km grid with explicit convection provides better results over the 9-km grid using parameterized convection for track, intensity as well as structure forecasts due to stronger inflow and consequently stronger moisture transport. Biswas et al. (2014) using triple nested HWRF model showed that the TC track and intensity predictions even from inner 3-km nest using explicit CMP are highly sensitive to the cumulus schemes in the outer domain due to their effect on the storm environment.

Chutia et al. (2019) on the simulation of MORA (2017) over the Bay of Bengal using WRF, have shown that cyclone track as well as other parameters related to the TC are sensitive to model horizontal resolution and predictions improved in 4-km simulations using microphysics over 9-km runs with parameterized convection. A few studies (Deshpande et al., 2012; Nasrollahi et al., 2012) showed that at even at higher grid resolution (<10 km) the cumulus physics has some impact on the track, distribution of rain and intensity of the storm. The study of Sandeep et al. (2018) on the impact of cloud physics parameterization schemes on the simulation of Vardah cyclone using triple nested WRF model indicated that 3-km grid using explicit microphysics slightly improved the track and intensity over the 9-km grid with parameterized convection.

1.4.2.2. Microphysics parameterization sensitivity studies

Much progress has been made in understanding and parameterizing cloud microphysics processes in the last decades (Seifert, 2011). Many studies have shown that more sophistication in microphysics parameterization can reduce model errors and outperform simpler CP. Lin et al. (1983) in their study to simulate a moderate intensity thunderstorm showed that the inclusion of snow improved the realism of the results when compared to the model without snow. These studies reveal that the choice of microphysics in numerical models becomes a critical factor in simulating deep convective processes in the absence of CP. The microphysics schemes in numerical models vary according to the complexity and are classified as diagnostic (effects of condensation, evaporation of falling precipitation), bulk (treatment of hydrometeors with size distribution) and bin physics (particle distribution). In the simulation of tropical convection microphysical processes are commonly parameterized using the bulk method with the following hydrometeors: cloud water, rain water, cloud ice, snow and graupel/hail (McCumber et al., 1991).

Several studies have investigated the evolution of convection and effect of cloud microphysics on TCs (Zhang et al., 2019; Mooney et al., 2019; Li et al., 2019; Parker et al., 2017; Makarieva et al., 2017; Khain et al., 2016; Maw and Min, 2017; Zhang and Sippel, 2008). Wang et al. (2001, 2002) tested the sensitivity of TC structure, intensification and intensity to the choice and details of cloud microphysics parameterization in a Triply Nested Movable Mesh Primitive Equation Model, TCM3. They found considerable differences in the simulated stratiform clouds and the associated downdrafts outside the eyewall of the TC and the intensification rate. However, their study indicated that the final intensity of the TC is not very sensitive to the cloud microphysics parameterizations. Deshpande et al. (2010) in their simulation study of super cyclone Gonu showed that explicit moisture schemes produce profound impact on the cyclone intensity and moderate impact on the cyclone track forecasts. Miglietta et al. (2015) reported similar results for a Mediterranean tropical-like cyclone. The simulation study of TC Nargis by Raju et al. (2011) showed that the cumulus convection controls the cyclone intensity while microphysics parameterization influences the track prediction. But recent studies show that explicit convection schemes produce considerable impact on TC tracks and intensities (Deshpande et al., 2012; Taraphdar et al., 2014) and the intensity is well predicted when no cumulus parameterization was used in the highest resolution domain. The recent study by Saikumar and Ramashri (2017) showed that the latent heat released in the clouds plays a very important role in intensifying or strengthening of TCs and this release is mainly dependent on the cloud microphysical and dynamical properties. Maw and Min (2017) found that the Lin scheme better predicted the TC intensity which is due to the better representation of melting and evaporation processes from frozen hydrometeors, and the large number of liquid hydrometeors improved the latent heat released in the storm which in turn improved the intensity simulation of the storm. In a numerical modelling study of hurricane Irene Khain et al. (2016) showed that the predictions of minimum pressure and maximum wind speed are highly sensitive to different bulk microphysics schemes. For the real-time prediction of TCs over NIO, the operational forecasting centers in India are presently using WRF with cloud resolving grid configuration (27, 9 and 3-km). Though many modelling studies were conducted to study the sensitivity of TC predictions to cloud microphysics, since they were limited to single cases the uncertainty of their application for operational predictions is not clearly addressed.

1.4.2.3. Studies on the role of SST boundary forcing

An important aspect of TC intensification through environmental interaction is the interaction between the ocean and the storm. Among various parameters, the Sea Surface Temperature (SST) influence the genesis, intensification and track characteristics of TCs (Gray, 1978; Nicholls, 1984; Bender et al., 1993; Chan et al., 2001) by controlling the air-sea fluxes of evaporation and the sensible heat. Several studies showed that warmer SST facilitates TC intensification (Hong et al., 2000; Shay et al., 2000; Bright et al., 2002), whereas negative SST anomalies associated with cold-core eddies or TC-induced cold wake would weaken the TCs (Bao et al., 2000; Bender and Ginis, 2000; Bender et al., 2007; Emanuel et al., 2004; Lin et al., 2005). SST has been shown to promote rapid intensification (RI) of TCs.

The RI of TC is largely determined by the thermal profile of the upper ocean, where the intensity increases with an increase in SST. An increase in SST leads to evaporation of moisture from the ocean surface resulting in latent heat increase that is utilized further to drive the circulation (Singh et al., 2016). There a large number of studies that concentrates on the RI of cyclones related to the convective characteristics, SST, vertical wind shear, TC heat potential etc. (Wada, 2009; Chen at al., 2011; Sun et al., 2013; Tao and Zhang, 2014; Wang et al., 2015; Kanada et al., 2017; Chen et al., 2018; Rai et al., 2019; Xu and Wang, 2018; Potter et al., 2019; Chih and Wu, 2019). The study of Wada, 2009 showed that a high initial SST accelerates the RI process. Similar results are reported by Lin et al. (2009) where the pre-existing warm ocean anomaly in the BOB lead to the RI of TC Nargis. In study of Tao and Zhang, 2014, they showed that SST contributes to the intensification, while the development of TC is largely dependent on the magnitude of vertical wind shear and diabatic heating. The study by Foltz and Balaguru, 2016 found that exceptionally warmer SSTs and deeper than normal thermocline driven by prolonged El

Niño conditions aided Hurricane Patricia's RI. Another study on SST impact on RI of Typhoon Megi (Kanada et al., 2017) showed that the RI took place by modulating the radial structure of core convection, when high SST appeared in the eye region. Recently Zhang et al., 2020 showed that SST as well as its radial gradient play an important role in the evolution of TC. Also, several studies have tested the influence of SST forcing on genesis, track and intensity of TCs. Nicholls, 1984 in his study of the interannual fluctuations in Australian TC activity based on the southern oscillation and SST suggests that, SST may be directly influencing cyclone generation with more cyclones generated when the SST is warmer than normal due to the strongest predictive relationship of SST anomalies and cyclone numbers found. The study also shows that rather than the SSTs itself, it may be the SST anomalies which directly influence the frequency of cyclone generation. The study of Steenhof and Gough (2008) on Atlantic TC activity also showed that the increase in SST could result in increased Atlantic basin hurricane activity.

Some studies (Evans, 1993; Demaria and Kaplan, 1994; Whitney and Hobgood, 1997; Vecchi and Soden, 2007; Kotal et al., 2009) have shown that SST alone is not an adequate predictor of TC intensity. Evans (1993) studied the relative importance of SST in TC intensification by examining the historical data record in a number of ocean basins. It was shown that while SST may well provide and upper bound on tropical storm intensity, above a minimum SST threshold, SST does not seem to be the overriding factor in determining either the instantaneous storm intensity or the actual maximum intensity attained by the storm. Vecchi and Soden (2007) studied the relationship between SST and TC potential intensity using various climate models and observational reconstructions. They found that the long-term changes in potential intensity are closely related to the regional structure of warming, but, the changes in local SST are not adequate for characterizing even the sign of changes in potential intensity. Similar study by Kotal et al.

(2009) also showed that SST alone is not a dominant factor for TC intensification. Similarly, Ralph and Gough (2009) in analyzing the influence of SST on TC activity over eastern north Pacific also found that increasing trends of SST are not accompanied by increasing trends in TC activity.

Mandal et al. (2007) using satellite observed SST data on Orissa super cyclone (1999) over the NIO has shown that SST has significant impact on the simulated storm track and intensity. Dailey et al. (2009) in their study on the relation between Atlantic SST and U.S hurricane landfall risk, found that the pattern on TC genesis shifts with warmer SSTs greatly influence the regional landfall. A study on tropical cyclone rainfall rates by Lin at al. (2015) has shown that TC rainfall area is controlled primarily by its environmental SST relative to the tropical mean SST. Srinivas et al. (2017) studied the impact of SST on the movement and intensity of TCs by performing numerical simulations altering the SST variable. The results showed that the experiments with increased SST produced higher intensity estimates close to the observations through changes in the transport of heat and moisture to the TC.

1.5. Objectives of the present study

The preceding review of TC modeling studies shows that increased model resolution in general produced better intensity and track predictions. However, unlike the Atlantic and Pacific Ocean regions only few studies using cloud-resolving grids with explicit convection exist for the TCs over NIO region. Most of the high resolution modeling studies over NIO were limited to1 or 2 cases and at grid-sizes of ≥ 5 km not clearly inferring statistically the extent of improvement by high resolution using explicit convection for their implications in operational forecasting. Similarly, most of the microphysics sensitivity studies (Mukhopadhyay et al., 2011; Choudhury and Das, 2017; Raju et al., 2011; Saikumar and Ramashri, 2017) on the NIO TCs are limited to 1 or 2 cyclones and with limited number of microphysics schemes not leading to definite conclusions for practical implications in operational forecasting. As many numbers of microphysics schemes are developed in advanced numerical models like WRF, their sensitivity on TC predictions needs to be studied. Also, most of the studies on the role of SST boundary forcing on TC intensity as well as rapid intensification were conducted for systems over Atlantic and Pacific oceans and very few studies exist for TCs over the NIO. The role of SST on the rapidly intensified cyclones remains to be studied over the NIO. With this gap, the current study is aimed at performing TC simulations over the BOB region of NIO using a high-resolution mesoscale model by conducting the following analysis:

- To examine the impact of horizontal resolution and convection physics on the intensity and track predictions for tropical cyclones over the BOB of NIO with respect to two horizontal grid resolutions i.e., 9km grid using parameterized convection and 3km grid using explicit microphysics.
- To study the sensitivity of cloud-resolving scale predictions of Tropical cyclones with WRF to various microphysics parameterizations considering six TCs over NIO.
- To examine the role of SST on rapid intensification of cyclones by conducting numerical simulations with various satellite derived SST data.

Chapter 2

Model, Data and Case studies

2.1. Brief description of the Numerical Atmospheric Model

The Advanced Research Weather Research and Forecasting (ARW) atmospheric model is used in this thesis work for simulation of the TCs. ARW is a community numerical weather prediction system designed for both atmospheric research and operational forecasting applications by National Center for Atmospheric Research (NCAR) in collaboration with universities and other government agencies in the US and collaborating laboratories in other countries. Advanced Research WRF is a fully compressible non-hydrostatic Euler model with an available run-time hydrostatic option. The time integration uses a 2nd- or 3rd-order Runge-Kutta scheme with a smaller time step for acoustic and gravity-wave modes. The model uses Arakawa C-grid staggering and 2nd- to 6th-order advection options in horizontal and vertical for spatial discretization. The model has a large bundle of parameterization schemes for sub-grid scale physical processes developed by research community (Skamarock et al., 2008). The various components of the model system are described below.

2.1.1. Model Structure

The Advanced Research WRF (WRF-ARW) solver developed at NCAR based on Eulerian mass dynamical core is used in the present study. The schematic structure of WRF-ARW system components is given in Figure 2.1. Primarily it consists of the dynamical solver, pre-processing system for preparing the initial and boundary conditions to the model, physics packages and a variational data assimilation system (WRF-Var) for incorporating observations into the initial conditions.

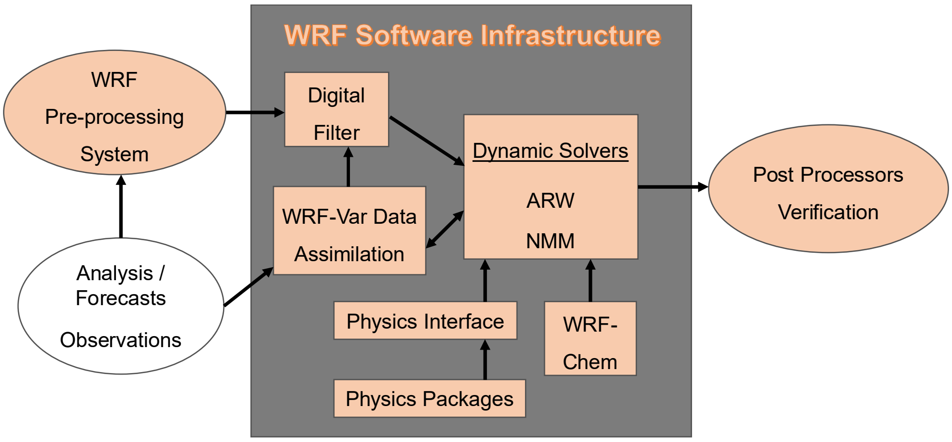

Figure 2.1. *The components of WRF system (referred from Skamarock et al., 2008).*

The model prognostic variables consist of the *u* and *v* velocity components in cartesian coordinates, vertical velocity *w*, perturbation potential temperature and geopotential, and perturbation surface pressure of dry air. The optional variables are turbulent kinetic energy and any number of scalars such as water vapor mixing ratio, rain/snow mixing ratio, cloud water/ice mixing ratio, and chemical species and tracers. The model has a hybrid sigma-pressure vertical coordinate that is terrain-following near the surface and becomes isobaric at a user level that is pre-defined. Several options such as periodic, open, symmetric, and specified are available for lateral boundary conditions. It has gravity wave absorbing constant pressure level at the top boundary along a material surface. The bottom boundary condition can be set as physical or free-slip. Also, full Coriolis terms are included for the effect of Earth's rotation. The model supports four map projections for real-data simulation: polar stereographic, Lambert conformal, Mercator and latitude-longitude along with the inclusion of curvature terms. The nesting in WRF can be one-way interactive, two-way interactive and moving nests. The model also supports grid and observation nudging.

The WRF Pre-processing system (WPS) (Fig. 2.1) program is primarily used for real-data simulations. It performs, 1) defining simulation domains with suitable map projections; 2) interpolating terrestrial data such as terrain, land use, and soil types to the simulation domains and 3) degribbing and interpolating meteorological data from another model to the simulation domains. WRF-Var Data Assimilation (WRF-DA) can be used to ingest observations into the interpolated analyses created by WPS. It can also be used to update WRF model's initial conditions when the model is run in cycling mode. WRF-DA is based on an incremental variational data assimilation technique (Barker et al., 2004), and has both 3D-Var and 4D-Var capabilities. ARW solver is the key component of the modelling system which is composed of several initialization programs for idealized, and real-data simulations, and the numerical integration program. A number of visualization tools are available to display WRF-ARW model results. The model data in NETCDF format can essentially be displayed using any tool capable of displaying this format of data. Various post-processing utilities such as NCL, RIP, ARWpost, etc. are supported (Skamarock et al., 2008).

2.1.2. Governing model equations

The flux-form prognostic Euler equations of WRF model are represented as follows.

$$\partial_t U + (\boldsymbol{\nabla}.\boldsymbol{V}u) - \partial_x\left(p\partial_\eta \phi\right) + \partial_\eta(p\partial_x\phi) = F_U \tag{2.1}$$

$$\partial_t V + (\boldsymbol{\nabla}.\boldsymbol{V}v) - \partial_y\left(p\partial_\eta \phi\right) + \partial_\eta\left(p\partial_y\phi\right) = F_V \tag{2.2}$$

$$\partial_t W + (\boldsymbol{\nabla}.\boldsymbol{V}w) - g\left(\partial_\eta p - \mu\right) = F_W \tag{2.3}$$

$$\partial_t \Theta + (\boldsymbol{\nabla}.\boldsymbol{V}\theta) = F_\Theta \tag{2.4}$$

$$\partial_t \mu + (\boldsymbol{\nabla}.\boldsymbol{V}) = 0 \tag{2.5}$$

$$\partial_t \phi + \mu^{-1}[(\boldsymbol{V}.\boldsymbol{\nabla}\phi) - gW] = 0 \tag{2.6}$$

$$\partial_\eta \phi = -\alpha\mu \tag{2.7}$$

$$p = p_0(R_d\theta/p_0\alpha)^\gamma \tag{2.8}$$

where, $\phi = gz$ is the geopotential, p is the pressure and $\alpha = 1/\rho$ is the specific mass. These are non-conserved variables whereas equations (2.1-2.6) are in conservative form. The equations (2.1, 2.2) represent the horizontal (x, y) components of momentum, (2.3) represents the vertical (z) component of momentum. Equation (2.4) is the thermodynamic energy equation, (2.5) is the equation of mass continuity and (2.6) is the geopotential equation. (2.7) is the equation for inverse density along with the diagnostic relation and (2.8) is the equation of state. The subscripts x, y and η in the above equations denote differentiation. The advection of any variable 'a' in the above equations is given by

$\boldsymbol{\nabla}.\boldsymbol{V}a = \partial_x(Ua) + \partial_y(Va) + \partial_\eta(\Omega a)$ and $\boldsymbol{V}.\boldsymbol{\nabla}a = U\partial_x a + V\partial_y a + \Omega\partial_\eta a,$

The terms F_U, F_V, F_W and F_Θ on the R.H.S of equations (2.1-2.4) represent the forcing terms arising from model physics, turbulent mixing, spherical projections, and the earth's rotation. $\gamma = c_p/c_v$ = 1.4 is the ratio of heat capacities for dry air, R_d is the gas constant for dry air, and p_0 is a reference pressure. The relation for hydrostatic balance (2.7) is a diagnostic relation and is the hydrostatic counterpart to the non-hydrostatic equation.

The prognostic equation for moisture is given by,

$$\partial_t Q_m + (\boldsymbol{\nabla}.\boldsymbol{V}q_m) = F_{Qm} \tag{2.9}$$

The above equation includes the mixing ratios of water vapor and other hydrometeors and microphysical variables.

2.1.3. Initial and boundary conditions

The programs that generate the specific initial conditions provide the ARW with:

- input data that is on the correct horizontal and vertical staggering.
- hydrostatically balanced reference state and perturbation fields, and
- metadata specifying information such as the date, grid physical characteristics, and projection details.

First, the model physical grid is defined by configuring the model domains using the GEOGRID program which includes the projection, number of grid points, location of the globe, nest locations, and grid distances etc. The 2-dimensional static terrestrial fields such as albedo, terrain elevation, Coriolis parameter, vegetation/land-use type, land/water mask, map scale factors, map rotation angle, vegetation greenness fraction, soil texture category, annual mean temperature, and latitude/longitude are interpolated the grid. The binary gridded data from an external global model analyses and forecasts is converted to internal format using program UNGRIB. These 2-dimensional time-dependent fields from the external model include: surface and sea-level pressures (Pa), layers of soil temperature (K) and soil moisture (kg/Kg, either total moisture or binned into total and liquid content), snow depth (m), skin temperature and sea surface temperature (K), and sea ice flag. The meteorological data [3-dimensional fields (including the surface) of temperature (K), relative humidity and the horizontal components of momentum] is horizontally interpolated onto the projected domain(s) using the METGRID program. The final output data from WPS provides a complete 3-dimensional snapshot of the atmosphere on the selected model grid's horizontal staggering at the selected time steps.

The specified lateral boundary conditions for the coarse grid is supplied by an external file that is generated by program *real* which contains records for the fields u, v, θ, q_v, ϕ', and μ'_d that are used by ARW to constrain the lateral boundaries. The lateral boundary file will be processed by WPS. This file consists for each of these variables, both a valid value at the initial time of the lateral boundary time and a tendency term to get to the next boundary time period. All fine domains use the nest time-dependent lateral boundary condition for nesting, where the outer row and column of the fine grid is specified from the parent domain. The remaining lateral boundary conditions are for use by the coarsest or parent domain.

Lateral boundary conditions in ARW can be specified as periodic in x (west-east), y (south-north), or doubly periodic in (x, y). The periodic boundary conditions constrain the solutions to be periodic; that is, a generic model state variable ψ will follow the relation

$$\psi\left(x + nL_x, y + mL_y\right) = \psi(x, y) \tag{2.10}$$

for all integer (n, m). The periodic lengths (L_x, L_y) are the dimensions of the domain in x and y.

All the four grid sides use specified lateral conditions for the outer domain. The specified lateral boundary condition is a relaxation boundary condition. The specified relaxation zone is determined entirely by temporal interpolation from an external forecast or analyses, for the coarse grid.

2.1.4. Model physics

ARW offers multiple physics parameterization schemes for microphysics, cumulus parameterization, planetary boundary layer (PBL), land-surface processes and atmospheric radiation that can be combined in any way. The physics schemes for Cumulus convection, PBL turbulent diffusion, surface layer transport, land surface processes, short and longwave radiation transfer in this study are chosen based on the earlier modelling studies for the TCs in the NIO region (Mukhopadhyay et al., 2011; Srinivas et al., 2013; Osuri et al., 2012; Greeshma et al., 2015) and were evaluated to provide better results. Various schemes for cloud microphysics are evaluated by conducting sensitivity experiments for their performance in the convective permitting simulations for TCs.

2.1.4.1. Radiation physics

Radiation physics parameterization schemes calculate the radiation transfer in the earth-atmosphere system and atmospheric heating due to radiative flux divergence and surface downward longwave and shortwave radiation for the ground heat budget. The processes include absorption, reflection, and scattering in the atmosphere and surfaces with the only source as the Sun. All the radiation schemes in WRF and one-dimensional schemes with each column treated independently. Following are the long wave and shortwave radiation schemes used in the present study.

- *RRTM (Rapid Radiative Transfer Model) long wave*

RRTM is a spectral band scheme which utilizes the correlated-k approach based on Mlawer et al. (1997) to calculate fluxes and heating rates efficiently and accurately. It uses pre-set tables to accurately represent long wave processes due to ozone, water vapor, CO_2 and other trace gases present and also accounts for cloud optical depth.

- *RRTMG (RRTM for GCM) long wave and shortwave*

RRTMG utilizes the correlated-k approach (Mlawer et al., 1997; Clough et al., 2005) to calculate fluxes and heating rates and it includes the Monte-Carlo Independent Column approximation (McICA) technique (Barker et al., 2007; Pincus et al., 2003) for representing sub-grid cloud variability. Regardless of the cloud type or amount for radiation calculations, this scheme also specifies the size of the hydrometeors (Bae et al., 2016).

- *Dudhia Shortwave*

This scheme is taken from MM5 and is based on Dudhia, (1989). It comprises of a simple downward integration of solar flux, that accounts for clear-air scattering, water vapor absorption (Lacis and Hansen, 1974), and cloud albedo and absorption. The scheme has an option to account for terrain slope and shadowing effects on the surface solar flux.

2.1.4.2. Land-surface physics

Land-surface schemes compute the heat and moisture fluxes over land points and sea-ice points. They use radiative forcing from the radiation scheme, precipitation forcing from the microphysics and convection schemes and atmospheric information from the surface layer scheme, and internal information on the land's state variables and land-surface properties to compute the surface energy budget. These fluxes provide a lower boundary condition for the vertical transport in the PBL schemes. Following are the land-surface physics used in the study.

- *5-layer thermal diffusion model*

This is a simple land surface model (LSM) based on the MM5 5-layer soil temperature model (Dudhia, 1996). The thickness of the layers is 1, 2, 4, 8 and 16 cm. The temperature is fixed at a deep-layer average below these layers. It includes radiation, sensible and latent heat flux in the energy budget and also allows for a snow-cover which is fixed in time. Soil moisture is fixed with landuse- and season-dependent constant value with no explicit vegetation effects.

- *Noah LSM*

The Noah LSM is a 4-layer soil temperature and moisture model with canopy moisture and snow cover prediction (Chen and Dudhia, 2001; Ek et al., 2003; Tewari et al., 2004). The thickness of layers is 10, 30, 60 and 100 cm from the top down. This scheme is consistent with the time-dependent soil fields provided in the analysis datasets. It also predicts canopy moisture and snow cover and accounts for the land-use-dependent vegetation effects on evapotranspiration, soil- type dependent infiltration and runoff effects on soil moisture budget. It uses a single vegetation layer, single layer bulk snowpack. It has an improved urban treatment considering surface emissivity properties.

2.1.4.3. Surface layer physics

The surface layer parameterization schemes calculate the friction velocities and exchange coefficients that enable the calculation of surface heat and moisture fluxes by the land-surface models and surface stress in the planetary boundary layer scheme. The surface fluxes and surface diagnostic fields are computed in the surface layer scheme itself, over water surfaces. The description of the surface layer physics scheme used for the study is given below.

- *MM5 Similarity theory*

This scheme is introduced in MM5 model and later in WRF model. This scheme uses the stability functions from Paulson, (1970), Dyer and Hicks, (1970) and Webb, (1970) for computing surface exchange coefficients for heat, momentum and moisture. Jiménez et al. (2012) have modified this scheme for application to full range of atmospheric stabilities. In the revised one, the turbulent fluxes are more (less) efficient during the day (night) that shows the largest impact in the planetary boundary layer meteorological variables. To enhance the surface fluxes of heat and moisture, a convective velocity following Beljaars, (1994) is used.

2.1.4.4. Planetary boundary layer physics

The PBL computes the vertical sub-grid scale fluxes due to eddy transports in the whole atmospheric column, not just the boundary layer. The surface fluxes are provided by the surface layer and land-surface schemes. The flux profiles within the well-mixed boundary layer and the stable layer are determined by the PBL schemes. Thus, they provide atmospheric tendencies of temperature, moisture (including clouds), and horizontal momentum in the entire atmospheric column. The schemes are one-dimensional, and assume that there is a clear scale separation between the sub-grid scale eddies and resolved eddies. Following are the PBL schemes used for the simulations.

- *Yonsei University (YSU)*

The YSU PBL (Hong et al., 2006) is a non-local scheme with first-order closure based on k-theory and uses the counter gradient terms (Hong and Pan, 1996) to represent fluxes due to non-local gradients with explicit treatment of the entrainment layer at the PBL top. The turbulent exchange coefficients for momentum and enthalpy follow a parabolic relationship with stability. According to the results from the large-eddy model studies (Noh et al., 2003), the entrainment is made proportional to the surface buoyancy flux. A critical bulk Richardson number of zero is used to define the PBL top that is effectively dependent on the buoyancy profile, in which PBL top is defined at the maximum entrainment layer.

- *Mellor-Yamada Nakanishi and Niino (MYNN) level 2.5*

MYNN level 2.5 PBL is a local scheme (Nakanishi and Niino, 2004) with a second-order closure where the expressions of mixing length and stability are based on large eddy simulation results rather than on observations. This scheme uses a prognostic turbulent kinetic energy (TKE) equation and the exchange coefficients are formulated through TKE. The mixing length expressions are applicable to a variety of static stability regimes (Cohen et al., 2015).

2.1.4.5. Cumulus physics

The sub-grid scale effects of convective and/or shallow clouds are represented using cumulus parameterization (CP). Various schemes are proposed to represent vertical fluxes due to unresolved updrafts and downdrafts and compensating motion outside the clouds through a cloud model. They provide vertical heating and moistening profiles by operating only on individual columns where the scheme is triggered. All the schemes provide the convective component of surface rainfall. The cumulus schemes are called implicit parameterization as it represents the subgrid scale processes on the grid scale variables. Cumulus parameterizations are theoretically valid only for coarser grid sizes (≥ 10 km), where they are necessary to release latent heat properly on a realistic time scale in the convective columns. Generally, cumulus schemes are not used at a very fine resolution (≤ 5 km grid) when the model can resolve the convective eddies itself. The details of the cumulus schemes used are given in the following.

- *Kain-Fritsch*

This cumulus convection scheme is based on the works of Kain and Fritsch (1990) and Kain (2004). It uses a Lagrangian parcel method and a simple cloud model with moist updrafts and downdrafts. It includes the effects of detrainment and entrainment. The scheme has a trigger function, a mass flux formulation and closure based on convective available potential energy (CAPE). In marginally unstable and relatively dry environments, a minimum entrainment rate is imposed in the scheme to suppress widespread convection. The entrainment rate is allowed to vary as a function of low-level convergence and shallow convection is also allowed for any updraft that does not reach the minimum cloud depth. This scheme is selected for the simulations based on its robust performance in the sensitivity study by Srinivas et al. (2013) for TCs in NIO region.

2.1.4.6. Cloud Microphysics (CMP)

The cloud microphysical processes include explicitly resolved hydrometeors, cloud and precipitation. The CMP includes the set of physical processes controlling the formation of cloud droplets and ice crystals, their growth, and their fallout as precipitation (Stensrud, 2007). The primary microphysical species are water vapour, cloud droplets, rain droplets, cloud ice crystals, snow, rimed ice, graupel, and hail. As a general rule, for grid-sizes less than 10 km, where updrafts may be resolved, mixed-phase schemes should be used, particularly in convective or icing situations. The schemes can be either single moment or double moment. The single moment schemes predict the mixing ratio of hydrometeors whereas the double moment schemes predict both the mixing ratio and number concentration of the hydrometeors. CMP schemes can be broadly classified into two categories - bin and bulk based on the representation of the size distribution of hydrometeors. While the bin approach distinguishes particle size distribution into a large number of bins, the bulk approach uses prescribed analytic form for the size distribution of each microphysical species. Recent studies show that bin approach provides a more realistic reproduction of cloud structure and convection than the bulk approach (Khain et al., 2009; Iguchi et al., 2008). However, bulk schemes are more preferred due to bulk schemes being computationally expensive. Six bulk microphysics schemes are used in the present study for microphysics sensitivity simulations and the details are given below.

- *Morrison double moment*

The Morrison scheme (Morrison et al., 2005, 2009) is a double moment scheme. It uses a gamma size distribution and prognostic variables including the number concentration and mixing ratio of six hydrometeors, water vapor, cloud water, rain water, cloud ice, rain, snow and graupel/hail. It has a user specified switch to include either graupel or hail. The prediction of two moments allows for a more robust treatment of the particle size distributions.

- *Lin*

The Lin scheme (Lin et al., 1983) is a single moment scheme with mixed-phase processes and predict six hydrometeors, water vapor, cloud water, rain water, cloud ice, rain, snow and graupel/hail. It uses the inverse size distribution for rain, snow and graupel.

The Lin scheme is a sophisticated scheme in WRF which is suitable for real-data high resolution simulations.

- *WRF Single-Moment 3-class (WSM3)*

The WSM3 scheme is a single moment scheme that follows (Hong et al., 2004) and predicts three categories of hydrometeors: water vapor, cloud water/ice, rain/snow. This scheme is computationally efficient for ice processes inclusion, but lacks supercooled water and gradual melting rates.

- W*RF Single-Moment 6-class (WSM6)*

The WSM6 scheme is a single-moment scheme and has six prognostic equations of microphysical processes for water vapor, cloud water, cloud ice, rain, snow and graupel. This scheme allows supercooled water to exist and the melting of the snow as it falls below the melting layer. It extends the WSM 5-class scheme to include graupel and associated processes (Hong and Lim, 2006). The WSM6 scheme is very suitable for cloud resolving grids due to its efficiency.

- *New Thompson*

The Thompson scheme is a single moment scheme (Thompson et al., 2008) that includes six prognostic equations of the hydrometeors (water vapor, cloud water, cloud ice, rain, snow and graupel) but double moment for ice and rain (number concentrations of ice and rain). The scheme explicitly predicts the mixing ratio of hydrometeors and uses a generalized gamma distribution shape for each hydrometeor species.

- *Goddard*

The Goddard is a one-moment scheme (Tao and Simpson, 1993) suitable for high-resolution simulations which includes the prediction of water vapor, cloud water, cloud ice, rain, snow and graupel. It uses the inverse size distributions and has an option to choose either graupel or hail as the third class of ice. The microphysics processes that do not involve melting, evaporation or sublimation are calculated based on one thermodynamic state that ensures equal treatment of all of these processes (Skamarock et al., 2008).

2.2. Overview of tropical low pressure / cyclonic cases selected

A brief description of the tropical low pressure and cyclone cases chosen for the study is given below.

2.2.1. Tropical low-pressure system with heavy rainfall event (27 Nov-02 Dec 2015)

A low-pressure system had formed in the southwest Bay of Bengal and adjoining Tamil Nadu on 27 November 2015 during the northeast monsoon (IMD, 2015; Mishra, 2016). This was associated with a cyclonic circulation extending up to 3.1 km from the sea level. The low pressure persisted till 2 December and produced extensive rainfall over north coastal Tamil Nadu and very heavy precipitation over the Chennai city of Tamil Nadu and surrounding areas on 1 December 2015. Though this system has not intensified further but it produced more rainfall along the coast. The trough moved westwards between 30 November and 1 Dec, and it passed along coastal Tamil Nadu extending from 9°N (1010 hPa) to 14°N (1014 hPa). Very heavy rains led to flooding across the entire stretch of coast from Chennai to Cuddalore. According to daily rainfall records of IMD, total amounts received from 00 UTC 1 December through 00 UTC 2 December in Tamil Nadu were 495 mm at Tambaram, and 218 mm at Puducherry. The hourly rainfall records of IMD show that the heaviest precipitation in Chennai occurred between 05 UTC and 15 UTC of 1 December. The low-pressure area moved off the south Tamilnadu coast and gradually dissipated with the westward movement of the trough. This extreme weather case was considered to study the sensitivity of high-resolution model simulations to cloud microphysics, so that the tested schemes can be further evaluated for TCs in the subsequent studies.

2.2.2. Laila (17-21 May 2010)

The SCS 'Laila' originated from a low-pressure area which developed over the southeast BOB on 15 May 2010. It concentrated into a depression at 0600 UTC of 17 May due to increase in low-level horizontal convergence and relative vorticity associated with the setting of Southwest monsoon over Andaman Sea and adjoining southeast BOB. The system moved northwestwards and became a SCS at 0600 UTC of 19 May with a minimum pressure of 986 hPa and a sustained maximum wind speed of 55 knots. The system crossed Andhra Pradesh (AP) coast near Bapatla between 1100 and 1200 UTC of 20 May as a SCS. It caused scattered heavy to very heavy rainfall with isolated extremely heavy rainfall (≥ 25 cm) over coastal Tamilnadu and coastal AP (IMD, 2011, RSMC-2010).

2.2.3. Jal (4-8 November 2010)

The SCS 'Jal' developed over the BOB from the remnant of a depression which moved from northwest Pacific Ocean to the BOB across southern Thailand on 1st November 2010. It developed into a deep depression and into a CS at 0600 UTC of 5th November due to higher SST (30-32°C), higher ocean heat content (> 100 KJ/cm^2), increased low-level relative vorticity and upper level divergence and low vertical wind shear. The system moved west-northwestwards and intensified into a SCS at 0000 UTC of 6 November with a minimum pressure of 988 hPa and maximum sustained winds of 60 knots. It crossed north Tamilnadu – south AP coast as a deep-depression, close to north of Chennai around 1600 UTC of 7 November. Heavy to very heavy rainfall occurred at most places over north Tamilnadu, Puducherry, coastal AP, Rayalaseema, south interior Karnataka and coastal Karnataka (IMD, 2011, RSMC-2010).

2.2.4. Thane (25-31 December 2011)

The VSCS storm ‘Thane’ originated from a low-pressure associated with a cyclonic circulation due to an active ITCZ over the southeast BOB on 24th December 2011. Under favorable conditions of low-level convergence and upper-level divergence associated with high ocean thermal energy and Madden Julian Oscillation (MJO) index laying over phase 5, the system moved north-northwestwards and further moved towards west intensifying into a VSCS at 0900 UTC 28 December with an estimated minimum pressure and sustained wind speed of 969 hPa and 75 knots respectively at 2100 UTC 29 December. The system crossed Tamilnadu and Puducherry coast, close to the south of Cuddalore between 0100 and 0200 UTC of 30th December. It caused heavy to very heavy rainfall at a few places over north Tamilnadu and Puducherry on 30th and 31st December including isolated heavy rainfall over south Tamilnadu, south coastal Andhra Pradesh, Rayalaseema during this period and over Kerala on 31stDecember (IMD, 2012, RSMC-2011).

2.2.5. Phailin (8-14 October 2013)

The ESCS ‘Phailin’ originated from a remnant cyclonic circulation from the South China Sea on 6th October 2013. Due to high SSTs, ocean thermal energy and low vertical wind shear, there was a rapid intensification of the cyclone from 10th morning. The system gradually intensified into an ESCS and attained it maximum intensity with a lowest pressure of 940 hPa and sustained wind speed of 115 knots at 0300 UTC of 11 October. The VSCS continued to move northwestwards at a speed of about 15 kmph and crossed Andhra Pradesh and Odisha coast near Gopalpur around 1700 UTC of 12 October. Phailin caused very heavy to extremely heavy rainfall over Andaman and Nicobar Islands, Odisha and isolated heavy to very heavy rainfall over North Coastal Andhra Pradesh, West Bengal, Jharkand, Bihar, Chhattisgarh and Sikkim (IMD, 2014, RSMC-2013).

2.2.6. Helen (19-23 November 2013)

The SCS 'Helen' originated from a trough associated with a tropical storm near the Andaman Islands on 16th November 2013. It gradually concentrated into a depression over the west central BOB in the early morning of 19th November due to warmer SSTs, low to moderate vertical wind shears and increase in low-level convergence along with upper-level divergence. The depression further intensified into a SCS in the early morning of 21st November with a lowest central pressure of 990 hPa and sustained winds of 55 knots. On 22nd November the system initially moved westwards and then west-southwestwards and crossed Andhra Pradesh coast close to south of Machilipatnam between 0800 and 0900 UTC of 22nd November as a CS. Isolated heavy to very heavy rainfall was recorded over coastal Andhra Pradesh and north Tamilnadu coast on 21stNovember (IMD, 2014, RSMC-2013).

2.2.7. Lehar (23-28 November 2013)

The VSCS 'Lehar' originated as low-pressure over the south Andaman Sea associated with the remnant of a tropical depression over the South China Sea, on 21st November 2013. Due to the adequate upper-level divergence associated with an upper tropospheric ridge, and the increase in relative vorticity and low-level convergence from 22nd to 23rd November, it concentrated into a depression at 1200 UTC 23 November. The system moved northwestwards and gradually intensified into a VSCS at 2100 UTC 25th November and attained its maximum intensity with a central pressure and sustained winds of 980 hPa and 75 knots respectively at 1800 UTC 25 November. It gradually weakened into a depression due to colder SST and high vertical wind shear and crossed AP coast around 0830 UTC 28 November close to south of Machilipatnam. Heavy to very heavy rainfall was recorded over Andaman and Nicobar Islands and coastal AP on 25th and 29th November (IMD, 2014, RSMC-2013).

2.2.8. Hudhud (7-14 October 2014)

The ESCS 'Hudhud' originated from a low-pressure area over Tenasserim coast and adjoining north Andaman Sea on 6th October 2014. While moving west-northwestwards, it concentrated into a depression over north Andaman Sea in the morning of 7th October. High poleward outflow associated with an upper tropospheric ridge, high SST (30-32°C) and MJO index over phase 6 favoured further intensification of the system. The system gradually intensified into an ESCS at 0600 UTC 11 October, attained the maximum intensity with 950 hPa and 100 knots of lowest central pressure and maximum sustained wind speed respectively and crossed north AP coast over Visakhapatnam between 0630 and 0730 UTC 12 October. Hudhud caused isolated heavy to very heavy rainfall at a few places with isolated extremely heavy rainfall over north AP and south Odisha and large-scale structural damage due to strong winds gusting to 110 knots (IMD, 2015, RSMC-2014).

2.2.9. Vardah (6-13 December 2016)

The VSCS 'Vardah' originated as a low-pressure area over southeast BOB and adjoining south Andaman Sea on 3rd December 2016. Initially moving northwards and then northwestwards, it gradually concentrated into a deep-depression at 1800 UTC 07 December due to low wind shear and favorable SSTs. The system moved northwards and intensified into a CS at 0000 UTC 8 December and then moved west-northwestwards intensifying further into a SCS at 1800 UTC 9 December. Vardah strengthened into a VSCS at 1200 UTC 10 December and attained maximum intensity on 0000 UTC 11 December with a lowest central pressure of 980 hPa and maximum sustained winds of 70 knots. The system weakened gradually into a SCS moving westwards and crossed Tamilnadu coast close to Chennai between 0930 to 1130 UTC 12 December. The system brought heavy to very heavy rainfall over Chennai, Tiruvallur and Kanchipuram districts of Tamilnadu on 12th December and caused extensive damage over Chennai (IMD, 2017, RSMC-2016).

2.2.10. Gaja (11-19 November 2018)

The VSCS 'Gaja' originated as a low-pressure system over the Gulf of Thailand on 5th November and crossing into the Andaman Sea. It concentrated into a depression and further intensified into a CS at 0000 UTC 11 November with favorable environmental conditions of increased low-level convergence, vorticity and moderate vertical wind shear due to MJO index in phase 4. The system then moved west-southwestwards and strengthened gradually into a VSCS at 0300 UTC 15 November and crossed Tamilnadu and Puducherry coast between Nagapattinam and Vedaranniyam around 1900 UTC to 2100 UTC 15 November with its maximum intensity of 976 hPa and 70 knots of central pressure and sustained wind speed respectively. The storm survived its crossing into the Arabian Sea and however dissipated in hostile conditions a few days later. Gaja caused extremely heavy rainfall ($\geq$ 20 cm) over Nagapattinam, Thanjavur, Cuddalore and Trichy districts of Tamilnadu (IMD, 2019, RSMC-2018).

2.2.11. Fani (26 April – 05 May 2019)

The ESCS 'Fani' originated as a depression over east equatorial Indian Ocean and adjoining southeast BOB at 0300 UTC 26 April 2018. The system intensified into a CS at 0600 UTC 27 April, moved north-northwestwards and further strengthened into a SCS at 1200 UTC 29 April, under the influence of warm sea waters (30-31°C), high low-level positive vorticity (130×10^{-6} sec^{-1}), high low-level convergence. Further enhancement of favorable environmental conditions led to a rapid intensification of the system into a VSCS in the subsequent 12 hours and to an ESCS in another 12 hours (12 UTC 30 April), while moving west-northwestwards. The system attained its maximum intensity on 1500 UTC 02 May with the lowest central pressure of 937 hPa and maximum sustained winds of 115 knots. The system then moved north-northeastwards and crossed Odisha coast close to Puri between 0230 to 0430 UTC 3 May with a sustained wind speed of 95 knots. Fani was the most intense storm to make landfall in Odisha since the 1999 Odisha super cyclone. It caused a massive environmental and infrastructure devastation worth US$1.74 billion (IMD, 2020, RSMC-2019).

2.2.12. Amphan (13-22 May 2020)

The Super Cyclonic Storm (SuCS) 'Amphan' originated from the remnant of a cyclonic circulation associated with a low-pressure area which occurred in the near Equatorial easterly wave over south Andaman Sea and adjoining southeast BOB during 1^{st}-5^{th} May 2020. Under favorable environmental conditions, it concentrated into a depression and intensified gradually into a CS at 1200 UTC 16 May. It underwent rapid intensification during subsequent 24 hours and an ESCS in the early hours of 18^{th} (2100 UTC 17 May) and into a SuCS at 0600 UTC 18 May. The rapid intensification was mainly due to low-vertical wind shear (10-15 knots), very warm SSTs (30-31°C), high TC heat potential (100-120 KJ/cm^2) and increased cross equatorial wind surge. It attained maximum intensity on 1800 UTC 18 May with 920 hPa and 130 knots of central pressure and sustained winds respectively. It maintained the intensity of SuCS over west central BOB for nearly 24 hours, before weakening into an ESCS at 0600 UTC 19 May under unfavorable environment. Thereafter it weakened slightly and crossed West Bengal – Bangladesh coasts as a VSCS, across Sundarbans during 1000-1200 UTC 20 May with a sustained wind speed of 85 knots. (RSMC-IMD, 16^{th} -21^{st} May 2020: Summary).

2.3. Data used for the study

In this section, a brief description of data sets used for initializing the model simulations as well as for the validation of the model results is provided. The initial and boundary conditions for the ARW model simulations are provided from the National

Center for Environmental Prediction (NCEP) Global Forecasting System (GFS) analysis and forecasts. For the simulations with lower boundary SST update, NCEP operational GFS SST analysis and NCEP/ National Oceanic Atmospheric Administration (NCEP/ NOAA) high resolution SST data are used. The climatological SST mean over a 11 years period was computed from NOAA Optimum Interpolation Sea Surface Temperature (OISST) high resolution data. The simulation results of tracks and intensity of TCs are compared with IMD best track data. The simulation on cloud structure is compared with the IMD Doppler Weather Radar (DWR) images. The Cooperative Institute for Research in Atmosphere (CIRA) Advanced Microwave Sounding Unit (AMSU) derived real time cyclone products are used for the comparison of wind shears, core warming, surface winds and tangential winds of the TCs. The radius of maximum winds is compared with the CIRA multiplatform satellite wind analysis. The simulated vertical velocity profiles are compared with the Mesosphere-Stratosphere-Troposphere (MST) radar data of National Atmospheric Research Laboratory (NARL), Gadanki. The Tropical Rainfall Measuring Mission (TRMM) data and IMD Automatic Weather Station (AWS) data are used validating the rainfall simulation. The details of the datasets used for the study is given below.

2.3.1. NCEP GFS

GFS is a weather forecast model produced by the NCEP. It is a coupled model, composed of four separate models (an atmosphere model, an ocean model, a land/soil model, and a sea ice model), which work together to provide an accurate picture of the weather conditions. The entire globe is covered by the GFS at a base horizontal resolution of 28 kilometers between grid points which is used to predict weather out to 16 days in the future. Gridded data are available for download through the NOAA National Operational Model Archive and Distribution System (NOMADS). For the present study, the GFS data of 50 km and 25 km horizontal grid resolution and temporal resolution of 3 hours are used. (https://www.ncdc.noaa.gov/data-access/model-data/model-datasets/global-forcast-system-gfs).

- ***GFS-SST***

The GFS-SST is the operational global SST analysis by NCEP that use 7 days of insitu and satellite SST. The data is derived by optimum interpolation of observations from past 7 days where the SST anomaly is damped with an e-folding time of 90 days over the forecast (Reynolds and Smith, 1994).

2.3.2. NCEP/NOAA High resolution SST

NCEP/NOAA SST is a daily, high-resolution, real time global SST (RTG_SST) analysis developed at the NCEP/Marine Modelling and Analysis Branch (NCEP/MMAB). The product is produced on a twelfth-degree grid with a two-dimensional variational interpolation analysis of the most recent 24-hours buoy and ship data, satellite retrieved SST data, and SST's derived from satellite-observed sea-ice coverage. Currently, the analysis uses satellite SST retrieval data from the GOES satellites. Satellite retrieved SST values are averaged within 1/12° grid boxes. The bias calculation and removal for the retrieved SST is the technique employed in the 7-day Reynolds-Smith climatological analysis (https://polar.ncep.noaa.gov/s st/rtg_high_res/description.shtml). The real-time SST data can be accessed from (ftp://ftp.nce p.noaa.gov/pub/data/nccf/com/gfs/prod).

2.3.3. NOAA OISST

NOAA OISST is an analysis data constructed by combining observations from different platforms (satellites, ships, buoys, and Argo floats) on a regular global grid. The methodology includes bias adjustment of satellite and ship observations (referenced to buoys) to compensate for platform differences and sensor biases (https://www.ncdc.noaa.

gov/oisst). Satellite retrieved SST values are averaged within 1/4° grid boxes on global grid. The daily mean of SST is available from 1981 to present (https://psl.noaa.gov/cgi-bin/db_search/DBListFiles.pl? did=132&tid=88563 &vid=2423).

2.3.4. IMD best track estimates

The best track data of cyclones in the NIO region is generated by the Regional Specialized Meteorological Centre for Tropical Cyclones, IMD following the Dvorak technique (IMD, 2003; Dvorak, 1975). To determine the best track, IMD takes account of all available surface and upper air observations from land and ocean, satellite observations and radar observations. Six hourly best track data sets containing the central position (lat/long), stage of intensity along with T/CI No., estimated central pressure, and sustained maximum surface wind are generated and archived since 1990. These data are also shared with WMO/ESCAP Panel member countries, WMO and other research institutes. The finalized best track, intensity and other parameters are published and shared by IMD/ RSMC, New Delhi (http://www.rsmcnewdelhi.imd.gov.in/images/pdf/archive/best-track/bestrack.pdf).

2.3.5. IMD DWR observations

IMD operates the DWR for cyclone detection and characterization of other extreme weather events. The base parameters available from DWRs are reflectivity (*Z*), radial velocity (*V*) and spectral width (ω). Various other meteorological products for issuing forecasts and warnings are derived from these base parameters, such as, plan position indicator, maximum reflectivity, vertical profile diagram of speed and direction, wind barbs, surface rainfall intensity, precipitation accumulation etc. Presently IMD has 25 radars distributed across India. For the present study the DWR images over Chennai (Tamil Nadu), Visakhapatnam (Andhra Pradesh), Gopalpur (Odisha) and Paradip (Odisha) accessed over internet from IMD (https://mausam.imd.gov.in/imd_latest/contents/index_radar.php) are used.

2.3.6. IMD AWS observations

The IMD AWS stations are used for continuous monitoring of weather systems such as cyclones, western disturbances, thunderstorms and monsoon etc. over continental India. Various weather parameters such as air temperature, relative humidity, atmospheric pressure, rainfall, wind speed, wind direction etc. are being measured at conventional observatories of IMD since 1875. (https://metnet.imd.gov.in/imdetp/lecture_notes/course11/LN_11_61_AWS%20and%20ARG%20-%20Phase%20II.pdf). The present study uses the measured rainfall data from IMD AWS rain-gauges (http://aws.imd.gov.in:8091/).

2.3.7. CIRA Regional and Mesoscale Meteorology Branch (RAMMB) products

The CIRA - Regional and Mesoscale Meteorology Branch (CIRA-RAMMB) of Colorado State University (CSU) generates TC products from multi-satellite remote sensing observations for the 7 TC basins in association with NOAA/NESDIS/STAR/RAMMB in a real-time manner to provide a better understanding of the TC characteristics. The CIRA data is prepared from various sensors of multiple satellites such as SSM/I, AMSU, MODIS, QuikSCAT, ASCAT etc. at ground resolutions of 25 km and above (Knaff et al., 2011). CIRA-RAMMB is also integrated to a database that can accommodate future product development in order to serve the data to the public and research community (https://rammb-data.cira.colostate.edu/tc_realtime/about.asp#strmstat). Following are the datasets used for the present study from CIRA-RAMMB (https://rammb-data.cira.colostate.edu/tc_realtime/). All the TC products are displayed in the CIRA website in graphical plots except the MSLP and CSLP which are available in data format, and the present study used the images for model comparison.

- *AMSU-based azimuthal mean radial/height cross sections*

  The radial/height cross sections of temperature anomaly and tangential wind are created using the AMSU-derived azimuthally averaged temperature and height files based on Demuth et al. (2004). These images are useful in determining the thermal structure of the TCs.

- *AMSU area averaged wind shears and layer means*

The area averaged vertical wind shear and mass weighted deep-layer mean winds in two layers (200-850 hPa and 500-850 hPa) are estimated using the balanced 3-D wind field derived from the AMSU temperature retrievals based on Zehr et al. (2008). The area averaging is calculated within 0-600 km from the cyclone center and displayed in an interval of 12 hours. These are useful for determining rapid changes in the synoptic wind fields. In the present study this data is used for comparing the simulated wind speed shear.

- *Radius of maximum wind (RMW)*

The RMW estimates are developed by CIRA based on several methods including estimates of intensity, latitude and information contained in IR images (Mueller et al., 2006), applying an inward slope from the 3km flight level (Stern et al., 2014). RMW estimates based on the behaviour of the angular momentum surfaces and a function of the current intensity, the Coriolis parameter and a measure of the TC size are also used to accompany the satellite-based methods (Chavas et al., 2014). This data is used to compare the simulated RMW to determine the intensity of the cyclones.

- *Multiplatform surface wind analysis*

The surface wind analysis by CIRA combines information from five data sources to create a mid-level wind analysis using a variational approach (Knaff and DeMaria, 2006). The mid-level resulting winds are then adjusted to the surface applying a very simple single column approach. The five datasets currently used are the ASCAT scatterometer, which is adjusted upward to 700 hPa. This data is used for the comparison of simulated spatial surface winds.

2.3.8. MST radar observations

The MST radar of NARL located at Gadanki (13.5°N, 79.2°E) is used for atmospheric probing in the regions of Mesosphere, Stratosphere and Troposphere covering up to a height of 100 km. It is a highly sensitive pulse-coded coherent very high frequency phased array radar that operates with 53 MHz with an average power aperture of $7x10^8$ Wm^2 with a peak power of 2.5 MW. The phase antenna array consists of two orthogonal sets, one for each polarization, of 1024 three-element Yagi-Uda antennas that is arranged in a 23 x 32 matrix over an area of 130 m x 130 m. The two sets are collocated with pairs of crossed Yagis mounted on the same set of poles (Rao et al., 1995).

2.3.9. TRMM Rainfall

The TRMM is a joint mission between NASA and the JAPAN Aerospace Exploration Agency (JAXA) to study rainfall for weather and climate research. The TRMM Microwave Imager (TMI) is a multi-channel, dual polarized, passive microwave radiometer aboard TRMM satellite. There are two types of daily SST data available - one is optimally interpolated (OI) data with 25 km resolution using only microwave (MW) and the other one is generated using microwave and IR (MW_IR) with 9 km resolution. In the present study the 25 km resolution data are used for rainfall comparisons (https://disc2.gesdisc.eosdis. nasa.gov /data/TRMM_L3/TRMM_3B42_Daily.7/).

Chapter 3

Impacts of convection permitting high resolution simulations

3.1. Introduction

There has been a considerable progress in TC tracks prediction due to increased model resolution, improved physics parameterizations, increased coverage of high-quality satellite observations and data assimilation techniques (Leslie et al., 1998; Houze et al., 2007; Miyoshi et al., 2010; Rogers et al., 2006; Rappaport et al., 2009). However, relatively little progress has been made in intensity forecasts. The application of high-resolution models with proper convection physics is required for resolving the moist convection for better prediction of TCs intensity. Most of the TC simulation studies over the NIO region evaluated the models at 9-km resolution or more using mostly parameterized convection (Mukhopadhyay et al., 2011; Srinivas et al., 2013; Osuri et al., 2013; Deshpande et al., 2012; Singh and Bhaskaran, 2019 among others). These studies indicated considerable intensity errors suggesting the application of explicit convection physics at near cloud-resolving grid spacing for error reduction.

A few studies using grid-sizes of ≥ 5km with explicit convection (Deshpande et al., 2010; Sandeep et al., 2018; Chutia et al., 2019) reported some improvements, but were limited to 1 or 2 cases not clearly inferring the quantitative improvements for their implications in operational forecasting. With this gap, the current study in this chapter examines the impact of convection permitting high resolution simulations on the intensity and track predictions for TCs over the BOB of NIO with respect to two horizontal grid resolutions i.e., 9km grid using parameterized convection and 3km grid using cloud microphysics using the WRF-ARW model. The study involves a comparison of the effects of CP at 9-km resolution with MP in the finer grids (3km) for ten severe TCs formed over the BOB during 2010-2019.

3.2. Methodology

Ten TCs which originated over the BOB of NIO during the period 2010-2019 (Laila 2010, Jal 2010, Thane 2011, Phailin 2013, Helen 2013, Lehar 2013, Hudhud 2014, Vardha 2016, Gaja 2018, Fani 2019) are selected for the study. The IMD tracks of the selected TCs are given in Figure 3.1b. The intensity including the lowest central sea level pressure (CSLP), maximum sustained winds (MSW), category, and model simulation period of each cyclone are provided in Table 3.1. The WRF-ARW model v.3.9 is used for the simulations. The model is configured with three two-way interactive nested domains (d01, d02, d03) (Fig. 3.1a) with horizontal resolutions of 27 km 9 km and 3 km respectively and 45 vertical levels with model top at 10 hPa. The simulations are initialized either at the stage of deep depression or cyclonic storm (http://imd.gov.in/section/nhac/termglossary.pdf) as per the IMD best track data and integrated until dissipating to depression stage

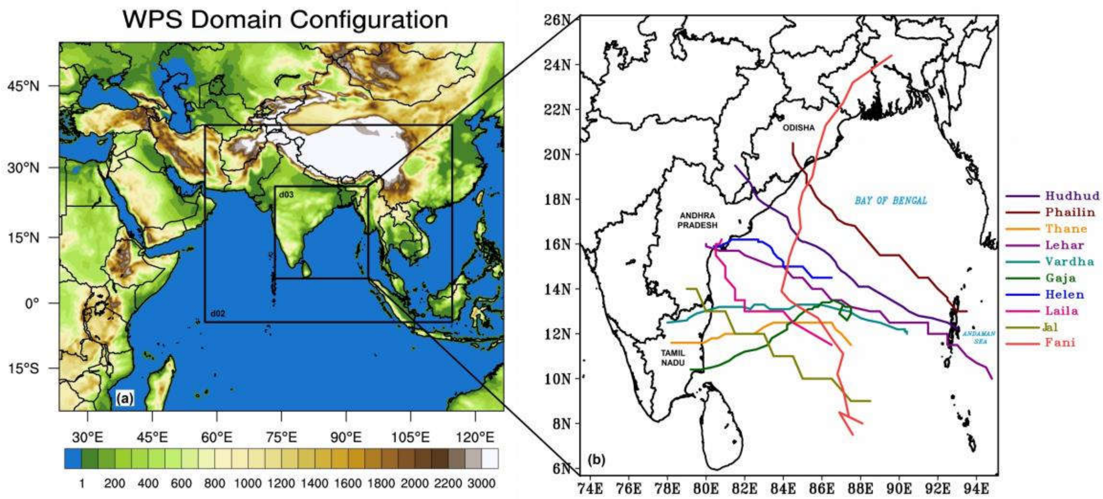

Figure 3.1. ***(a)*** *Simulation domains used for the study with terrain height (m) and* ***(b)*** *IMD tracks of the 10 cyclones selected for the study along the east coast.*

Table 3.1. *Details of TC cases used for the study.*

TC	Category (MSW in m/s and CSLP in hPa)	Model simulation period (YYYYMMDDHH-YYYYMMDDHH) (hrs)
Laila	SCS (28.27, 986)	2010051800-2010052100 (72)
Jal	SCS (30.84, 988)	2010110500-2010110800 (72)
Helen	SCS (28.29, 990)	2013111900-2013112212 (84)
Thane	VSCS (38.58, 969)	2011122700-2011123012 (84)
Lehar	VSCS (38.58, 980)	2013112400-2013112812 (108)
Vardah	VSCS (36.01, 975)	2016120900-2016121300 (96)
Gaja	VSCS (36.01, 976)	2018111200-2018111600 (96)
Phailin	ESCS (59.1, 940)	2013100900-2013101300 (96)
Hudhud	ESCS (48.8, 950)	2014100800-2014101300 (120)
Fani	ESCS (66.6, 937)	2019042800-2019050400 (144)

after making the landfall. The NCEP-GFS 0.5° × 0.5° analysis data is used for initialization and the boundary conditions are updated with the GFS forecasts at every 3 hours. The SST is updated from the GFS data. The model physics options used for the simulations are provided in Table 3.2. The cumulus parameterization is used only in the outer domains (27 km, 9 km).

Two numerical experiments are conducted for each cyclone to study the impact of horizontal resolution on the simulations using i) a parent domain of 27 km resolution with a 9 km nest (27:9) using cumulus convection (9km-CP) ii) a parent domain of 27 km resolution with inner 9 km and 3 km nests (27:9:3) where cumulus physics is used in the 27 km and 9 km domains and only microphysics in the 3 km domain (3km-MP). The model is run with same initial conditions in both simulations (9km-CP, 3km-MP). The results from the simulations are compared with the IMD best track parameters and structure of convective rain bands with IMD DWR products. Further, the radius of maximum wind, deep layer (850-200 hPa) shear and surface wind pattern from the simulations are compared CIRA AMSU derived satellite data. The structural parameters like azimuthally averaged temperature anomaly, tangential winds are also compared with the CIRA products.

Table 3.2. *Model physics used for the study.*

Physics	Scheme
Longwave radiation	RRTM (Mlawer et al., 1997)
Shortwave radiation	Dudhia (Dudhia, 1989)
Surface layer	MM5 similarity theory
Land surface processes	5-layer thermal diffusion (Dudhia, 1996)
Planetary boundary layer	YSU (Hong et al., 2006; Noah et al., 2003)
Cumulus	Kain Fritsch (Kain and Fritsch, 1993; Kain, 2004)
Microphysics	Goddard (Tao and Simpson, 1993)

3.3. Results and discussion

The simulations from 9km-CP and 3km-MP for all the 10 cyclones are analyzed for the tracks, and time variation of CSLP and MSW. Given the large number of cyclone cases, their variability and hourly model outputs, the results are presented in a statistical sense by segregating the cases in to different homogenous samples rather than individual cases. Based on the period of intensification (time taken for maximum intensification) and cyclone category, three groups are considered: i) group-1 (30-50 hours; SCS; Laila, Jal and Helen), ii) group-2 (51-80 hours; VSCS; Vardah, Thane, and Lehar), iii) group-3 (81-120 hours; Hudhud ESCS, Gaja VSCS). The approximate period of intensification/

deepening, peak intensity and decay phases are (40, 16, 40 hrs) in group-1, (65, 24, 16 hrs) in group-2, and (90, 6, 12 hrs) in group-3 respectively. Besides these samples, there are two rapid intensification (RI) cyclones Phailin and Fani of ESCS category which are analyzed separately. The first 12 h of each simulation is considered as model spin-up period and results are analyzed from 12 h onwards till the end of simulation. The computed mean errors include all 10 cyclones for 72 hours, 8 cyclones for 84 hours, 6 cyclones for 96 hours and 3 cyclones for ≥ 108 hours of simulation period. The results from the homogenous groups are discussed in terms of error metrics such as (i) absolute track errors and (ii) intensity errors (absolute and bias).

The detailed structural and intensity parameters including the warming produced in the cyclone core region, wind field, equivalent potential temperature, convergence, relative vorticity and cloud reflectivity are analyzed for two ESCS cases, (1) Hudhud (most intensive cyclone among the three groups) and (2) Phailin (one RI case) during their peak intensification phase, though similar features are found in all cases. Hudhud attained peak intensification during 15 UTC 11 Oct –06 UTC 12 Oct 2014 with an average maximum pressure drop of 60 hPa from the mean sea level pressure and maximum sustained wind speed of 48.8 m/s. The cyclone Phailin attained peak intensification during 06 UTC 11 Oct – 12 UTC 12 Oct 2013 with an average maximum pressure drop of 70 hPa and maximum sustained wind speed of 59 m/s. The period of maximum intensity of simulated cyclone is same as that of IMD estimate for Phailin, but roughly 10 h more (early peak) than the IMD estimate for Hudhud. For the purpose of inter-comparison of simulations,18 UTC 11 Oct 2014 for Hudhud and 03 UTC 12 Oct 2013 for Phailin in the middle of maximum intensification period are selected for the analyses.

3.3.1. Track predictions

The movement of cyclone (track) is controlled by several factors such as large-scale flow, surface pressure, sea surface temperature, air temperature, wind shear, Coriolis force etc. (Riehl, 1954). The predicted tracks from the experiments 9km-CP, 3km-MP are analyzed for all the cyclone cases (Fig. 3.2). A large variation is observed in the predicted tracks in the two simulations for each cyclone. The predicted tracks are deviated to the north of the observed track for ESCS and VSCS cases, Hudhud, Thane, Lehar, Vardah, Gaja, and to the south for SCS cases, Helen, Laila, Jal. The Predicted tracks from 9km-CP and 3km-MP in the case of RI cyclones Phailin and Fani are deviated to the north and south of best tracks showing random cross-track errors. A gradual divergence can also be observed in the two experiments from the initial position; the 3km-MP experiment produced closer tracks to the IMD estimates indicating drastic improvement of track prediction.

The mean vector track errors (vector displacement errors) were analyzed individually for the three groups of cyclones and is presented in Figure 3.3. As shown in Figure 3.3, the mean vector track errors steadily increased in all the three groups, the error level and growth rate are more in group-2 and group-3 of very severe to extremely severe cyclones with moderate to long period of intensification, followed by group-1 cyclones with short duration of intensification. However, the error differences between 3km-MP and 9km-CP are large in group-1 followed by group-2 and group-3. The track error differences increased with simulation time towards decay and landfall phase (72-108 h). The mean track errors are reduced in 3km-MP with respect to 9km-CP by 40%, 37.5%, 73.3%, 41.9%, 0% in group-1 (Fig. 3.3a), 33.3%, 11.4%, 10%, 34%, 46.2% in group-2 (Fig. 3.3b), 36.4%, 20.8%, 7.2%, 7.5%, 26.8% in group-3 (Fig. 3.3c) at 24, 48, 72, 96 and 108 h respectively. In the case of the RI cyclones Phailin (Fig. 3.3d) and Fani (Fig. 3.3e),

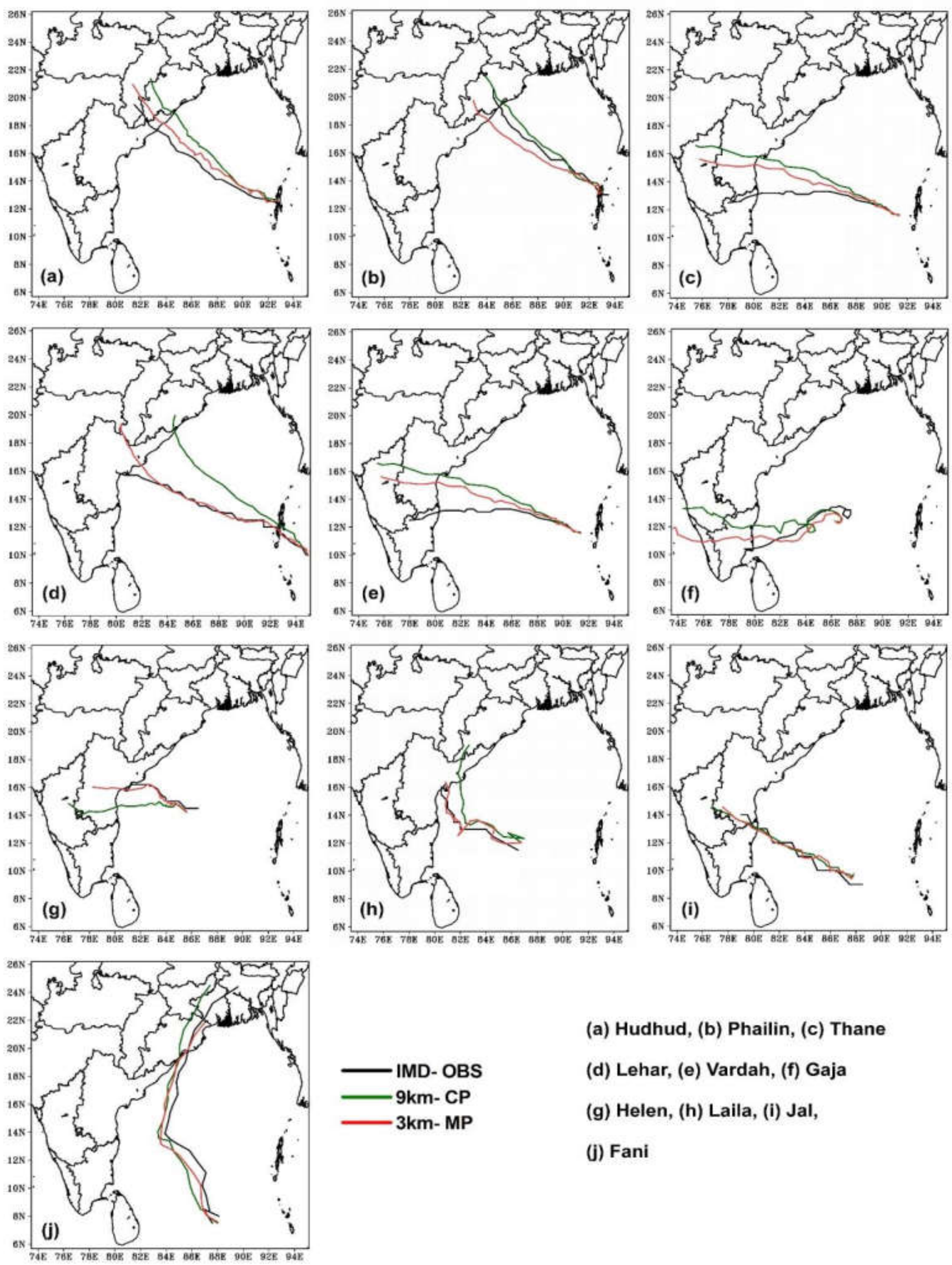

Figure 3.2. *Simulated tracks at 6-hour intervals compared with IMD best track for* ***(a)*** *Hudhud,* ***(b)*** *Phailin,* ***(c)*** *Thane,* ***(d)*** *Lehar,* ***(e)*** *Vardha,* ***(f)*** *Gaja,* ***(g)*** *Helen,* ***(h)*** *Laila,* ***(i)*** *Jal,* ***(j)*** *Fani cyclones.*

the track errors in 3km-MP decreased during the RI phase (12-48 h for Phailin; 24-48 h for Fani) and increased subsequently till the end of the simulation relative to 9km-CP. For these cyclones the 9km-CP produced larger track errors (60-90%) relative to 3km-MP during the RI phase and marginally smaller track errors (25-50%) towards the decay and landfall. The results of the ten TCs shows a consistent improvement in track prediction in the 3-km simulation using explicit convection by 31.7%, 3.8%, 27.65%, 7.6%, 19.2% at 24, 48, 72, 96, 108 h respectively over the 9-km experiments with implicit convection. These differences in mean track errors are statistically significant at most forecast periods up to 72 h (all 10 TCs), 84 h (8 TCs), 96 h (6 TCs) and 108 h (3 TCs).

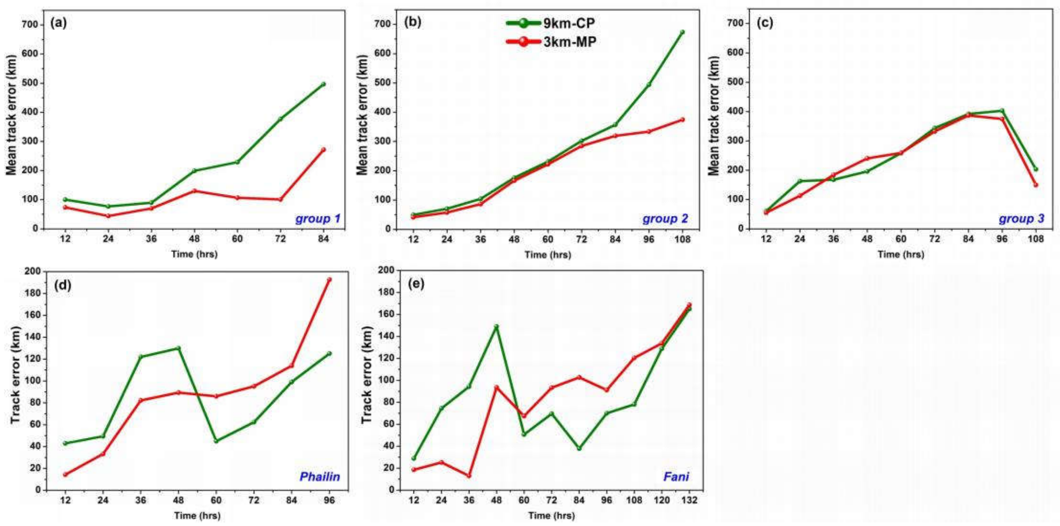

Figure 3.3. *Time variation of mean vector track errors with respect to IMD data for different homogenous groups of cyclones* ***(a)*** *group-1,* ***(b)*** *group-2,* ***(c)*** *group-3, and RI cyclones* ***(d)*** *Phailin,* ***(e)*** *Fani.*

The mean track errors for ten cyclones are presented in Table 3.3. It is observed that the 3km- MP consistently produced lesser errors compared to 9km-CP. The mean vector track error of all 10 cyclones (from Table 3.3) for the 9km-CP, 3km-MP experiments are (98 km, 67 km) at 24h, (163 km, 156 km) at 48h, (287 km, 208 km) at 72h and (327 km, 302 km) at 96 h respectively. The differences in track positions in the two simulations are likely due to the variation in the intensity of vortex at different stages and its interaction with largescale environment. TC motion is a result of interaction of complex internal and external factors, even though environmental steering is the most prominent mechanism.

Table 3.3. *Mean track errors computed from 3 hourly interval model outputs excluding the first 12-h spin-up period for 10 cyclones for 9km-CP and 3km-MP.*

Time (hrs)	Mean Track Error (km)	
	9 km	3 km
12	70.68	55.469
24	98.562	67.282
36	109.55	109.66
48	163.16	156.95
60	202.14	171.42
72	287.3	207.87
84	317.46	288.08
96	327.66	302.81
108	320.73	259.13

3.3.2. Relative vorticity tendency and tracks

Results from the previous section confirm that the tracks of the TCs are influenced by model horizontal resolution and convection physics. Changes in convergence and convection leads to changes in the extent of latent heat release which would modify the TC thermodynamical structure and the vertical wind shear. The altered convection would also modify the transport of heat and momentum between different vertical layers due to variation in the updrafts and downdrafts. This coupling of thermodynamical and dynamical processes would influence the prediction of TCs in baroclinic flow. The TC movement can be studied by vorticity which represents a coupling of the dynamic and thermodynamic variations (Chan, 1984, 2005; Marks, 2003). The relative vorticity tendency is given by the sum of contributions from horizontal advection of total vorticity (ζ+ f), vortex stretching, tilting by shear, and friction (Holton, 2004). Marks (2003) and Chan (2005) related the movement of the storm to the relative vorticity advection through the storm center. The earlier modelling studies on TCs over NIO (Hari Prasad, 2007; Srinivas et al., 2015) have shown that the horizontal advection and stretching terms mainly contribute for the net vorticity variation with the horizontal advection playing an overriding role. Microphysical parameterizations can affect the movement of cyclones by altering the temperature and pressure gradients affected by changes in diabatic heating and convection which are generated by small scale processes of cloud formation, growth and dissipation (refer section 3.3.4) which in turn influence the generation of winds and hence the advection of vorticity. Although a detailed vorticity budget analysis is not attempted in this study, the differences in the net vorticity between the two simulations for two extremely severe cyclones Hudhud and Phailin are provided.

The time evolution of maximum relative vorticity at 850 hPa averaged over a 2°×2° area around the centre of cyclones Hudhud and Phailin is presented in Figure 3.4. A progressive increase in vorticity during the growing phase (0000 UTC 08 Oct- 1200 UTC 10 Oct for Hudhud; 0000 UTC 09 Oct – 0009 UTC 11 Oct for Phailin) and a decrease during the decay and landfall are well represented in both the simulations. The 3km-MP produced higher relative vorticity all through the simulation. Further, the peak vorticity lasted longer in 3km-MP (30 h for Hudhud, 24 h for Phailin) relative to 9km-CP (12 h each for Hudhud and Phailin) indicating a longer sustenance of intense cyclonic activity in 3km-MP compared to 9km-CP. The stronger vorticity in 3km-MP can be related to a stronger frictional flow convergence in the boundary layer, stronger tangential and radial winds, higher core warming and vertical motion (refer sections 3.3.4, 3.3.5) through coupling of thermodynamics and dynamics.

The relative vorticity distribution along with flow field at 850 hPa during peak intensification of Hudhud and Phailin is presented in Figure 3.5. For both the cyclones, the 3km-MP (Fig. 3.5b, d) produced a stronger vorticity (800-900 x 10^{-5} sec^{-1}) relative to 9km-CP (300-400 x 10^{-5} sec^{-1}) with smaller and well-defined inner core structure indicating higher stretching effect. The stronger vorticity is related to stronger frictional convergence

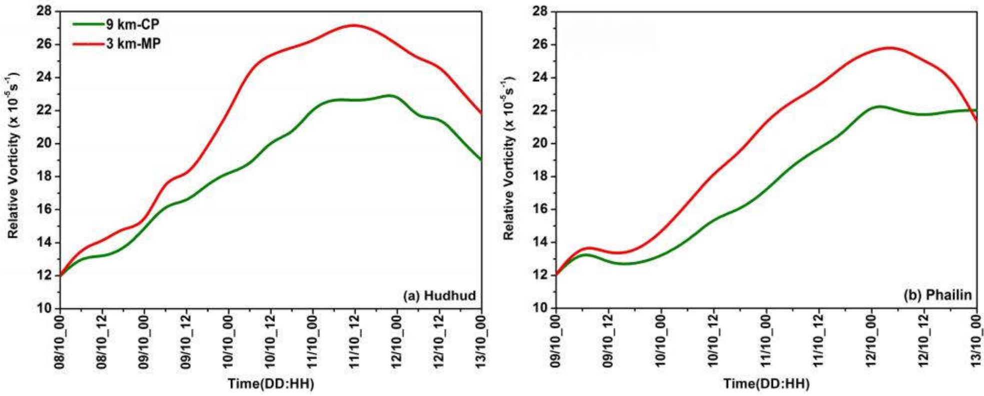

Figure 3.4. *Time evolution of simulated maximum relative vorticity (x 10^{-5} s^{-1}) at 850 hPa averaged over 2°×2° from the centre of* ***(a)*** *Hudhud and* ***(b)*** *Phailin. The time labels on the x-axis are DD for day and HH for hour.*

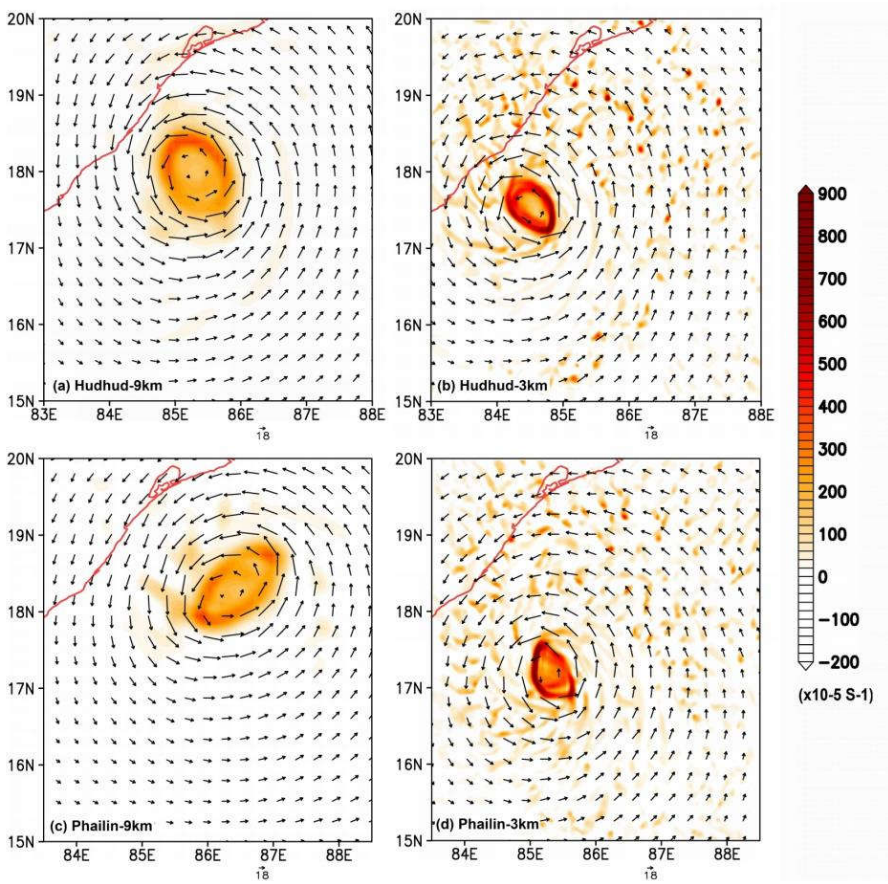

Figure 3.5. *Spatial distribution of relative vorticity (x 10^{-5} s^{-1} in shaded contours) and wind vectors at 850 hPa during peak intensification for* ***(a, b)*** *Phailin and* ***(c, d)*** *Hudhud for* ***(a, c)*** *9km-CP and* ***(b, d)*** *3km-MP.*

of air in the boundary layer and it is associated with lower theta-e in the middle layers and stronger vertical motions (refer section 3.3.4). The smaller core in 3km-MP indicates higher stretching effect relative to 9km-CP. The vortex of Hudhud is stretched horizontally in southeast- northwest sectors in 9km-CP and east-southeast–west-northwest sector in 3km-MP. The net positive vorticity is concentrated in the northwestern sector in 9km-CP and west-northwest sector in 3km-MP indicating higher vorticity gradients and thus the cyclone moved in those respective directions in the two simulations. In the case of Phailin the vortex is stretched horizontally in northeast-southwest sectors in 9km-CP and southeast-northwest sectors in 3km-MP. The net positive vorticity is distributed in the west sector in 9km-CP and west-northwest sector in 3km-MP thus enabling the cyclone to move in those respective directions in the two simulations. These results indicate that the net vorticity variation due to combined influences of advection by environmental flow, vortex stretching, Coriolis force resulted in changes in the direction of movement of the cyclone in the two simulations with different resolution and convection treatments. Further it is observed that the 3km-MP produced smaller landfall position errors (Table 3.4) over 9km-

Table 3.4. *Comparison of landfall position error with respect to IMD for 10 cyclones for 9km-CP and 3km-MP.*

TC	Error during Landfall position with respect to IMD (km)	
	9km-CP	3km-MP
Laila	180.49	127.3
Jal	195.4	102.91
Helen	534.79	198.08
Thane	310.63	242.79
Lehar	652.03	339.93
Vardha	390.74	346.63
Gaja	642.35	680.49
Phailin	111.85	179.61
Hudhud	190.74	106.53
Fani	92.06	301.76

CP for most of the cyclones except for Gaja, Phailin and Fani. The relative speed of movement of cyclones is analyzed and compared with IMD in Table 3.5. It can be found that in the case of Gaja, the 3km-MP produced relatively faster moving cyclones indicating stronger influence of environmental flow which resulted in the large simulated track errors by 3km-MP.

Table 3.5. *Comparison of speed of movement of cyclone computed at 6 hours for Phailin, Gaja and Fani between model and IMD.*

TC	**Time (hrs)**	**Speed computed at 6 hourly intervals (kmph)**		
		IMD	**Model**	
			9 km	**3 km**
Phailin	12	13.1	8.5	5.2
	24	13.1	9.5	13.2
	36	13.1	7.5	10.6
	48	20.7	19.7	14.0
	60	15.7	15.1	13.9
	72	13.1	16.2	17.0
	84	14.5	20.8	15.6
	96	19.3	22.0	20.5
Gaja	12	9.3	7.6	4.6
	24	5.6	23.7	12.7
	36	11.3	11.0	20.3
	48	5.9	26.9	13.5
	60	13.4	23.5	19.7
	72	14.5	28.0	29.0
	84	16.6	8.2	28.0
	96	20.5	16.3	5.0
Fani	12	20.94	9.261	4.5
	24	3.7	11.83	12.13
	36	17.075	11.12	18.8
	48	16.761	14.5	13.85
	60	22.6	15.61	13.17
	72	10.47	6.07	3.52
	84	13.48	17.74	10.55
	96	14.92	13.05	11.11
	108	14.81	18.17	13.54

3.3.3. Intensity predictions

The intensity of the cyclone is closely related to its CSLP and MSW speed. The MSW in a TC is a function of the radius of maximum wind and the local maximum pressure gradient (Atkinson and Holliday 1977).

The trends in intensity predictions are analyzed in different groups of cyclones in this paragraph. The mean CSLP and MSW errors (model value minus IMD value) at 12h forecast interval for the three groups of cyclones and RI cases are presented in Figures 3.6 and 3.7 respectively. Though the error trends are similar in general, the 3km-MP produced smaller errors compared to 9km-CP. Both 9km-CP and 3km-MP produced stronger simulated cyclones (-ve CSLP, +ve MSW errors) for group-1 and group-3 cyclones (Laila, Jal, Helen, Hudhud, Gaja) and weaker cyclones (+ve CSLP, -ve MSW errors) for group-2 (Vardah, Thane, Lehar). For group-1 (Fig. 3.6a) the mean CSLP errors in 3km-MP/9km-CP gradually increased from 2 at 12 h to -3 hPa/-11 hPa during intensification (48 h) and reduced to 4 hPa/5 hPa during decay and landfall stage (80 h). The mean MSW errors (Fig. 3.7a) correspondingly increased from 6 ms^{-1}/4 ms^{-1} at 12 h to 18 ms^{-1}/20 ms^{-1} during intensification (48 h) and reduced to +5 ms^{-1}/-8 ms^{-1} in 3km-MP/ 9km-CP during decay and landfall stage (80 h). This shows stronger cyclones in both 3-km and 9-km simulations during intensification and weaker cyclones during decay and landfall for group-1. We find that the 3km-MP produced consistently less CSLP and MSW errors during all the phases. For group-2 (Fig. 3.6b), the mean CSLP errors increased from -6 hPa/-8 hPa at 12 h to 9 hPa/9 hPa in 3km-MP/9km-CP during intensification (72h) and then varied as -5 hPa/-14 hPa during decay and landfall phase (96 h) indicating stronger simulated cyclones during growing and decay stages and weaker cyclones during peak intensification. The mean MSW errors (Fig. 3.7b) correspondingly varied as 35 ms^{-1}/22 ms^{-1} at 12h, -26 ms^{-1}/-35 ms^{-1} during intensification (72 h) and 18 ms^{-1}/22 ms^{-1} during decay and landfall (96h). For group-3 (Fig. 3.6c) the mean CSLP errors in 3km-MP/9km-CP increased from -3 hPa/-4 hPa at 12 h to -8 hPa/-6 hPa during intensification (84 h) and to 2 hPa/2 hPa during decaying and landfall stage. The mean MSW errors (Fig. 3.7c) decreased from 15 ms^{-1} to -5 ms^{-1} for 3km-MP and increased from 10 ms^{-1} to -25 ms^{-1} for 9km-CP from 12h to decay and landfall stages (84 h).

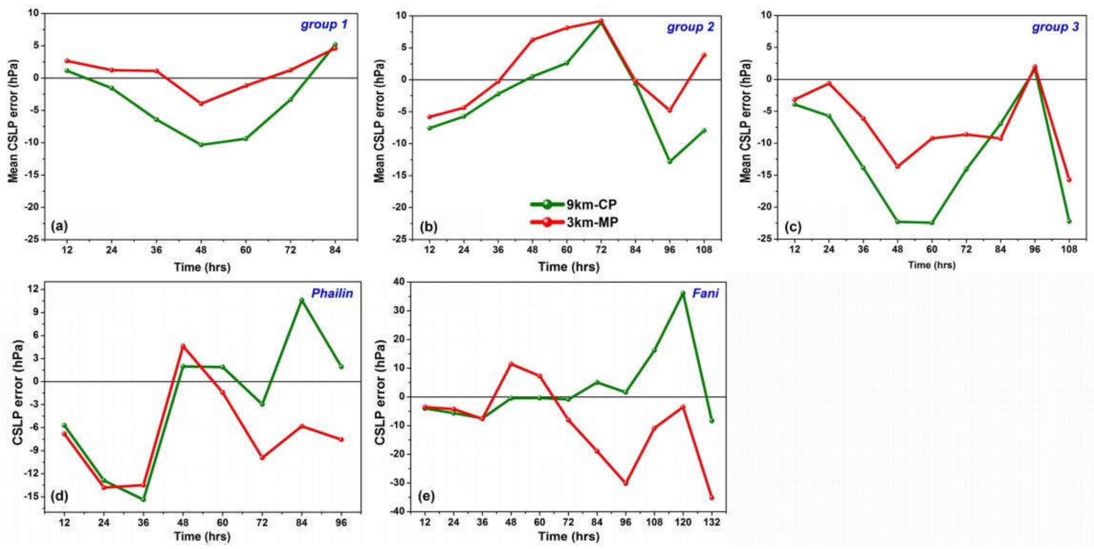

Figure 3.6. *Time variation of mean CSLP errors with respect to IMD data for different homogeneous groups of cyclones **(a)** group-1, **(b)** group-2, **(c)** group-3 and RI cyclones **(d)** Phailin, **(e)** Fani.*

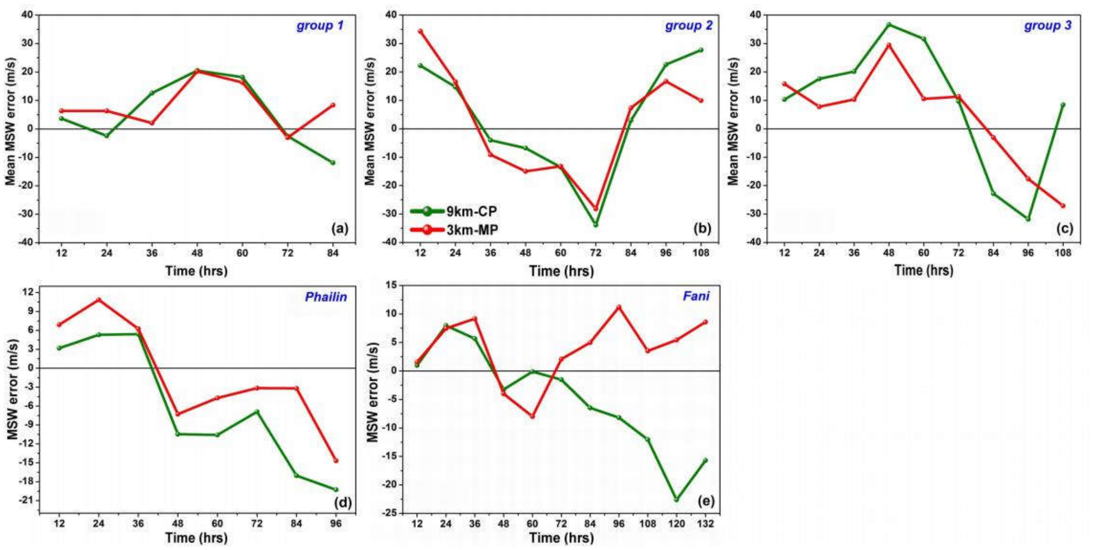

Figure 3.7. *Time variation of mean MSW errors with respect to IMD data for different homogeneous groups of cyclones **(a)** group-1, **(b)** group-2, **(c)** group-3 and RI cyclones **(d)** Phailin, **(e)** Fani.*

The 9km-CP produced relatively higher intensity during the growing phase of up to 48 h for group-1 (SCS with short period of intensification), 60 h for group-2 (VSCS moderate period of intensification), and 72 h for group-3 (VSCS and ESCS with very long period of intensification). However, it underpredicted the intensity during the peak and decay phases for group-2 and group-3 cyclones while giving almost similar intensity for group-3 as that of 3km-MP. Overall, the MSW prediction in 3km-MP with respect to 9km-CP is improved by 2-96% in group-1 and 55-43% in group-3 at 24-96 h forecast interval. However, for group-2 the MSW is under-predicted by -14 to -15% at 24-48 h but subsequently improved by 20-32% at 72-96 h interval. The intensity error differences are more in group-3 followed by group-2 and group-1 cyclones. For most of the cyclones, while the 9km-CP produced a higher intensity during the growing phase, the 3km-MP produced slightly higher intensity only during the peak intensification stage. For the RI cases (Phailin and Fani), the 3km-MP produced slightly higher intensification during the RI phase. For these RI cyclones, the MSW is improved roughly by 17-97% in 3km-MP over 9km-CP.

The mean absolute errors (model - IMD estimate) in CSLP and MSW at 12 hours forecast interval computed for the ten cyclones are presented in Table 3.6. The results show that 3km-MP consistently produced lesser CSLP errors from 12 h to 96 h when compared to 9km-CP. In the case of MSW from the time of intensification (36 h) 3km-MP showed lesser errors relative to 9km-CP. The 3-km experiment produced stronger simulated cyclone all through whereas the 9-km experiment initially produced stronger cyclone in the growing phase and a less intensive cyclone during the peak growth and dissipation phases. These results indicate that the 3 km domain produced the lowest errors in CSLP and MSW throughout the simulation for all cyclones studied. Overall, the MSW predictions are improved by 29%, 31%, 44%, 101% in 3km-MP over 9km-CP. The improved predictions by 3km-MP are due to better resolving the convection using high resolution and explicit cloud physics (Gopalakrishnan et al., 2012).

The radius of strongest winds from the center of the TC, termed as the 'radius of maximum winds' (RMW) is an important parameter relating the dynamics and structural aspects of the TC. The CIRA RMW estimates are used to evaluate the WRF predicted RMW. The procedure used in Zhang et al. (2011) and Gopalakrishnan et al. (2012) is followed here to evaluate the WRF predicted RMW from different groups of cyclones. The cumulative distribution function (CDF) of the RMW from WRF predictions at 6 h interval along with corresponding values from CIRA analysis are presented in Figure 3.8.

Table 3.6. *Mean CSLP and MSW errors computed from 3 hourly interval model outputs excluding the first 12-h spin-up period for 10 cyclones for 9km-CP and 3km-MP.*

Time (hrs)	Mean CSLP Error (hPa)		Mean MSW Error (m/s)	
	9 km	3 km	9 km	3 km
12	-3.654	-2.509	3.019	4.986
24	-5.147	-2.722	2.855	3.692
36	-7.67	-2.596	2.512	1.099
48	-8.008	-1.768	2.759	1.896
60	-7.03	0.0953	2.066	0.568
72	-1.581	0.4584	-2.883	-1.618
84	0.0051	-2.9	-3.744	1.952
96	-4.107	-2.637	-4.701	0.056
108	-15.09	-5.935	-3.916	-0.541

The slope of the CDF values indicates wide variation in the RMW between CIRA analysis and WRF predictions. For group-1 (Fig. 3.8a), as per the CIRA analysis, 70% of the observed RMW are distributed over 20-65 km. For the 9km-CP and 3km-MP simulations, 70% of the RMW are distributed over 25- 100 km and 30-250 km respectively. For group-2 (Fig. 3.8b), 70% of the observed RMW are distributed over 15-60 km. For the 9km-CP and 3km-MP simulations for this group 70% of the RMW are distributed over 40-90 km and 50-110 km respectively. For group-3 (Fig. 3.8c), 70% of the observed RMW are distributed over 15-55 km. For the 9km-CP and 3km-MP simulations for this group 70% of the RMW are distributed over 25-75 km and 40-150 km respectively. These results suggest that the storm size is successively reduced from group-1 (SCS) to group-3 (ESCS) and that the high resolution simulations (3km-CP) provide better storm size estimates compared to the low-resolution forecasts consistently in all the three groups. It can be seen that for both the RI cyclones (Phailin and Fani) (Figs. 3.8d, e), the 3km-MP produced smaller size compared to the 9km-CP and in better match with the observed RMW values.

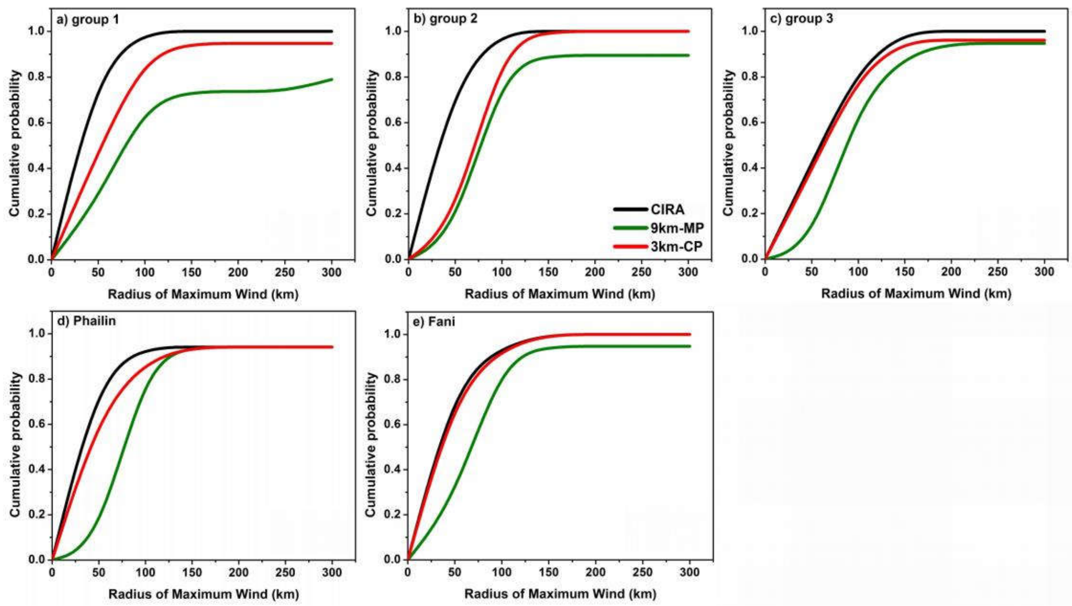

Figure 3.8. *Cumulative distribution function of RMW at 10 m above the ground compared with CIRA data for different groups of cyclones* ***(a)*** *group-1,* ***(b)*** *group-2,* ***(c)*** *group-3, and RI cyclones* ***(d)*** *Phailin,* ***(e)*** *Fani.*

Another important factor which controls the development and intensification of a TC is the vertical shear of horizontal wind. For TC to develop and to sustain its intensity the winds should be uniform vertically through the troposphere. Significant vertical differences in wind results in sweeping away of the latent heat carried aloft, and will not lead to a converging motion through considerable depth of the atmosphere favoring development of convection and warming. Mean absolute errors of WRF predicted deep layer (850-200 hPa) wind shears with respect to CIRA satellite derived estimates provided in Figure 3.9 show that, the 3km-MP produced lower wind shear differences compared to the 9km-CP for group-1 (Fig. 3.9a) and group-3 (Fig. 3.9c) cyclones but slightly higher errors during peak intensification for group-2 (Fig. 3.9b). For both the RI cyclones the 3km-MP produced slightly higher errors than the 9km-CP at the early stages (12-24 h) but during the intensification period (24-72 hrs) it produced considerably lower errors. These results suggest that the 3km-MP produced consistently lower shear for most of the cyclones indicating better prediction of wind shear and so the intensity.

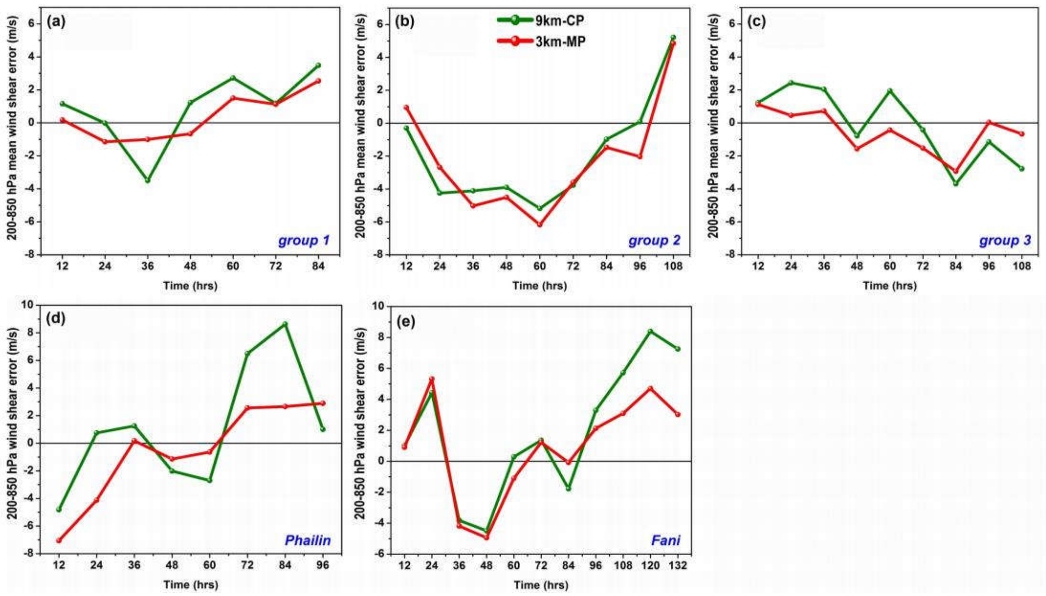

Figure 3.9. *Time variation of mean errors of deep layer (850 hPa-200 hPa) shear (m/s) with respect to CIRA data for different homogeneous groups of cyclones **(a)** group-1, **(b)** group-2, **(c)** group-3, and RI cyclones **(d)** Phailin, **(e)** Fani.*

3.3.4. Storm Dynamics and Thermodynamics

Results in the sections 3.3.1-3.3.3 indicate that the 3km-MP produced more realistic simulation of tracks as well as intensity than 9km-CP for different groups of cyclones. However, it produced slightly stronger cyclones compared to 9km-CP during peak intensification phases. The reasons for the differences are examined from the storm thermodynamical and dynamical characteristics in the following. Results are shown mainly for Hudhud and Phailin as mentioned in section 3.3.

The divergence, vertical velocity and radial wind fields are analyzed to examine the differences in the dynamics due to change in horizontal resolution and convection physics. The time evolution of divergence and vertical velocity at 850 hPa averaged over a 2°×2° area from the two simulations (Fig. 3.10) shows that the 3km-MP predicted a stronger convergence in the lower layers throughout the life-cycle of the storms relative to 9km-CP. The stronger convergence in 3km-MP is also associated with a stronger vertical motion relative to 9km-CP for both the cyclones.

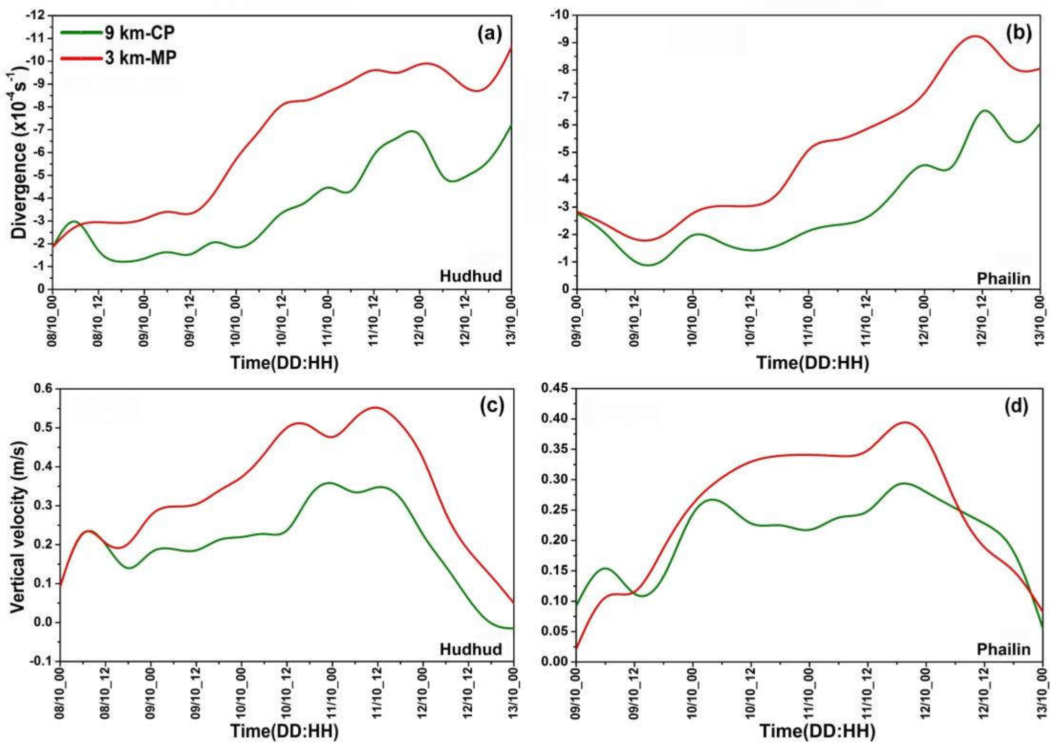

Figure 3.10. *Time evolution of simulated* ***(a, b)*** *divergence (x 10^{-4} s^{-1}),* ***(c, d)*** *vertical velocity (m/s) at 850 hPa averaged over 2°×2° from the centre of* ***(a, c)*** *Hudhud and* ***(b, d)*** *Phailin.*

The convergence/divergence, equivalent potential energy (theta-e) and vertical velocity fields averaged over a 2°×2° area around the center of Hudhud and Phailin cyclones during their peak intensification at different levels for both the cyclones are also presented in Figure 3.11. The divergence profile (Fig. 3.11a, b) indicates a stronger convergence in the lower layers and stronger divergence in the upper layers in 3km-MP compared to 9km-CP. Vertical distribution of theta-e suggests (Fig. 3.11c, d) formation of unstable layers in the lower atmosphere (below ~5 km) and stable layers in the upper atmosphere (above 6 km). It also shows a local minimum in theta-e in the mid-troposphere, suggesting development of dry region associated with subsidence into the eye. Relatively high theta-e values in the lower levels (0-1 km) and at upper levels (11–16 km) are found. The high theta-e in the lower levels is due to convergence of moisture towards the center of TC. Both the simulations produced a decreasing theta-e with height up to 4 km in 9km-CP and 6 km in 3km-MP and increasing theta-e further upwards. The vertical profiles of theta-e suggest formation of stronger and larger unstable convective layers in the lower troposphere (1-6 km for Hudhud and 1-5 km for Phailin) in 3km-MP compared to 9km-CP (2-5 km for Hudhud and 2-4 km for Phailin). The strength of the TC is characterized by the intensity of convective scale vertical motions. The updrafts/downdrafts occur in the vertical zone where inflows converge radially outward at about 2 kilometers from the horizontal wind maxima (Smith, 2006). The heating of the core will produce vertical motions (updrafts) and this facilitates an enhanced low-level moist radial inflow. Stronger vertical motions will lead to stronger vertical transport of mass flux leading to more convective warming and consequently a more intense cyclone. Also, the structure of the diabatic heating is controlled by the structure of the vertical velocity. The simulated vertical velocities for both cyclones (Fig. 3.11e, f) steadily increased from 2 km upwards, the 3km-MP produced more rapid increase compared to 9km-CP. For both the cyclones

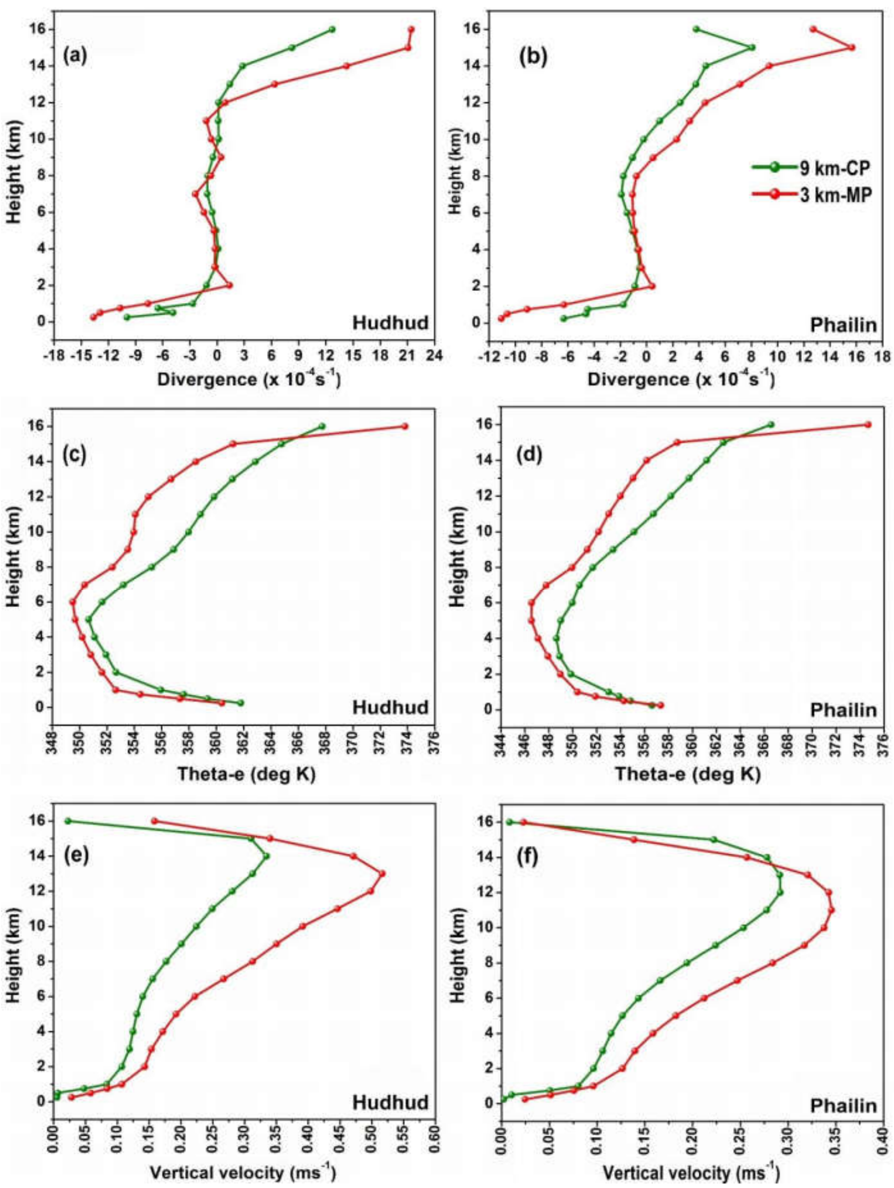

Figure 3.11. *Vertical profiles of simulated* ***(a, b)*** *divergence (x 10^{-4} s^{-1})* ***(c, d)*** *theta-e (K) and* ***(e, f)*** *vertical velocity (m/s) averaged over an area of 2°×2° from the centre of* ***(a, c, e)*** *Hudhud and* ***(b, d, f)*** *Phailin at peak intensification.*

the 3km-MP predicted the higher updraft velocities (52 cm/s for Hudhud, 35 cm/s for Phailin) relative to 9km-CP (33 cm/s for Hudhud, 28 cm/s for Phailin) in the upper troposphere. The maximum updrafts occurred in the layer 12–14 km for Hudhud and 10-13 km for Phailin. The simulated vertical motions are in agreement with the degree of convective instability (Fig. 3.11c, d) produced in the two simulations. The high resolution simulations predicted stronger vertical motions by simulating highly convective atmospheres compared to 9km-CP. The stronger convergence in 3km grid (Fig. 3.11a, b) has led to stronger vertical motion (Fig. 3.11e, f) and higher moisture transport thus producing more heat of condensation (Gopalakrishnan et al., 2011).

Azimuthally averaged radial wind in the lower troposphere (up to 5 km) for Hudhud and Phailin during their peak intensification is analyzed (Fig. 3.12) to study the inflow/outflow characteristics. As shown in Figure 3.12, the 3km-MP produced a more intensified cyclone with well-defined core as compared to 9km-CP. A striking feature is that the central calm region (eye) is more clearly distinguishable in 3km-CP compared to the 9km-CP. The core of maximum radial winds is spread to a higher range (75 km for Hudhud and 70 km for Phailin) in 3km-MP than 9km-CP (55 km for Hudhud and 45 km in Phailin). The 3km-MP produced stronger inflow (-30 m/s, -22 m/s for Phailin) and stronger outflow (22 m/s for Hudhud, 7 m/s for Phailin) than 9km-CP (inflow -22 m/s; outflow 7 m/s for both Hudhud and Phailin). In both the cyclones the outflow begins from about 1 km upwards in 3km-MP and roughly 1.25 km upwards in 9km-CP. Chan and Chan (2015) suggested that the changes in inner core dynamics lead to differences in the inflow and outflow characteristics. A stronger TC in 3km-MP simulations is related to stronger upper level outflow which leads to a decrease in surface pressure and consequent rise in low-level inflow (Fig. 3.12b, d) near the inner core. The strong inflow in the boundary layer in 3km-MP leads to stronger outflow in the middle and upper troposphere which is generally observed in all the cyclones. Overall, the high resolution simulations with explicit convection (3km-MP) better produced the radial wind structure over the low-resolution 9km-CP. The stronger radial winds in 3km-MP are due to stronger convergence in the boundary layer ($\leq$ 2 km) and a stronger divergence in the upper troposphere (12-15 km) than 9km-CP (Fig. 3.12a, b) (Gopalakrishnan et al., 2011) which consequently produced stronger vertical motions (Fig. 3.12e, f).

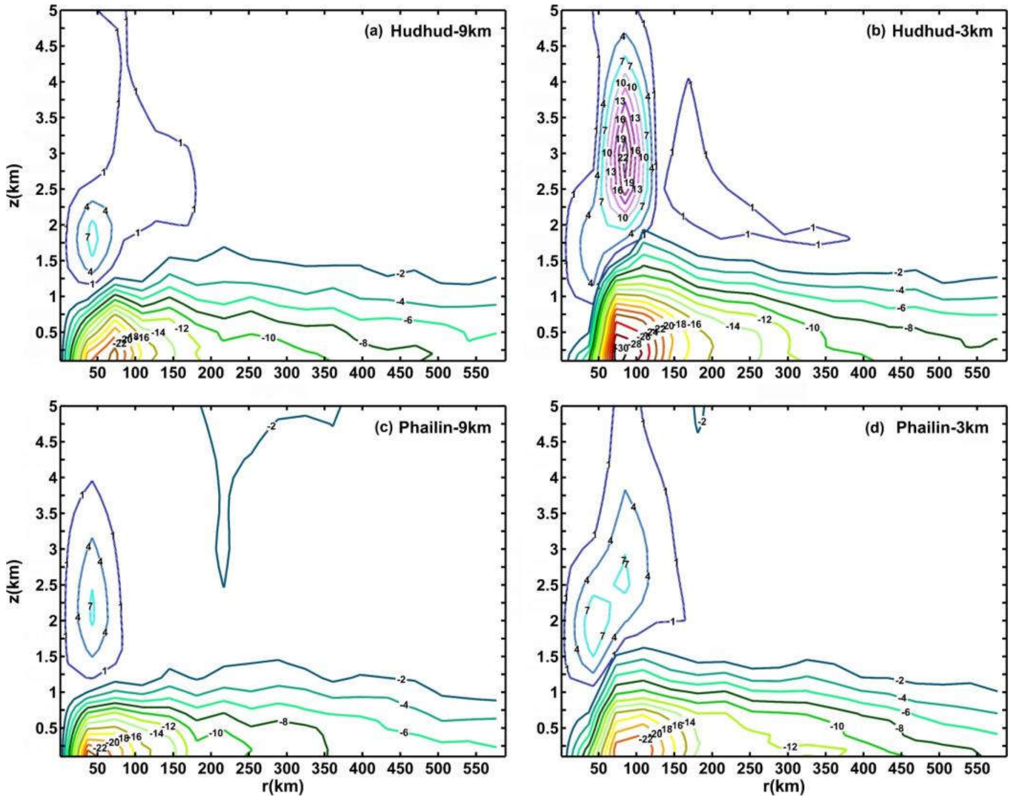

Figure 3.12. *Azimuthally averaged radius height cross section of radial wind (m/s) for* ***(a, b)*** *Hudhud and* ***(c, d)*** *Phailin at peak intensification for* ***(a, c)*** *9km-CP and* ***(b, d)*** *3km-MP.*

TCs are characterized by warming in the upper troposphere and cooling in the lower troposphere with time (Anthes, 1982). The warming in the upper layers in the core region is due to subsidence and condensation processes whereas the cooling in the lower layers is by evaporation and moisture convergence. These processes influence the coupling between the thermodynamics and dynamics, thereby affect the intensity of the system. The intensification of a TC is closely associated with the buoyancy produced by the collective effects of deep convection (Smith, 2006). The buoyancy is related to simulated diabatic heating and thus it is associated with moist convection (Zhang et al., 2007; Taraphdar et al., 2014) which controls the error growth in ultimately limiting the intrinsic predictability of TCs. Figure 3.13 shows the zonal variation of simulated diabatic heating with height at peak intensification for Hudhud and Phailin. This shows that the 3km-MP experiments predicted a more prominent core with more heating (6° C in 500-250 hPa in Hudhud; 4°C in 500-300 hPa in Phailin) extending to deeper layers relative to 9km-CP (3°C in 700-300 hPa in Hudhud; 2.5°C in 650-300 hPa in Phailin). The greater diabatic heating found in 3km-MP is attributed to stronger convergence, vertical motion and moisture transport and the stronger convectively unstable atmosphere predicted (Figure 3.13) producing more heat of condensation relative to 9km-CP. The higher diabatic heating over a deeper layer

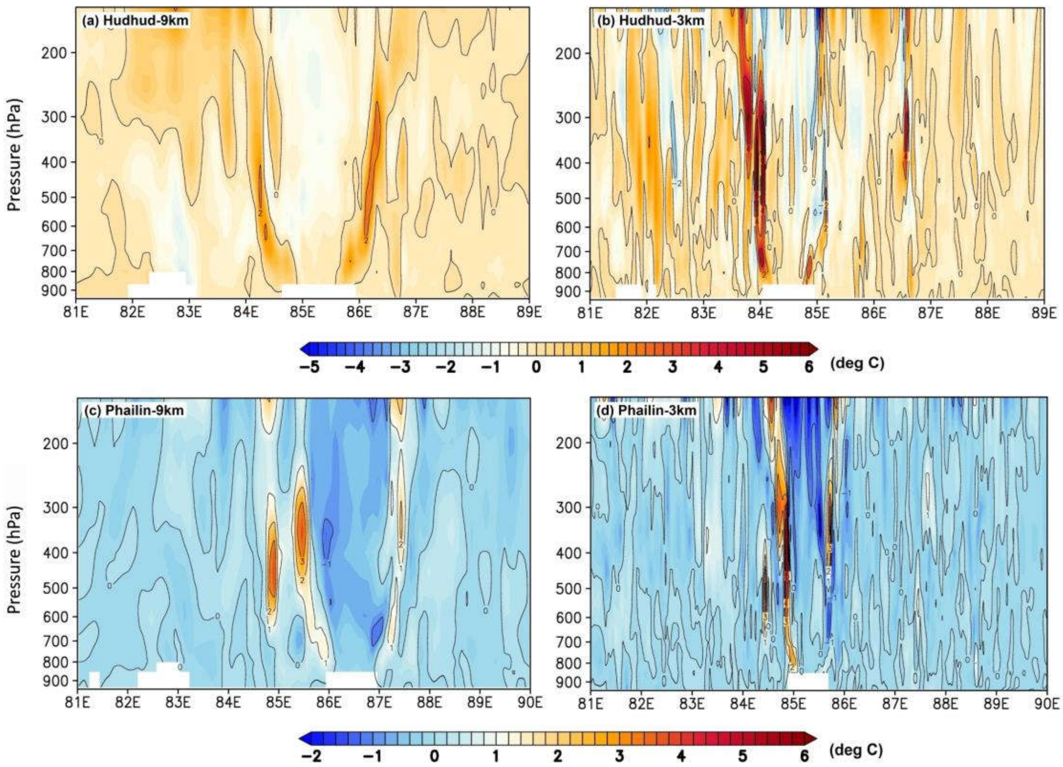

Figure 3.13. *Zonal variation of simulated diabatic heating (℃) with height for* ***(a, b)*** *Hudhud and* ***(c, d)*** *Phailin at peak intensification for* ***(a, c)*** *9km-CP and* ***(b, d)*** *3km-MP.*

compared to 9km-CP indicates a stronger simulated cyclone in 3km-MP relative to the 9km-CP. Similar results are also reported by Gopalakrishnan et al. (2012) for Atlantic hurricanes. The amount of water condensed and latent heat released in 9km-CP is determined in terms of grid-scale variables (e.g., by horizontal gradients of saturated moist entropy in the troposphere to largescale processes that produce CAPE, convective mass fluxes etc.) without considering the details of individual clouds whereas in 3km simulation convection is explicitly resolved and the distribution of diabatic heating depends on the phase changes (Stern and Nolan, 2012). Thus, both increased resolution and microphysics lead to higher diabatic heating in 3km-MP.

The two most common variables used to characterize the warm core are its strength defined by the magnitude of the maximum deviation in temperature (also called thermal anomaly or warming) and its vertical extent (Stern and Nolan, 2012). An increased core warming would lead to a more intensified cyclone by enhancing the convection. Azimuthally averaged radius-height section of warming produced during the peak intensification phase for Hudhud and Phailin cyclones relative to the initial time along with the CIRA observation is presented in Figure 3.14. As compared to the 9km-CP (Fig. 3.14a, d), the radius of the warm core has increased in the 3km domains (Fig. 3.14b, e). The maximum warming in the simulations for Hudhud is 10°C in the 9km-CP and 11°C in 3km-MP against the CIRA estimate of 7°C. The warming extended to a deep vertical layer 4-15 km in 9km-CP and 4-16 km in 3km-MP against the 7-13 km warm layer in the CIRA estimates. Similarly, the region of strong warming (as shown by contour of 5°C) extended radially up to 60 km in 9km-CP and 130 km in 3km-MP against the CIRA data of 150 km. Compared to the simulated thermal structure, the analyzed CIRA data indicates smooth temperature profiles. The highest warming in the simulations for Phailin was 9°C in 9km-CP and 11°C in 3km-MP against the CIRA value of 8°C. The vertical extent of warming is 4-15 km in 9km-CP and 4-17 km in 3km-MP against the 9-13 km layer in CIRA estimates. The region of intense warming (≥ 5°C) extended horizontally up to 60 km in 9km-CP and 100 km in 3km-MP against the CIRA estimate of 125 km. These results indicate that the cyclone thermal structure could be better predicted by the features of warming found in CIRA estimates, the extent of warm core and its strength are better simulated by 3km-MP. The stronger and deeper warming in 3km-MP is partly related to the higher diabatic heating (Fig. 3.13) produced by the latent heat released by convection and condensation in the eye wall.

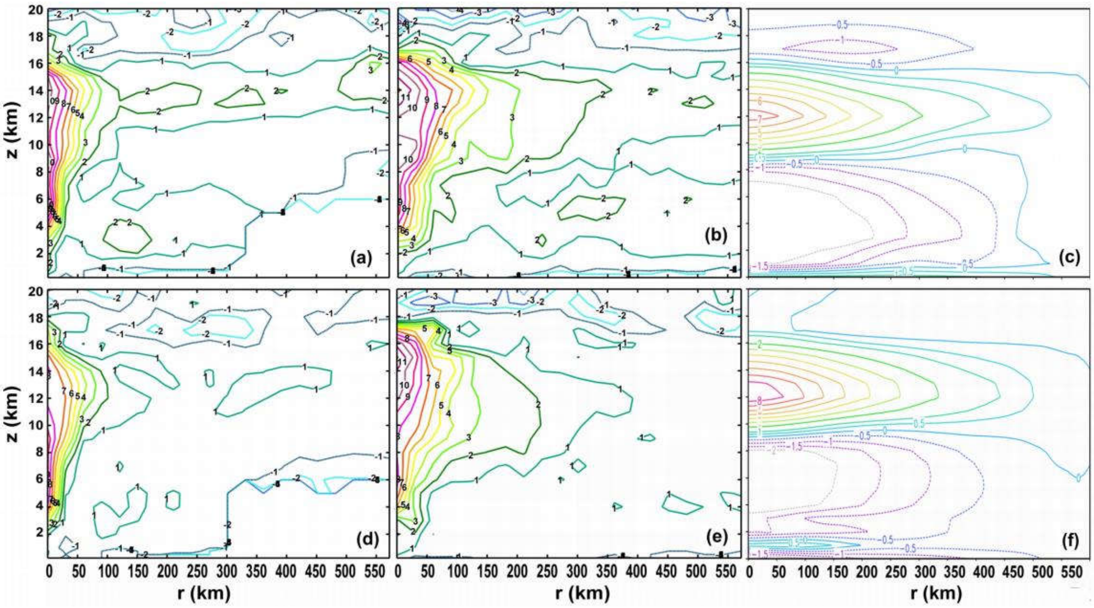

Figure 3.14. *Azimuthally averaged radius height cross section of temperature anomaly (°C) for* ***(a-c)*** *Hudhud and* ***(d-f)*** *Phailin at peak intensification relative to the initial time for* ***(a, d)*** *9km-CP,* ***(b, e)*** *3km-MP compared with* ***(c, f)*** *CIRA data.*

Figure 3.15 shows the differences in the thermal anomaly at 300 hPa layer in the 9 and 3 km simulations for Phailin and Hudhud. It is apparent that for the 9km-CP simulation, the Kain Fritsch convective parameterization provides more heating in the first 40-h period for both the cyclones relative to the microphysics in 3km-MP. This heating difference is more for the RI cyclone Phailin (~2 C) compared to the Hudhud (~1 C). During the peak intensification and decay phases the heating produced in the 3km-MP is nearly 2°C more than the 9km-CP. These variations of thermal anomaly differences between the 3km and 9 km simulations in different phases are generally noticed for all the cyclones, except that the warming differences are more for the RI cyclones (Phailin and Fani). The higher heating produced by convective parameterization during the intensification period in 9km-CP and microphysics during peak intensification phases explain the different intensification characteristics in different phases in the two simulations.

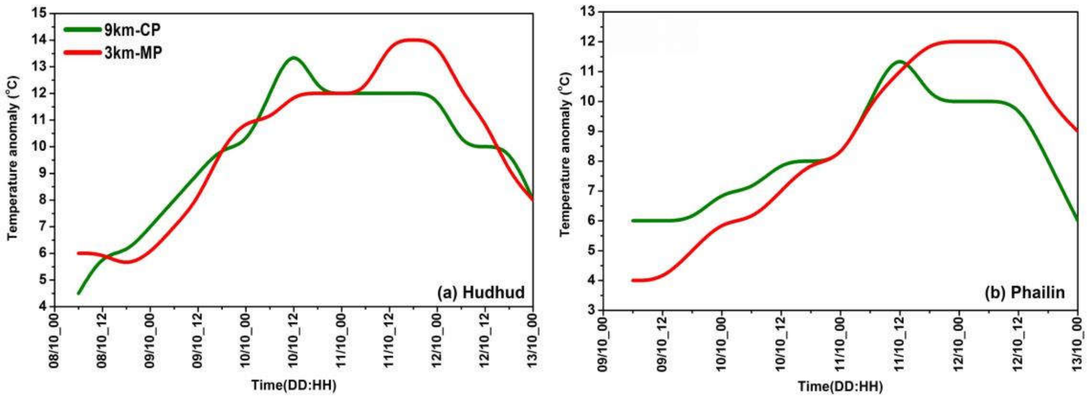

Figure 3.15. *Time evolution of simulated temperature anomaly (°C) at 300 hPa over 2°×2° area from the centre of* ***(a)*** *Hudhud and* ***(b)*** *Phailin.*

3.3.5. Wind flow structure

WRF simulated surface wind flow pattern is compared with the CIRA surface wind analysis (Fig. 3.16) during peak intensification of Hudhud and Phailin. As shown in the figure the CIRA wind data indicates intense cyclonic storms with maximum winds of up to 80 knots (~41 ms^{-1}) in the core region for Hudhud (Fig. 3.16c) and of 110 knots (55 ms^{-1}) for Phailin (Fig. 3.16f) and winds decreasing gradually away from the core. The simulated storms are little advanced relative to the positions indicated in CIRA towards the coast in both the simulations, approximately to the west in 3km-MP and northwest in 9km-CP due to difference in the predicted movement. While the strength of the winds in the core region for both the cyclones is more realistic in the 3km-MP (80 knots for Hudhud; 110 knots for Phailin), it is underestimated in 9km-CP (65 knots for Hudhud; 95 knots for Phailin). As explained by Fovell et al. (2016) the microphysical processes like phase changes, condensation can modulate inner core diabatic heating, temperature and pressure gradients which in turn influence the strength and breadth of winds. The band of strongest tangential winds is predicted at higher radial distance (60 km, 100 km in 3km-MP, 9km-

CP against 40 km in CIRA for Hudhud; 45 km, 70 km in 3km-MP, 9km-CP against 30 km in CIRA for Phailin) relative to the CIRA. The relatively small RMW of the storms as noticed from CIRA is well simulated by 3km-MP indicating the storm size better represented in it. The differences in storm structure between simulations and CIRA are due to position errors relative to the coastline, and related wind field differences resulting from land surface friction. These differences are more predominant in 9km-MP which predicted more proximity of the storm to the coastline. These results suggest that the structure of the winds in the cyclone core and intensity are better simulated by 3km-MP than 9km-CP. The variation in the position of the cyclones in the two simulations is attributable to the differences in the storm scale dynamics discussed earlier.

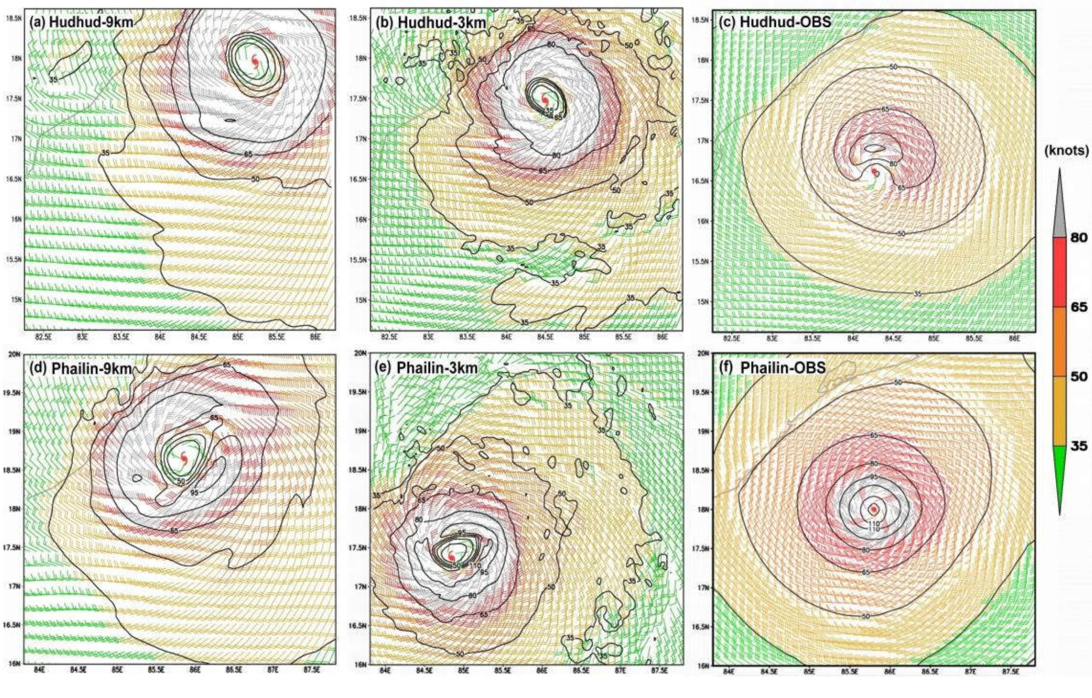

Figure 3.16. *Simulated surface wind field for* ***(a-c)*** *Hudhud and* ***(d-f)*** *Phailin at peak intensification for 9km-CP* ***(a, d)*** *and* ***(b, e)*** *3km-MP compared with* ***(c, f)*** *CIRA analysis.*

The temperature distribution in a TC is related to the tangential wind distribution through thermal wind balance (Willoughby, 1990). Figure 3.17 provides azimuthally averaged radius-height cross section of tangential winds for Hudhud and Phailin during peak intensification along with CIRA estimates. As compared to the CIRA estimates (Fig. 3.17c, f) both simulations (9km-CP, 3km-MP) slightly overestimated the tangential winds. Since the analyzed CIRA data is at 25 km × 25 km resolution it may under-represent the strength of actual cyclone. As in the case of core warming it is noticed that the core of maximum winds is simulated to a higher range in 3km-MP relative to 9km-CP. The core of maximum tangential winds (45 m/s) in CIRA analysis for Hudhud (Fig. 3.17c) extended radially up to 110 km and vertically up to 11 km. Tangential winds of 45 m/s simulated in 3km-MP, 9km-CP extended radially up to 100 km, 50 km and vertically up to 10 km, 5 km respectively indicating better representation of winds in 3km-MP relative to 9km-CP. The larger core with stronger winds (60-65 m/s) in 3km-MP compared to relatively smaller core with 55-60 m/s in 9km-CP indicates stronger simulated cyclone in 3km-MP. Similar results are noticed for Phailin cyclone (Fig. 3.17d-e) as well, except that both the simulations indicate less strong and smaller core of tangential winds relative to the CIRA estimate. An important result is the 3km-MP produced slightly more intensive and bigger

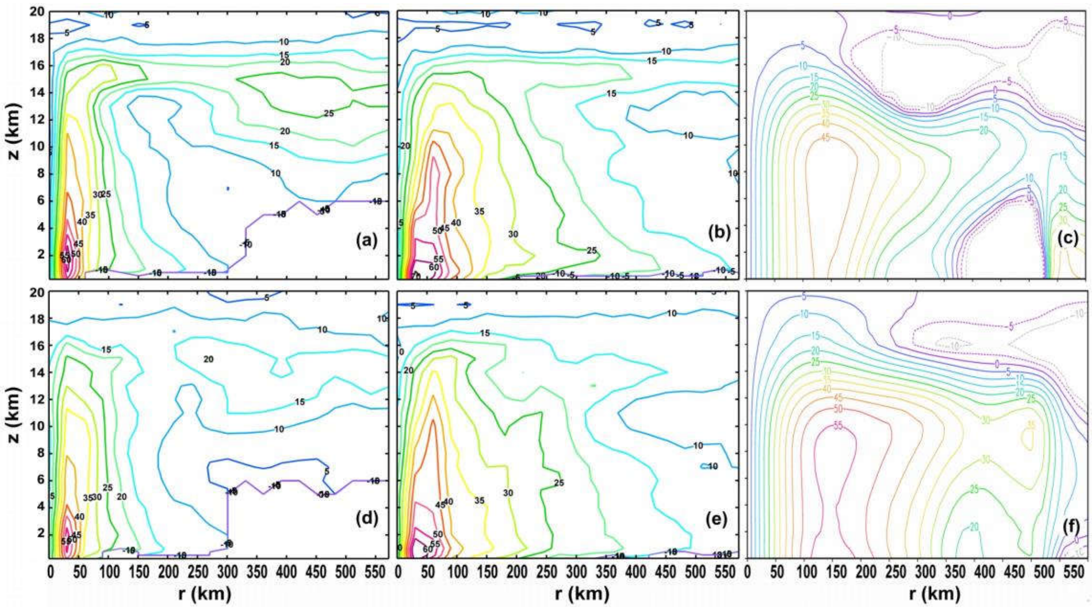

Figure 3.17. *Azimuthally averaged radius height cross section of tangential wind (m/s) for* ***(a-c)*** *Hudhud and* ***(d-f)*** *Phailin at peak intensification for* ***(a, d)*** *9km-CP,* ***(b, e)*** *3km-MP compared with* ***(c, f)*** *CIRA data.*

core of tangential winds indicating stronger simulated cyclones than 9km-CP. Wang et al. (2009) and Wang (2012) suggested that a greater diabatic heating in rainbands produces stronger inflow in the lower levels and stronger outflow in the upper levels (Fig. 3.12), with stronger upward motion outside the eyewall. The stronger inflow in the lower troposphere in 3km-MP results in stronger inward transport of angular momentum leading to stronger spin up of the tangential wind near the eyewall and consequent increase in TC intensity. Here we observe that the structure of the tangential winds is only slightly influenced by the microphysics and only the higher grid resolution is responsible for the structure, since the low-resolution has also predicted the intense winds. Similar to the results of warm core, the 3km-MP simulations predict the tangential wind distribution in better agreement with CIRA estimates compared to 9km-CP in terms of location of maximum winds and their vertical extension.

3.3.6. Radar reflectivity

Simulated maximum cloud reflectivity during peak intensity stage of Hudhud and Phailin (Fig. 3.18) indicate stronger storms relative to DWR observed storms in terms of areas of deep convection and rainfall distribution (Fig. 3.18c, f). The DWR data for Hudhud shows higher reflectivity in the western sectors, followed by southern and southeastern sectors. In the simulations the reflectivity on the western portion of eyewall is underestimated and that on the southern sectors are overestimated, especially in 9km-CP. The relatively low simulated reflectivity in the western parts is due to larger wind shear and high reflectivity in the southern sectors is by stronger warming, vertical motion and development of deep convection. The reflectivity for Hudhud, though slightly over estimated, is better predicted in 3km-MP. Similar results are found for Phailin. As seen from Figure 3.18, the structure and morphology of cloud bands are better represented in the 3km-MP compared to the 9km-CP. The 3km-MP indicates clusters of cloud bands indicating mesoscale convective organization which is smoothed out in the 9km-CP. This indicates that high resolution simulations would be useful in identifying the areas of deep convection and heavy rainfall more precisely thus giving advantage for disaster management than the coarse domain simulations.

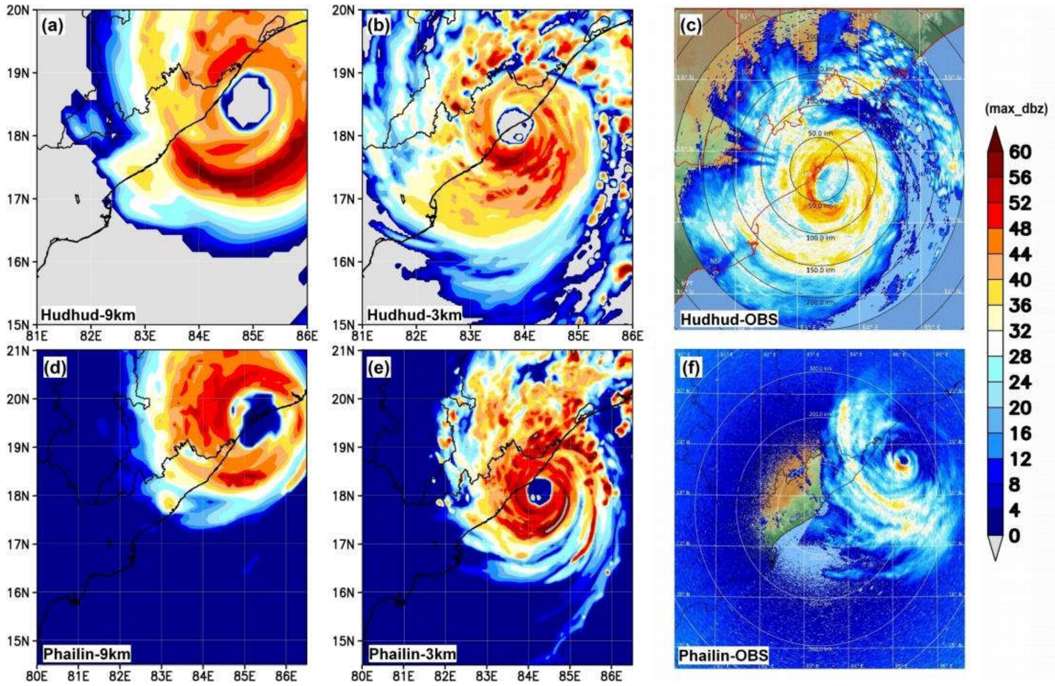

Figure 3.18. *Spatial distribution of simulated maximum radar reflectivity for* ***(a-c)*** *Hudhud and* ***(d-f)*** *Phailin at peak intensification for* ***(a, d)*** *9km-CP,* ***(b, e)*** *3km-MP compared with* ***(c, f)*** *DWR, IMD.*

3.4. Summary

In this chapter impact of convection permitting high resolution simulations on the track and intensity prediction of ten severe tropical cyclones in the BOB of NIO region using WRF-ARW model is examined. The results show that 3km-MP using explicit convection produced the best predictions for both intensity and track. The track errors in 3km-MP are reduced by 31%, 5%, 28% and 8% at 24h, 48h, 72h and 96h forecast intervals respectively over 9km-CP. The 9km-CP produced relatively weaker vorticity thereby the TC experienced stronger environmental steering force thus leading to northward deviating tracks and higher error compared to the 3km-MP which produced stronger vorticity. The

3km-MP produced significant improvements in intensity forecasts. Overall, the errors are reduced by 47%, 78%, 128%, 36% for CSLP and 29%, 31%, 44%, 101% for MSW at 24, 48, 72 and 96 h respectively in 3km-MP over 9km-CP. The study shows that the 9km-CP produced relatively higher (lower) intensity during the growing phases (peak and decay phases) for all cyclones due to producing higher (lower) thermal anomaly than the 3km-MP during growing phase indicating different impacts of cumulus and microphysics in the respective phases. Various structural characteristics of the TCs (RMW, surface winds, thermal anomaly, radial winds, cloud reflectivity etc.) though slightly overestimated relative to 9km-CP during peak growth, they are better represented in the 3km-MP as seen from comparison with CIRA multi-satellite cyclone products. Overall, the increased resolution of 3km-MP better resolved the inflow, convergence and updrafts and also produced higher diabatic heating due to explicit treatment of cloud microphysical processes and therefore shows improvements over low-resolution simulations using cumulus parameterization.

Chapter 4

Sensitivity of microphysics in the high resolution simulation of a tropical low pressure system

4.1. Introduction

In this chapter the relative sensitivities of various cloud microphysical parameterization schemes in the simulation a tropical low pressure system over the southwest BOB that produced heavy rainfall over north-coastal Tamilnadu, Chennai and surrounding areas are examined, using the WRF-ARW model. In a recent WRF simulation of the event, Srinivas et al. (2017) showed that the distribution and location of maximum rainfall were better predicted using a high resolution (1-3 km) with explicit convection due to better representation of the mesoscale upper air circulation and associated low-level moisture convergence. Hence, this low pressure system is simulated employing a high resolution of 1-km to study the representation of convection and rainfall using various mixed-ice-phase cloud microphysics schemes. Based on the sensitivity results the microphysics schemes are further used in the next chapter (Chapter 5) for TC prediction.

4.2. Methodology

The WRF-ARW model v.3.4 is used for the simulations. The model is configured with four interactive nested domains (Fig. 4.1) with 51 vertical levels with model top at 10 hPa. The outer domain is configured with 27 km resolution. The second, third, and fourth domains have horizontal resolution of 9, 3, and 1 km respectively. The simulations are initialized at 00 UTC 30 November 2015 and the model is integrated till 00 UTC 2 December 2015 (72 hours). The initial and boundary conditions for the simulations are obtained from NCEP-GFS 0.25° × 0.25° analysis and the boundary conditions are updated every 3 hours with the GFS forecasts. The model physics options including the six microphysics schemes used for the simulations are provided in Table 4.1. In the inner domains 3 and 4, only microphysics is employed and no convective parameterization is used. Five numerical experiments with five different microphysics parameterization schemes are performed, keeping all other physics options same. In the present study, both single and double-moment schemes are used.

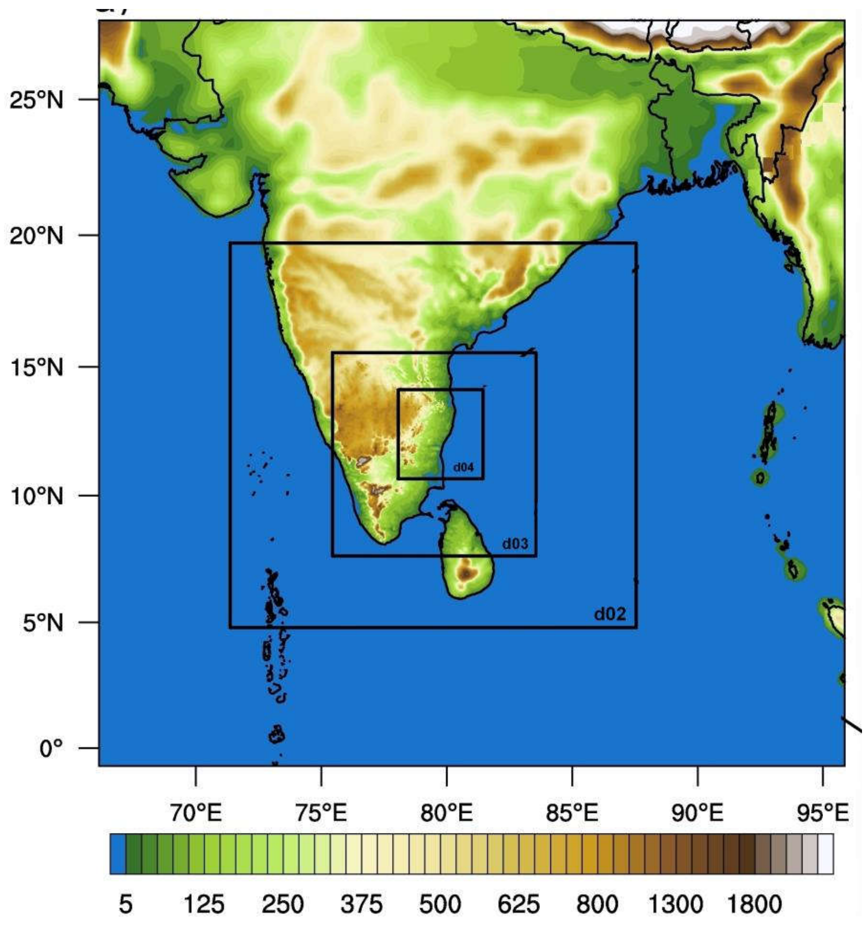

Figure 4.1. *Simulation domains used for the study with terrain height (m).*

The Chennai DWR data images are used for comparison of model cumulative rainfall and the hourly rainfall analysis are compared with the Automatic Weather Station (AWS) observations of IMD.

Table 4.1. *Model physics used for the study.*

Physics	Scheme
Longwave radiation	RRTMG (Mlawer et al., 1997; Clough et al., 2005)
Shortwave radiation	RRTMG (Mlawer et al., 1997; Clough et al., 2005)
Surface layer	MM5 similarity theory
Land surface processes	Noah LSM (Chen and Dudhia, 2001; Tewari, 2004)
Planetary boundary layer	MYNN level 2.5 (Nakanishi and Niino, 2004)
Cumulus	Kain Fritsch (Kain and Fritsch, 1993)
Microphysics	1. Morrison double moment (Morrison et al., 2009) 2. Lin (Lin et al., 1983) 3. WSM3 (Hong et al., 2004) 4. WSM6 (Hong and Lim, 2006) 5. New Thompson (Thompson et al., 2008) 6. Goddard (Tao and Simpson, 1993; McCumber et al., 1991)

4.3. Results and Discussion

All the analyses are carried out for 1 December, since the maximum rainfall was recorded on this day. Flow field at different levels, rainfall and thermodynamic parameters and hydrometeors are analyzed from simulations using different microphysics in the following.

4.3.1. Wind flow analysis

Simulated wind field and geopotential at 925 hPa and 500 hPa at 12 UTC of 1 Dec 2015 are analyzed for Morrison, Lin and Thompson schemes (Fig. 4.2). Since simulated wind field and geopotential for WSM3 WSM6 and Goddard schemes are similar to the Lin scheme they are not shown separately. Simulations indicate a cyclonic flow in the region of low pressure trough along the north coastal areas and extending vertically up to mid-tropospheric levels (500 hPa) with some differences in the location of the low-pressure trough among the three microphysics schemes. For Morrison and Lin, the position of trough is located over the ocean, whereas for Thompson, the axis of the trough is along the coast but slightly south of Chennai. The Thompson scheme also predicted high relative

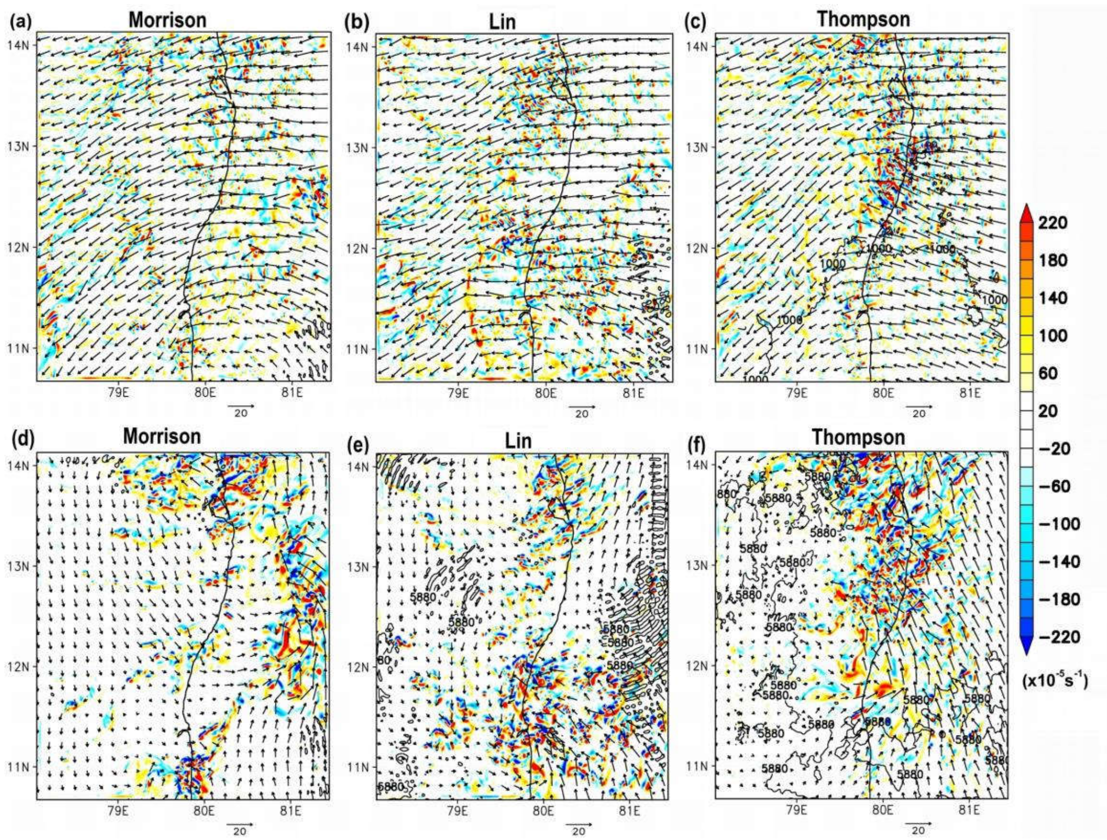

Figure 4.2. *Geopotential (m, in contours) and relative vorticity (x $10^{-5}s^{-1}$, shaded) for 1 Dec 2015 at 12 UTC from 1-km domain simulations with different microphysics schemes. Top panels* ***(a-c)*** *are for 925 hPa and bottom panels* ***(d-f)*** *are for 500 hPa.*

vorticity values (180-220 x $10^{-5}s^{-1}$) relative to the Morrison and Lin over Chennai. The lower to mid-tropospheric cyclonic circulation associated with concentration of high relative vorticity is simulated around Chennai and adjoining southern coastal areas (13.12°N - 12.75°N) for Thompson, over north Chennai (13.5°N) for Morrison and near Podicherry-Cuddalore (11.25-12.0°N) for Lin, WSM3 and WSM6 simulations. The cyclonic circulation is simulated slightly inland of Chennai and adjoining coastal areas in the case of Thompson. This simulation also shows strong surface winds and convergence on the right quadrant of cyclonic flow, resulting in heavy rainfall over the area.

The previous studies (Srinivas et al., 2017) showed that the low pressure is associated with strong moisture convergence in the lower atmosphere. Integrated lower tropospheric moisture convergence in the layer 1000- 850 hPa at 12 UTC is shown in Figure 4.3. It can be seen that the Morrison, Lin, WSM6, and Thompson predicted high

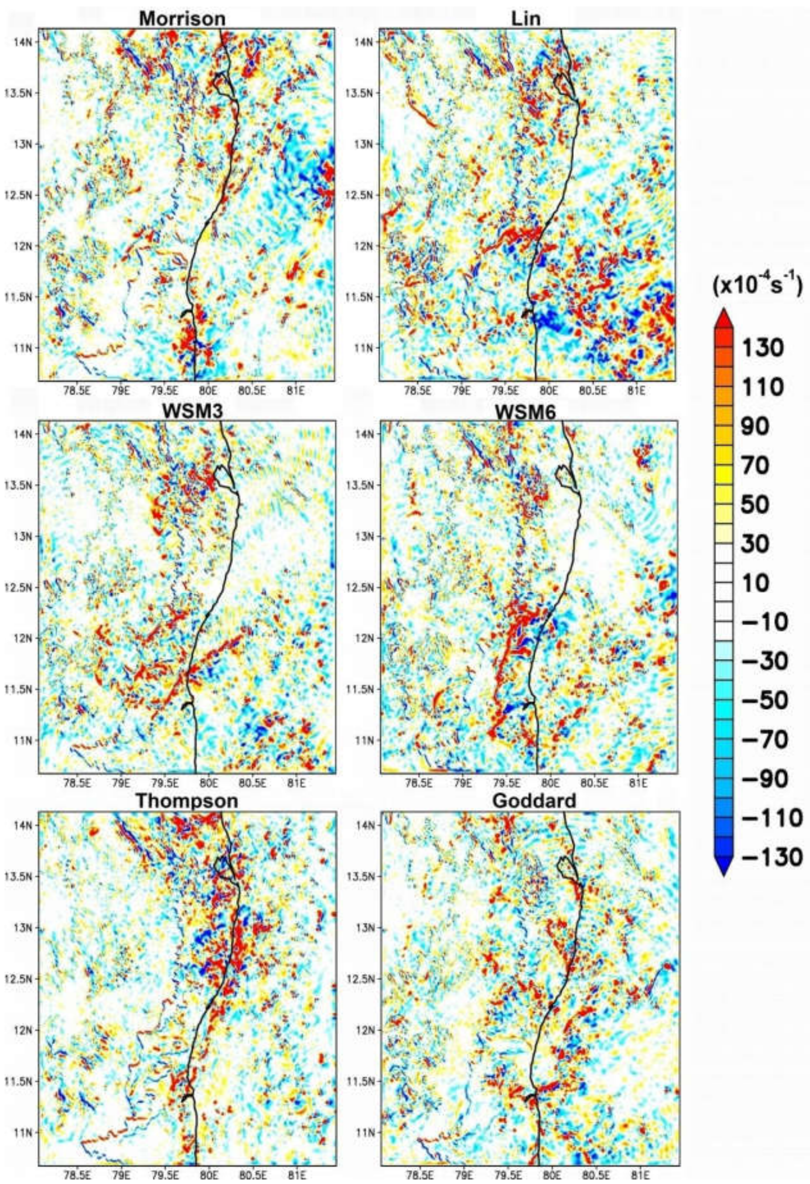

Figure 4.3. *Spatial distribution of integrated lower tropospheric moisture convergence (x 10^{-4} s^{-1}) at 12 UTC of 1 Dec 2015 by different microphysics schemes.*

values of moisture convergence (130 x $10^{-4}s^{-1}$), but at different locations. For Morrison, the convergence can be observed over the ocean and far away from the coast. The Lin scheme simulated a large area of moisture convergence but over the ocean near to the southern coastal areas of Chennai. The WSM6 scheme produced notable convergence inland but far south of Chennai i.e., along the coasts of Puducherry and Cuddalore. It is noted that the Thompson scheme simulated strong moisture convergence over south of Chennai and the adjoining coastal areas in good agreement with the spatial rainfall pattern. The differences in the circulation, convergence and vorticity features among different microphysics simulations are due to the changes in the atmospheric warming by diabatic heating and consequently, the circulations through coupling between thermodynamics and dynamics that ultimately impacts the rainfall. These features are discussed in the following sections.

4.3.2. Rainfall prediction with different microphysics schemes

The spatial simulated 24-hour cumulative rainfall for 1 December is shown in Figure 4.4 along with corresponding DWR precipitation estimates. This shows that the simulation with Thompson better reproduced the rainfall pattern with maximum rainfall over Chennai and the adjoining southern coastline. Simulations with Morrison and Lin, produced high rainfall (250-340 mm) distributed over the ocean rather than over the land area. The WSM3, WSM6 and Goddard schemes simulated less amount of rainfall among all the other schemes.

Figure 4.5 depicts the time series of hourly rainfall at Chennai (13.1°N, 80.2°E) predicted by the six microphysics schemes. From the results, it is noted that Thompson, though overestimates the rainfall (45 mm, 70 mm against 20 mm and 35 mm at 11 UTC and 13 UTC respectively), reproduces the timing of peak rainfall (09UTC to 15UTC) in better agreement with the observations. While the observations indicate an extended period of lighter precipitation, the simulation with Thompson produced a shorter and quick period of very heavy precipitation compared to the observed extended period of precipitation. Though the Lin, WSM3, WSM6 and Goddard schemes predicted the heavy rainfall, they simulated it far after (between 18 UTC to 22 UTC) the actual event. Morrison simulated a heavy rainfall of about 15 mm at 22 UTC. Thus, these results suggest that while the total precipitation is well-produced by the Thompson scheme, it produces a brief, very heavy precipitation event, compared to the observed extended moderate intensity rainfall.

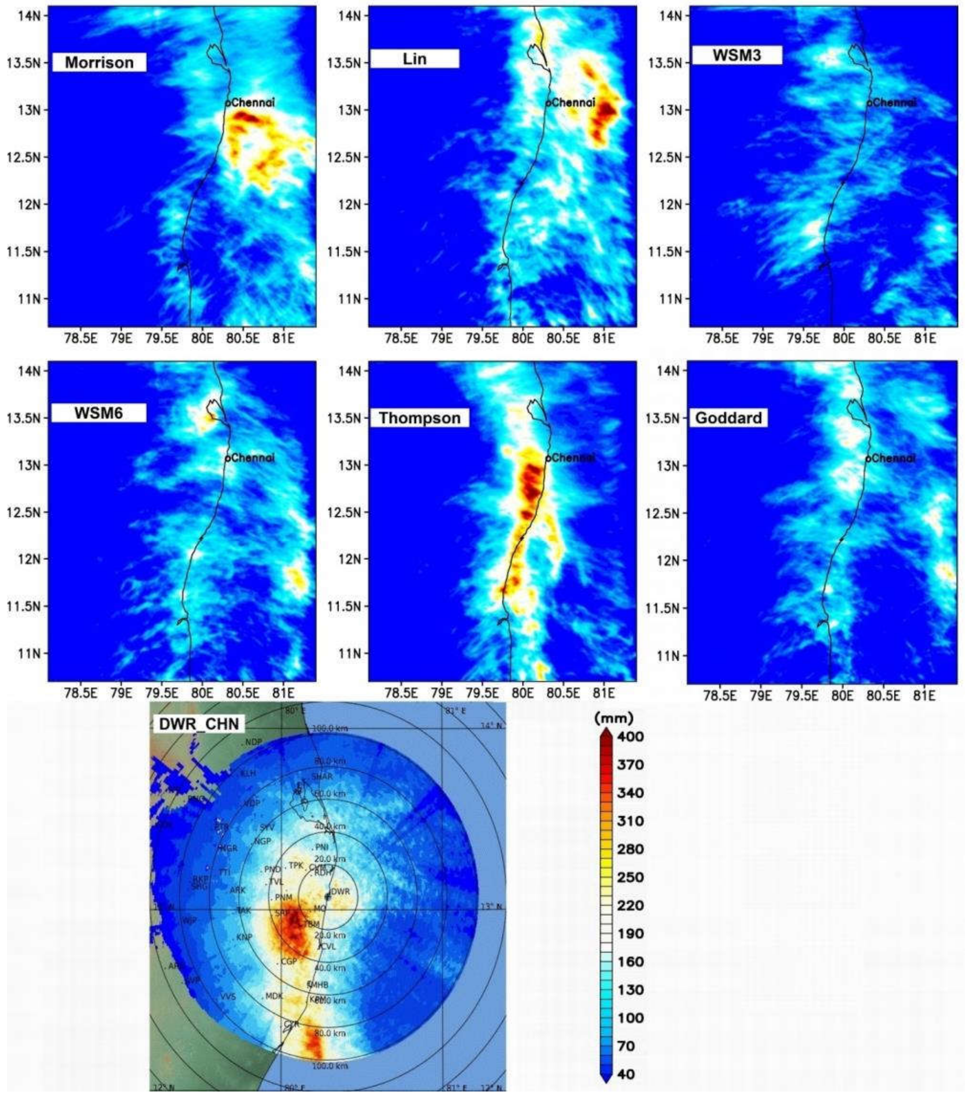

Figure 4.4. *The model-simulated cumulative rainfall received on 1 Dec 2015 by different microphysics schemes compared with DWR, Chennai Precipitation Accumulation.*

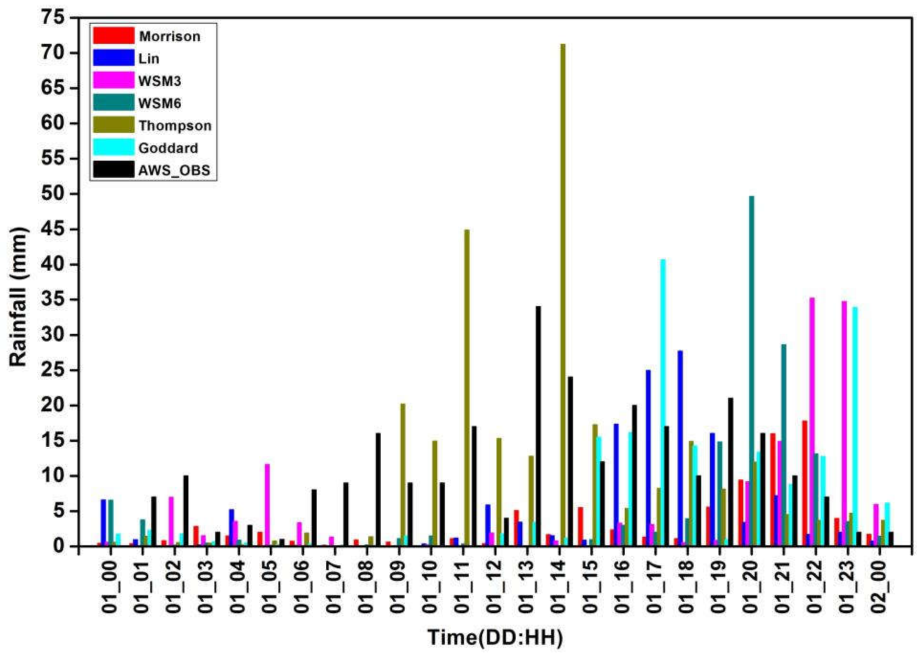

Figure 4.5. Simulated h*ourly rainfall at Chennai (13.1°N, 80.2°E) for the period from 00 UTC 1 Dec 2015 by different microphysics schemes compared with AWS observation of IMD.*

Error statistics [mean error (ME), mean absolute error (MAE), root mean square error (RMSE)] of simulated rainfall computed from each of the sensitivity runs against IMD rain gauge data computed for eight different stations (Madhavaram, Chennai, Ennore, Sriharikotta, Taramani, Chembarambakkam, Tambaram, Kalpakkam) are shown in Table 4.2. The Thompson scheme produced the least ME and MAE of 2.25 mm and 10.5 mm

Table 4.2. *Hourly rainfall error with respect to IMD on 1 Dec 2015 for five microphysics schemes, averaged for 8 stations including Chennai.*

Microphysics	Error statistics of rainfall (mm)		
	RMSE	***MAE***	***Bias***
Morrison	13.86	11.03	8.235
Lin	16.13	11.47	5.304
WSM3	15.7	11.9	8.7
WSM6	16.1	12.53	7.6
Thompson	14.14	10.51	2.25
Goddard	16.23	12.25	4.825

respectively whereas the WSM6 and Goddard schemes produced higher RMSE (16.1mm, 16.23 mm) and MAE (12.53 mm, 12.25 mm) compared to other schemes followed by the WSM3 scheme which also produced the highest ME/Bias (8.7 mm). The rainfall errors produced by Lin and Morrison are in the moderate range.

4.3.3. Analysis of thermodynamic parameters

As microphysics influences the thermodynamics through condensation/ sublimation and resultant heating/cooling processes, which in turn affect the storm dynamics (Hazra et al., 2017), various thermodynamic parameters are analyzed. Figure 4.6a shows the time series of area average CAPE for the region (12.96°N-80.15°E; 13.36°N-80.55°E) over Chennai. The simulations show that the CAPE increases gradually, and attains peak values between 09 and 18 UTC 1 December, during the period of heavy rainfall. Among the six schemes, the WSM3 followed by WSM6 and Thompson produced the highest CAPE (2500-2800 J/kg) and Lin, Morrison and Goddard produced the lowest (1900-2300 J/kg) -values. The peak CAPE is predicted during 11-14 UTC for Lin, Morrison, Goddard and 14-19 UTC for Thompson, WSM3 and WSM6 simulations. The Thompson scheme produced higher CAPE during the period of heavy rainfall than other schemes. The tendencies of CAPE among different simulations suggests that the model produces different instabilities both spatially and temporally, which may influence the drop size and the rain/precipitation mechanism through vertical motions (Chaudhuri and Bhowmick, 2006).

The area average vertical velocity at 500 hPa over Chennai (Fig. 4.6b) shows that the Thompson and Morrison produce the highest vertical motions (~7.3 m/s) followed by Goddard (6.5 m/s), WSM3, WSM6 and Lin (2.5 m/s). Moreover, the highest vertical motions are produced at different times (11 UTC, 18 UTC for Thompson; 21 UTC for Morrison; 17 UTC for Lin; 21 UTC for WSM3; 18 UTC, 23 UTC for WSM6; 15 UTC for

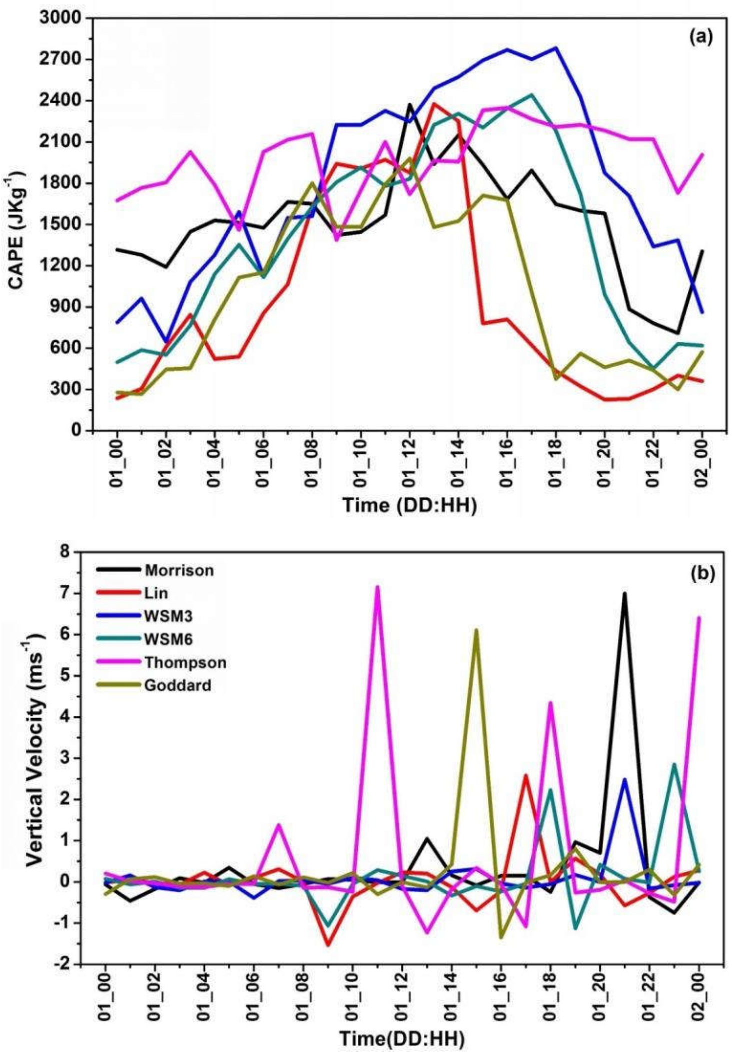

Figure 4.6. *Time variation of model simulated **(a)** CAPE averaged for the region (12.96°N-13.36°N, 80.15°E-80.55°E) and **(b)** vertical velocity at 550 hPa at Chennai (12.93°N, 80.30°E) for the period from 00 UTC 1 Dec to 00 UTC 2 Dec 2015.*

Goddard) on 1 December. The microphysics schemes influence the convection in the simulations by changes in the diabatic heating and the resulting low-level convergence. Strong updrafts can carry the warm-rain generated liquid drops above the environmental 0°C level, where they subsequently freeze into ice pellets. These frozen drops can further grow in size, transforming to graupel and hail, and can ultimately lead to intense precipitation (Kumjian et al., 2012). The results of the study show that strong updrafts of 5-7 m/s associated with high CAPE (>1500 Joules) in the case of Thompson promote the growth of particles size in the mixed phase, thus facilitating intense precipitation. Although Morrison simulated large updrafts, the strong updrafts occurred in the post storm phase. The diabatic warming in the atmosphere through condensation and freezing will influence the vertical motion.

The temperature change from 00 UTC to 15 UTC of 1 December is analyzed in a vertical cross-section over Chennai (80.3°E) for different microphysics simulations (Figure 4.7). Cooling in the lower layers (≤3 km) and warming in the upper troposphere (12-14 km) is noticed indicating high conditional instability in the case of Morrison and Thompson. Warming in the lower layers as well as upper troposphere is noticed in the case of Lin, WSM3 WSM6 and Goddard schemes. The stronger warming in Thompson is associated with large CAPE and strong vertical motions while the other simulations are marked with low CAPE and low vertical motions. Zhang (1989) found that the freezing and sublimation through ice microphysics can provide a positive forcing for the rapid development of mid-tropospheric warm-core vortex circulation. The higher warming in Thompson microphysics could be due to the role of solid hydrometeors which in the process of freezing release large latent heat in the upper troposphere. These results suggest that the explicit incorporation of ice microphysics into the simulation of mesoscale cloud precipitation process is very important for the realistic simulation of mesoscale structure and evolution of convective weather systems (Zhang, 1989) and associated precipitation.

The equivalent potential temperature (theta-e) is a critical indicator to potential instability and the high values of theta-e will result in the formation of more unstable and saturated convective environment (Im et al., 2013). Figure 4.8 shows the vertical cross-section of vertical velocity and theta-e at Chennai from 00 UTC 1 December to 00 UTC 2 December for the six simulations. Only the Morrison, WSM6 and Thompson schemes

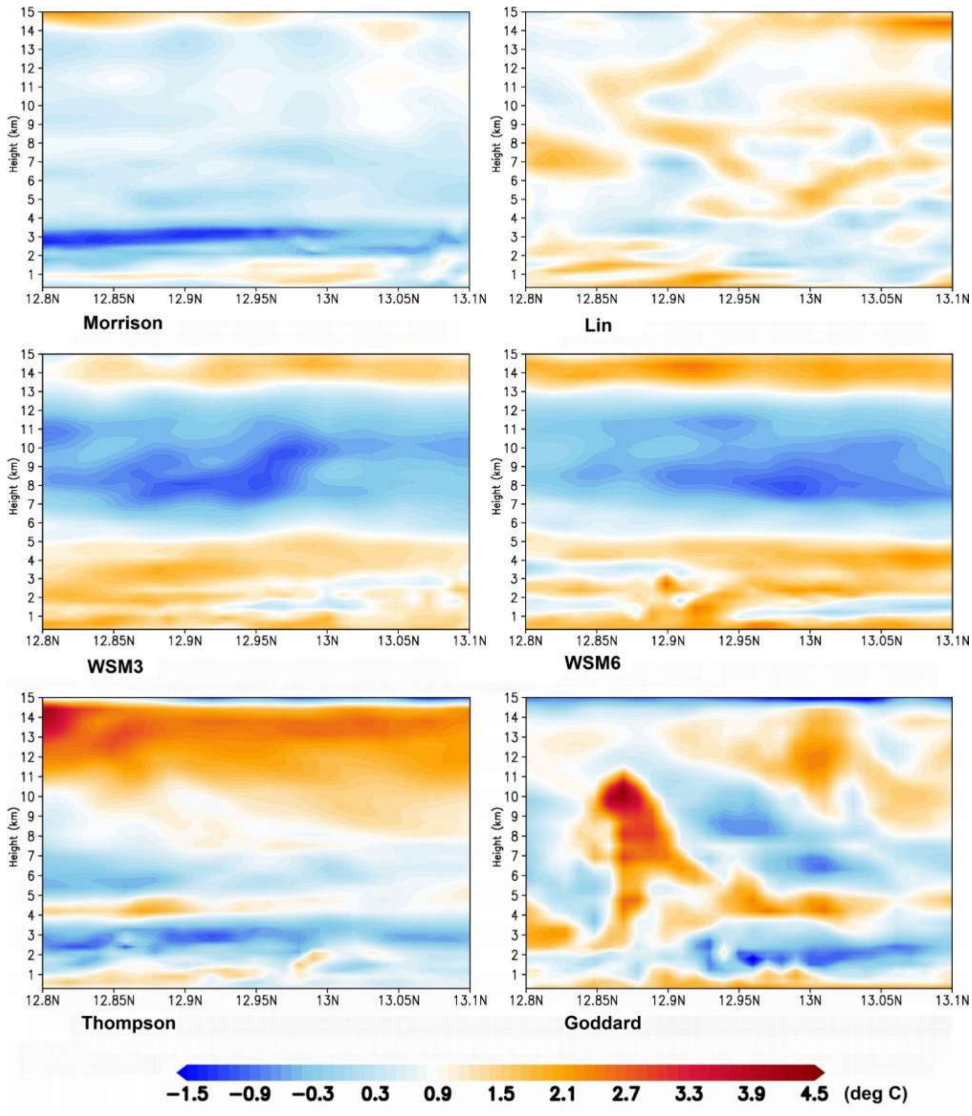

Figure 4.7. *Latitude-height section of simulated diabatic heating/cooling over Chennai (80.30°E) at 15 UTC 1 Dec by different microphysics schemes.*

simulated strong vertical motions along with downdrafts. Compared to other schemes WSM3 and Goddard simulated weak vertical motions (2-3 ms^{-1}) as well as smaller theta-e indicating less moist convection. For Morrison, prominent vertical motion in the layer 2-7 km is simulated at 21 UTC in later phase, and it is associated with high theta-e (high moist convection) values (350-354 K) extending up to 10 km and above. For the WSM6 scheme the timing of theta-e and strong vertical motions is simulated at a later phase from 18 UTC to 19 UTC, which explains as to why the WSM6 scheme produced heavy rainfall after 18 UTC. Most of the time, the simulation with WSM6 had weak vertical motion and thus did not produce much rainfall between 14 -16 UTC. The Lin scheme produced relatively weak vertical motion and low theta-e resulting in limited rainfall. Im et el. (2013) pointed out the steep rise of theta-e values in the lower to mid-tropospheric levels along with veering wind favours the development of deep convective systems which produce

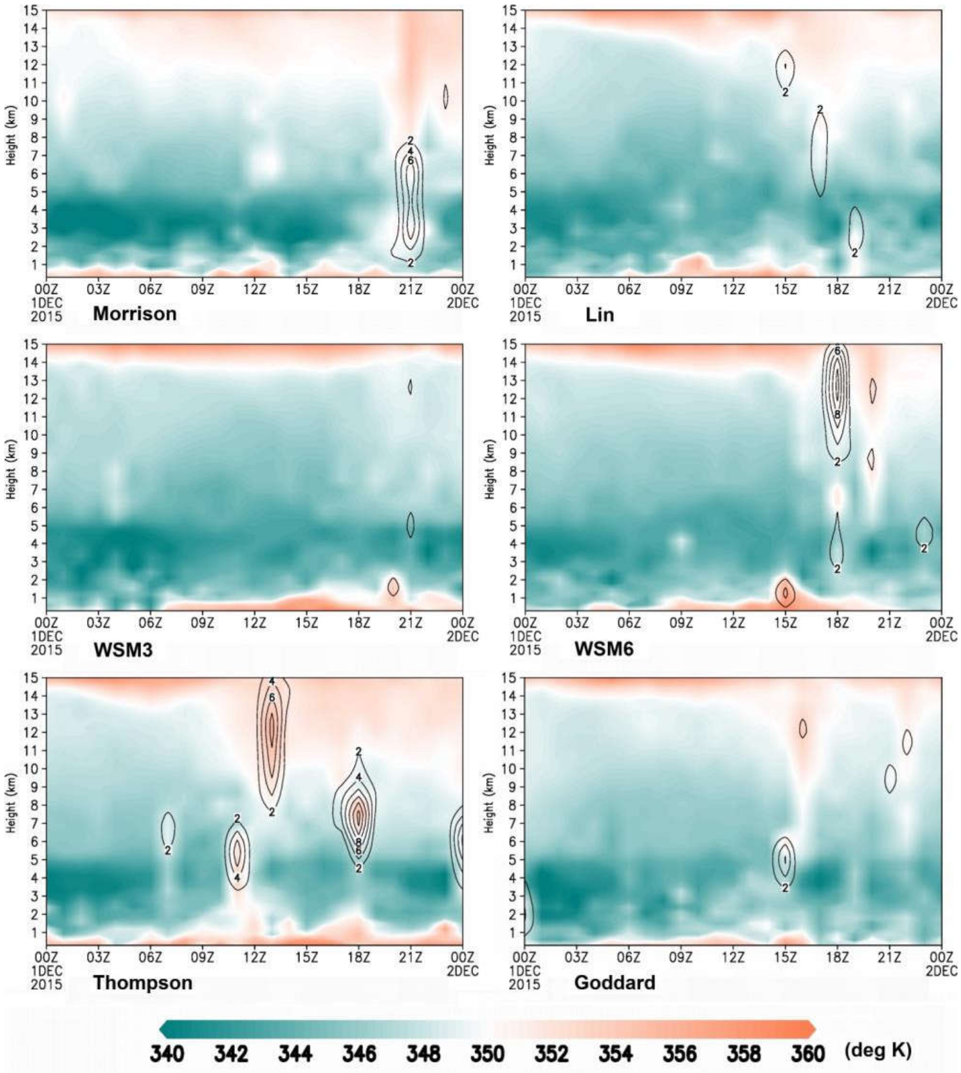

Figure 4.8. *Time variation of model simulated equivalent potential temperature (shaded) and vertical velocity (contours) with height averaged for the region (12.55°N-13.45°N, 79.8°E-80.2°E) by different microphysics schemes for the period from 00 UTC 1 Dec to 00 UTC 2 Dec 2015.*

heavy rainfall. For Thompson, the region of high theta-e and large vertical motions extended beyond 9 km in the upper troposphere. At 13 UTC and 11 UTC strong updraft can be observed. Among all schemes, Thomson produced the highest vertical velocity (16 m/s) and also high theta-e (~355 K) thus giving the reasonable rainfall simulation. The strong vertical motions in Thompson are associated with high moist convection, likely due to the sublimation and freezing of solid hydrometeors.

4.3.4. Hydrometeors structure and composition

For a more detailed understanding of the microphysics schemes, the time variation of mixing ratio of the various hydrometeors as per their vertical abundance (water vapor at 1000 hPa, cloud water at 500 hPa, rain water at 600 hPa, cloud ice and snow at 200 hPa and graupel at 400 hPa) is analyzed (Fig. 4.9) on 01 December. As shown in Figure 4.9, the WSM3 scheme predicts only liquid hydrometeors, which are qvapor, qcloud, and qrain. All the schemes produced nearly similar time variation of qvapor (Fig. 4.9a), with higher values during the heavy rainfall period. Among all the schemes Thompson predicted relatively higher values of qvapor at 15 UTC of 1 December. The Thompson scheme also predicted relatively high values of qcloud (Fig. 4.9b) between 07 UTC and 20 UTC followed by the Goddard at 15 UTC and Morrison between 12 UTC and 21 UTC. All the other schemes predicted comparatively less values of qcloud. The Thompson produced relatively high values of rain mixing ratio between 06 UTC and 18 UTC followed by the Goddard scheme which produced notable rain at 15 UTC The Morrison and Lin schemes also produced significant amount of rain at 21 UTC and 18 UTC respectively. The Thompson scheme produced very low ice while Lin produced the highest ice (between 15-17 UTC 01 December) compared to other schemes (Morrison, Lin, WSM6, Goddard) which produced moderate values. From the time series of qsnow at 200 hPa (Fig. 4.9e) it is observed that Thompson predicted highest values of qsnow (1.5-6.5 g/Kg) between 13 UTC and 18 UTC followed by Morrison and WSM6 (after 18 UTC). Lin and Goddard microphysics did not produce any notable presence of qsnow. All the schemes produced good presence of qgraup (Fig. 4.9f) between 16 UTC and 23 UTC with Morrison, Goddard and Thompson giving the highest graupel. Thus, the above results suggest that the Thompson scheme predicted most of the hydrometeors as well as their time of occurrence (except qice) coinciding with the maximum observed rainfall event. Next to Thompson, Morrison produced notable values of hydrometeors when compared to other schemes, but at a later time (3-4 hours delay) of actual event of heavy rainfall.

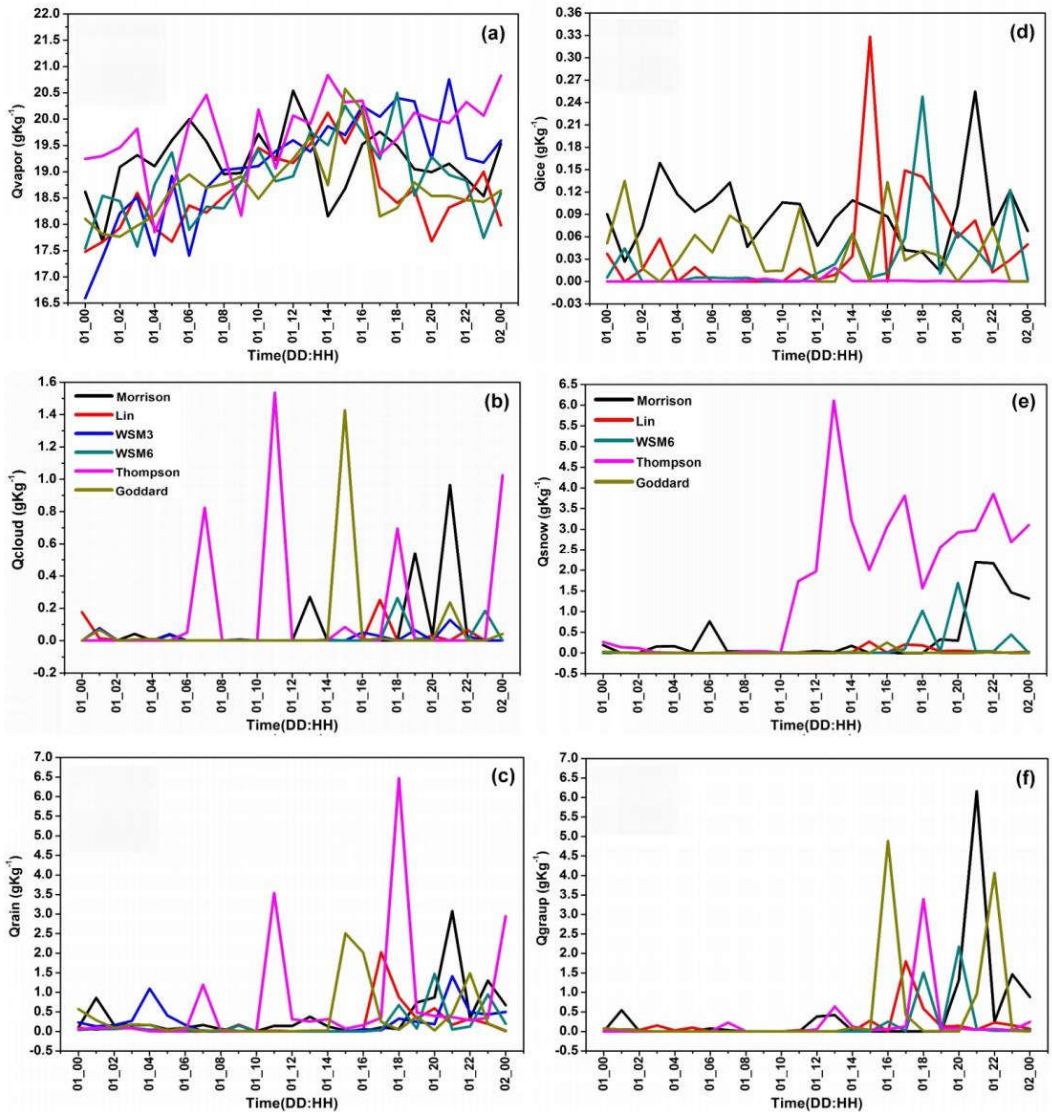

Figure 4.9. *Time variation of model simulated* ***(a)*** *qvapor (1000 hPa),* ***(b)*** *qcloud (500 hPa),* ***(c)*** *qrain (600 hPa),* ***(d)*** *qice (200 hPa),* ***(e)*** *qsnow (200 hPa),* ***(f)*** *qgraup (400 hPa) with time at Chennai (12.93N, 80.30E) for the period from 00 UTC 1 Dec to 00 UTC 2 Dec.*

Vertical profiles of hydrometeors at Chennai analyzed at 18 UTC of 1 December (Figure 4.10) show that the Thompson scheme produced the highest cloud water, rain water, snow and graupel, whereas Goddard, WSM6 and Lin produced highest ice. All the schemes have produced water vapor similarly (Fig. 4.10a). Thompson has not produced ice. The Goddard scheme produced the highest value of qice (0.27 g/Kg) followed by WSM6 (0.24 g/Kg) and Lin (0.15 g/kg). The Thompson scheme produced highest amount of graupel (6 g/kg). The WSM3 scheme has not simulated any hydrometeor notably, except 1.5 g/kg of rain water. Also, the Goddard scheme could significantly produce cloud ice only. These vertical hydrometeor distributions show that Thompson simulated high amount of all the hydrometeors except for ice.

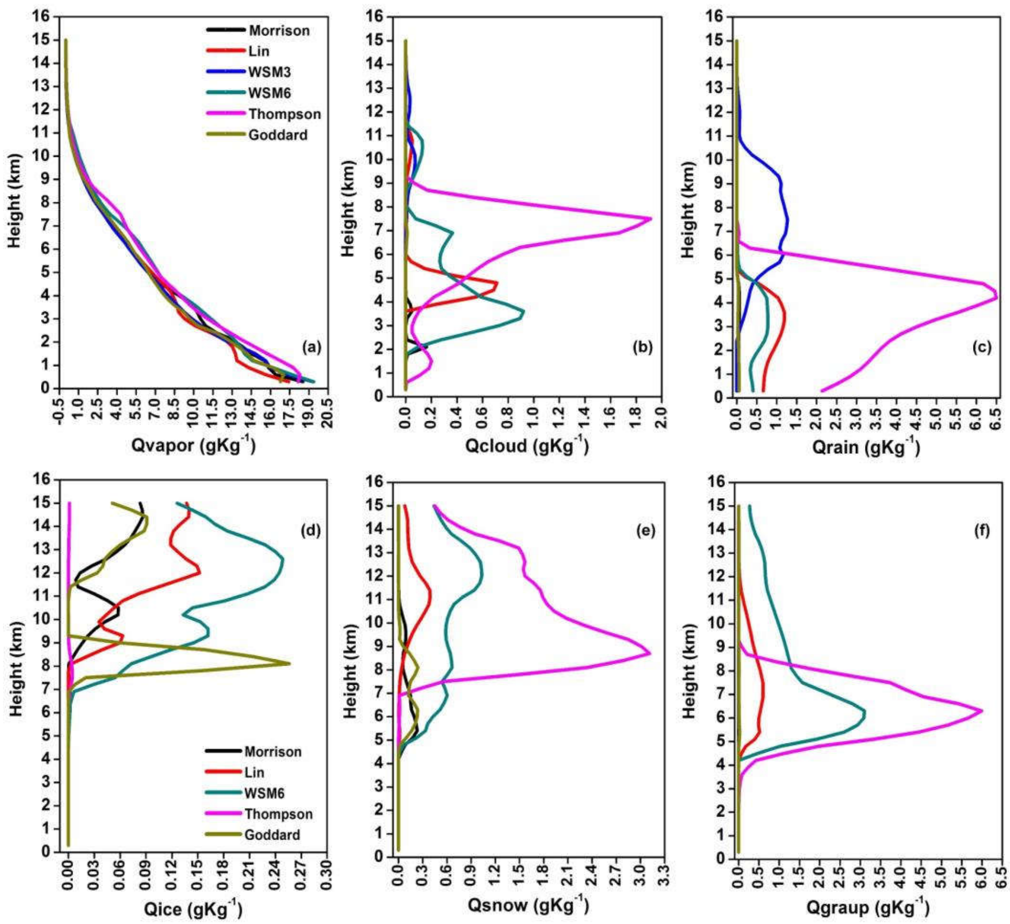

Figure 4.10. *Simulated vertical profiles of **(a)** qvapor, **(b)** qcloud, **(c)** qrain, **(d)** qice, **(e)** qsnow and **(f)** qgraup at 18 UTC of 1 Dec 2015 by different microphysics schemes at Chennai (12.93°N, 80.30°E).*

The maximum radar reflectivity predicted by the five microphysics schemes is compared with the Chennai DWR reflectivity at 12 UTC (Fig. 4.11) of 1 December. The DWR observations show the areas of deep convection around Chennai city in a radius of 50-km and along the coast up to 100 km. It is seen that simulations with Morrison, Lin, and WSM6 overestimated the reflectivity and also represented the areas of deep convection south of Chennai near Pondicherry in Morrison scheme and near Kalpakkam

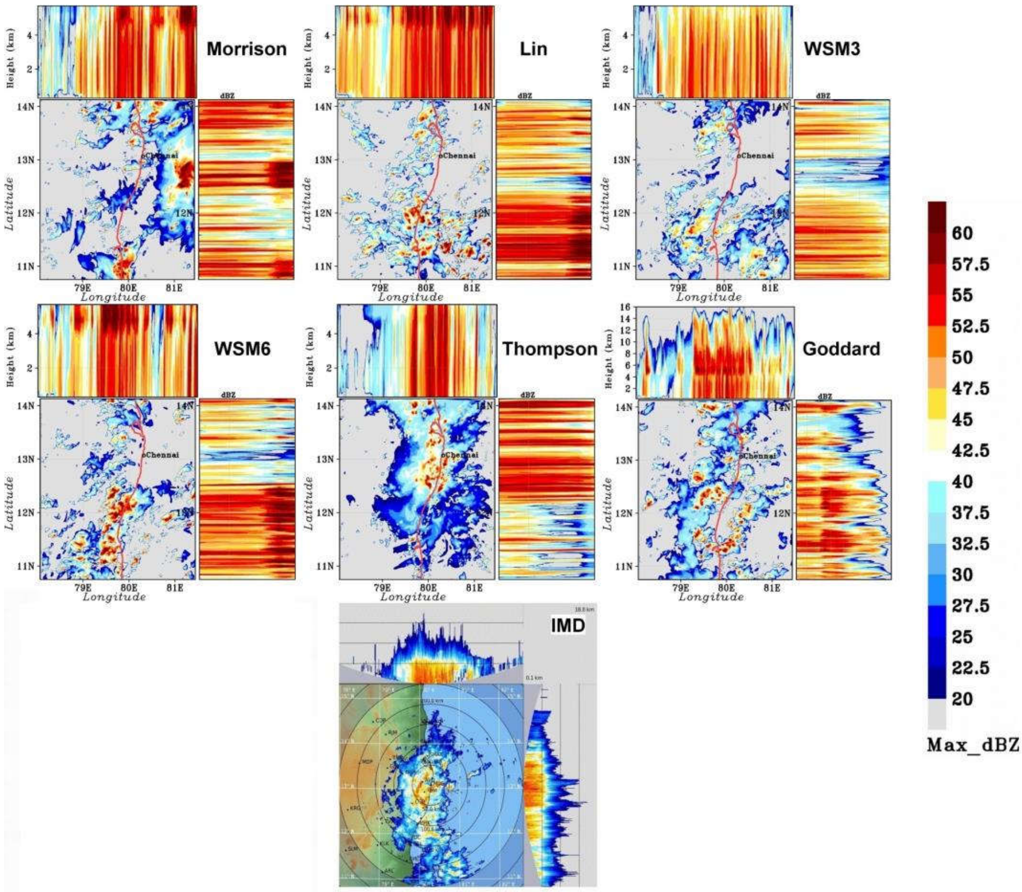

Figure 4.11. *Model simulated maximum radar reflectivity by different microphysics schemes at 12 UTC 1 Dec 2015 compared with Chennai DWR reflectivity.*

in WSM6 and Lin schemes. WSM3 underestimated the radar reflectivity indicating underestimation of convective clouds and underestimation of rainfall. The Goddard scheme could produce significant reflectivity but the areas of convection is scattered southward and more inland. Among the different microphysics the Thompson scheme produced the reflectivity pattern in good agreement with DWR observations. The hydrometeor reflectivity over Chennai and adjacent regions is simulated well by Thompson (45-60 dBz) in better match with the DWR reflectivity while it is highly scattered for all the other schemes.

The time-height profile of model-produced radar reflectivity is also analyzed at Chennai (12.93°N, 80.30°E) (Fig. 4.12). The six schemes have shown different evolution of distribution of cloud reflectivity. For the Morrison scheme, the highest values (50-55

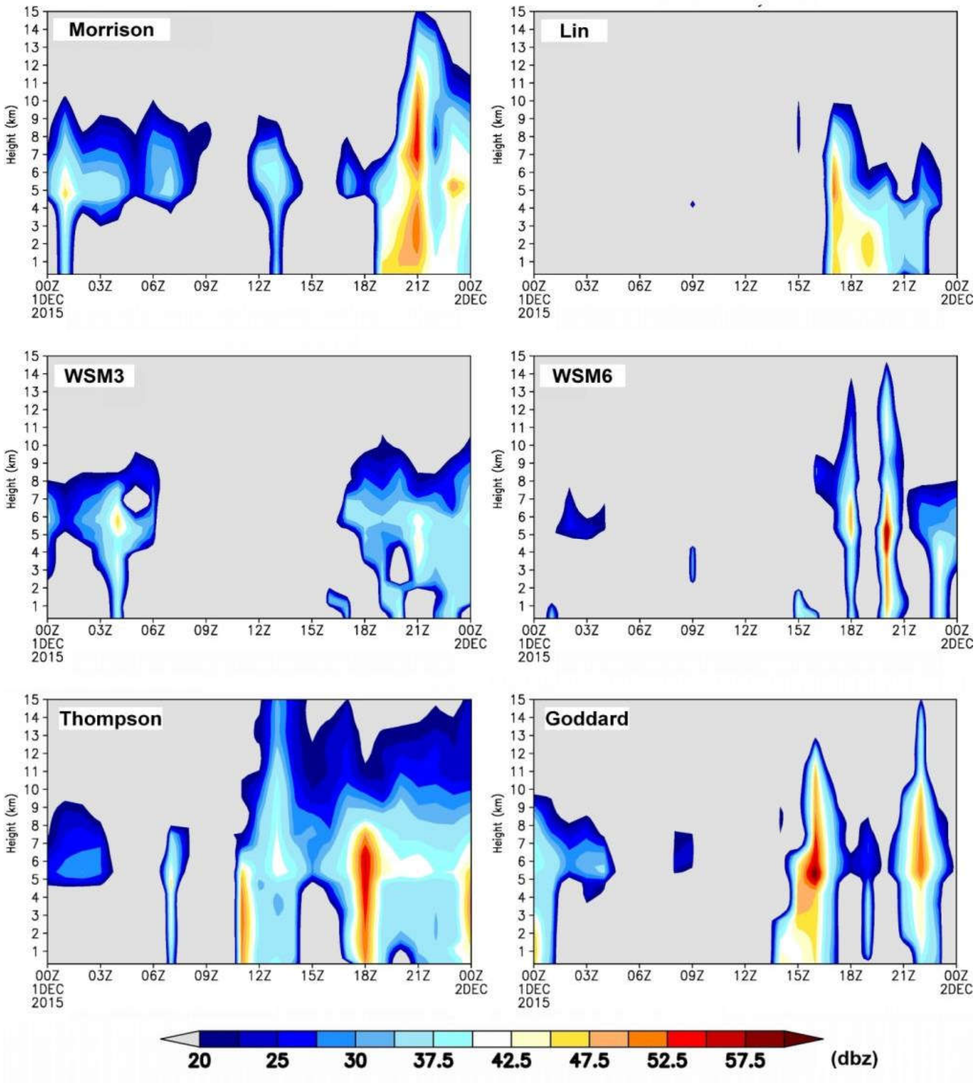

Figure 4.12. *Time variation of model simulated radar reflectivity with height by different microphysics schemes at Chennai (12.93°N, 80.30°E) for the period from 00 UTC 1 Dec to 00 UTC 2 Dec 2015.*

dBZ) propagating up to 13 km are predicted during 18 UTC of 1 December to 00 UTC of 2 December, whereas low values (20-45 dBZ) are observed at other time steps at lower heights (0-10 km). For Lin and WSM6, notable values of reflectivity (27-50 dBZ) covering the layer of 0-9 km are seen between 18-21 UTC only. During the period of highest rainfall (09-15 UTC), low reflectivity (20 dBZ) is observed in the simulations using Lin, WSM3, and WSM6 at all heights. For WSM3, predicted value of the maximum reflectivity is 45 dBZ between 4 and 7 km. In the case of Goddard, notable reflectivity is observed between 15-17 UTC and after 21 UTC. In the case of Thompson, a continuous reflectivity distribution can be observed from 11 UTC 1 December to 00 UTC of 2 December throughout the altitudes from 0 to 15 km. The highest values obtained are at 11 UTC and 18 UTC with a marked decrease between 15-17 UTC. During the heavy rainfall period, the Thompson scheme has shown good distribution of clouds as compared to all the other schemes.

4.4. Summary

In this chapter, the tropical low pressure system over the Bay of Bengal and associated heavy rainfall event over north coastal Tamil Nadu on 1 December 2015 is simulated using a 1-km horizontal resolution to study the sensitivity to cloud microphysics. Simulations revealed that the microphysics schemes affect the location of the low pressure trough, atmospheric circulation and low level convergence through changes in the diabatic heating and its coupling to dynamics ultimately influencing the distribution and location of rainfall. It is noticed that among all the schemes the Thompson scheme has realistically produced the low-pressure trough, circulation and rainfall pattern compared to other schemes. From the detailed analysis, it is found that though the Morrison and WSM6 schemes also gave good prediction of hydrometeors, they represented slow evolution of rainfall towards 00 UTC of 2 December.

The model results show that, the location of maximum rainfall, intensity, and distribution are differently simulated in the six simulations. While the Morrison and Lin schemes simulated the maximum precipitation over the ocean area adjacent to Chennai, the WSM3, WSM6 and Goddard schemes simulated along the coast but with significantly lower intensity. The Thompson microphysics scheme produced the maximum rainfall (450 mm) over Chennai and its surroundings and the heavy rainfall extension along the coast with its time of occurrence in better agreement with observations compared to all the other schemes. Still some uncertainties are to be explored in the case of Thompson scheme.

Among the microphysics schemes used in the study, the Thompson and Goddard schemes follow a gamma distribution for the size distribution of different hydrometeors. Microphysics sensitivity results revealed that the Thompson predicted most of the hydrometeors mixing ratios (except ice), their vertical distribution as well as the time of occurrence coinciding with the maximum observed rainfall event better than the other schemes. Especially it showed a remarkable distribution of snow from 11 UTC 1 December to 00 UTC of 2 December indicating the contribution of snow for the heavy rainfall. According to IMD, the highest rainfall occurred at 5 UTC to 15 UTC of 1 December. The results from Thompson showed that it reproduced the rainfall peaks and time variation before 15 UTC and the heavy rainfall extended till 18 UTC of 1 December. Comparisons of model-produced rainfall at rain-gauge station at Chennai indicate that the Thompson scheme better produced the rainfall variation and the maximum values are simulated between 08 UTC and 15 UTC as in the observed rainfall.

Chapter 5

Sensitivity of high resolution TC simulations to cloud microphysics

5.1. Introduction

Many numerical modelling studies on TCs show that high resolution models with explicit convection physics (Gopalakrishnan et al., 2011; Gopalakrishnan et al., 2012; Seifert, 2011; Gentry and Lackman, 2010; Yu and Lee, 2010; Craig and DÖrnbrack, 2008) considerably improve the intensity and structure predictions. However, some of the recent studies reported that the evolution of convection and intensification in the convection permitting simulations are (Zhang et al., 2019; Mooney et al., 2019; Li et al., 2019; Parker et al., 2017; Makarieva et al., 2017; Khain et al., 2016; Maw and Min, 2017) highly sensitive to the cloud microphysics schemes. Wang et al. (2001, 2002) tested the sensitivity of TC structure, intensification and intensity to the choice and details of cloud microphysics parameterization. They found considerable differences in the simulated stratiform clouds and the associated downdrafts outside the eyewall of the TC and the intensification rate. A few studies for TCs over NIO region also show that explicit convection schemes produce considerable impact on TC tracks and intensities (Deshpande et al., 2012; Taraphdar et al., 2014) and the intensity is well predicted when no cumulus parameterization was used in the highest resolution domain. Though many modelling studies were conducted to study the sensitivity of TC predictions to cloud microphysics, there still exist large uncertainty and complexity of cloud microphysics in predicting TC tracks and intensity. As several microphysics parameterizations are developed and incorporated in the community mesoscale model WRF it is required to study their performance towards developing better forecast skills for the TCs over the NIO. In this chapter the sensitivity of high resolution (3 km) predictions of TCs WRF-ARW are examined. Six TCs which formed over BOB are chosen for the study using 5 microphysics schemes. The microphysics schemes were chosen based on the results from the previous chapter.

5.2. Methodology

Six very severe TCs namely Phailin, Hudhud, Thane, Lehar, Fani and Gaja which formed over the BOB from 2011 to 2014 period are chosen for the study. The model simulation period of the cyclones is same as in the study of Chapter 3 (refer Table 3.1 of Chapter 3). The WRF-ARW model v.3.9 is used for the simulations. The model domain configuration is same as that of in Chapter 3 (refer Fig. 3.1 of Chapter 3). The IMD tracks of the selected cyclones are illustrated in Figure 3.1 of Chapter 3. The NCEP-GFS 0.25° × 0.25° analysis data is used for model initialization and the boundary conditions are updated every 3 hours with the GFS forecasts. The SST is updated from the GFS data. The model physics options including the various microphysics schemes used for the simulations are provided in Table 5.1.

The cumulus parameterization is used only in the outer domains (27 km, 9 km). The results from the simulations are compared with the IMD best track parameters, the CIRA satellite observation derived products of TC structural parameters, IMD Doppler Weather RADAR (DWR) products and the Mesosphere Stratosphere Troposphere (MST) radar data of Gadanki station. The error statistics (mean error) obtained as model value minus observation is computed from 3-hourly model outputs for each microphysics case after the model spin up period of 12 h.

Table 5.1. *Model physics used for the study.*

Physics	Scheme
Longwave radiation	RRTM (Mlawer et al., 1997)
Shortwave radiation	Dudhia (Dudhia, 1989)
Surface layer	MM5 similarity theory
Land surface processes	5-layer thermal diffusion (Dudhia, 1996)
Planetary boundary layer	YSU (Hong et al., 2006; Noah et al., 2003)
Cumulus	Kain Fritsch (Kain and Fritsch, 1993)
Microphysics	1. Morrison double moment (Morrison et al., 2009) 2. Lin (Lin et al., 1983) 4. WSM6 (Hong and Lim, 2006) 5. New Thompson (Thompson et al., 2008) 6. Goddard (Tao and Simpson, 1993; McCumber et al.,1991)

5.3. Results and Discussion

The simulated tracks, respective track errors (vector displacement errors), CSLP and MSW from best track estimates, relative vorticity and wind field are analyzed from all the experiments with different microphysics schemes. In addition, the warming produced in the cyclone core region, wind field, theta-e, convergence, relative vorticity and cloud reflectivity are also analyzed during peak intensification period for cyclone Hudhud. The peak intensification period of Hudhud is considered as 15 UTC 11 Oct – 06 UTC 12 Oct 2014 (refer section 3.3 of chapter 3). For the purpose of inter-comparison of simulations, 18 UTC 11 Oct 2014 for Hudhud in the middle of maximum intensification period is selected for the analyses. The vertical distribution of ice hydrometeors and the radar reflectivity are analyzed in order to understand the simulated cloud band distribution. Further, simulated vertical velocity for Fani and Gaja cyclones are compared with MST Radar observed vertical velocity profiles over Gadanki station, during the period when the cyclones passed close to the observation station to assess the model performance in resolving the vertical motion. The results of the track and intensity, and the structure of simulated cyclones are presented in the following.

5.3.1. Track and intensity predictions

The tracks of six cyclones simulated by the five different experiments along with the observed track (IMD best track data) are presented in Figure 5.1 and the corresponding error in vector track positions is shown in Figure 5.2.

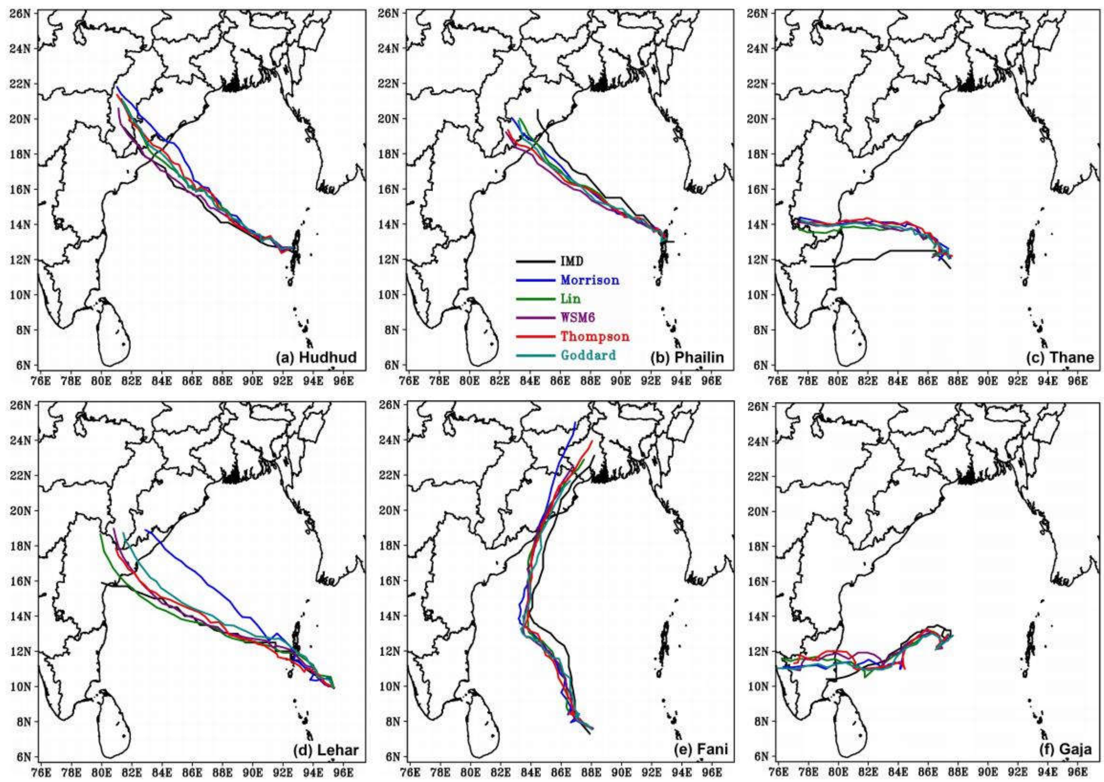

Figure 5.1. *Simulated tracks at 6-hour intervals compared with IMD best track data for **(a)**Hudhud, **(b)** Phailin, **(c)**Thane, **(d)** Lehar, **(e)** Fani and **(f)** Gaja.*

In general, it is found that the deviations in predicted tracks among different microphysics simulations are meager in the initial stages but moderately increase from cyclone stage (about 48 h) onwards till the landfall and further. These results of moderate influence of microphysics on track forecasts corroborate with Deshpande et al (2012). A qualitative comparison of track errors (Figs. 5.1 and 5.2) indicates that the WSM6 followed by Lin and Goddard produce least errors for Hudhud; Morrison followed by Lin and Goddard for Phailin; Lin followed by Goddard and WSM6 for Thane; Goddard followed by Thompson and WSM6 for Lehar; Thompson followed by Lin and WSM6 for Fani; and Morrison followed by Thompson and WSM6 for Gaja.

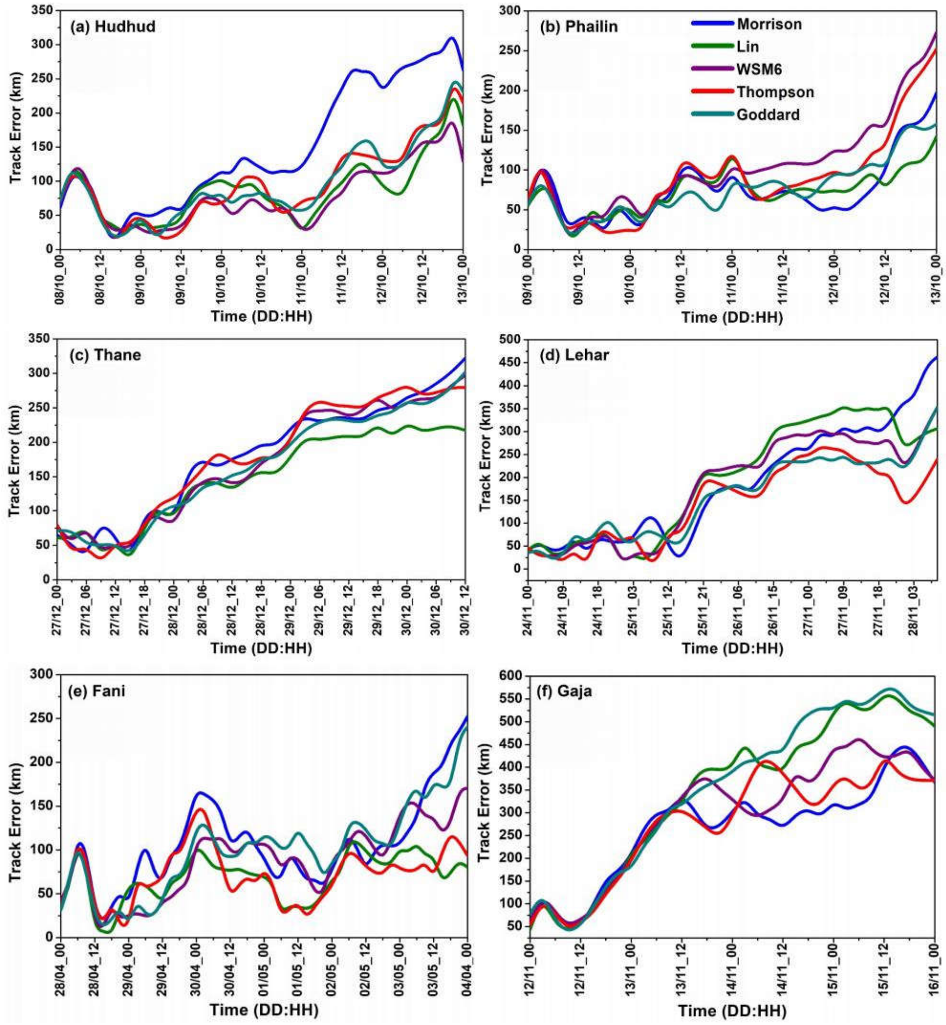

Figure 5.2. *Simulated track errors with respect to IMD best track data for* ***(a)*** *Hudhud,* ***(b)*** *Phailin,* ***(c)*** *Thane,* ***(d)*** *Lehar,* ***(e)*** *Fani and* ***(f)*** *Gaja. The time labels on the x-axis are DD for day and HH for hour.*

Statistical analysis of track forecasts for all the four cyclones (Table 5.2) indicates that the Thompson produced the minimal error (157.51 km) followed by WSM6 (169.25 km), Lin (169.68 km), Morrison (176.75 km) and Goddard (183.5 km) schemes. To better understand the model performance, the mean track errors for the six cyclones computed at different forecast intervals are analyzed (Fig. 5.3). It is analyzed that from 48 h to 96 h, the Thompson scheme produced the least errors relative to other schemes, even though it could not produce least values during the initial stages (12 h-36 h). The Lin scheme produced least errors at 12 h, WSM6 at 24 h and Goddard at 36 h. The error produced by Morrison and Goddard schemes are higher towards the final stages of simulation (84 h, 96 h). However, no scheme other than Thompson could consistently produce the minimal track errors in consecutive time intervals. It is important to note that even though the errors are higher (not highest though) during the initial stages, Thompson produced least errors from intensification stage till ending stage. The changes in tracks in different microphysics simulations are due to the variation in the phase transformation, hydrometeor mixing ratios among different schemes which produce changes in warming and dynamics (see section 5.3.4). As discussed subsequently in section 5.3.4, Goddard, WSM6 and Lin schemes simulated more rain whereas Morrison scheme produced more cloud. Sun et al. (2015)

Table 5.2. *Mean track errors with respect to IMD computed from 3 hourly interval model outputs excluding the first 12-h spin-up period for six TCs for the five microphysics schemes.*

TC	Mean Track error (km)				
	Morrison	**Lin**	**WSM6**	**Thompson**	**Goddard**
Hudhud	158.97	87.37	78.82	97.19	98.28
Phailin	78.96	78.31	114.57	98.06	81.9
Thane	203.85	168.7	193.86	205.26	189.09
Lehar	207.78	219.22	201.5	160.92	176.97
Fani	111	69.28	91.53	72.04	105.14
Gaja	299.97	395.22	335.26	311.63	449.6
Mean	176.75	169.68	169.25	157.51	183.5

showed that simulation of excess hydrometeors i.e., either more cloud or more precipitating components in a TC can result in condensate warming above 500 hPa or evaporative cooling below 500 hPa in the TC outer region. The relative variations of rain, cloud, ice, snow mixing ratios affects the temperature profile in terms of warming in the upper layers and cooling in the lower layers thus altering the storm scale thermodynamic and dynamics and its interaction with largescale-environment leading to changes in the movement of the storm among different MP schemes.

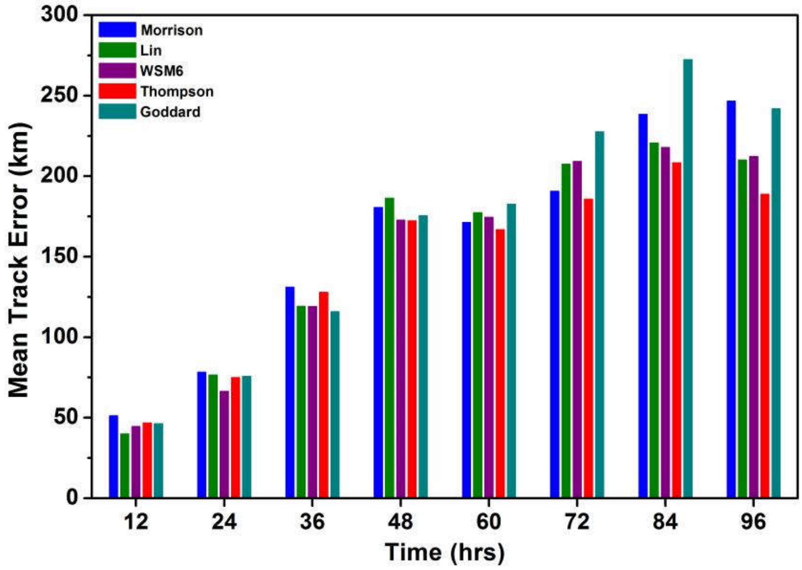

Figure 5.3. *Mean errors in track with respect to IMD estimates by different microphysics schemes at 12 h interval computed for the six cyclones.*

The time evolution of model simulated CSLP and MSW along with IMD estimates are presented in Figure 5.4 and Figure 5.5 respectively. They indicate that an increase in wind speed is associated with a fall in the central pressure for each storm. It can be seen that the intensity is generally over estimated by all the microphysics schemes for both Hudhud and Lehar and underestimated for Thane and Gaja. For Phailin all the schemes produced similar trends of CSLP and slightly higher pressure drop relative to the IMD estimates. For Fani, except Morrison all the other schemes produced slightly higher pressure drop during peak intensity stage (06 UTC 2 May – 00 UTC 3 May). Morrison considerably underestimated the pressure drop (Δp ~ hPa) during the peak intensity stage for Fani. For a majority of cases, Thompson, followed by Lin and Morison produced a better agreement with observations throughout the simulation. Though all the schemes have shown nearly same magnitude of MSW the Lin scheme has produced slightly stronger (Fig.5.5) winds during the deepening phase. In the case of Lehar, for both CSLP

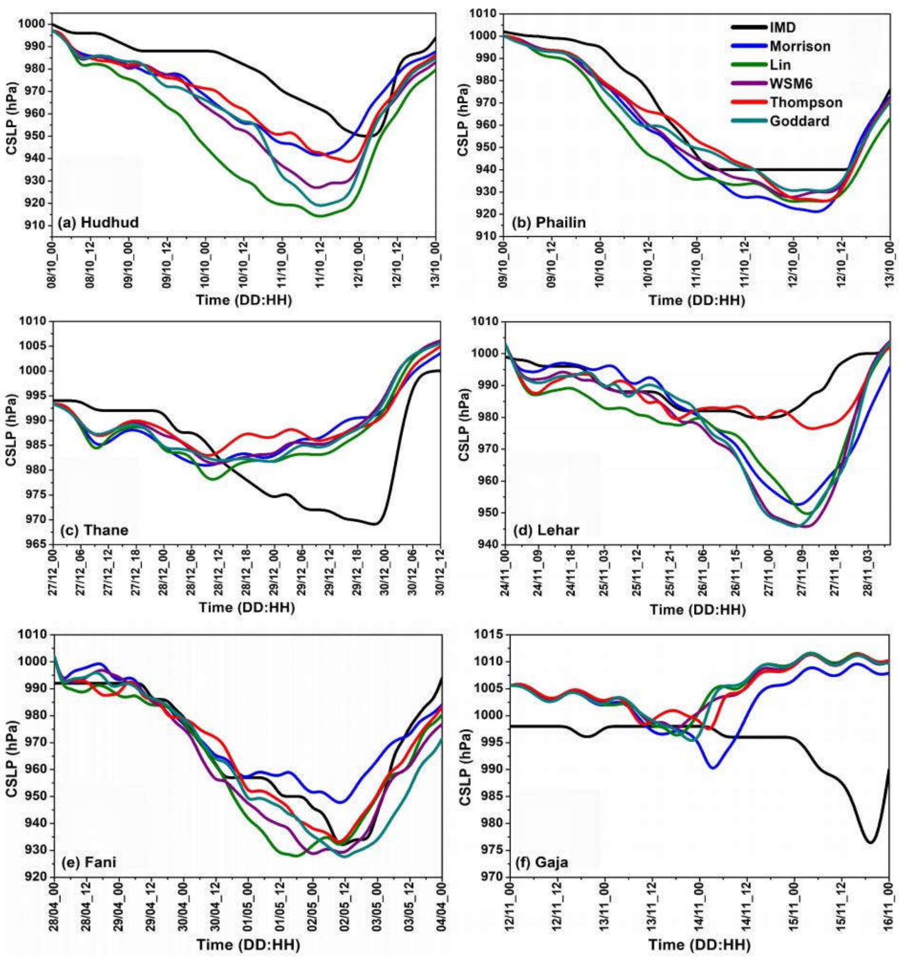

Figure 5.4. *Simulated CSLP compared with IMD best track data for* ***(a)*** *Hudhud,* ***(b)*** *Phailin,* ***(c)****Thane,* ***(d)*** *Lehar,* ***(e)*** *Fani and* ***(f)*** *Gaja.*

(Fig. 5.4) and MSW (Fig. 5.5), even though all the schemes produced good comparison with the IMD estimates during the initial stages, the Thompson alone could closely simulate the CSLP and MSW during the deepening phase. It may be noted that the results of improved track predictions in some cases of microphysics do not show corresponding improvements in intensity predictions thus indicating the complication in predicting both intensity and movement of cyclones with any particular microphysics accurately. The intensity predictions are highly influenced by far less predictable internal dynamics that is modulated by the large-scale environment (Emanuel, 1999).

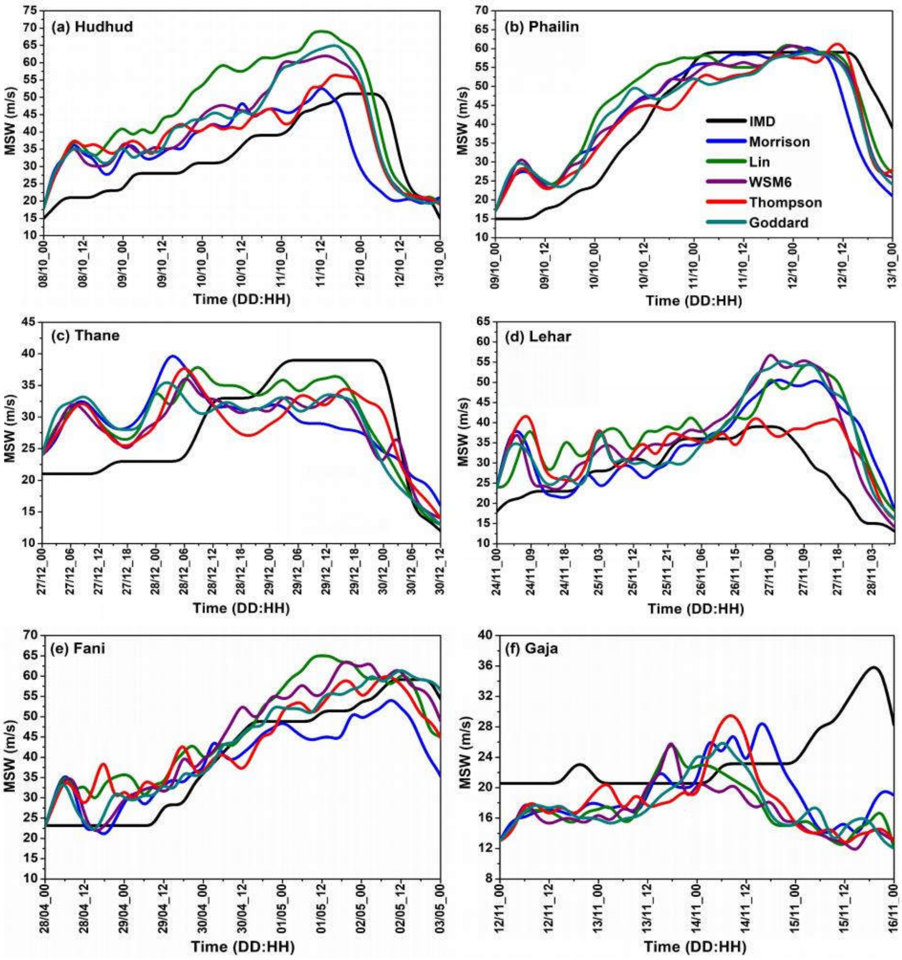

Figure 5.5. *Simulated MSW compared with IMD best track data for* ***(a)*** *Hudhud,* ***(b)*** *Phailin,* ***(c)*** *Thane,* ***(d)*** *Lehar,* ***(e)****Fani and* ***(f)*** *Gaja.*

To better understand the model performance for intensity parameters the mean errors (predicted – observed) for CSLP and MSW with respect to IMD estimates for the four cyclones at different forecast intervals are analyzed (Fig. 5.6a and Fig. 5.6b). It is found that for CSLP, Thompson followed by the Goddard and Morrison produced the least error at different forecast intervals (Fig. 5.6a) while the other two schemes (Lin, WSM6) produced inconsistent error trends at different intervals. For MSW (Fig. 5.6b), both

Thompson and Morrison produced least errors at different forecast intervals. While the MSW (Fig. 5.6b) error decreased towards peak intensification, the CSLP errors remained nearly uniform throughout the simulation.

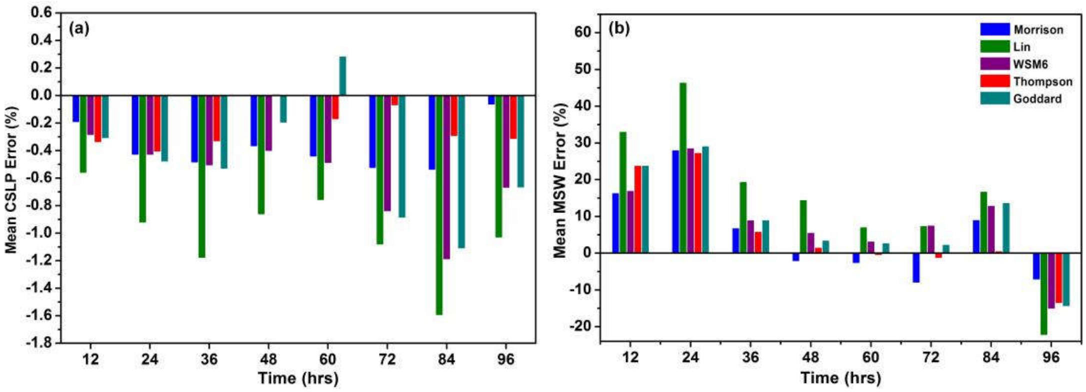

Figure 5.6. *Mean percentage errors in **(a)** CSLP and **(b)** MSW with respect to IMD estimates at 12 h interval computed for the six cyclones.*

The mean errors (model - observation) and the mean absolute errors in CSLP and MSW for the entire simulation period (excluding the spin up time of 12 h from model initialization) for different TCs with respect to different microphysics are presented in Table 5.3 and Table 5.4 respectively. The error statistics indicates that the Thompson scheme produced the least error in CSLP (-0.52 hPa) followed by the Morrison (-2.23 hPa), Goddard (-4.37 hPa), WSM6 (-4.54 hPa), and Lin (-7.92 hPa) (Table 5.3). The Thompson scheme also produced the least mean absolute error in CSLP (8.54 hPa) followed by the Morrison (10.52 hPa), WSM6 (11.36 hPa), Goddard (11.53 hPa) and Lin (14.31 hPa) (Table 5.4). For MSW, the Thompson scheme produced the least error (0.21 ms^{-1}) followed by Morrison (-0.49 ms^{-1}), Goddard (1.53 ms^{-1}), WSM6 (1.68 ms^{-1}), and Lin (3.17 ms^{-1}). The Thompson scheme produced the least mean absolute error (6.42 ms^{-1}) followed by the WSM6 (7.18 ms^{-1}), Goddard (7.21 ms^{-1}), Morrison (7.39 ms^{-1}) and Lin (8.78 ms^{-1}) schemes. Considering both CSLP and MSW Thompson produced the best intensity estimates followed by Morrison, Goddard, WSM6 and Lin. The mean intensity and track errors (Tables 5.2-5.4) indicate that except Thompson, the schemes which produced good track prediction have not come up with a good intensity prediction. Though Morrison also gave a better intensity pattern next to Thompson, it produced high error in track. The Thompson scheme gave the best track as well as best intensity predictions. The Lin scheme produced lesser track error than other schemes next to the Thompson, but produced the highest intensity error. For both the track and intensity Goddard produced comparatively large errors than other microphysics schemes. The error statistics indicate that the Thompson scheme provided the best prediction for track and intensity estimates.

Table 5.3. *Mean CSLP and MSW errors with respect to IMD computed from 3 hourly interval model outputs excluding the first 12-h spin-up period for six TCs for the five microphysics schemes.*

TC	Morrison		Lin		WSM6		Thompson		Goddard	
	CSLP (hPa)	MSW (m/s)	CSLP (hPa)	MSW (m/s)	CSLP (hPa)	MSW (m/s)	CSLP (hPa)	MSW (m/s)	CSLP (hPa)	MSW (m/s)
Hudhud	-11.74	1.31	-31.13	13.63	-18.6	7.19	-12.53	4.69	-19.34	7.58
Phailin	-10.21	-1.17	-14.06	-2.46	-7.61	-0.17	-4.81	-1.78	-6.01	-1.17
Thane	5.92	-0.7	5.1	0.37	6.86	-1.25	7.4	-.91	6.25	-1.25
Lehar	-10.33	6.19	-12.47	9.9	-13.09	8.19	-3.02	4.25	-12.2	7.51
Fani	4.53	-3.96	-6.58	4.31	-6.29	3.54	-1.5	0.99	-6.3	3.13
Gaja	8.45	-4.61	11.57	-6.68	11.44	-7.4	11.33	-5.96	11.37	-6.57
Mean	-2.23	-0.49	-7.92	3.17	-4.54	1.68	-0.52	0.21	-4.37	1.53

Table 5.4. *Mean absolute errors of CSLP and MSW with respect to IMD computed from 3 hourly interval model outputs excluding the first 12-h-spin-up period for six TCs for the five microphysics schemes.*

TC	Morrison		Lin		WSM6		Thompson		Goddard	
	CSLP (hPa)	**MSW (m/s)**	**CSLP (hPa)**	**MSW (m/s)**	**CSLP (hPa)**	**MSW (m/s)**	**CSLP (hPa)**	**MSW (m/s)**	**CSLP (hPa)**	**MSW (m/s)**
Hudhud	14.26	8.86	31.13	15.69	19.24	10.41	13.56	8.02	19.99	10.86
Phailin	11.08	6.82	14.06	7.1	8.04	5.75	7.63	6.28	7.82	6.82
Thane	9.01	7.7	8.37	5.04	8.82	5.5	8.93	5.75	8.57	5.91
Lehar	12.59	7.93	12.51	9.96	13.32	8.25	4.28	5.16	13.61	8.8
Fani	6.28	6.54	8.02	7.17	7.23	5.1	5.34	5.83	7.4	3.44
Gaja	9.92	6.5	11.78	7.76	11.53	8.09	11.52	7.5	11.79	7.43
Mean	10.52	7.39	14.31	8.78	11.36	7.18	8.54	6.42	11.53	7.21

To gain an understanding of the factors leading to the differences in the performance of different microphysics schemes in the track and intensity predictions, the thermodynamics, wind field and hydrometeors from different simulations are analyzed. The VSCS Hudhud is considered for this analysis as many observational estimates are available for this cyclone.

5.3.2. Analysis of storm thermodynamics

The warming in the upper layers in the core region of TCs is due to subsidence as well as condensation whereas the cooling in the lower layers is due to convergence and evaporation of moist air. The coupling between thermodynamics and dynamics by the above processes determines the intensification of the system. The microphysical processes (phase changes) influence the heating or cooling within the TC as a resultant of condensation or sublimation, which in turn will influence the dynamics of the storm. The thermodynamic environment simulated by the microphysics schemes is analyzed through parameters like temperature anomaly, vertical velocity, theta-e and the relative vorticity. Figure 5.7 shows the azimuthally averaged radius-height cross section of temperature anomaly representing the atmospheric warming produced at the time of peak intensification stage (18 UTC 11 Oct 2014) relative to the initial time of cyclone Hudhud. The corresponding CIRA Multiplatform TC analysis data is used for comparison. Compared to CIRA data all the schemes overestimated the warming as well as its horizontal and vertical extent near the center of the TC. The CIRA data indicates that the maximum warming is distributed in the 10-14 km layer and radially up to 70 km from the center of the cyclone. Some of the differences in the features such as the horizontal and vertical extents of warming could be due to the differences in the resolution of the model and the datasets. The warmest temperatures are found in the eye itself since the air temperature within the TC shows a steady rise as the air converges inward towards the eyewall and then a rapid rise as it enters the eye. All the simulations show the warming to start above the boundary layer and extend vertically up to 16 km. Among the different microphysics Morrison best predicted the warming with a vertical extent of 13 km and horizontal extent of 50 km, followed by the WSM6, Goddard and Thompson even though the warming was overestimated by 5°C by the schemes. The cloud microphysical processes cause the diabatic heating due to phase transitions (condensation) which will influence the dynamical processes. Though none of the schemes could exactly match with the CIRA estimates, the distribution of warming including the radius and vertical extent are well predicted by Morrison and Thompson schemes.

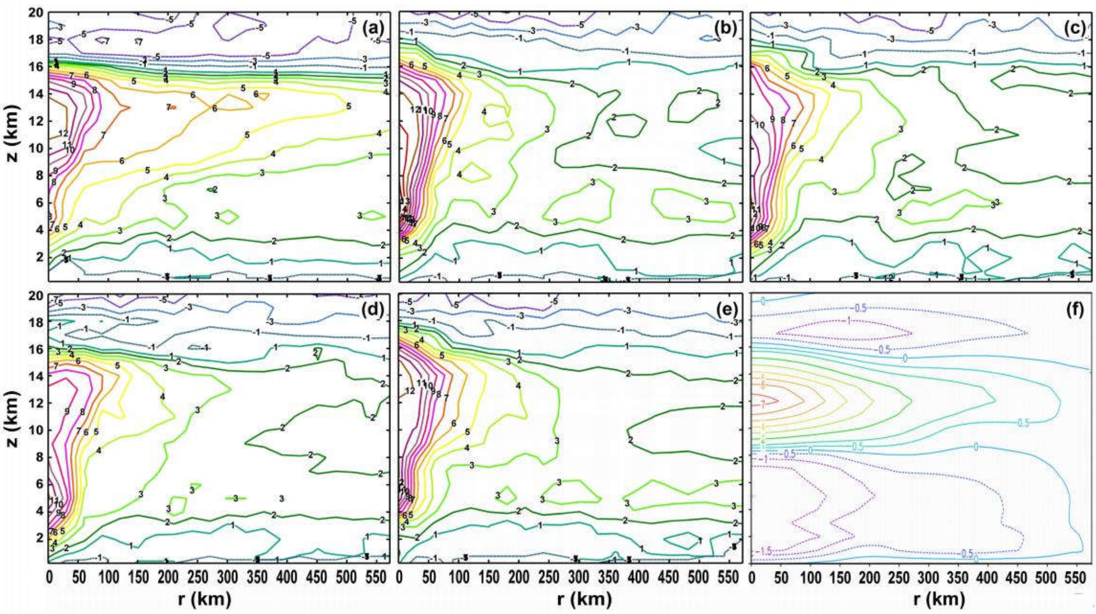

Figure 5.7. *Azimuthally averaged radius height cross section of temperature anomaly (°C) from 00 UTC 8 Oct to 18 UTC 11 Oct 2014 by* ***(a)*** *Morrison,* ***(b)*** *Lin,* ***(c)*** *WSM6,* ***(d)*** *Thompson,* ***(e)*** *Goddard for TC Hudhud compared with* ***(f)*** *CIRA data.*

The vertical section of area average theta-e over a 2° × 2° area around the centre of the cyclone Hudhud during its intense phase at 18 UTC 11 Oct 2014 (Fig. 5.8) indicates the formation of a convectively unstable region in the lower layers and stable divergent region in the upper layers. A local minimum in theta-e is found in the middle troposphere, reflecting drying associated with subsidence into the eye. Relatively higher theta-e values are noted at the lower levels (0-1km) and at upper levels (10 -16 km). Generally, all the schemes produced a gradual decrease in theta-e with height up to 4 km and an increase further upwards. The highly convective layer from 3 to 5 km of the cyclone is well reproduced by the model with a decrease in theta-e. The increase in theta-e in the upper troposphere indicates stable divergent layer of the TC. A high value of theta-e in the lower levels is due to the convergence of moisture towards the center of TC. The WSM6 scheme produced highly unstable layer followed by the Goddard, Lin, Thompson and Morrison.

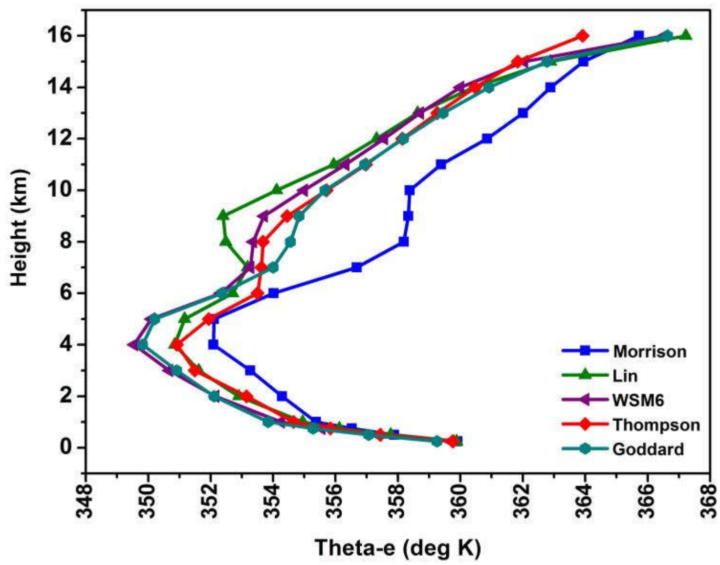

Figure 5.8. *Vertical profile of simulated theta-e averaged over an area of 2° × 2° from the center of Hudhud at 18 UTC 11 Oct 2014.*

The convective scale vertical motions (updrafts/downdrafts) occur in the vertical zone where inflows converge just a kilometer or two radially outward from the horizontal wind maxima (Smith, 2006). The vertical profile of a 2° × 2° area averaged vertical velocity around the center of Hudhud (Fig. 5.9) shows that Goddard produced the maximum updraft of 34 cm/s in the layer 12-13 km followed by Lin and WSM6 (33 cm/s) in the layer 12-13 km, Thompson (30 cm/s) and the Morrison (25 cm/s) in the layer 13-14 km. It is seen that the simulated vertical motions by various schemes are in agreement with the degree of convective instability produced by them. The Goddard and WSM6 schemes produced the maximum vertical motions by simulating highly convective atmospheres while Morrison produced minimum vertical motions by simulating less convective layers than other schemes. All the other schemes simulated moderate vertical velocities and convective structures.

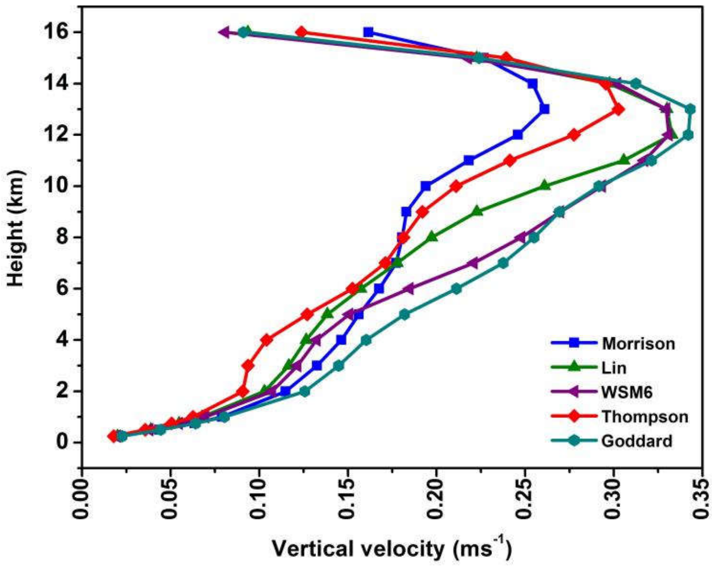

Figure 5.9. *Vertical profile of simulated vertical velocity averaged over an area of 2° × 2° from the center of Hudhud at 18 UTC 11 Oct 2014.*

5.3.3. Wind flow and structure

The vertical section of azimuthally averaged radial wind of cyclone Hudhud at its peak intensification from different experiments is presented in Figure 5.10. Since the radial wind represents the inflow (negative values) which is prominent at the lower levels of the cyclone, the analysis was confined to the lower 2.5 km layer of the atmosphere. From the results it is observed that the Lin, WSM6 and Goddard schemes predicted the maximum amount of inflow (-26 to -28 m/s). Morrison and Thompson produced relatively lower values of inflow. Morrison produced its maximum inflow at about 80-100 km. All other schemes produced their maximum value of inflow at 50 km from the core. Strong radial winds in the lower levels indicate stronger convergence, intense vertical motion and a strong warming of the core which promotes the strengthening of the cyclone. It is noticed that in general in all the schemes (except Thompson and Morrison), the outflow (positive values) is prominent from 1.5 km upwards. Goddard and Lin produced stronger outflow of 16 m/s and 13 m/s respectively thereby promoting to produce stronger cyclone. The highest value of theta-e produced by the Lin, WSM6, and Goddard schemes (Fig. 5.8) is due to the stronger radial winds in these cases. The Morrison and Thompson schemes produced minimum inflow and outflow which shows the early weakening of the cyclone.

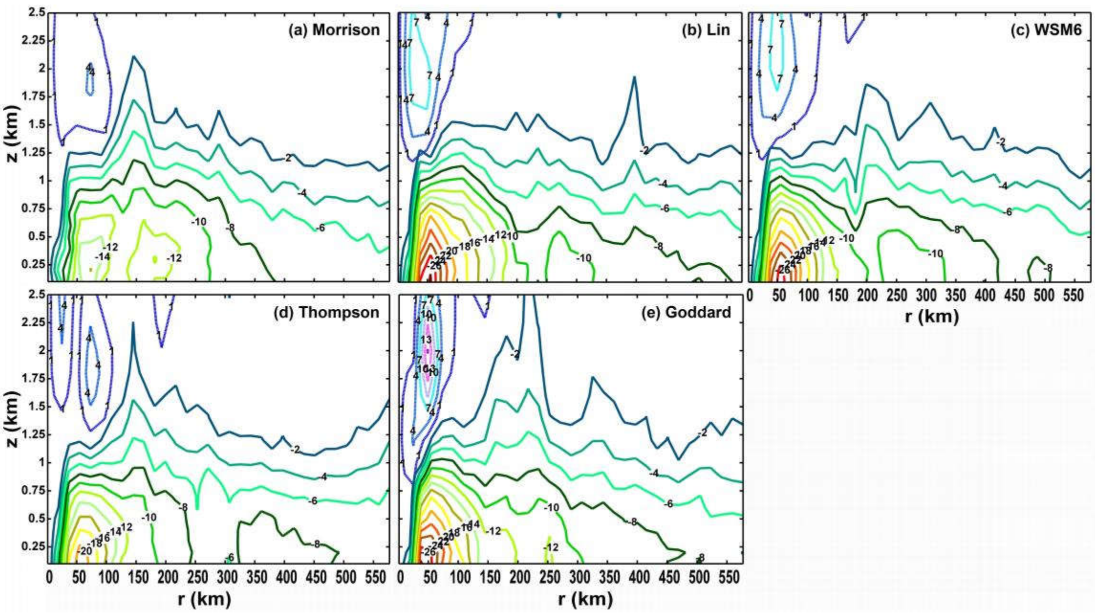

Figure 5.10. *Azimuthally averaged radius height cross section of simulated radial wind (m/s) by **(a)** Morrison, **(b)** Lin, **(c)** WSM6, **(d)** Thompson, **(e)** Goddard for TC Hudhud at 18 UTC 11 Oct 2014.*

The vertical structure of azimuthally averaged tangential winds for Hudhud at 18 UTC 11 Oct is compared with corresponding data from CIRA (Fig. 5.11). From the tangential wind speed distribution for a steady axisymmetric vortex, one can determine the radial distribution of the vertically-averaged wind speed components in the boundary layer as the functions of radius as well as the induced vertical velocity at the top of the boundary layer. From Figure 5.11 it is observed that all the schemes except Morrison overestimated the wind speed (60-75 m/s) relative to the observation (50 m/s). While the maximum wind speed in CIRA data (Fig. 5.11f) prevails vertically up to 10 km, it extended vertically to about 2 km only in different simulations. These differences in the maximum winds and their vertical extents between model and the CIRA data could be due to difference in resolutions as also seen in Figure 5.7. Secondly, the horizontal resolution of AMSU instrument (25 km) results in a smooth temperature field and low tangential wind speeds extending to unrealistically high elevations.

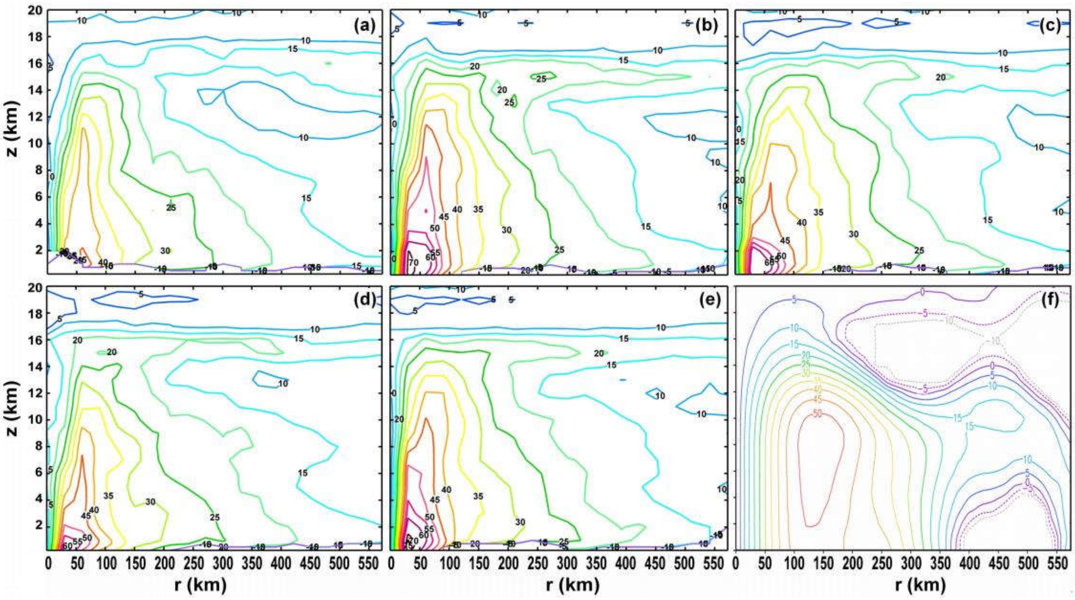

Figure 5.11. *Azimuthally averaged radius height cross section of tangential wind (m/s) at 18 UTC 11 Oct 2014 by **(a)** Morrison, **(b)** Lin, **(c)** WSM6, **(d)** Thompson, **(e)** Goddard for TC Hudhud compared with **(f)** CIRA data.*

5.3.4. Hydrometeors distribution

McCumber et al. (1991) showed that the use of ice microphysics simulated better results in reproducing some features of the observed convection, and that for the tropical convection the optimal mix of bulk ice hydrometeors is ice, snow and graupel. Takahashi and Shimura (2004) in a study of tropical rain characteristics and microphysics indicated the importance of diffusive and riming growth of ice particles and the associated release of latent heat in the development of convection and rain. Franklin et al. (2005) in a numerical simulation study of a cyclone, found that the model was sensitive to the increase in graupel fall speeds which thus confined it to the convective regions causing high rain rates at the inner core of the storm. In the present work, the mixing ratios of six hydrometeors namely water vapor (qvapor), cloud water (qcloud), rainwater (qrain), cloud ice (qice), snow (qsnow) and graupel (qgraup) are analyzed to understand their contribution to the intensity of TC. The analysis is carried out for cyclone Hudhud at its peak intensification stage (18 UTC 11 Oct).

Figure 5.12 shows the vertical distribution of area average mixing ratios of various hydrometeors (qvapor, qcloud, qrain, qice, qsnow, and qgraup) over a 2° × 2° area around the center of Hudhud at its peak intensification. It is observed that except for qvapor large variation in hydrometeors distribution is observed among different microphysics simulations. In general, Goddard and Thompson schemes produced high amount of qcloud while Lin and WSM6 produced low amount (Fig. 5.12b) both in the lower and upper troposphere. Morrison produced the largest amount of qcloud above 6 km. Goddard and WSM6 produced high amount of qrain below 6 km, followed by Lin, Morrison and Thompson. It is noticed that the ice (Fig. 5.12d) is mainly distributed in the upper layers above 6 km amsl and that most of the schemes simulated the maximum ice in the layer 8-14 km except Morrison which showed the peak ice in the layer 13-16 km. The Goddard scheme produced the highest amount of ice followed by WSM6, Lin and Morrison. The Thompson scheme hardly produced any ice and this result corroborates with the results for the heavy rainfall event associated with 2015 tropical low pressure system in the Bay of Bengal reported in Chapter 4 and the earlier study on extreme rainfall event by Dasari and Salgado (2015). Unlike qice, qsnow is mainly distributed in the layer 6-13 km in most of the simulations (Fig. 5.12e). The Thompson scheme followed by the Goddard, Morrison and WSM6 simulated considerable amounts of snow extending vertically between 6 and 13 km. Lin produced very small amount of snow. The ability of the Thompson scheme to predict considerable amount of snow is also reported in the previous chapter on tropical low pressure system. Unlike other hydrometeors the qgraup is concentrated in the 5-8 km middle tropospheric layers (Fig. 5.12f) in all the simulations. Goddard and WSM6 simulated the largest amount of graupel followed by Lin, Morrison and Thompson.

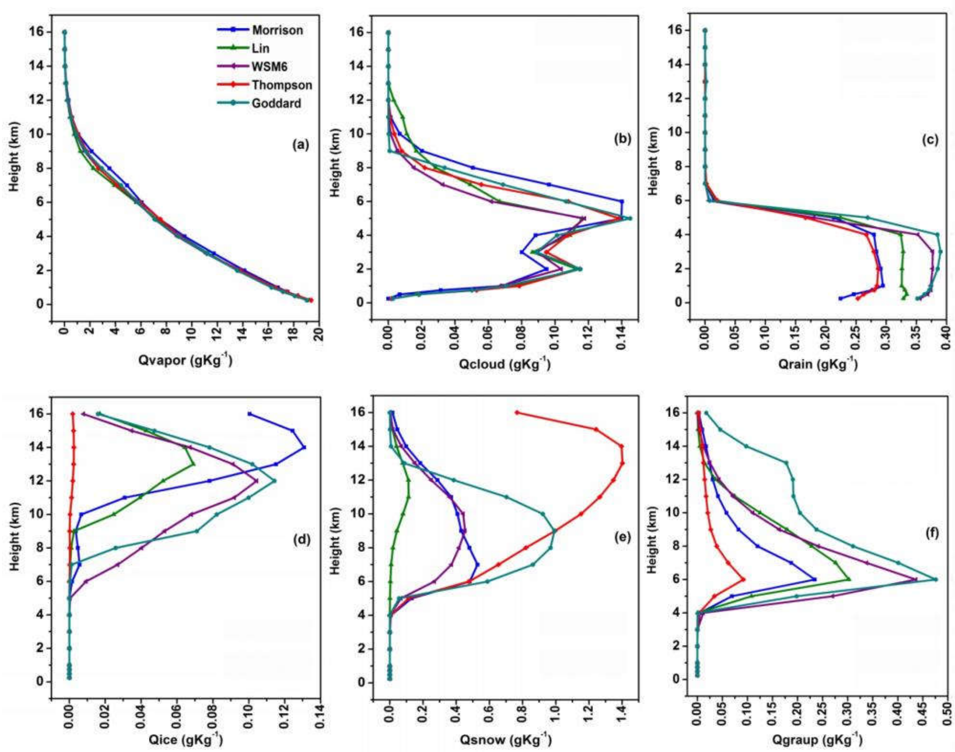

Figure 5.12. *Vertical profiles of simulated **(a)** Qvapor, **(b)** Qcloud, **(c)** Qrain, **(d)** Qice, **(e)** Qsnow, **(f)** Qgraup averaged over an area of 2° × 2° from the center of Hudhud at 18 UTC 11 Oct 2014.*

The zonal variation of the mixing ratios of three ice hydrometeors, cloud ice (qice), snow (qsnow) and graupel (qgraup) are also analyzed to understand their contribution to the intensity of TC and is respectively presented in Figures 5.13, 5.14 and 5.15. It is noticed that the overall production of ice (Fig. 5.13) is very small in amount for all the schemes. Also, the Goddard scheme produced the highest amount of ice between 8-14 km which is prominent along the eyewall. All the other schemes (WSM6, Morrison, Lin) except Thompson produced only moderate values of ice. The spatial qsnow distribution (Fig. 5.14) shows that Goddard followed by Thompson and Morrison simulated considerable

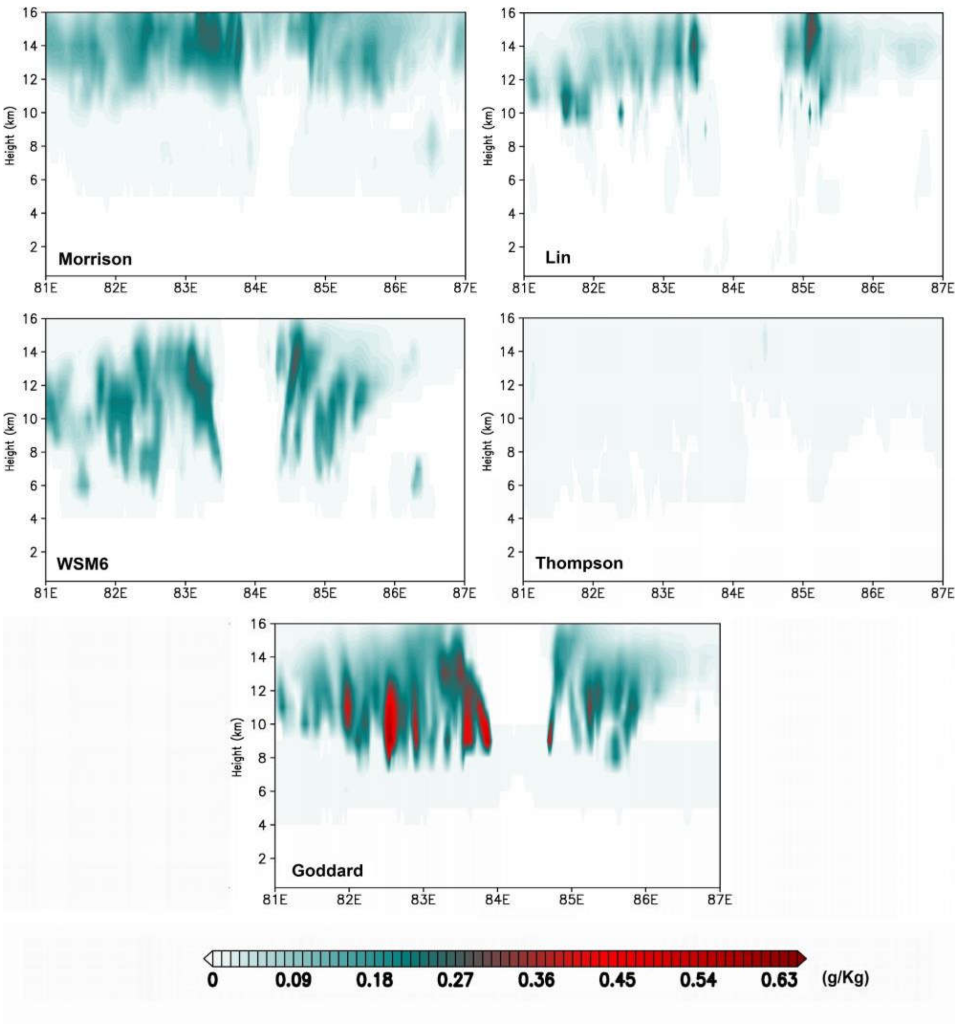

Figure 5.13. *Zonal variation of simulated qice with height for TC Hudhud at 18 UTC 11 Oct 2014 by Morrison (18.69°N), Lin (17.48°N), WSM6 (17.07°N), Thompson (17.64°N) and Goddard (17.80°N).*

amounts of snow extending vertically between 6 and 16 km, with Goddard producing the largest amount and the Lin scheme giving very small amount. For Morrison snow is distributed along the eyewall, extending from 6-16 km, whereas for Goddard it, is distributed along the rain bands as well though it extended only up to 12 km. For Thompson, a large amount of snow can be found along the eyewall. From the zonal variation of qgraup (Fig. 5.15) indicates that the Lin, WSM6, and Goddard schemes simulated high amounts of graupel along the eyewall. The heating within the inner core is greatly influenced by the production of graupel in that region (Mukhopadhyay et al., 2011;

Kanase and Salvekar, 2015). This correlates with theta-e (Fig. 5.8) where the Lin, WSM6 and Goddard produced maximum theta-e at the inner core and also very unstable middle layers.

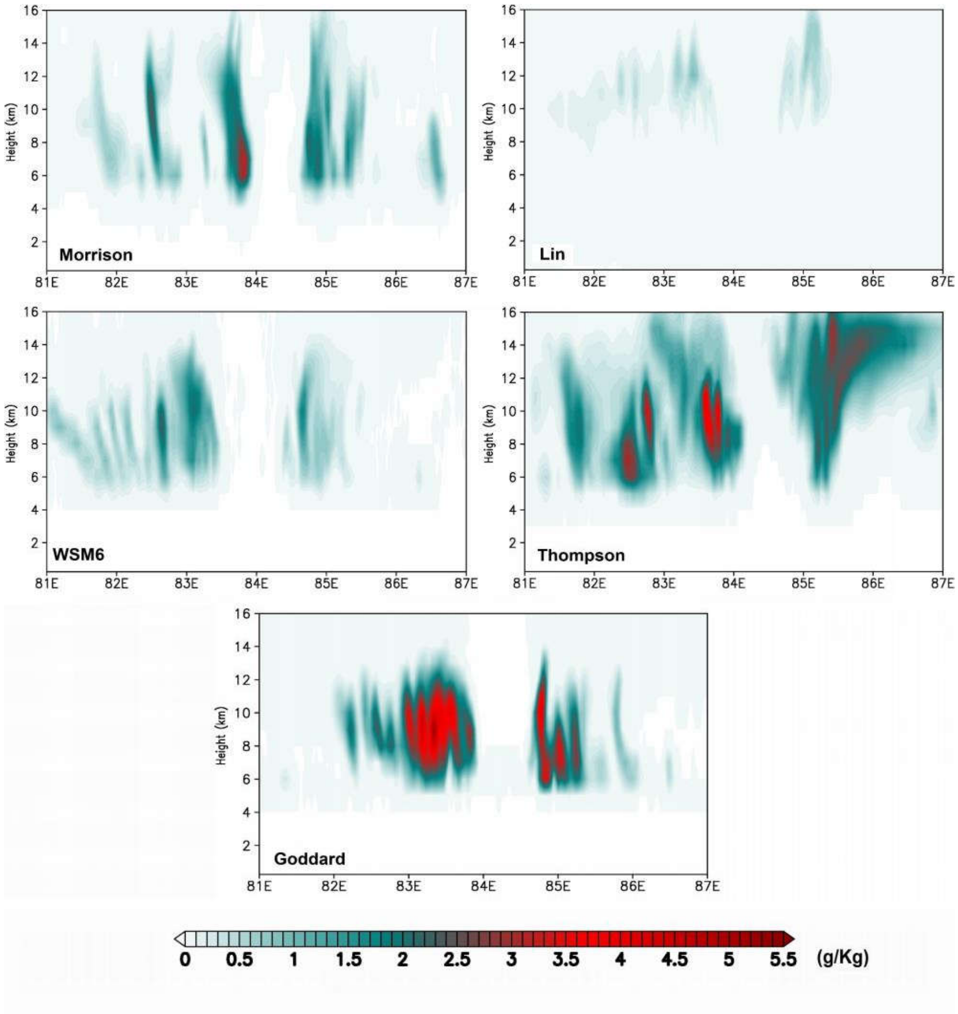

Figure 5.14. *Zonal variation of simulated qsnow with height for TC Hudhud at 18 UTC 11 Oct 2014 by Morrison (18.69°N), Lin (17.48°N), WSM6 (17.07°N), Thompson (17.64°N) and Goddard (17.80°N).*

The hydrometeor analysis suggests that the Goddard, WSM6 and Lin schemes simulated most of the hydrometeors with good vertical distribution. Morrison produced a high amount of ice with very small quantities of other hydrometeors. Similarly, Thompson produced very little quantity of ice, rain and graupel. The cloud microphysics influences the simulations by vertical heat and water vapor distributions and their feed back to the largescale environment by enhancing the convection. The heating within the inner core is greatly influenced by the graupel production in the inner core region (Mukhopadhyay et al., 2011; Kanase and Salvekar, 2015). The present simulations show that Goddard, WSM6 and Lin produced highly intensive cyclone whereas Thompson and Morrison simulated weaker cyclone. The strong intensification of Hudhud in the case of Goddard, WSM6 and

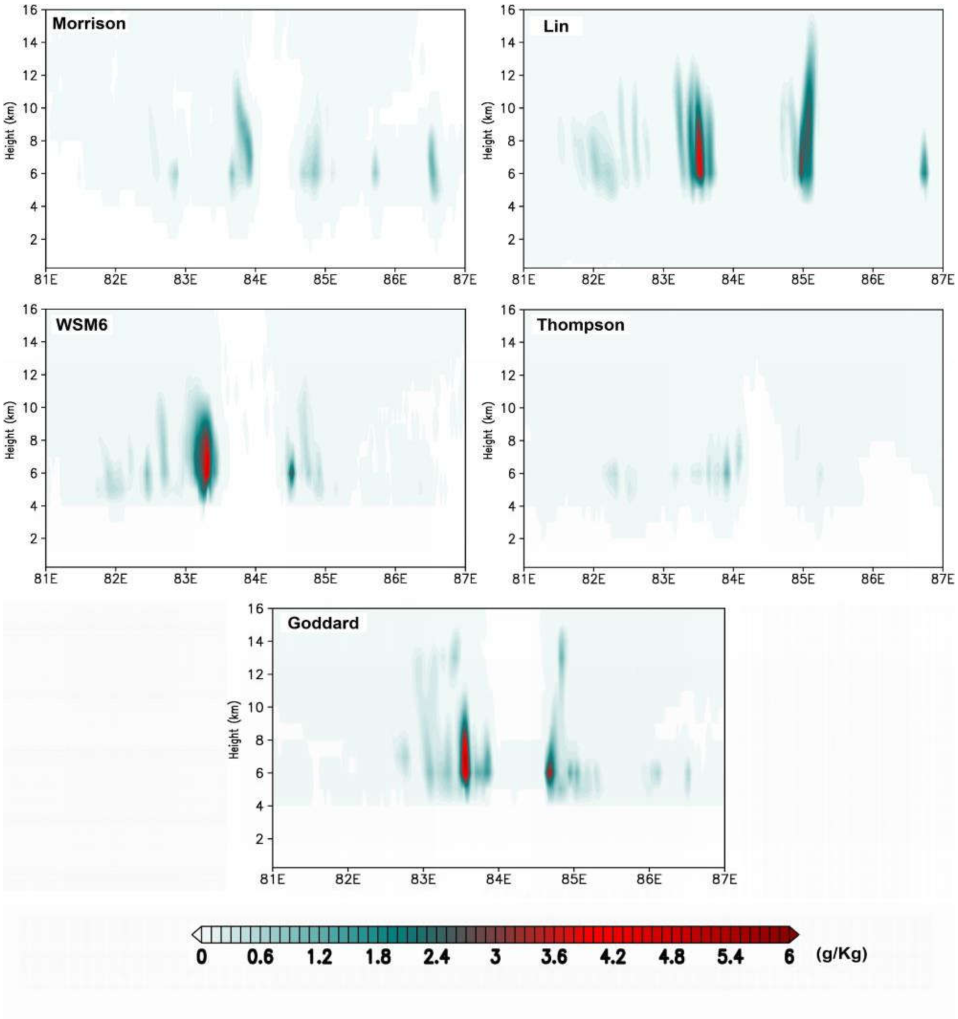

Figure 5.15. *Zonal variation of simulated qgraup with height for TC Hudhud at 18 UTC 11 Oct 2014 by Morrison (18.69°N), Lin (17.48°N), WSM6 (17.07°N), Thompson (17.64°N) and Goddard (17.80°N).*

Lin is due to simulation of a majority of the hydrometeors in good quantity and distribution which enhanced the latent heating and vertical motion and thus facilitated formation of deep convectively unstable layers as evident from theta-e and vertical velocity distributions seen in Figures 5.8, 5.9 respectively.

5.3.5. Vertical motions

An important aspect in the numerical modelling of TCs is how well the models can resolve the convection to obtain realistic intensity and track predictions. It is expected that high resolution ($\leq$ 3 km) models with microphysics alone can fully resolve the convection and precipitation processes without the need of cumulus schemes (Seifert, 2011; Gopalakrishnan et al., 2011; 2012). The lack of comprehensive observational data especially of vertical motion in the region of TCs limits detailed model evaluation for convection. However, with the advancement of land-based RADAR wind profilers some information on the vertical motion in TCs is now possible whenever the TCs approach or pass near to the observation stations. Here, the efficiency of various microphysics schemes in resolving the convective motions in high resolution simulations is examined using a few MST RADAR vertical velocity profiles available for Fani and Gaja cyclones.

Model derived vertical velocity profiles are compared with the corresponding data from MST RADAR at Gadanki station during the period when the cyclones passed near to the observation station Gadanki. Gadanki station (13.5°N, 79.2°E) is situated about 100 km northwest of Chennai near Tirupati in Andhra Pradesh. As per the best track data, Gadanki station falls at a range of about 400-600 km from the centre of cyclones Fani and Gaja during their passage in the east central Bay of Bengal near to the station. The information on the nearest positions of Fani and Gaja cyclones to Gadanki station during their movement over east central Bay of Bengal is obtained from the IMD best track data.

The time-height profiles of simulated vertical velocities at Gadanki by different microphysics experiments are presented in Fig. 5.16 and Fig. 5.17 for Fani and Gaja respectively. As seen from these figures' strong updrafts (0.7 m/s) are simulated in the layer 8-15 km between 00 UTC 30 April and 00 UTC 1 May 2019 for Fani (Fig. 5.18) and between 00 UTC 14 Nov and 00 UTC 15 Nov 2018 for Gaja (Fig. 5.19) in most of the simulations. The simulations also show downdrafts (-0.2 m/s for Fani and -0.5 m/s for Gaja) in the upper layers. Both updrafts and downdrafts are stronger in the upper layers compared to the lower layers.

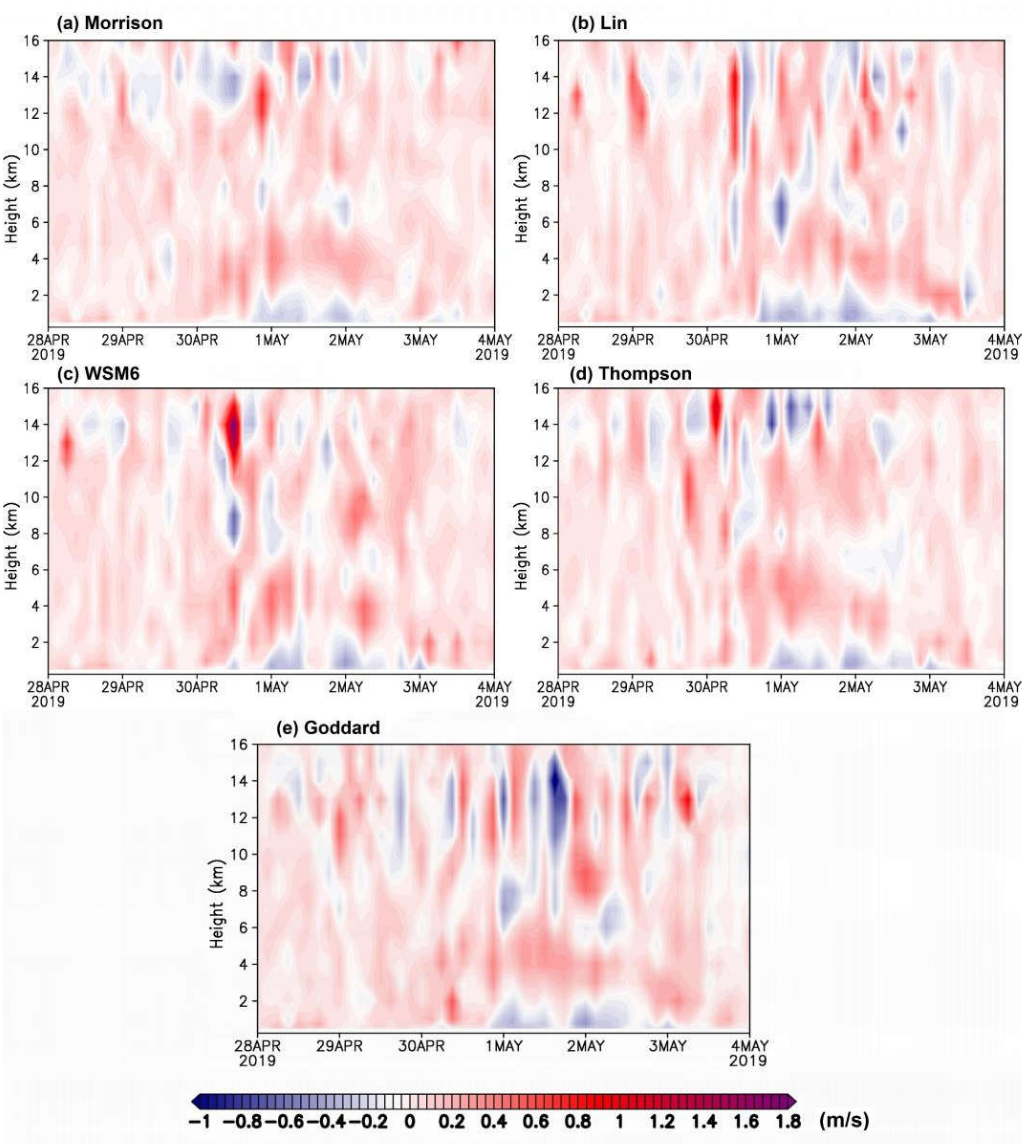

Figure 5.16. *Time height profiles of simulated vertical winds for Fani at Gadanki by* ***(a)*** *Morrison,* ***(b)*** *Lin,* ***(c)*** *WSM6,* ***(d)*** *Thompson and* ***(e)*** *Goddard.*

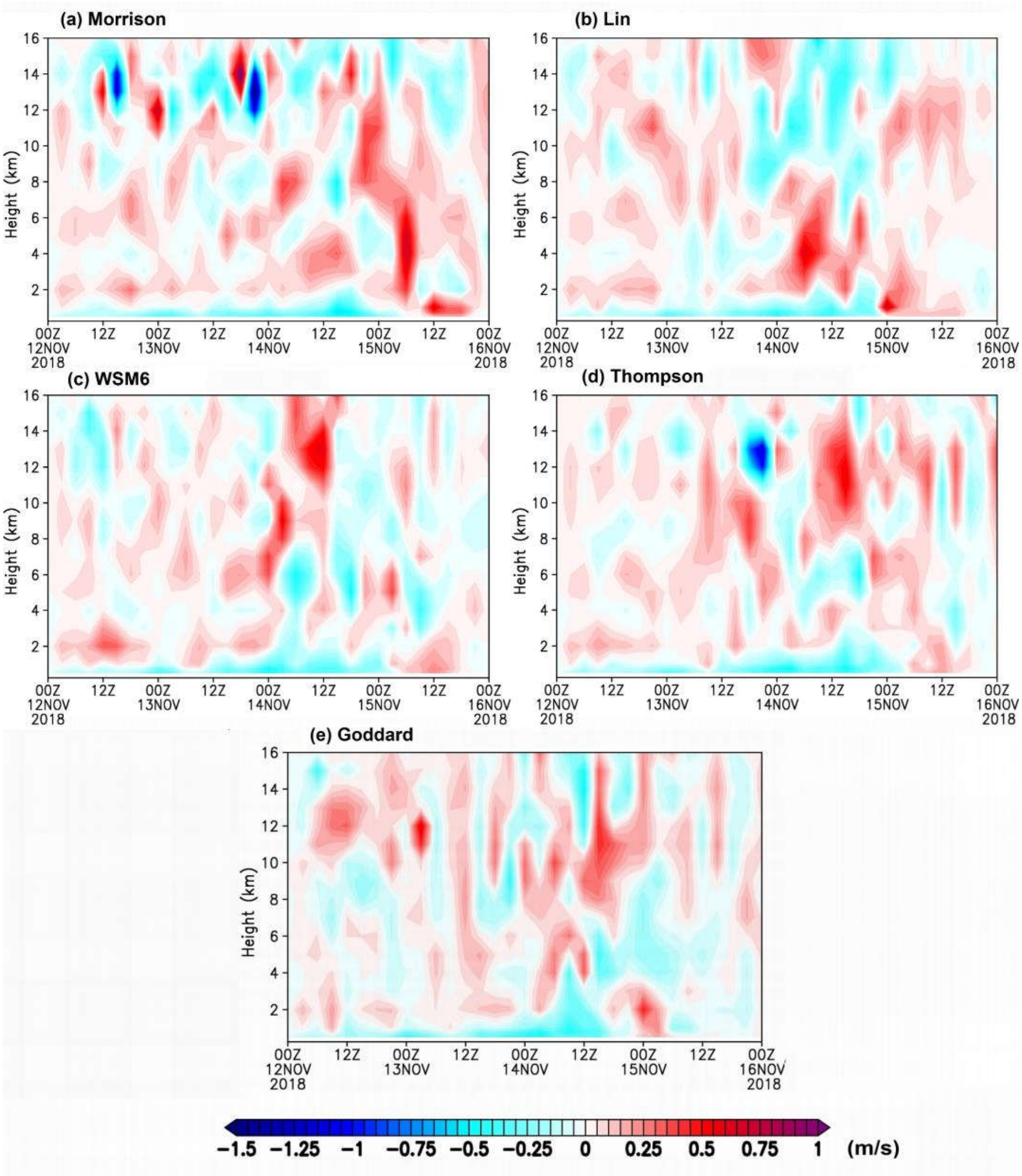

Figure 5.17. *Time height profiles of simulated vertical winds for Gaja at Gadanki by **(a)** Morrison, **(b)** Lin, **(c)** WSM6, **(d)** Thompson and **(e)** Goddard.*

Figure 5.18 shows the MST Radar observed vertical wind profiles for Fani between 30 April and 1 May 2019. The Radar profiles at different times shows large variation of vertical winds especially in the upper 10 - 16 km region in Troposphere representing random upward as well as downward motions. To obtain a convenient way of comparison the vertical wind profiles from simulations are averaged over a 24 h window (00 UTC 30 April – 00 UTC 1 May 2019 for Fani; 00 UTC 14 Nov - 00 UTC 15 Nov 2018 for Gaja) and compared (Fig. 5.19) with corresponding average observation profiles from MST

Radar. As shown in Figure 5. 19a we notice strong upward motions (0.05 m/s- 0.15 m/s) in the lower and upper layers 3-7 km, 10-13 km, and downward motion (-0.05 m/s) in middle layers 8-10 km for Fani. The model could capture these vertical variations in vertical motion with some differences in different experiments. It can be seen that for Fani, the Goddard, Thompson and Morrison show closer agreement with the observations at lower altitudes (1-5 km) and Thompson, WSM6 and Morrison produce a closer match in the middle layers (5-9 km). At higher altitudes (13-16 km), Morrison, Goddard, and WSM6 give a better prediction. Overall, Morrison followed by Thompson produced the vertical wind profile in better agreement with the observations when compared to other schemes throughout the troposphere. The WSM6 scheme shows largest deviations from observations at the most of the heights indicating overestimation. For Gaja cyclone (Fig. 5.19b), the experiments with Thompson followed by Morrison and Goddard produced better agreement of vertical velocities with observations and WSM6, Lin produced large deviations in both lower and upper layers.

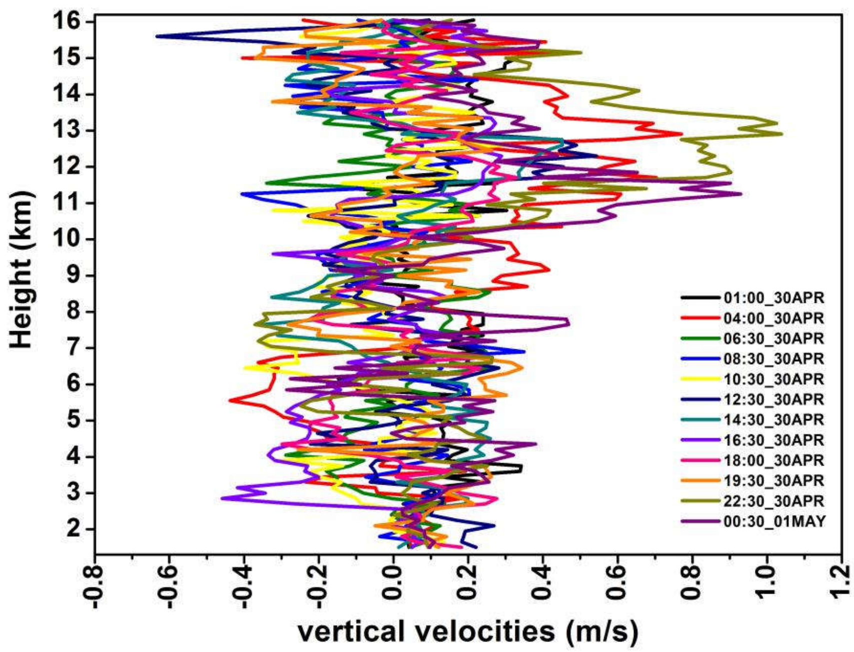

Figure 5.18. *Vertical winds from MST radar at different times (IST) during 30 April to 1 May for Fani.*

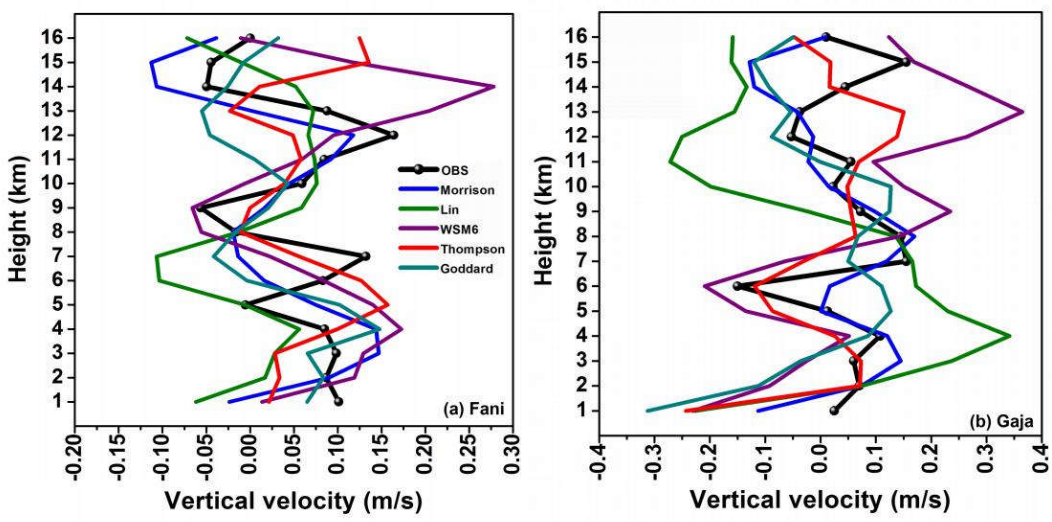

Figure 5.19. Simulated vertical wind profiles by different microphysics schemes compared with MST radar profiles at Gadanki for **(a)** Fani and **(b)** Gaja.

For a better understanding of the performances of different microphysics in representation of convection, the deviations of simulated mean vertical wind profiles from the corresponding mean radar profiles are analyzed for as shown in Figure 5.20. The vertical line in these plots indicates perfect fit of simulated convection with observed convection. We find that the deviations in vertical velocities are minimum in the experiments with Morrison, Thompson and Goddard schemes at different layers for both the cyclones. Among these three schemes the Thompson and Morrison schemes showed highly consistent trends of vertical motions in the lower, middle and upper layers giving closer comparison to observed vertical motion and indicating better representation of convection. Owing to the limitation of stationary observations at a range of 400-600 km and their availability only during the developing stages of the storms a complete characterization of simulated vertical motions for the entire life cycle could not be provided. Nevertheless, the current analysis shows the fidelity of the convective permitting simulations in reproducing the observed cyclone vertical motions and the better representation of convection with Thompson and Morrison microphysics schemes.

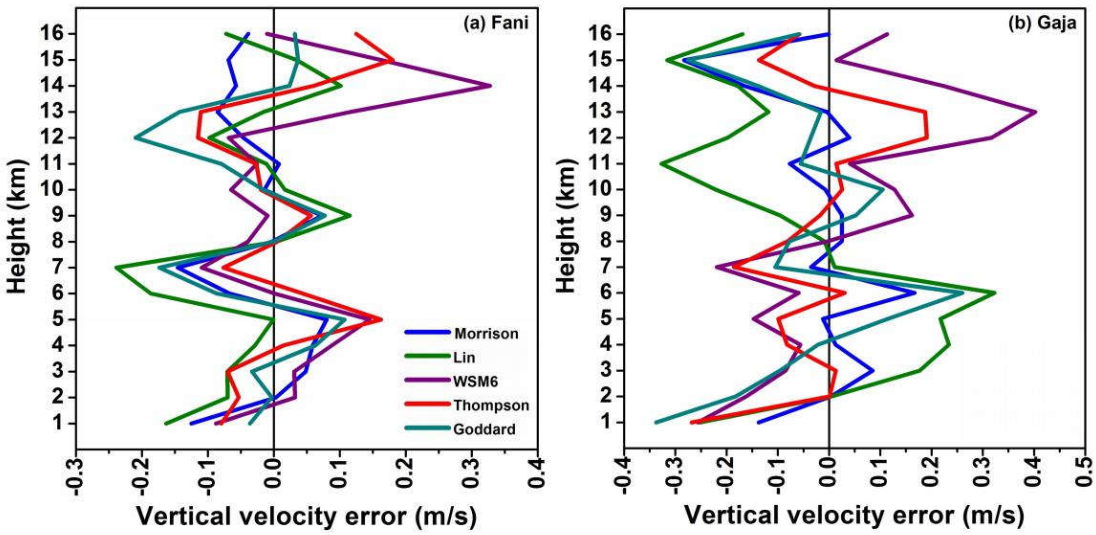

Figure 5.20. *Statistical errors of simulated vertical winds against MST radar profiles for **(a)** Fani and **(b)** Gaja.*

5.3.6. Maximum radar reflectivity

Simulated maximum cloud reflectivity is compared with the Chennai DWR data to examine the fidelity of reproducing the deep convective cloud bands by various microphysics experiments. Figure 5.21 shows the spatial distribution of maximum radar reflectivity for Hudhud at 03 UTC 12 Oct from different simulations along with DWR observation. All the schemes have over predicted (40-60 dbZ) the radar reflectivity indicating deeper convective cloud organization than the observed case (36-52 dbZ). In terms of the areas of convection all the schemes except Morrison represented the reflectivity in good agreement with the observation. These schemes though overestimated the reflectivity they reproduced the morphology of cloud reflectivity more accurately in terms of location and area extent of deep convection, clouds and high rainfall and the distribution of different intensities of rain bands as compared to the Morrison. They also better simulated the position of the cyclone as well as the features of comma structure, and eye development. Compared to Goddard, Thompson simulated the observed band with high reflectivity just west of the eye, as well as the low reflectivity area east of the eye.

The Morrison scheme simulated a weakened cyclone without eye which can be due to the erroneous landfall at that time (Fig. 5.2 and Fig. 5.3).

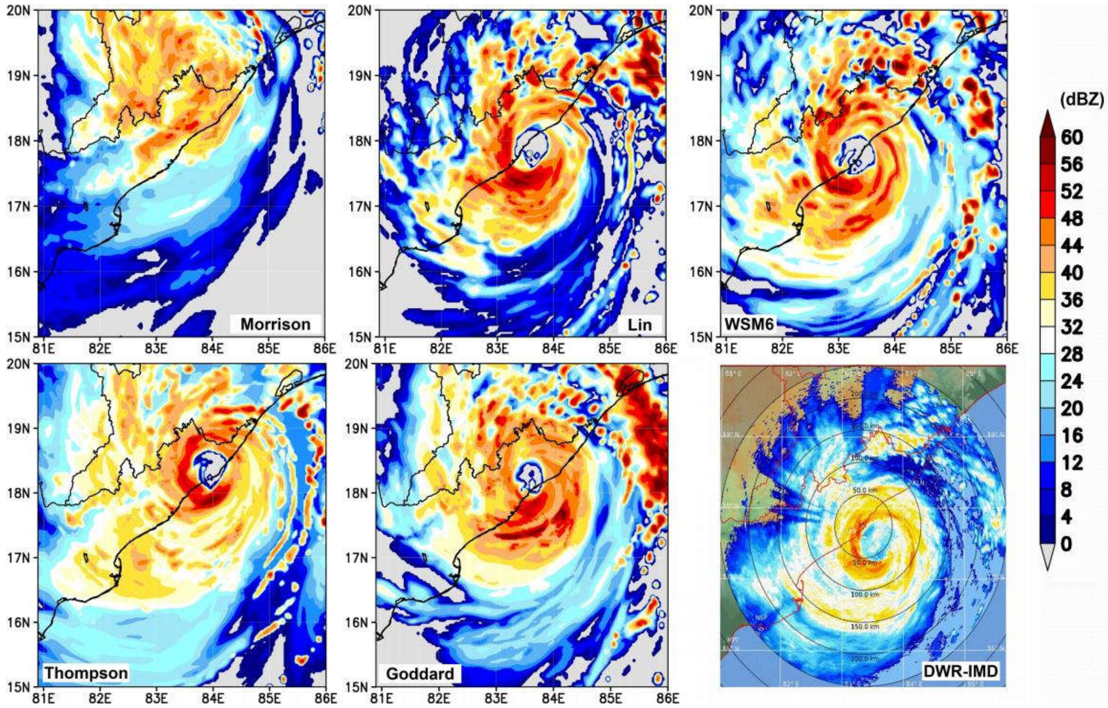

Figure 5.21. *Spatial distribution of simulated maximum radar reflectivity by different microphysics schemes compared with DWR, IMD, for TC Hudhud at 03 UTC 12 Oct 2014.*

Figure 5.22 shows the zonal variation of radar reflectivity with height for Hudhud at its peak intensity (18 UTC 11 Oct) for all the schemes. As in the previous analysis, the Lin, WSM6, and Goddard schemes have produced higher values of radar reflectivity along the eyewall where they predicted high values of vertical velocity (Fig. 5.9) and lower values of theta-e (Fig. 5.8). This can be attributed to the relatively stronger inflow, vertical motions and thus formation of large graupel (Fig. 5.12f) predicted by the three schemes. Morrison and Thompson produced relatively lower values of reflectivity which is due to the relatively weaker inflow, low vertical motions, upper level warming and low amounts of graupel.

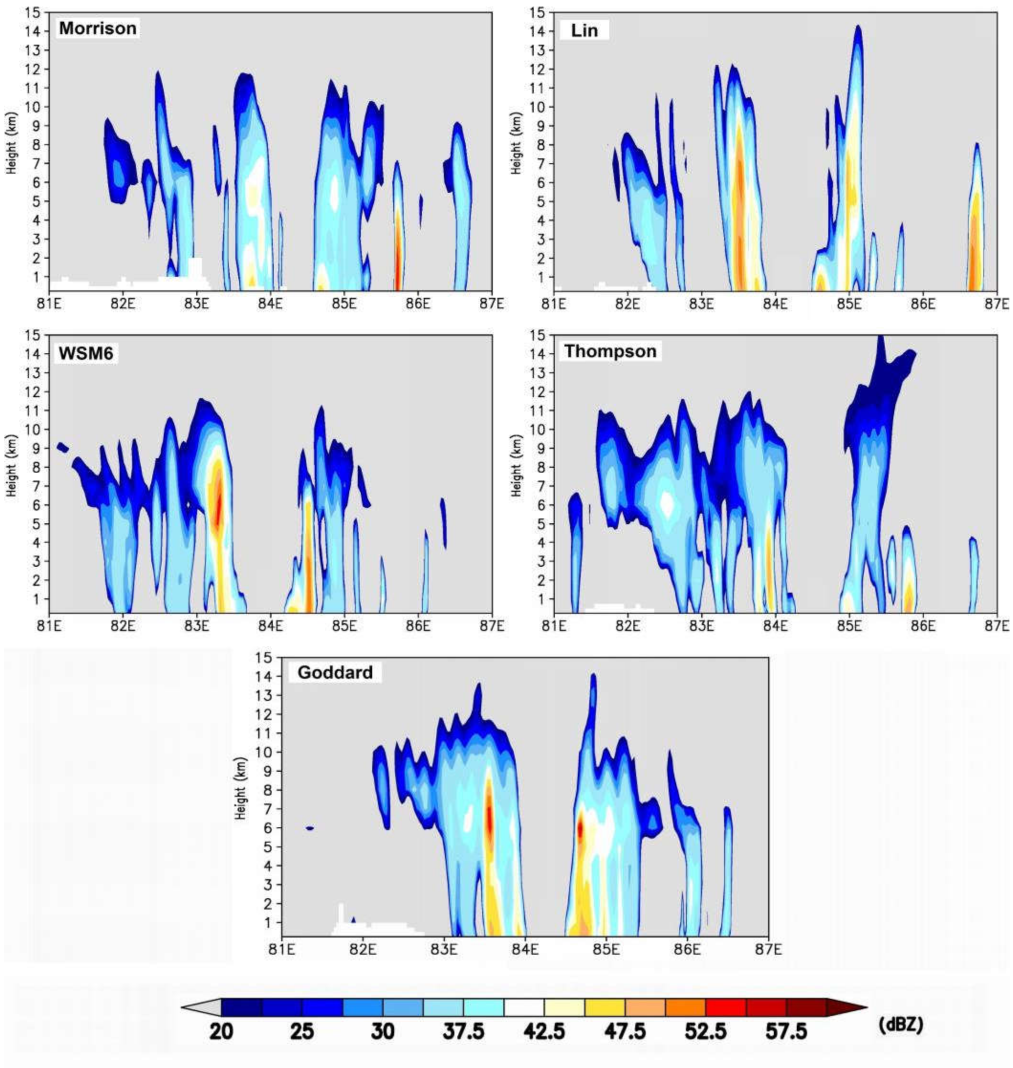

Figure 5.22. *Zonal variation of simulated radar reflectivity height for TC Hudhud at 18 UTC 11 Oct 2014 for Morrison (18.69°N), Lin (17.48°N), WSM6 (17.07°N), Thompson (17.64°N) and Goddard (17.80°N).*

5.4. Summary

In this chapter the sensitivity of track and intensity predictions of TCs over the BOB of NIO with the WRF-ARW model to different microphysics schemes is examined for six very severe cyclones. The study reveals the complexity in TC forecasting using explicit convection schemes. Results of simulated CSLP, MSW and track positions indicate that the microphysics schemes mainly affect the intensity and produce moderate impact on track. Overall, based on aggregate error statistics for all the six cyclones it is found that Thompson produced the best predictions for both tracks and intensity. Next to

Thompson, the Morrison and Goddard gave the best intensity prediction. Results suggest that the Thompson scheme gives least errors for both the track and intensity parameters thus indicating the better performance for high resolution operational TC forecasting in the NIO.

A detailed analysis of various parameters for cyclone Hudhud indicated that WSM6, Goddard, and Lin schemes produced large heating (high theta-e), convective vertical motions and highly unstable layer in the middle troposphere. All the schemes over predicted the tangential wind speed and none of the schemes could produce the core of maximum winds, unlike the temperature anomaly and radial winds. A comparison of simulated vertical motions in the case of Fani and Gaja cyclones with MST Radar observed vertical velocities indicated that the Morrison and Thompson schemes best simulated the convective motions compared to the other tested microphysics. Overall, this analysis indicated that the sensitivity of the simulated TC activity to microphysics schemes is due to the variations in the phase transitions, diabatic heating and instability and convection which coupled to storm scale dynamics led to change in the intensity and track predictions. The Thompson scheme produced better intensity and track predictions due to producing more realistic representation of convective motions in the cyclone.

Chapter 6

Impact of SST surface boundary condition on TC intensification

6.1. Introduction

The phenomena of Tropical cyclonic storms involve complex ocean-atmospheric processes during their formation and further development stages. The TCs are coupled to ocean mixed layer through the heat and moisture exchanges at the air-sea interface and the necessary energy to maintain or strengthen the TCs comes mainly from these air-sea fluxes. Among various parameters, the upper ocean heat content and SST influence the genesis, intensification and track characteristics of TCs (Gray, 1978; Nicholls, 1984; Bender et al., 1993; Chan et al., 2001) as it influences the moisture transport through evaporation as well as the sensible heat transfer to the atmosphere. The oceanic effects on TC intensification through SST include both positive and negative contributions. Schade and Emanuel (1999) using a simple coupled ocean-atmospheric model found that the feedback of SST cooling could significantly reduce TC intensity. Warmer SST associated with large ocean heat content causes TC intensification (Hong et al., 2000; Shay et al., 2000; Bright et al., 2002), whereas negative SST anomalies associated with cold-core eddies or TC-induced cold wake weakens the TC systems (Bao et al., 2000; Bender and Ginis, 2000; Bender et al., 2007; Emanuel et al., 2004; Lin et al., 2005). There are also studies which show that changes in local SST alone is not a dominant factor for TC (Kotal et al., 2009; Ralph and Gough, 2008), and long term SST changes do have an influence on TC intensification (Vecchi and Soden, 2007). The rapid intensification (RI) of TCs is largely determined by the thermal profile of the upper ocean, where the intensity increases with an increase in SST. Several studies investigated the RI of cyclones with reference to the convective characteristics, SST, vertical wind shear, TC heat potential etc. (Wada, 2009; Tao and Zhang, 2014; Kanada et al., 2017, Potter et al., 2019). However, most of these studies were mainly focused on the cyclones over Atlantic or Pacific Oceans, where RI is quite common compared to the NIO. In contrast to the large number of studies on the role of SST in RI cyclones over other basins, very few studies are available over the NIO. Lin et al. (2009) have shown that the pre-existing warm ocean anomaly in the BOB lead to the RI of TC Nargis. With this gap, the current study in this chapter examines the role of SST in RI phase of two pre-monsoon TCs over NIO by conducting numerical simulations with satellite derived real-time SST and climatological SST data sets.

6.2. Methodology

Two rapidly intensified cyclones Amphan and Fani that formed over the BOB of NIO during the pre-monsoon period of 2020 and 2019 respectively are chosen for the study. The intensity parameters such as the CSLP, MSW, intensity category, model simulation period and the total period of RI phase of the cyclones are provided in Table 6.1.

Table 6.1. *Details of TCs used for the study.*

TC	Category (MSW in m/s and CSLP in hPa)	Model simulation period (YYYYMMDDHH-YYYYMMDDHH) (hrs)	RI phase
Amphan	SuCS (66.8, 920)	2020051600-2020052100 (120)	2020051700-2020051821 (69 h)
Fani	ESCS (59.1, 932)	2019042800-2019050400 (144)	2019042900-2019043000 (24 h)

6.2.1. Brief description of RI phases

RI is defined as the sustained wind speed increase of ≥ 30 kts in 24 h (Kaplan and DeMaria, 2003). Cyclone Amphan has two RI phases (1) 00 UTC 17 May to 00 UTC 18 May, in which the wind speed increased from 45 kts to 100 kts (55 kts in 24 h) and (2) 00 UTC 18 May to 21 UTC 18 May, in which the wind speed increased from 100 kts to 130 kts (30 kts in 21 h). The intensity category of Amphan changed from CS to ESCS during the first phase and then to SuCS during the second phase. The wind speed increased from 45 kts to 130 kts (85 kts in 45 h) during the entire RI period (00 UTC 17 May to 21 UTC 18 May) (RSMC-IMD, 16^{th} -21^{st} May 2020: Summary). In the case of Fani, there is only one RI phase, 00 UTC 29 April to 00 UTC 30April, in which the wind speed increased from 45 kts to 80 kts (35 kts in 24 h). The intensity category of Fani changed from CS to VSCS during the RI phase (IMD, 2020, RSMC-2019).

6.2.2. Experiment

The WRF-ARW model v.3.9 is used for the simulations. Based on the results obtained with high resolution simulations in Chapters 3, and 5 for better predictions of TC characteristics for a large number of cyclones with 3-km resolution, the model is configured with two interactive nested domains (Fig. 6.1) with horizontal resolutions of 9 km and 3 km respectively and 45 vertical levels with 10 hPa at the top. The simulations are initialized either at the stage of cyclonic storm as per the IMD best track data and integrated until dissipating to CS stage after making the landfall. The NCEP-GFS 0.25° × 0.25° analysis data is used for initialization and the boundary conditions are updated every 3 hours with the GFS forecasts. The model physics options used for the simulations are provided in Table 6.2. The cumulus physics is used in the outer 9 km resolution domain and only microphysics is used in the inner 3 km resolution domain.

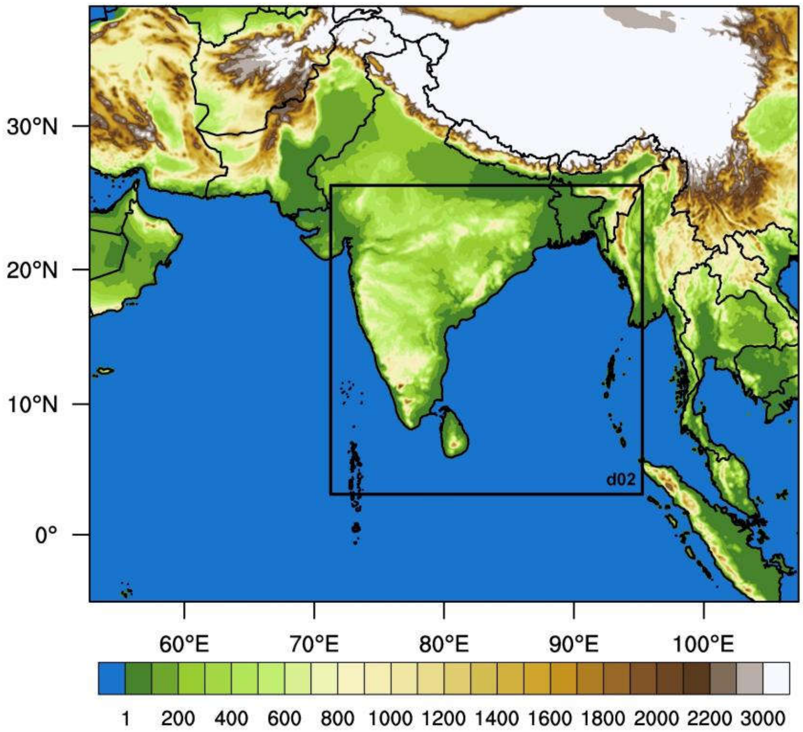

Figure 6.1. *Simulation domains used for the study with terrain height (m).*

Table 6.2. *Model physics used for the study.*

Physics	Scheme
Longwave radiation	RRTM (Mlawer et al., 1997)
Shortwave radiation	Dudhia(Dudhia, 1989)
Surface layer	MM5 similarity theory
Land surface processes	Noah LSM (Chen and Dudhia, 2001; Tewari, 2004)
Planetary boundary layer	YSU (Hong et al., 2006; Noah et al., 2003)
Cumulus	Kain Fritsch (Kain and Fritsch, 1993)
Microphysics	New Thompson (Thompson et al., 2008)

Two numerical experiments are conducted with WRF for each of the cyclones Amphan and Fani. In the first experiment (GFS-SST) the SST initial and boundary conditions are obtained from the GFS analysis and forecasts. In the second experiment (NOAA-SST), the NOAA/NCEP real-time global SST analysis is used for the SST initial and boundary conditions. In the third experiment (CLIM-SST) the model SST initial and boundary conditions are defined from a 11-year climatological mean SST computed from NOAA OISST data. The climatological mean SST for the model simulation days is derived from the daily SST mean for the period 2009 to 2019 for Amphan and 2008 to 2018 for Fani cyclone. The results of CLIM-SST are compared with GFS-SST and NOAA-SST simulations to understand the influence of SST change on TC intensity for the two cyclones. The GFS SST represents average SST conditions over 7-day period (refer section 2.3.1 of Chapter 2) and thus may not represent the variations during the life cycle of cyclones. The NOAA/NCEP SST is a high-resolution (10 km) analysis arrived by two-dimensional variational interpolation technique (Gemmill et al., 2007) of the most recent 24 h buoy and ship data, satellite SST data, and satellite-observed sea ice coverage-based SSTs.

6.3. Results and Discussion

The influence of the SST parameter on the intensification of the two cyclones is analyzed by comparing the model results from CLIM-SST (control run) with those from GFS-SST and NOAA-SST experiments. The SST differences between climatological SST and actual SST (either GFS or NOAA SST data) in these simulations account for the effect of variation of SST from the mean conditions.

Initially, the spatial SST field from GFS-SST, NOAA-SST and CLIM-SST over model 2nd domain and the averaged SST over the oceanic area of whole cyclone path at different instances were examined to analyze the resulting differences in the three experiments. The results of the simulations for CSLP, MSW from the experiments with GFS-SST, NOAA-SST and CLIM-SST (control run) are compared with the IMD best track data for the two cyclones. In addition, the time variation of wind shear, vertical velocity, sensible and latent heat fluxes, diabatic heating etc. are also analyzed to understand their differences among the three simulations and the underlying factors during the RI phase of the two cyclones.

Figure 6.2 shows the SST field along with the cyclone tracks from GFS-SST, NOAA-SST and CLIM-SST for Amphan at 00 UTC 17 May (24 h), 00 UTC 00 UTC 18 May (48 h), 00 UTC 19 May (72 h) and 00 UTC 21 May (120 h) which is followed by Figure 6.3 for Fani at 00 UTC 29 April (24 h), 00 UTC 30 April (48 h), 00 UTC 2 May (96 h), 00 UTC 3 May (120 h). It is observed that the SST in GFS-SST simulation has not varied much at different time intervals for both the cyclones (Fig. 6. 2a-d, Fig. 6.3a-d). For Amphan, the NOAA-SST shows a spatially varying SST and a higher SST (~1.5°C) than the GFS-SST. Moreover, unlike GFS-SST the NOAA-SST shows cooling on the rear sectors of the cyclone indicating cyclone induced cold wake formation. Unlike NOAA-SST, the GFS-SST does not indicate any variations of SST along the cyclone track. For NOAA-SST in the case of Amphan (Fig. 6.2e-h), cooling of ocean can be observed during both the RI phases, 24-48 h (Fig. 6.2f) and 48-72 h (Fig. 6.2g), with higher cooling at the second phase. The cooling induced by the cyclone is enhanced by ~ 4°C at 120 h (Fig. 6.2h), showing cooling over a major area over which the cyclone has passed. In the case case of Fani, the GFS-SST shows a higher SST (1 to 3°C from 24 h to 120 h) than the NOAA- SST in the 10-16°N belt of BOB (Fig. 6.3 a-d). The experiment NOAA-SST (Fig. 6.3e-h) shows that SST is initially 30.5-31.5°C at 24 h over east and central BOB but gradually reduced in the central and northern BOB indicating cooling with time along the track of the cyclone with large areal cooling at 120 h (Fig. 6.3h). It is also observed that both the cyclones moved along the areas of positive SST gradient which is clearly seen in the case of NOAA-SST. The CLIM-SST for both the cyclones (Fig. 6.2i-l, Fig. 6.3i-l) is ~ 1.5°C lesser than the SST in GFS and NOAA data. This shows that the sea was warmer than the normal during the formation of Amphan and Fani. A prominent variation with time is not observed for CLIM-SST as it represents a long-term average field.

Figure 6.4 shows the time variation of SST averaged over an area (7-19°N, 82-89°E) from the three experiments GFS-SST, NOAA-SST and CLIM-SST for Amphan and Fani. In the case of Amphan (Fig. 6.4a), the NOAA SST and GFS SST are warmer by about 1.65°C and 1°C respectively over the CLIM-SST in the period 00 UTC 16 May – 00 UTC 19 May during which the cyclone had an RI phase. Subsequent to 00 UTC 19 May while the SST difference reduced gradually to 0.65°C for NOAA SST, it remained

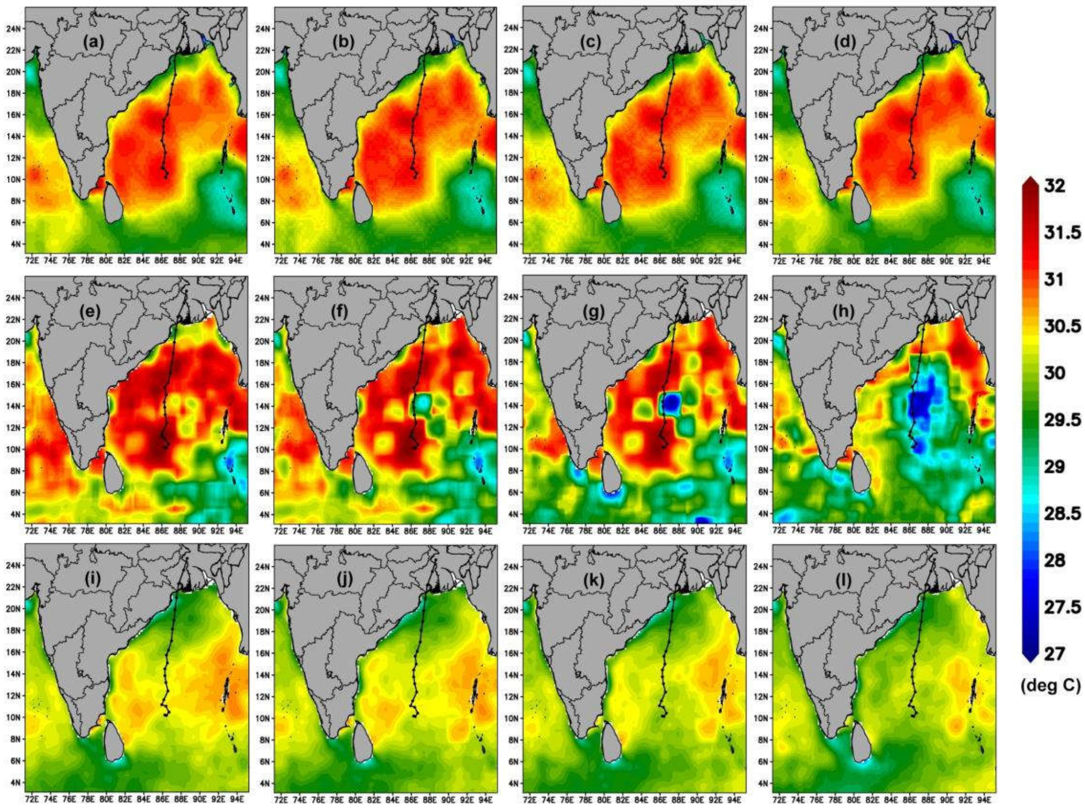

Figure 6.2. *SST field for Amphan cyclone from* ***(a-d)*** *GFS-SST,* ***(e-h)*** *NOAA-SST and* ***(i-l)*** *CLIM-SST at* ***(a, e, i)*** *24 h,* ***(b, f, i)*** *48 h,* ***(c, g, k)*** *72 h and* ***(d, h, l)*** *120 h.*

uniform for GFS SST. This clearly indicates a positive SST anomaly of 1.5°C from normal seasonal value during May 2020 when cyclone Amphan formed. The SST in the case of

GFS-SST is 0.75°C lesser than the NOAA-SST and 1.0°C higher than the CLIM-SST in the period 00 UTC 16 – 00 UTC 19 May 2020, suggesting a lesser positive SST anomaly

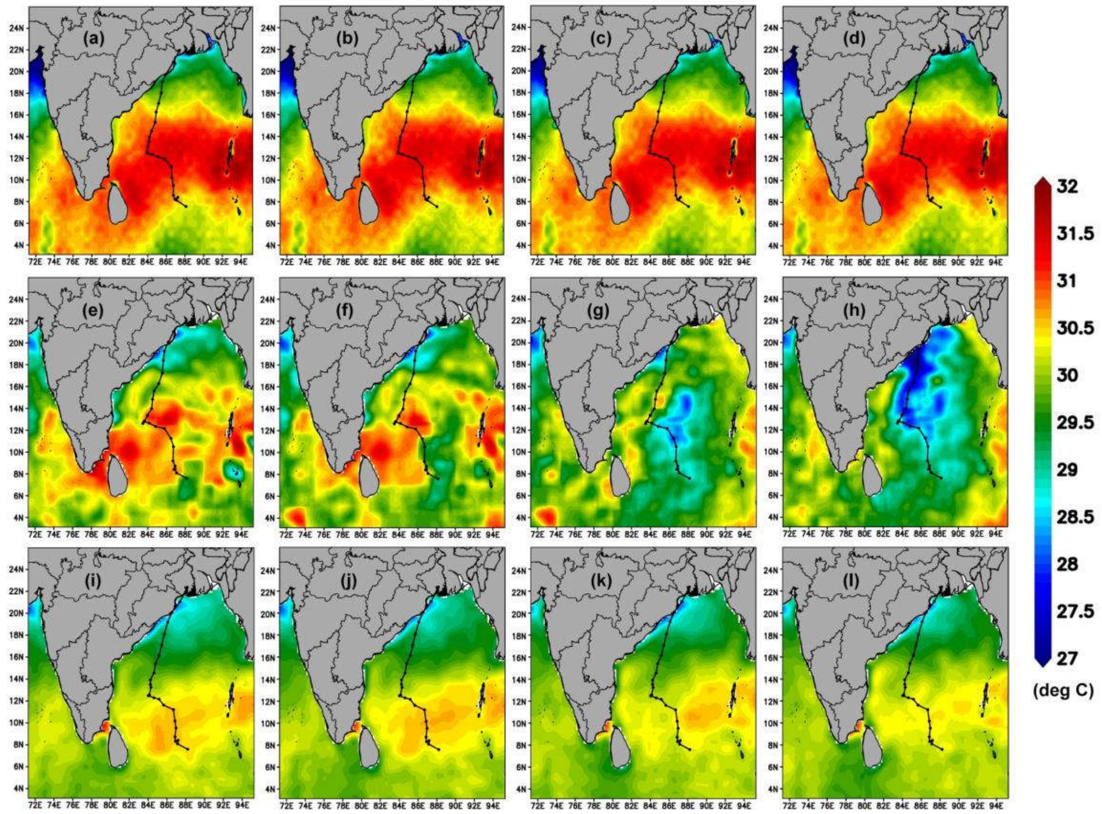

Figure 6.3. *SST field for Fani cyclone from* ***(a-d)*** *GFS-SST,* ***(e-h)*** *NOAA-SST and* ***(i-l)*** *CLIM-SST at* ***(a, e, i)*** *24 h,* ***(b, f, i)*** *48 h,* ***(c, g, k)*** *72 h and* ***(d, h, l)*** *120 h.*

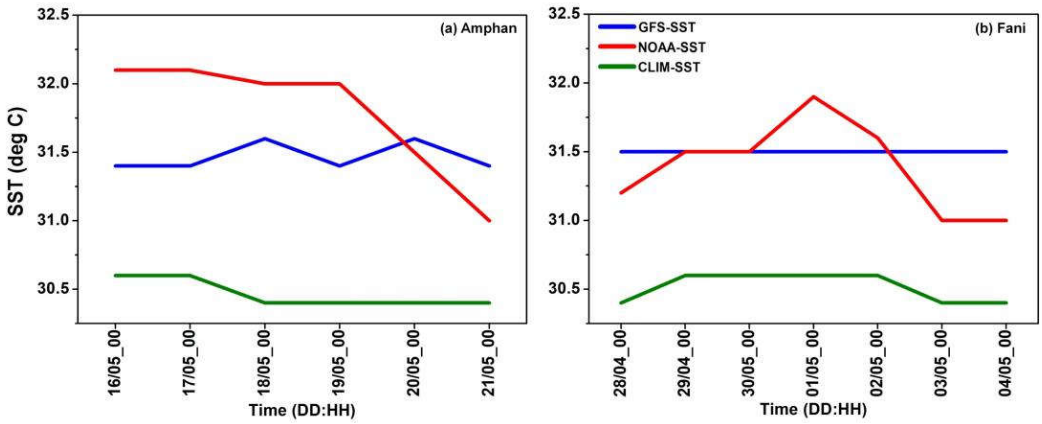

Figure 6.4. *Daily difference in SST datasets used during the whole simulation period for* ***(a)*** *Amphan and* ***(b)*** *Fani.*

in GFS-SST relative to NOAA-SST. For Fani (Fig. 6.4b), both the GFS-SST and NOAA-SST indicates a warmer SST by roughly 0.75°C and 1.25°C respectively over the CLIM-

SST during 00 UTC 28 April - 00 UTC 04 May 2018 indicating positive SST anomaly over normal seasonal value. While the GFS-SST indicates a uniform positive SST anomaly (1.0°C), the NOAA-SST shows a rising positive anomaly from 0.75°C at 00 UTC 28 April, peaking to 1.25°C at 00 UTC 01 May and then reducing to 0.5°C at 00 UTC 03 May. During the RI phase of the cyclone Fani, the NOAA SST has a higher positive SST anomaly over GFS-SST although during other times it has a relatively low SST anomaly. An increase in SST leads to an increase of evaporation of moisture from the ocean surface resulting in latent heat release which is further utilized to drive the circulation (Singh et al., 2016). The time series of areal average SST confirms the invariant nature of SST field in GFS-SST compared to the NOAA-SST during the life cycle of both the cyclones.

6.3.1. Intensity predictions

The intensity variations of the simulated cyclones from different experiments are examined from the time evolution of simulated CSLP and MSW for Amphan and Fani. As shown in Figure 6.5 all the experiments have captured the RI phase of Amphan (Fig. 6.5a, c) with slightly higher intensity compared to the IMD estimates. However, the simulations with GFS and NOAA produced lower CSLP and higher MSW (Fig. 6.5a, c) than the CLIM-SST which is possibly due to the increased SST compared to CLIM-SST. The NOAA-SST produced the highest intensity compared to others. All the simulations for Fani (Fig. 6.5b, d) indicate a delayed and less intensive RI phase between 12 UTC 29 April and 12 UTC 30 May against the observed RI phase between 00 UTC 29 May and 00 UTC 30 May. Unlike for Amphan the CLIM-SST produced the lowest CSLP and highest MSW for Fani (Fig. 6.5b, d) compared to both GFS-SST and NOAA-SST in better agreement with the observations especially during the deepening and peak intensification stages (00 UTC 01 May – 00 UTC 03 May). This indicates that the anomalous increase in SST has not influenced the RI of Fani cyclone as the CLIM-SST also produced nearly similar intensity as in the case of GFS-SST and NOAA-SST. In the GFS-SST and NOAA-SST simulations, the peak RI phase was predicted at 00 UTC 1 May against the observed RI phase at 12 UTC 30 April with little underestimation by 5 ms^{-1} compared to IMD data for Fani. Further, the peak intensity is slightly underestimated and delayed by 12 hours in NOAA-SST relative to GFS-SST and CLIM-SST experiments.

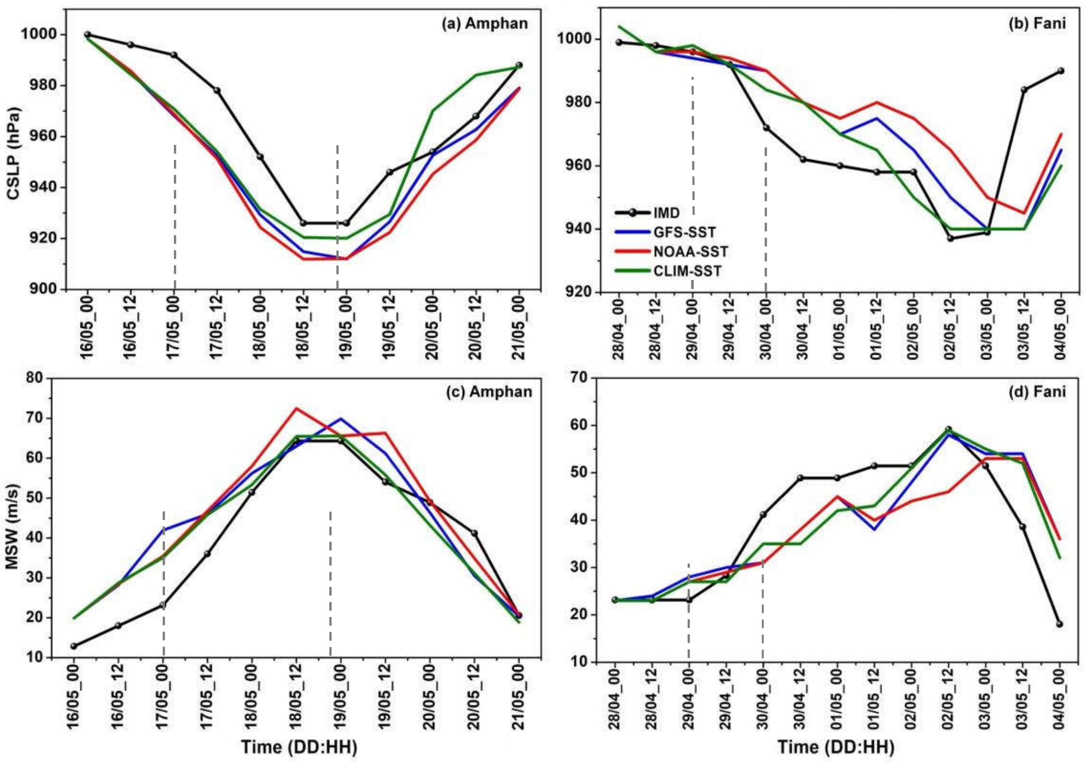

Figure 6.5. *Simulated **(a, b)** CSLP and **(c, d)** MSW compared with IMD best track for **(a, c)** Amphan and **(b, d)** Fani. The dotted lines indicate the RI phase.*

6.3.2. RH and wind shear

Some of the favorable factors for RI of cyclones in general are higher SST, higher humidity in the mid-troposphere and low vertical shear of horizontal winds etc., which are analyzed from different experiments. The growth of a TC is closely associated with increase of low-level convergence and vertical motions in the core region. The time evolution of divergence and vertical velocity at 925 hPa averaged over a 2° × 2° area of the cyclone is analyzed for Amphan (Fig. 6.6a, c) and Fani (Fig. 6.6b, d). For Amphan, all the experiments have predicted the first RI phase with a sharp increase in convergence

(Fig. 6.6a) and vertical velocity (Fig. 6.6c) from 24 h to 48 h. The NOAA-SST during the first RI phase and the GFS-SST during the second RI phase (peak time, 69 h) produced the highest convergence and vertical velocity respectively. However, the CLIM-SST predicted the lowest values throughout the simulation consistent with CSLP and MSW (Fig. 6.6a, c) parameters. In the case of Fani (Fig. 6.6b, d), NOAA-SST produced higher

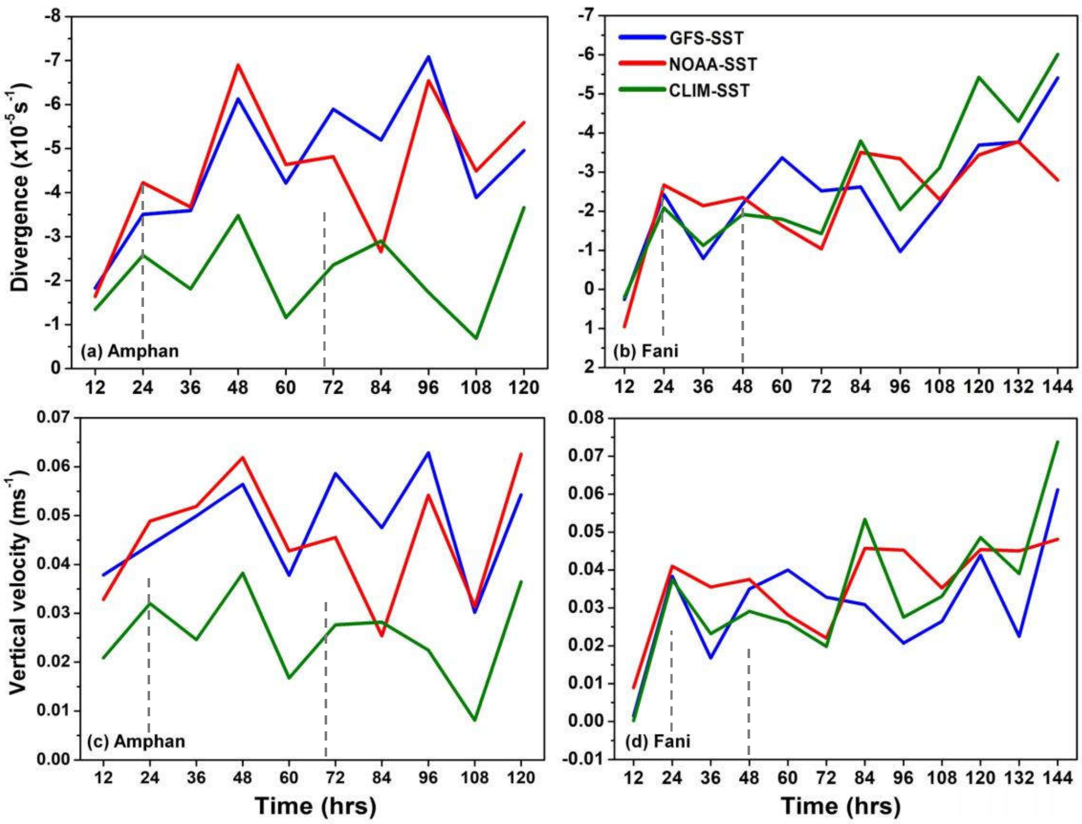

Figure 6.6. *Simulated **(a, b)** convergence and **(c, d)** vertical velocity for **(a, c)** Amphan and **(b, d)** Fani. The dotted lines indicate the RI phase.*

values of convergence and vertical motion during the RI phase compared to both GFS-SST and CLIM-SST. The GFS-SST produced slightly higher convergence and vertical motion during 48h–72 h and subsequently both NOAA-SST and CLIM-SST produced higher convergence and vertical motion relative to GFS-SST. The stronger convergence and higher vertical motion are consistent with the positive SST anomaly in GFS-SST and NOAA-SST experiments suggesting that SST anomaly indeed has some influence on the intensification during the RI and subsequent phases of both the cyclones, though the effect is much stronger in Amphan over Fani.

For a TC to develop the humidity level in the mid troposphere must be high as the entrainment of moist air will lead to the growth of cumulonimbus clouds. The time evolution of mid-tropospheric (600 hPa) relative humidity (RH) averaged over a 2° × 2° area from the cyclone centre is shown in Figure 6.7. The simulations for Amphan (Fig. 6.7a) show the RH is nearly similar during the first 12 h of simulation in all the experiments but subsequently enhanced in GFS-SST and NOAA-SST relative to CLIM-SST till 120 h. In general, there is an increased RH (88-90%) during the RI phase which reduced below 88% subsequent to RI phase in both GFS and NOAA simulation cases for Amphan. An interesting feature in the case of Amphan cyclone is that the simulated RH in GFS-SST and NOAA-SST is about 6% - 9% more during the RI phases relative to CLIM-SST. The

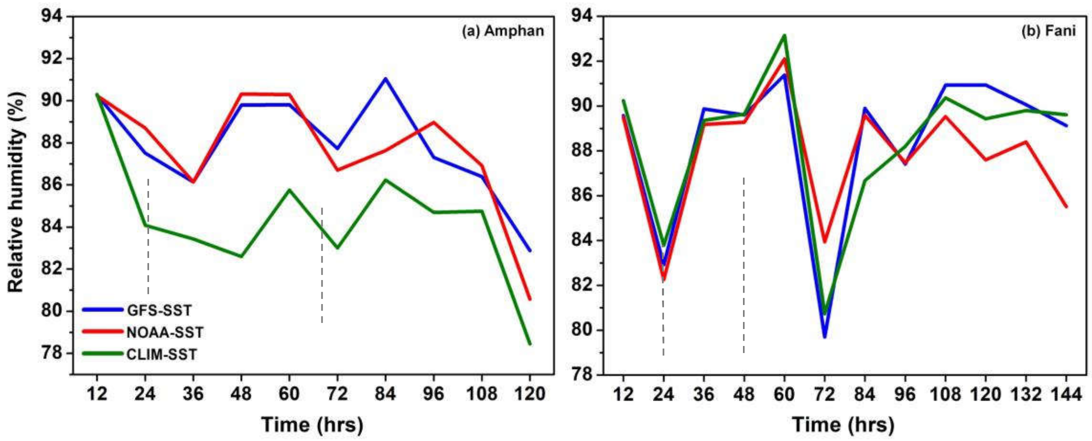

Figure 6.7. *Simulated relative humidity for **(a)** Amphan and **(b)** Fani. The dotted lines indicate the RI phase.*

enhanced RH could be due to enhanced moisture transport by increased evaporation led by the higher SST in the GFS-SST and NOAA-SST simulations over CLIM-SST. A sharp increase of RH during the RI phase from 82% to 89% can be seen from all the simulations for Fani (Figure 6.7b) suggesting that the high RH in the middle atmosphere has a positive effect during intensification. In contrast to Amphan, all the experiments produce more or less similar RH during the RI and subsequent phases which suggests very little role of positive SST anomaly in GFS-SST and NOAA-SST on the moisture transport and intensification of Fani.

The vertical shear of horizontal winds should be lower and uniform throughout the troposphere so that it facilitates convergence of moisture fluxes from the ocean for the TC to develop and intensify (Gray, 1978). The deep-layer (850-200 hPa) wind shear averaged over a 2° × 2° area from the centre of each cyclone is analyzed (Fig. 6.8). In the case of Amphan (Fig. 6.8a) a sharp decrease of the wind shear at the onset of the RI phase (24 h) and its rapid increase during the RI phase till 72 hours are noticed. This suggests that the low wind shear during 24-36 hours may have contributed to the intensification of Amphan to some extent but has no effect in the sub-sequent phases. All the three experiments produced nearly similar variation of wind shear throughout the life-cycle of Amphan. In the case of Fani (Fig. 6.8b) all the simulations show a sharp fall of shear during the rapid phase followed by a sharp rise up to 72 hours and again a fall up to 96 h. The drastically reduced shear (~7 ms^{-1}) between 12 UTC 29 April and 12 UTC 01 May suggests the significant role of shear in the RI phase of Fani which is well simulated by NOAA-SST and GFS-SST experiments. The slight underestimation of intensity in NOAA-SST from 72 h to 96 h (Fig. 6.5d) is associated with a stronger shear in that simulation. From 96 h onwards a comparatively lower and uniform wind shear can be observed till the end of the simulation, that resulted in the prediction of maximum intensity by all the three experiments (Fig. 6.5d).

During premonsoon period high accumulated TC heat potential due to high SST results in higher intensity of TCs whereas during post-monsoon season the presence of higher enthalpy fluxes and thicker barrier layer favors the TC intensification even with relatively smaller heat potential (Vissa et al., 2013). This is clearly noticed in the case of Amphan for which all the simulations produced nearly the same amount of shear but produced large SST variation. For Fani, the stronger simulated cyclone intensity correlates better with the low vertical wind shear than the SST variations. The simulations are not much sensitive to the changes in SST as anomalous SST increase of 1.25°C during the developing period of Fani in NOAA-SST and GFS-SST has not produced corresponding increments of intensification, as evidenced with similar intensification during the RI phase and higher intensification in subsequent phase with the CLIM-SST (Fig. 6.5d).

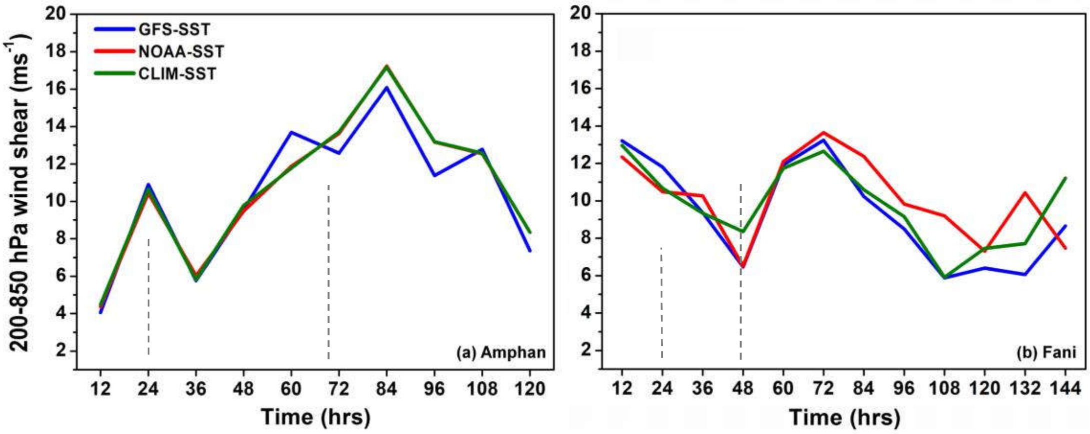

Figure 6.8. *Simulated deep layer (850-200 hPa) vertical wind shear for **(a)** Amphan and **(b)** Fani. The dotted lines indicate the RI phase.*

Further analysis is focused on Amphan, to understand the physical mechanism of influence of SST on the RI phase of this cyclone. The moisture, latent and sensible heat fluxes, diabatic heating, theta-e etc. are analyzed and presented in the following.

6.3.3. Latent and sensible heat fluxes

The heat fluxes from the warm ocean surface greatly influence the TC formation and intensification through the WISHE feedback mechanism (Emanuel, 1986). An increase in SST will increase the latent heat flux (LHF) due to high humidity resulting from a rise in temperature (Kumar et al., 2017). As the SST increases the increased ocean-atmospheric temperature difference leads to increased transfer of heat through surface heat fluxes. The time evolution of surface fluxes of moisture, latent heat (LHF) and sensible heat (SHF) averaged over a 2° × 2° area from the cyclone centre for Amphan is presented in Figure 6.9. Simulations indicate a continuous increase of LHF (Fig. 6.9a) throughout the RI phase associated with a corresponding increase in the moisture flux with the CLIM-SST producing lowest values compared to GFS-SST and NOAA-SST. The LHF in GFS-SST and NOAA-SST increased roughly by 100-200 Wm^{-2} over CLIM-SST. An increase

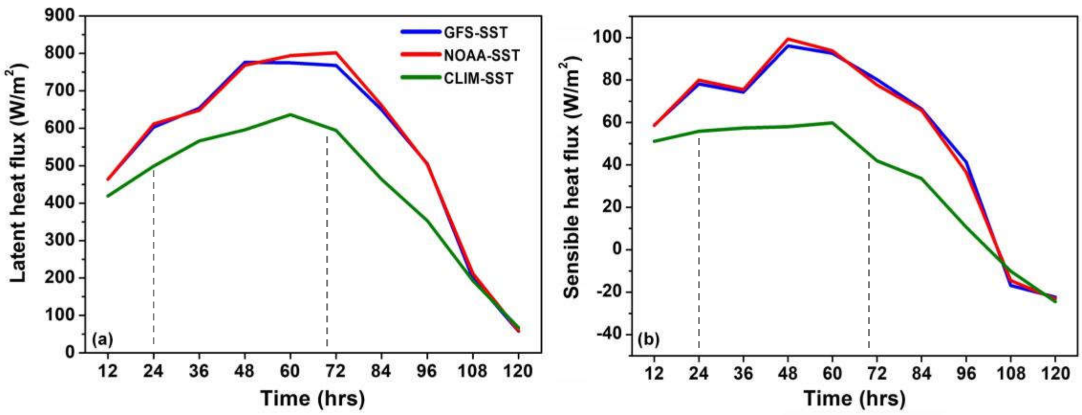

Figure 6.9. *Simulated surface* ***(a)*** *LHF and* ***(b)*** *SHF for TC Amphan. The dotted lines indicate the RI phase.*

(20-50 Wm^{-2}) in SHF (Fig. 6.9b) in the first phase of RI (24-48 h) can also be observed associated with an increase in the SST in the GFS-SST and NOAA-SST experiments. However, the SHF by CLIM-SST remains nearly uniform up to 60 h with lower values than both GFS-SST and NOAA-SST and decreases further. This shows that the surface moisture and energy fluxes considerably increased with positive SST anomaly for Amphan. The NOAA-SST produced the highest moisture, latent and sensible heat fluxes leading to the intensification of the system as seen from corresponding increments in the wind speed (Fig. 6.5c). An increase in MSW till 72 h is associated with enhancement of moisture and energy fluxes and a decrease in MSW from 72 h onwards is associated with decrease of fluxes (Fig. 6.5c; Fig 6.9a).

The variation of azimuthally averaged LHF and SHF in a 150 km radius from the cyclone centre against time are illustrated in Figure 6.10 and Figure 6.11 respectively. High LHF (Fig. 6.10) and SHF (Fig. 6.11) are present at the eyewall (25-50 km) where the maximum winds are observed (not shown) for all the experiments. An increase of fluxes can be observed from all the simulations as the RI phase begins. The maximum fluxes can be noticed during the second RI phase when the peak intensification of the cyclone occurred. The maximum LHF of 1400-1600 Wm^{-2} are simulated over 20-60 km in NOAA-

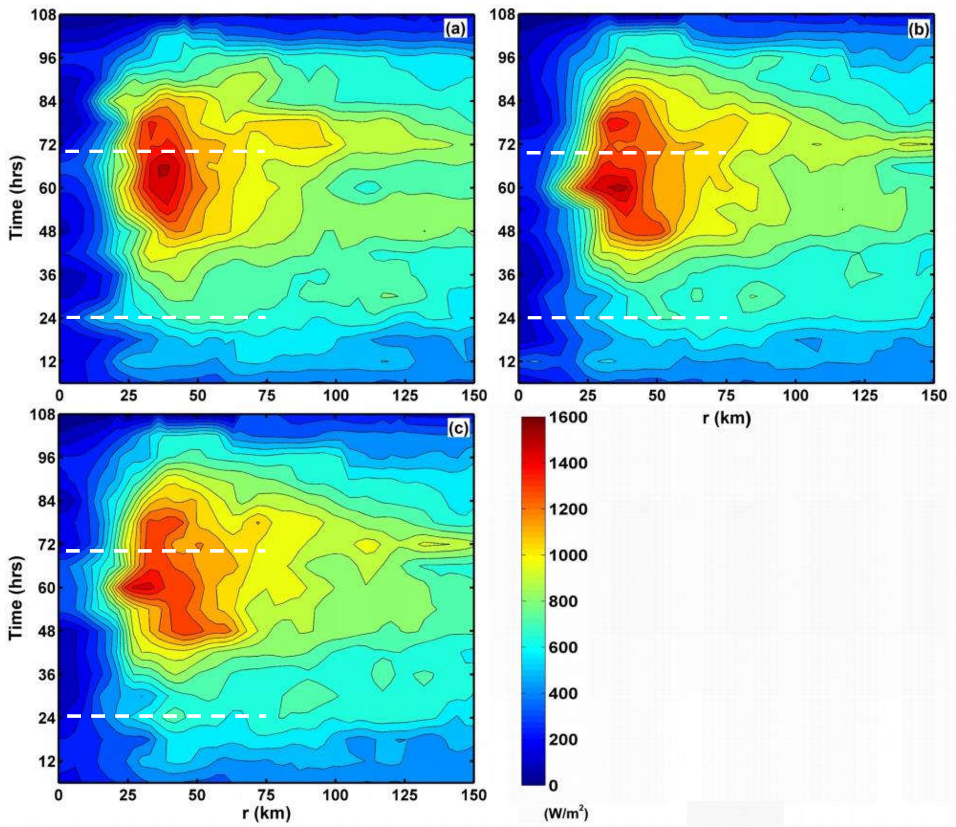

Figure 6.10. *Time-radius hovmuller diagram of azimuthally averaged surface LHF for Amphan by **(a)** GFS-SST, **(b)** NOAA-SST, **(c)** CLIM-SST. The white dotted lines indicate the RI phase.*

SST, 30-45 km in GFS-SST compared to 1200-1400 Wm^{-2} in 25-50 km in CLIM-SST. Similar to previous results, the CLIM-SST (Fig. 6.10c, Fig. 6.11c) produced least values of LHF and SHF. The NOAA-SST (Fig. 6.10b, Fig. 6.11b) produced high moisture and LHF for a prolonged period (till 86 h) compared to GFS-SST (Fig. 6.10a, Fig. 6.11a) (till

75 h) and CLIM-SST (till 72 h) beginning from the RI phase. The lower heat fluxes resulting from a decrease in SST in CLIM-SST is again evident from this analysis.

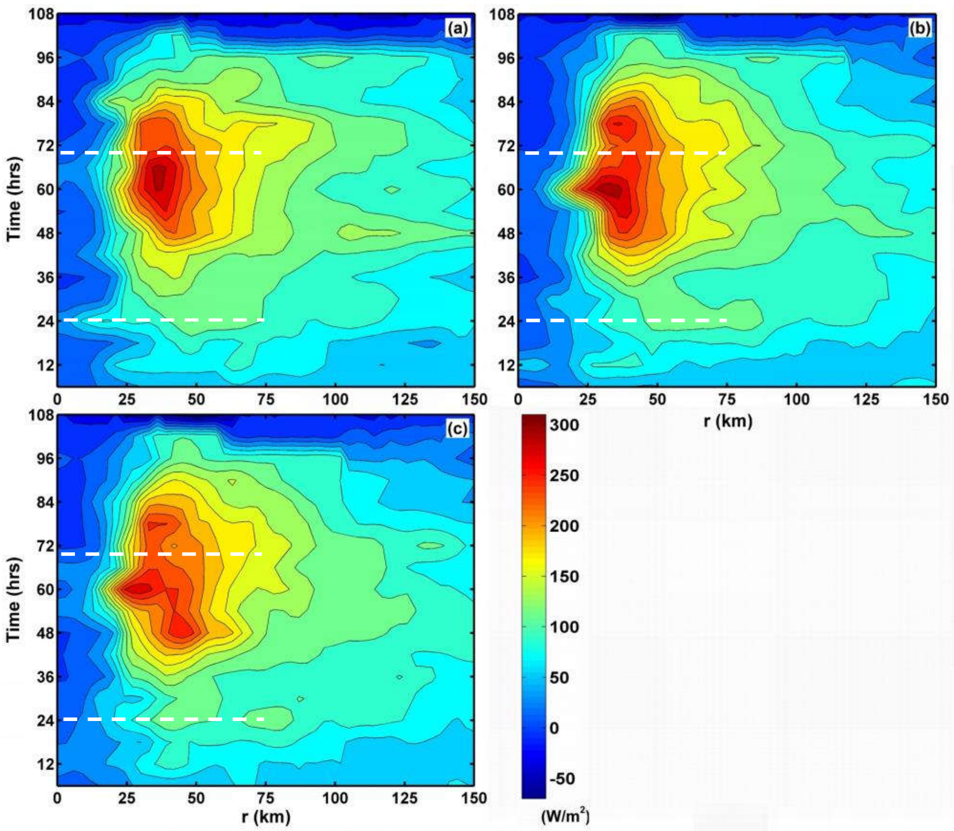

Figure 6.11. *Time-radius hovmuller diagram of azimuthally averaged surface SHF for Amphan by **(a)** GFS-SST, **(b)** NOAA-SST, **(c)** CLIM-SST. The white dotted lines indicate the RI phase.*

6.3.4. Storm Thermodynamics

Azimuthally averaged radius-height profile of temperature anomaly (total warming given by subsidence and diabatic processes) from the initial time at the two rapid intensification phases (48h, 69 h) along with the beginning of RI phase (24 h) is analyzed and presented in Figure 6.12. An increase in core warming will lead to more intensification of the cyclone by enhancing convection as discussed in section 3.3.4 of Chapter 3. All the simulations show increase in warming with time with maximum warming occurring in the second RI phase (69 h), where the maximum intensification was also produced. As noted in simulations in all the RI phases. For example, the NOAA-SST produced the highest warming of 13°C during the second RI phase (69 h) followed by GFS-SST (12°C) (Fig. 6.12c) and CLIM-SST (Fig. 6.12i) produced the least warming (10°C). Maximum warming is observed at the middle levels (4-8 km) which may be due to mainly by diabatic heating. Secondly the higher warming is also observed to extend to the upper levels (12-16 km) due to the subsidence and condensation process. All the simulations show their highest warming within 0-25 km radius which is the core. At 69 h, the warming shows an increase of 8°C, 7°C and 5°C for NOAA-SST (Fig. 6.12f), GFS-SST (Fig. 6.12c) and CLIM-SST (Fig. 6.12i) respectively from the beginning of RI phase (24 h). An increase in SST will impact the evaporation from the ocean surface which will produce more LHF as observed from the previous section. This will cause strengthening of cyclone low, more convergence and vertical motion at the lower levels which will further enhance moist convection.

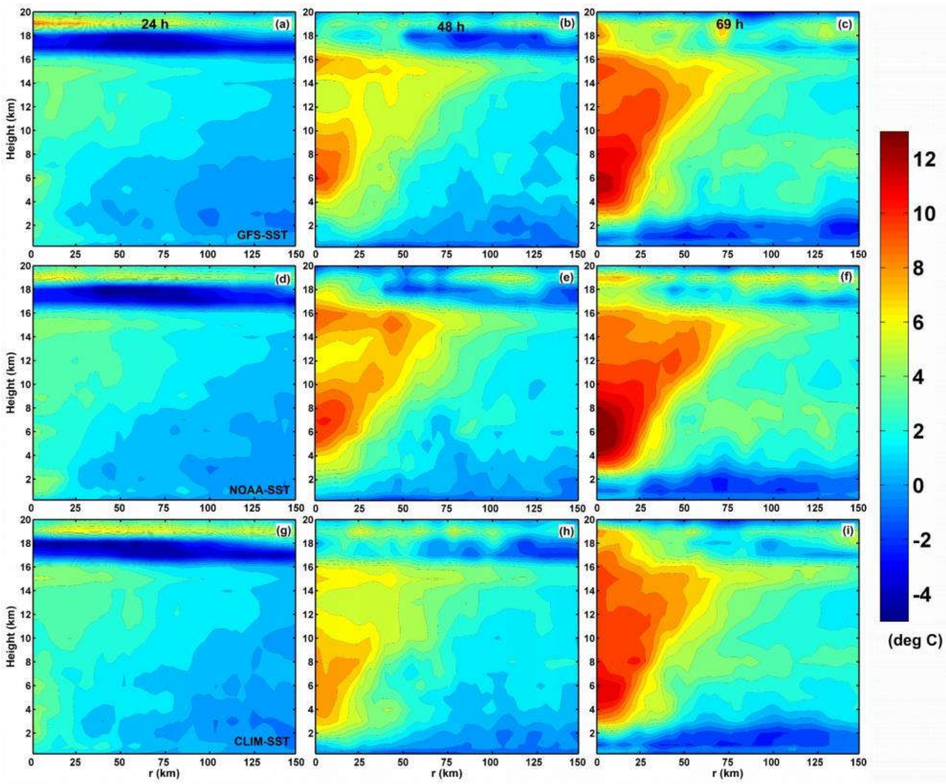

Figure 6.12. *Radius-height profile of azimuthally averaged warming produced relative to the initial time of simulation for Amphan by* ***(a-c)*** *GFS-SST,* ***(d-f)*** *NOAA-SST,* ***(g-i)*** *CLIM-SST at* ***(a, d, g)*** *24 h,* ***(b, e, h)*** *48 h and* ***(c, f, i)*** *69 h.*

The moist convection is determined by the diabatic heating and the intensity of a TC is closely related to the buoyancy produced through diabatic heating. The time evolution of diabatic heating in the layer 950 hPa- 150 hPa averaged over a 2° × 2° area from the centre of Amphan is presented in Figure 6.13. This shows the changes in the diabatic heating with SST variation. A rapid increase in diabatic heating is seen in the first RI phase (24-48 h) in the simulations with NOAA-SST producing the highest heating followed by GFS-SST and CLIM-SST. The diabatic heating will be more prominent at the eyewall (refer Fig. 3.15 of Chapter 3), where the maximum latent heat is released and this rise is attributed to the higher latent heat fluxes in NOAA-SST and GFS-SST (Figs. 6.9-6.11). The larger LHF and stronger convergence (Fig. 6.6a) has caused a higher diabatic heating (Fig. 6.13) and thereby stronger vertical motion (Fig. 6.6c) in the case of NOAA-

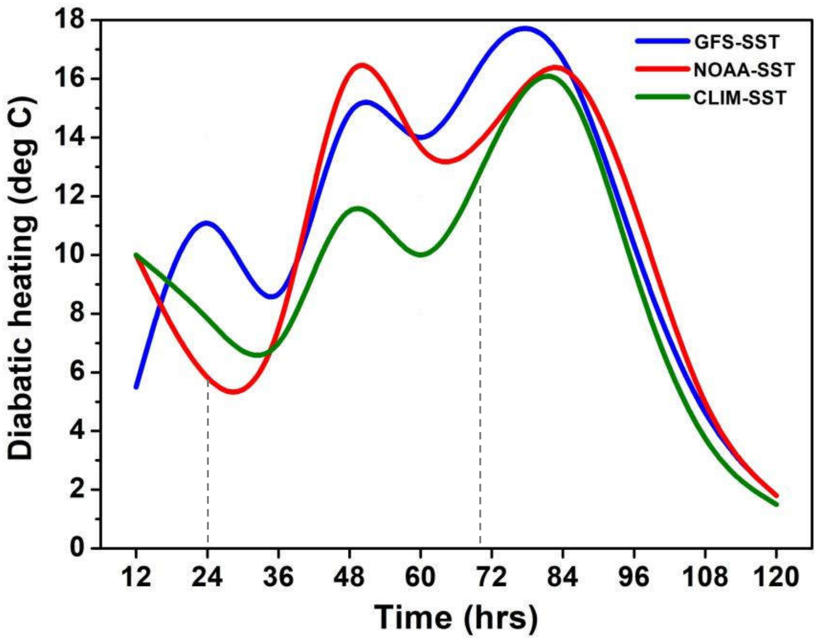

Figure 6.13. *Variation of simulated diabatic heating for Amphan relative to the initial time. The dotted lines indicate the RI phase.*

SST over CLIM-SST. The differences in distribution of RH (Fig. 6.7a) in the three experiments are also related to the distribution of diabatic heating (Fig. 6.13), where stronger heating is observed whenever there is an increase in RH (moisture transport) and vice-versa. From this analysis it is evident that an increase in SST has very much influenced the RI of Amphan through increased moisture, surface energy fluxes, convergence and the buoyancy caused by increased diabatic heating.

Azimuthally averaged radius-height cross-section of theta-e was analyzed at different RI phases from all the three experiments to understand the instability produced at different levels for the TC intensification. As shown in Figure 6.14, a decrease of theta-e in the middle layers and increase in the upper layers is seen indicating convectively unstable conditions in the middle layers at different stages of the cyclone. Further, the unstable core becomes more prominent with subsequent phases of RI. High theta-e values are observed at the lowest and highest levels in all the experiments. At 48 h comparatively

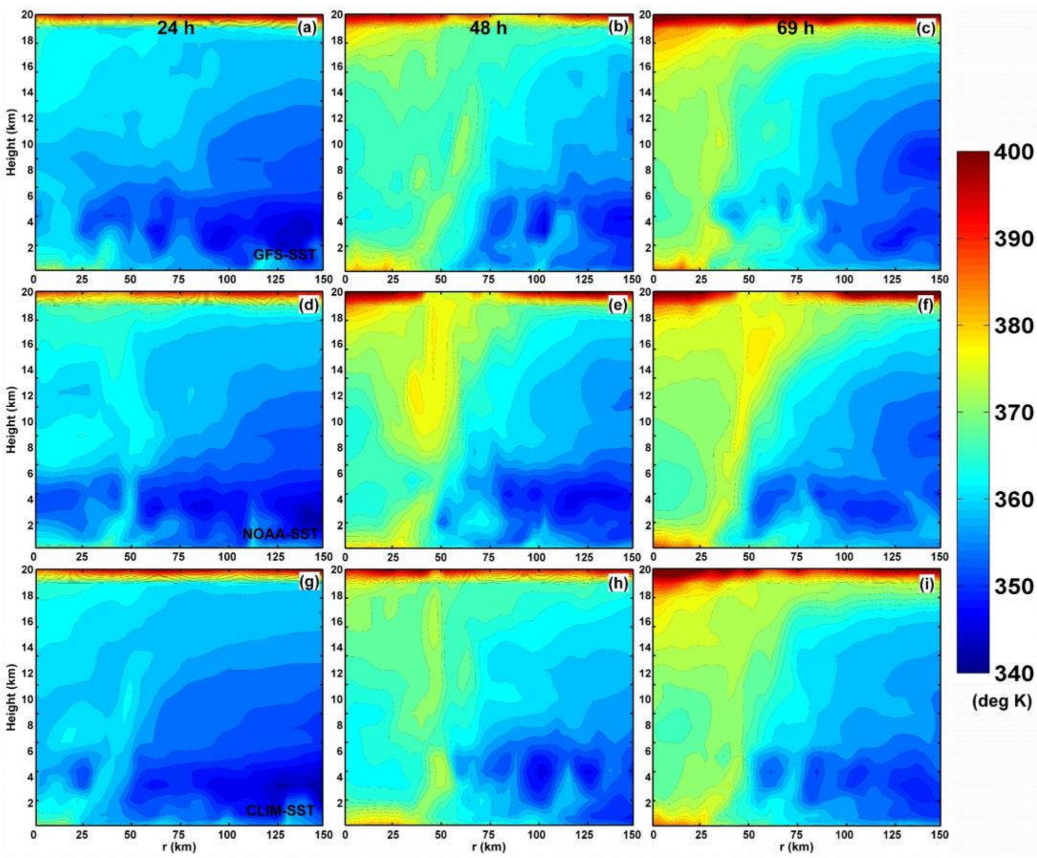

Figure 6.14. *Radius-height profile of azimuthally averaged theta-e for Amphan by* ***(a-c)*** *GFS-SST,* ***(d-f)*** *NOAA-SST,* ***(g-i)*** *CLIM-SST at* ***(a, d, g)*** *24 h,* ***(b, e, h)*** *48 h and* ***(c, f, i)*** *69 h.*

well-defined unstable core is produced by NOAA-SST (Fig. 6.14e) compared to GFS-SST (Fig. 6.14b) and CLIM-SST (Fig. 6.14h) correlating with relatively higher SST anomaly in it. The vertical theta-e gradient clearly indicates more stronger unstable layers and hence more intensification in NOAA-SST compared to the other two experiments. This is more clearly evident at the second RI phase (69 h) in which NOAA-SST (Fig. 6.14f) produced the highly unstable well-defined core with maximum warming at the lower and upper layers followed by GFS-SST (Fig. 6.14c). Both NOAA-SST (Fig. 6.14f) and GFS-SST (Fig. 6.14c) produced a smaller core (0-30 km) of unstable atmosphere compared to CLIM-SST (Fig. 6.14i) which produced a larger core (0-50 km) indicating a weak cyclone in CLIM-SST. Also, the layer of maximum instability (lowest theta-e) for NOAA and GFS is located in lower middle layers 3-6 km when compared to CLIM-SST, where it is found in 6-8 km which again indicates a weaker cyclone in the case of CLIM-SST.

To analyze the extent of variation in the convective motion due to the SST induced warming, the radius-height analysis of azimuthally averaged vertical velocity during different RI phases is analyzed for Amphan (Fig. 6.15). The highest (lowest) RI phases by NOAA-SST (CLIM-SST) is again evident from this analysis. A gradual increase in vertical winds is simulated from 24 h to 69 h (Fig. 6.15). The highest vertical motions (6-7 ms^{-1}) are produced by NOAA-SST at 48 h (Fig. 6.15e) and 72 h (Fig. 6.15f) followed by GFS-SST (Fig. 6.15b, c) (5 ms^{-1} at 48 h and 3 ms^{-1} at 69h) and CLIM-SST (3 ms^{-1} at 48 hand 69h). However, for GFS-SST more intensification is found at the first phase (Fig. 6.15 b) compared to the second phase (Fig. 6.15c). In the case of CLIM-SST, though the model produced slightly stronger updrafts at the beginning of RI phase (Fig. 6.15g) it shows prominent downdrafts at 48 h and 69 h indicating decline of convection. The updrafts produced by CLIM-SST are very less compared to GFS-SST and NOAA-SST at

48 h and 69 h. The maximum intensification produced by NOAA-SST is once again evident from this result.

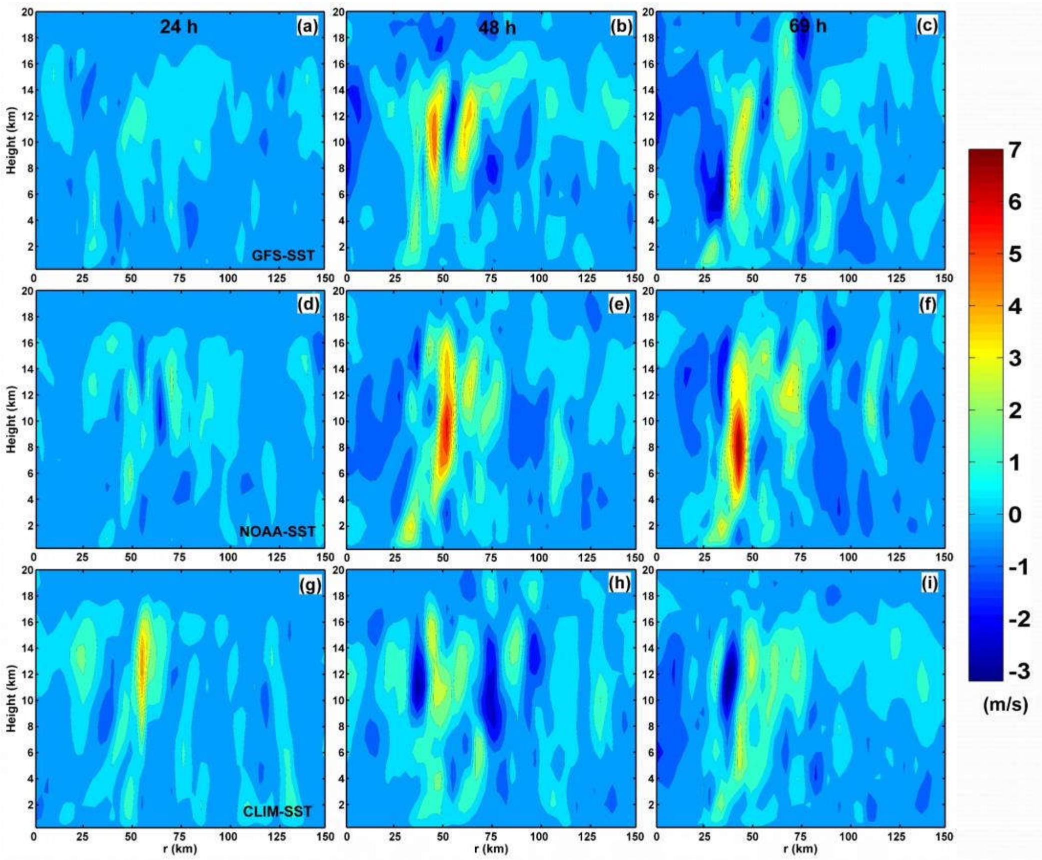

Figure 6.15. *Radius-height profile of azimuthally averaged vertical velocity for Amphan by **(a-c)** GFS-SST, **(d-f)** NOAA-SST, **(g-i)** CLIM-SST at **(a, d, g)** 24 h, **(b, e, h)** 48 h and **(c, f, i)** 69 h.*

6.3.5. Winds

Azimuthally averaged radius-height cross section of tangential winds at different RI phases is analyzed (Fig. 6.16) as the temperature distribution in a TC is related to the tangential wind distribution through thermal wind balance (Willoughby, 1990). The 10-m winds analysis (Fig. 6.17) for the whole simulation period with track is also presented. As shown in Figure 6.16, as noted generally in all the simulations the RI phases are noted with wind speed increase of ~30 m/s and ~45 m/s respectively at 48 h and 72 h from the beginning of RI phase (24 h). The winds produced by NOAA-SST (Fig. 6.16d-f) are comparatively stronger in all the phases followed by GFS-SST (Fig. 6.16a-c) and CLIM-SST (Fig. 6.16g-i). At 48 h, the maximum winds produced are 69 ms^{-1}, 75 ms^{-1} and 63 ms^{-1} for GFS-SST (Fig. 6.16b), NOAA-SST (Fig. 6.16e) and CLIM-SST (Fig. 6.16h) respectively. Similarly, at 72 h, highest winds are produced by NOAA-SST (83 m/s) (Fig. 6.16f) followed by GFS- SST (81 m/s) (Fig. 6.16c) and CLIM-SST (75 m/s) (Fig. 6.16i).

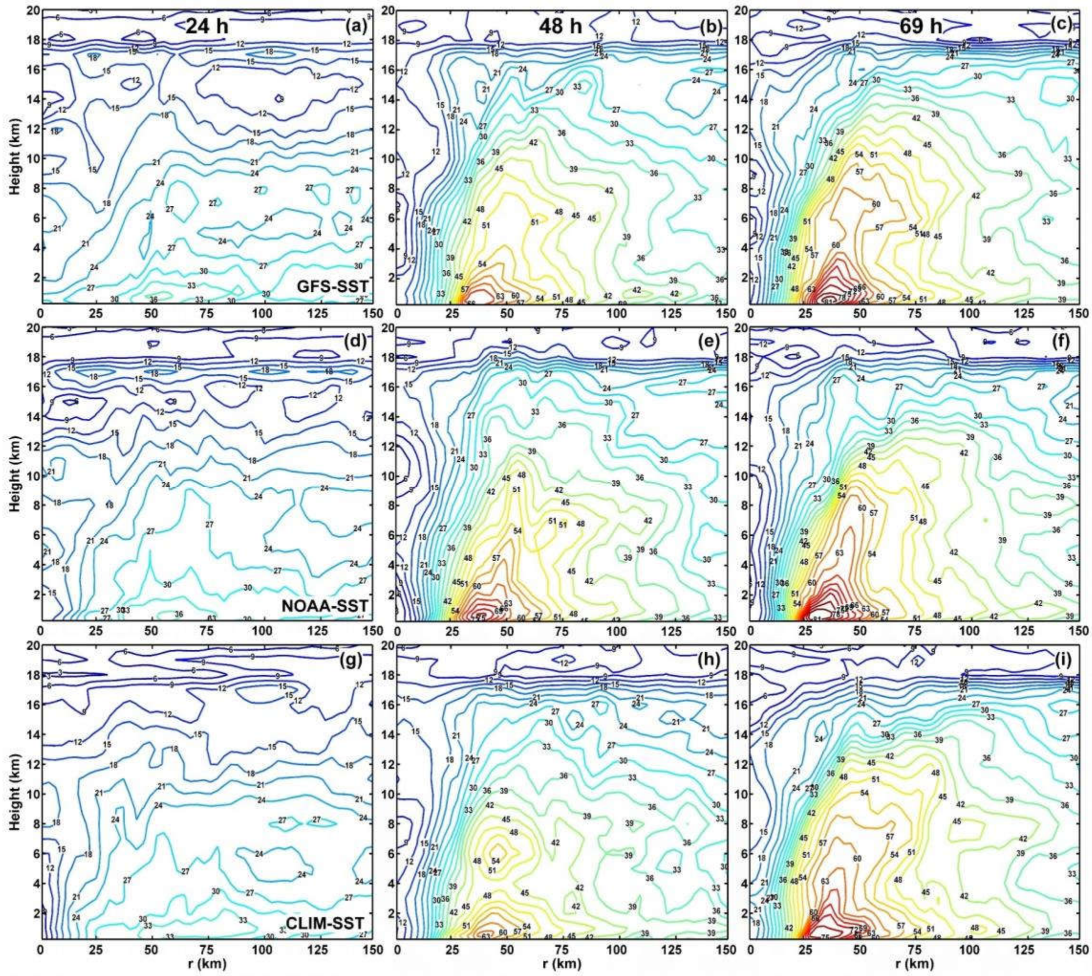

Figure 6.16. *Radius-height profile of azimuthally averaged tangential winds for Amphan by **(a-c)** GFS-SST, **(d-f)** NOAA-SST, **(g-i)** CLIM-SST at **(a, d, g)** 24 h, **(b, e, h)** 48 h and **(c, f, i)** 69 h.*

The RI of Amphan cyclone due to high tangential winds caused by increased warming, induced by an anomalous rise in SST is again well evident from this analysis. The distribution of 10 m winds throughout the simulation (Fig. 6.17) also shows that CLIM-SST (Fig. 6.17c) produced lesser sustained winds compared to NOAA (Fig. 6.17b) and

GFS (Fig. 6.17a). Also, high winds are observed to affect smaller areas relative to NOAA and GFS.

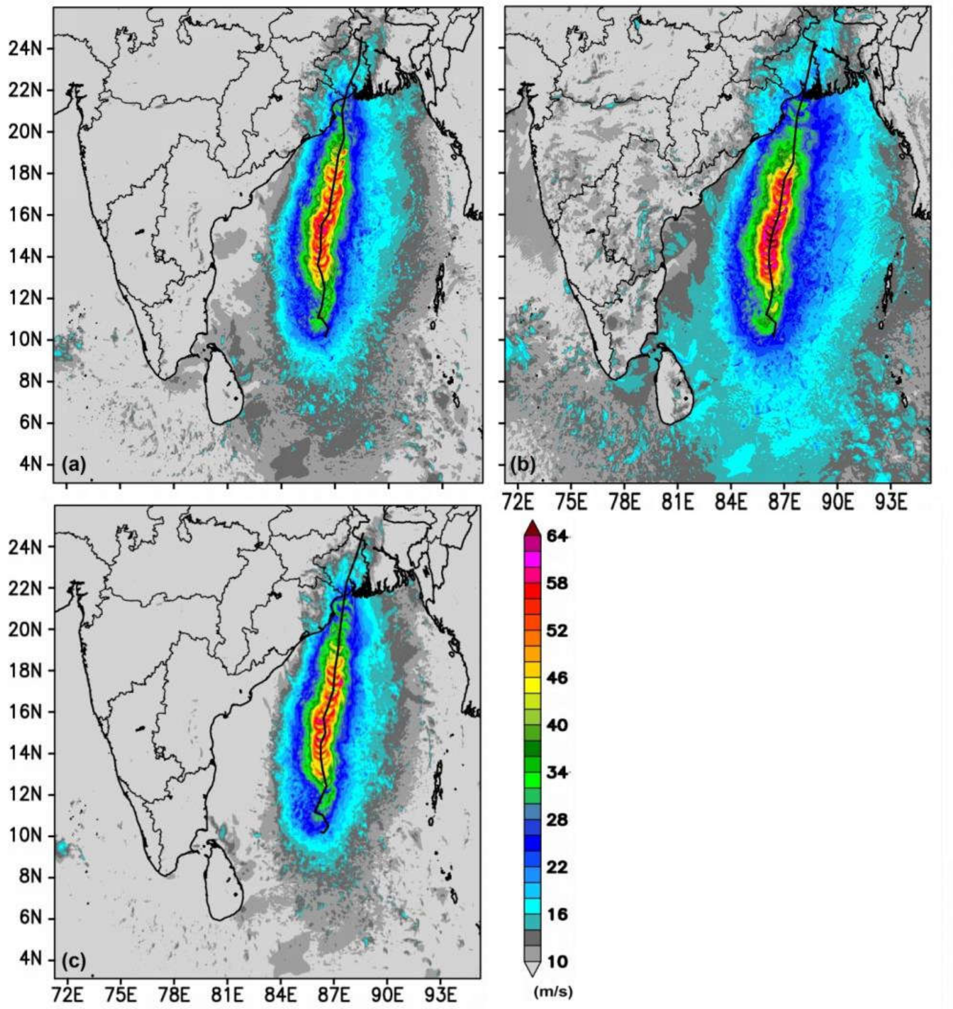

Fig. 6.17. *Simulated 10 m wind speed in along the track of cyclone for **(a)** GFS-SST, **(b)** NOAA-SST, **(c)** CLIMSST.*

6.4. Summary

In this chapter, the role of SST on rapid intensification of TCs in the Bay of Bengal of North Indian Ocean is examined taking two recent cases of rapidly intensified extremely severe tropical cyclonic storms Amphan and Fani that formed during the premonsoon season over the BOB in 2020 and 2019 respectively. Numerical simulations are conducted with a high resolution WRF-ARW model using the SST initial and boundary conditions from three different sources (i) NCEP operational GFSSST (GFS-SST) analysis and forecasts, ii) NOAA satellite SST data (NOAA-SST) and iii) 11-year climatological mean SST (CLIM-SST). The real-time NOAA SST and GFS SST field over the Bay of Bengal are found to be about 1.5°C and 1.25°C higher for Amphan and Fani cyclones respectively than the climatological mean. The SST sensitivity experiments showed that positive SST anomaly has greatly influenced the intensification of TC Amphan. Though all the experiments could capture the RI phase for TC Amphan with some variation in the intensity according to the SST data, the NOAA-SST produced the maximum intensification in response to the highest positive SST anomaly in NOAA SST data. All the experiments for Amphan similarly simulated the deep-layer shear. Although the wind shear reduced slightly at the onset of first RI phase it progressively increased during the RI phases thereby indicating that the wind-shear is not an influencing factor of RI for Amphan. The positive SST anomaly from climatological mean produced corresponding increments in total warming, diabatic heating, low-level convergence and vertical motion in NOAA-SST followed by GFS-SST at different intensity stages clearly indicating the role of SST on the rapid-intensification process for Amphan. However, for TC Fani, an increase in SST from the climatological mean has not influenced RI much, as the CLIM-SST simulation with lowest SST produced nearly the same intensity as that of NOAA-SST and GFS-SST during the RI phase and highest intensity during the peak intensification. However, all the simulations for Fani produced a decrease in the deep layer shear during the RI phase (24- 48 h) which is more predominantly simulated in NOAA-SST and GFS-SST indicating that low wind-shear mainly influenced its rapid intensification.

The results of surface energy fluxes and storm thermodynamics in the case of TC Amphan shows that the increased SST from the climatological mean indicated a large impact on the intensification through increased latent and sensible heat fluxes leading to increased convergence, warming, convection and tangential winds all indicating a WISHE type of feed-back to the storm. These results corroborate with the modelling findings by Cheng and Wu, 2020 conducted for super Typhoon Megi, 2010 formed in the western Pacific basin. In the case of Fani cyclone, the low wind-shear during the initial stages played a higher role compared to the smaller SST change in RI.

Chapter 7

Summary, conclusions and scope of future work

The information on the genesis, intensification and movement of the TCs over tropical oceanic regions is considered highly important for advanced preparations needed in disaster mitigation along the highly vulnerable tropical coastal areas. The prediction of the movement, intensity and structure of TCs over global tropical oceans has been a challenging task for the research community. The Bay of Bengal of North Indian Ocean is one of the potential basins with high annual frequency for intensive TCs. The east-coast of India is highly vulnerable to the TC related natural disasters due to the shallow and plain topography, curved coast line and the intensive TCs that form in the BOB region. Reliable numerical atmospheric models incorporating all the physical processes especially of convection are highly essential to produce robust predictions of the TCs. The previous modelling studies of TCs over the NIO mainly used coarse grids ($\geq$9 km) with parameterized convection for TC intensity and track forecasting. With advances in high resolution models convection can be explicitly represented to resolve the cloud and convection processes which would offer advantages over the traditional approach of using implicit convection.

In this study an attempt is made to study the impact of horizontal resolution and explicit convection, sensitivity of high resolution predictions to cloud microphysical processes on the track and intensity predictions of TCs over BOB region of NIO, and the role of SST in rapidly intensifying TCs using the WRF-ARW mesoscale numerical

weather prediction modelling system. To achieve these objectives towards improving the TC predictions over the NIO, the study is organized into four major chapters i) impact of convection permitting high resolution simulations ii) sensitivity of high resolution simulations to cloud microphysics schemes and iii) role of SST boundary forcing on the rapid intensification of TCs using GFS model analysis SST, satellite-derived SST and climatological SST data sets. Results of simulations are compared with various available observational datasets. A summary of the results of various simulations focused on the above aspects are presented in this chapter along with the conclusions, their applications and constraints. Discussions on comparisons with the earlier studies conducted and extension of the study as a future scope are also provided in the current chapter.

In essence, the increased grid resolution of 3 km better resolved the inflow, convergence and vertical motions and also produced higher diabatic heating due to explicit treatment of cloud microphysical processes and therefore produced improvements for both track and intensity predictions over low-resolution simulations (9 km) using cumulus parameterization. Among various microphysics schemes, the Thompson scheme produced stronger convergence and vertical motion up to 6 km and stronger upper air divergence associated with strong cyclonic vorticity in the atmosphere and also captured the time evolution of different hydrometeors that led to produce the observed pattern of the rainfall associated with a low-pressure system both spatially and temporally. Also, the Thompson scheme produced least errors for track and intensity and good prediction of thermodynamic parameters which suggest that it is more suitable for high-resolution operational TC forecasting in the NIO. The SST played a significant role in the rapid intensification of TC Amphan due to large positive SST anomaly from climatological mean associated with a high wind shear, whereas it has shown only a minor influence in RI phase of Fani due to smaller SST anomaly associated with low wind-shear. This suggests the RI phase is caused

mainly by SST anomaly for Amphan and low wind-shear for Fani cyclones. The chapter wise summary and conclusions of the study are given below.

In **Chapter 1** an introduction on the general characteristics of the TCs like formation, structure etc. of global TCs along with the climatology, intensity and a review of earlier numerical modelling studies of TCs over NIO was given. The importance of high-resolution TC simulations with explicit convection in the context of previous studies over NIO and current advancements over other basins and the objectives of the present study were also discussed.

In **Chapter 2**, a detailed description of WRF-ARW modelling system and its components which includes the governing equations, grid nesting, initial and boundary conditions and model physics used for the study were presented. Subsequently, a brief description of the history of the TCs along with their characteristics selected for the simulations were also presented. Finally, the details of the global data sets used for model initialization and integration and various observational data sets that include surface, upper air, DWR and satellite data products used for validation of simulations were provided.

In **Chapter 3** the results of convection permitting high-resolution simulations on the prediction of ten TCs during 2010-2019 in the BOB of NIO were presented. The study was conducted using two horizontal grid resolutions i.e., 9km grid using parameterized convection (9km-CP) and 3km grid using explicit microphysics (3km-MP). The study involved a comparison of the effects of cumulus physics at 9-km resolution with those of microphysics in the finer grids (3km). The results showed that the 3km-MP using explicit convection provided superior track and intensity predictions over the 9-km grids using implicit convection. The track errors in 3km-MP were reduced by 31%, 5%, 28% and 8% at 24h, 48h, 72h and 96h forecast intervals respectively over 9km-CP. The 9km-CP

produced relatively weaker vorticity, thereby the TC experienced stronger environmental steering force which thus led to northward deviating tracks and higher error compared to the 3km-MP which produced stronger vorticity. The 3km-MP produced significant improvements in intensity forecasts. Overall, the errors were reduced by 47%, 78%, 128%, 36% for CSLP and 29%, 31%, 44%, 101% for MSW at 24, 48, 72 and 96 h respectively in 3km-MP over 9km-CP. The study showed that the 9km-CP produced relatively higher (lower) intensity during the growing phases (peak and decay phases) for all cyclones due to producing higher (lower) thermal anomaly than the 3km-MP indicating different impacts of cumulus and microphysics in the respective phases. While both the simulations over-estimated the intensity for a majority of the cyclones, the 3km-MP reduced the overestimation of intensity during growing phases and underestimation during peak and decay phases and also improved the timing of maximum intensification in most cases. Various structural characteristics of the TCs (RMW, surface winds, thermal anomaly, radial winds, cloud reflectivity etc.) were found to be better represented in the 3km-MP as seen from comparison with CIRA multi-satellite observational cyclone products. Overall, the increased resolution of 3km-MP better resolved the inflow, convergence and updrafts and also produced higher diabatic heating due to explicit treatment of cloud microphysical processes and therefore suggests improvements over low-resolution simulations using cumulus parameterization. The results clearly demonstrate better model performance for track and intensity predictions compared to the earlier results reported by Srinivas et al. (2013) using 9 km with parameterized convection which showed considerable overestimation of the intensity. The results of this study using high-resolution modelling framework with explicit convection and statistical error evaluation for a large number of TCs over the BOB of NIO region show promising forecast strategy.

In **Chapter 4**, the results of sensitivity experiments with various cloud microphysical parameterization schemes (Morrison, Lin, WSM3, WSM6, Thompson, Goddard) in the simulation of tropical low-pressure system that produced heavy rainfall over north-coastal Tamilnadu, Chennai and surrounding areas were presented. Simulations revealed that the microphysics schemes affect the location of the low-pressure trough, atmospheric circulation and low-level convergence through changes in the diabatic heating and its coupling to dynamics ultimately influencing the distribution and location of rainfall. It was noticed that among all the schemes the Thompson scheme had realistically produced the low-pressure trough, circulation and rainfall pattern compared to other schemes. While the Morrison and Lin schemes simulated the maximum precipitation over the ocean area adjacent to Chennai, the WSM3, WSM6 and Goddard schemes simulated along the coast but with significantly lower intensity. The Thompson microphysics scheme produced the maximum rainfall (450 mm) over Chennai and its surroundings and the heavy rainfall extension along the coast with its time of occurrence in better agreement with observations compared to all the other schemes. Thompson predicted most of the hydrometeors mixing ratios (except ice), their vertical distribution as well as the time of occurrence coinciding with the maximum observed rainfall event and the corresponding hydrometeor reflectivity better than the other schemes. Based on these sensitivity results the microphysics schemes were further used in the next chapter (Chapter 5) for the prediction of TCs to obtain a better conclusion on the performance of various microphysics schemes for tropical cyclonic storms.

In **Chapter 5**, the sensitivity results of cloud-resolving scale predictions of TCs with a high resolution of 3 km to cloud microphysics schemes were presented. Six TCs which formed over the Bay of Bengal (BOB) were chosen for the study using 5 microphysics schemes. The microphysics schemes (Thompson, Goddard, Lin, Morrison,

WSM6) were chosen based on the results from Chapter 4. Results of simulated CSLP, MSW and track positions indicated that the microphysics schemes mainly affect the intensity and produce moderate impact on track. Overall, based on aggregate error statistics for all the six cyclones it was found that Thompson produced the best predictions for both tracks and intensity. Next to Thompson, Morrison and Goddard gave the best intensity prediction; WSM6 and Lin produced the best track prediction. Moreover, a comparison of simulated vertical winds with the corresponding data from MST radar profiles at Gadanki station during the passage of Gaja and Fani cyclones showed that the simulations with Morrison, Thompson and Goddard schemes produced more realistic representation of vertical motions indicating better prediction of convection in TCs. Overall, the results from the two chapters (Chapters 4 and 5) suggest that the Thompson scheme gave a good prediction of rainfall, thermodynamic variables and least errors for both the track and intensity parameters thus promising the scheme's application for high resolution operational TC forecasting in the NIO.

In **Chapter 6** the results of SST sensitivity experiments on the RI phase of two rapidly intensified cyclones Amphan and Fani that formed over the BOB during pre-monsoon season in 2020 and 2019 respectively were presented. The simulations with real-time SSTs (GFS-SST, NOAA-SST) were compared with a control run in which a 11-year climatological mean SST (CLIM-SST) was taken for SST initial and boundary conditions. The results showed that the anomalous increase in SST from the climatological mean greatly influenced the intensification of TC Amphan which is seen from the GFS-SST and NOAA-SST simulations with higher intensification than the CLIM-SST, though in general all the simulations overestimated the intensity. All the experiments also captured the RI phase for TC Amphan with variation in the intensity according to the observed SST values. The NOAA-SST produced the maximum intensification and CLIM-SST the least. The

simulations for Amphan revealed that the RI phase was associated with a positive SST anomaly and also an increase in vertical shear of horizontal wind in upper atmosphere indicating a greater role of SST in the RI process. However, for TC Fani, an increase in SST from the climatological mean did not influence much the intensification, as the CLIM-SST simulation also produced the highest intensity. Simulations for Fani revealed that though the SST anomaly is relatively small compared to Amphan, there was a low vertical shear of horizontal winds during the RI phase which facilitated the cyclone to undergo rapid intensification. The wind-shear was relatively low in both NOAA-SST and GFS-SST during the RI phase thus producing slightly higher intensification during the RI phase in these experiments. The analysis of surface fluxes and storm thermodynamics conducted for TC Amphan showed that an increase in SST has a great impact on the intensification through a WISHE type of feed-back by increasing the latent and sensible heat fluxes, low-level convergence and the diabatic heating thereby resulting in larger vertical velocities. Overall, the results from this chapter suggest that positive SST anomaly has a major role in rapid intensification as the simulations also showed a higher wind shear during the RI phase. On the other hand, simulations for Fani revealed a less important role of SST during the RI phase which is associated with a low-wind shear.

The present work has conducted numerical modelling studies for 11 TCs during 2010-2020 period and showed very promising results with 3-km resolution using explicit convection for the improvement of TC forecasting over NIO. Though there are a lot of uncertainties associated with the cloud microphysics and convective parameterization schemes in numerical models, the present study finds that the convection permitting simulations in general produce better simulations for TC tracks, intensities and structural parameters than the simulations using convective parameterization. However, these results may be specific to the Kain Fritsch convection scheme in the 9km grid. This may require

further sensitivity analysis with simulations with parameterized convection in the coarse domain to reduce uncertainties in model performance. Although there may be competing effects of decreasing flux moisture convergence and increasing convection at increasing horizontal resolution, numerical modelling studies at 1 km grid resolution are needed to test this limit for further possible improvements in TC intensity especially during the entire life cycle and structure prediction.

It is known that the TC simulations are sensitive to the initial conditions; however, most studies were focused on the impact of data assimilation at 9 km resolutions. The present results with high resolution convective permitting simulations can be further improved by data assimilation for thermodynamical parameters with data from sources such as GPS- Osculati humidity and temperature profiles using data assimilation techniques such as 3DVAR. Also, most of the previous air-sea interaction studies in numerical models were conducted at 9 km resolution. The air-sea coupled simulations need to be conducted at 3 km grid resolution to address the role of accurate air-sea fluxes on cloud-resolving simulations. The present study also finds the best microphysics scheme (Thompson scheme) applicable for both TC tracks, intensity and rainfall, from simulations conducted for six TCs and a tropical low-pressure convective system. However, there is further scope for detailed studies on microphysics sensitivity in the context of development of a large number of new cloud microphysics in WRF-ARW by analyzing the heating profiles associated with hydrometeor phase changes, fall speed and particle size distributions of frozen hydrometeors etc. The SST sensitivity experiments showed that even though SST has an impact in RI phase of cyclones it is not always a dominant factor for TC intensification as evident from the analysis of Amphan and Fani. The results of high SST anomaly and high wind-shear for Amphan and low SST anomaly and low wind-shear for Fani indicate SST influenced the RI phase only for Amphan whereas the wind-

shear played major role for Fani. These results suggest that in order to obtain more robust conclusions on the role of SST for RI further sensitivity studies have to be conducted with longer term climatological mean SST and for more cyclone samples including the post-monsoon cyclones that have undergone rapid intensification.

Thesis Abstract

The problem of Tropical Cyclone (TC) intensity forecasting continues to challenge both weather forecasters and researchers. Large variability of TC intensity and structure in numerical prediction systems arises from imperfect initial conditions, model physics parameterizations (radiation, convection, microphysics, planetary boundary layer), model resolutions, numerical discretization and approximation to the continuous equations and limits of predictability. Prediction of the TCs in the North Indian Oceans is highly challenging due to the highly variable nature of the TCs in NIO, variation in the sea surface temperature and seasonal variation in the largescale atmospheric conditions. Though the TC predictions are greatly improved in the last decade due to increase in the observations, data assimilation systems and improved physics parameterizations, not many studies are focused on the impact of horizontal resolution and explicit convection physics for the TCs in the North Indian Ocean (NIO). In the present work, numerical simulations for a number of TCs over the Bay of Bengal (BOB) region of NIO are conducted using a high-resolution mesoscale model and the results are compared with various observational datasets.

In the first part, the impact of horizontal resolution and convection physics on the intensity and track predictions for 10 TCs over the BOB of NIO is examined with respect to two horizontal grid resolutions i.e., 9km grid using parameterized convection (9km-CP) and 3km grid using explicit microphysics (3km-MP). The results of all 10 TCs indicated that the convection permitting 3km-MP experiment provided superior track and intensity predictions over the 9km-CP using implicit convection. Overall, the increased resolution of 3km-MP better resolved the inflow,

convergence and updrafts and also produced higher diabatic heating due to explicit treatment of cloud microphysical processes and therefore shows improvements over low resolution simulations using cumulus parameterization. In the second- and third-part sensitivity studies with various cloud microphysical parameterization schemes (Morrison, Lin, WSM3, WSM6, Thompson, Goddard) in the simulation of a tropical low pressure system and six TCs which formed over BOB are conducted. The results suggest that Thompson scheme gave a good prediction of rainfall, thermodynamic variables and least errors for both the track and intensity parameters thus promising the scheme's application for high resolution operational TC forecasting in the NIO. Sea Surface Temperature (SST) sensitivity experiments on the rapid intensification (RI) of two rapidly intensified cyclones (Amphan, Fani) formed over BOB are conducted in the final part comparing with a climatological mean SST for 11 years. Overall, the results suggest that positive SST anomaly has a major role in rapid intensification as the simulations also showed a higher wind shear during the RI phase. On the other hand, simulations for Fani revealed a less important role of SST during the RI phase which is associated with a low-wind shear.

The present study finds that the convection permitting simulations in general produce better simulations for TC tracks, intensities and structural parameters than the simulations using convective parameterization. The study also finds the best microphysics scheme (Thompson scheme) applicable for both TC tracks, intensity and rainfall, from simulations conducted for six TCs and a tropical low-pressure convective system. The results of high (low) SST anomaly and high (low) wind-shear for cyclone Amphan (Fani) indicate that SST influenced the RI phase only for Amphan whereas the wind-shear played major role for Fani.

Thesis Highlight

Name of the Student: Reshmi Mohan P
Name of CI: Indira Gandhi Centre for Atomic Research **Enrolment No.:** PHYS02201504027
Thesis Title: Numerical modelling studies on the impact of horizontal resolution, explicit convection and SST boundary forcing on the prediction of Tropical Cyclones over North Indian Ocean
Discipline: Physical Sciences **Sub-Area of Discipline:** Atmospheric Sciences
Date of viva voce: 15/05/2021

In the present work, an attempt is made to study the impact of horizontal resolution and explicit convection, sensitivity of high resolution predictions to cloud microphysical processes on the track and intensity predictions of Tropical Cyclones (TCs) over Bay Of Bengal (BOB) region of North Indian Ocean (NIO), and the role of SST in rapidly intensifying TCs using the WRF-ARW mesoscale numerical weather prediction modelling system. In the first part the study was conducted with two horizontal grid resolutions i.e., 9km grid using parameterized convection (9km-CP) and 3km grid using explicit microphysics (3km-MP) for ten TCs from 2010-2019. In the second and third parts microphysics sensitivity experiments were conducted for an extremely heavy rainfall event associated with a tropical low-pressure system followed by Tropical Cyclones. In the final part, SST sensitivity experiments were conducted on the Rapid Intensification (RI) of two pre-monsoon cyclones, Amphan and Fani.

In essence, the increased grid resolution of 3 km better resolved the inflow, convergence and vertical motions and also produced higher diabatic heating (Fig. 1a) due to explicit treatment of cloud microphysical processes and therefore produced improvements for both track and intensity predictions over low-resolution simulations (9 km) using cumulus parameterization. Among various microphysics schemes, the Thompson scheme produced stronger convergence and vertical motion up to 6 km and stronger upper air divergence associated with strong cyclonic vorticity in the atmosphere and also captured the time evolution of different hydrometeors that led to produce the observed pattern of the rainfall (Fig. 1b) associated with a low-pressure system both spatially and temporally. Also, the Thompson scheme produced least errors for track and intensity due to simulating the vertical motions in good agreement with the observation as observed for Fani and Gaja cyclones (Fig. 1c), which suggest that it is more suitable for high-resolution operational TC forecasting in the NIO. It has been found that the positive SST anomaly played a significant role in the rapid intensification of TC Amphan in spite of large wind shear during the developing stages due to highly symmetric organization of convection induced by warm SST. SST has only a minor influence in RI phase of Fani due to smaller SST anomaly associated with low wind-shear which promoted rapid intensification. This suggests the RI phase is caused mainly by SST anomaly for Amphan and low wind-shear for Fani cyclones.

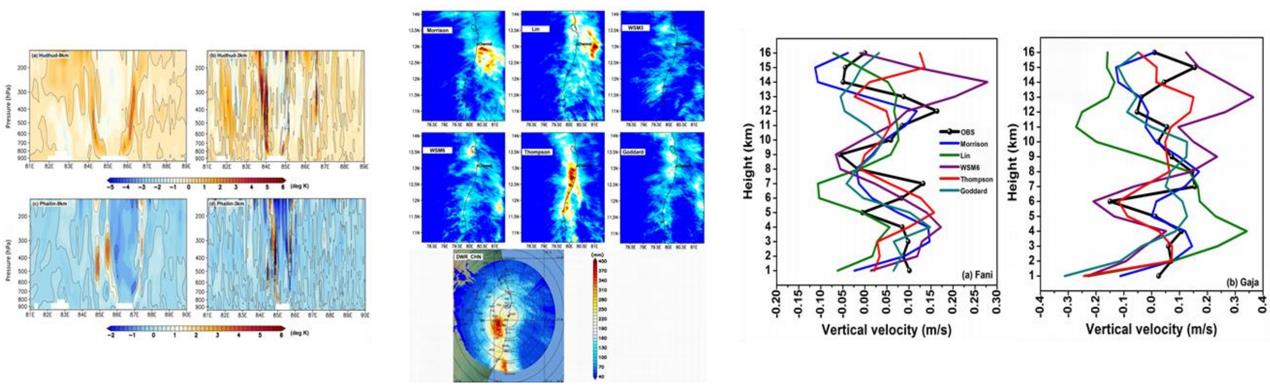

Figure 1. (a) Longitude height cross-section of diabatic heating for Hudhud (top panels) and Phailin (bottom panels) by 9km-CP (left panels) and 3km-MP (right panels), (b) 24 hour cumulated rainfall produced by different microphysics schemes compared with Chennai DWR image, (c) Simulated vertical motions by different microphysics schemes compared with MST radar data over Gadanki.